ADDIS ABABA UNIVERSITY

COLLEGE OF TECHNOLOGY AND BUILT ENVIRONMENT

SCHOOL OF CHEMICAL AND BIOENGINEERING

Photocatalytic-Adsorptive Abatement of Tetracycline Using a Green Synthesis of ZnO-NPs/Cassava Peel-Activated Carbon: Machine Learning Optimization

Ph.D. DISSERTATION

DEREJE EMISHAW MANYAZEWAL

ADDIS ABABA, ETHIOPIA

MAY 28, 2026

Photocatalytic-Adsorptive Abatement of Tetracycline Using a Green Synthesis of ZnO-NPs/Cassava Peel-Activated Carbon: Machine Learning Optimization

By

DEREJE EMISHAW MANYAZEWAL

A Ph.D. Dissertation

Submitted to the School of Chemical and Bioengineering of the College of Technology and Built Environment,

Addis Ababa University, Addis Ababa, Ethiopia

in Partial Fulfilment of the Requirements

for the Degree of

DOCTOR OF PHILOSOPHY

in

CHEMICAL ENGINEERING (PROCESS ENGINEERING)

MAY 28, 2026

STATEMENT OF THE AUTHOR

By signing below, I attest that this doctoral dissertation is entirely original and has not been submitted to any other university for credit toward a degree or exam. I have met the recognized standards for originality and quality, and I have adhered to all ethical principles in accordance with the university's regulations.

All scholarly content presented in this dissertation has been properly acknowledged to credit the sources. I confirm that every source used in the development of this thesis has been appropriately referenced. To prevent plagiarism, I have made every effort in the preparation of this dissertation

Dereje Emishaw Manyazewal		May 28, 2026
Ph.D. Candidate	**Signature**	**Date**

APPROVAL SHEET

The dissertation, entitled **"Photocatalytic-Adsorptive Abatement of Tetracycline Using a Green Synthesis of ZnO-NPs/Cassava Peel-Activated Carbon: Machine Learning Optimization**,**"** prepared and submitted by Dereje Emishaw Manyazewal in partial fulfillment of the requirements for the Degree of Doctor of Philosophy in Chemical Engineering, complies with the regulations of the university and meets the accepted standards with respect to originality and quality.

Approved by the Examination Committee

Dr. Kebede Niguse Mekonnen (Associate Prof.)	_____	_____
Internal Examiner	**Signature**	**Date**
Dr. Kenatu Angassa Wakuma (Associate Prof.)	_____	_____
External Examiner	**Signature**	**Date**
Professor Dr. Ing. Zebene Kiflie	_____	_____
Major Advisor	**Signature**	**Date**
Dr. Shimelis Kebede Kassahun (Associate Prof.)	_____	_____
Co-Advisor	**Signature**	**Date**
Dr. Anteneh Marelign (PG. Coordinator)	_____	_____
Chairperson	**Signature**	**Date**
_____	_____	_____
VEDAA, CTBE-AAU	**Signature**	**Date**

DEDICATION

I dedicate my dissertation to my family and many friends. I am profoundly thankful to my loving parents and my younger brother, Mr. Aboneh Emishaw Manyazewal. His unwavering support, encouragement, and love have sustained me throughout every stage of my life. This dissertation is also dedicated to my friends, whose words of support and inspiration for tenacity resonate in my ears, always by my side, and are truly special.

ACKNOWLEDGEMENTS

First and foremost, my deepest gratitude to Almighty God for blessing me with strength, wisdom, and perseverance to endure this long journey toward my goal, which has been very challenging yet rewarding in the end. I am profoundly thankful to my principal supervisors, Professor Zebene Kiflie and Dr. Shimelis Kebede Kassahun. Their invaluable daily suggestions and comments, combined with their immense knowledge and extensive experience, have been tremendously helpful at all stages of my study and have provided me with essential support for my academic research career. I express my additional, sincerest thanks to Dr. Shimelis Kebede Kassahun for his priceless contributions, supporting resources, publishing assistance, and encouraging words during all my learning. His generous support and hopeful words throughout this journey have been immensely valuable, and I deeply cherish his daily guidance.

My sincere gratitude goes to the specific individuals and laboratory personnel who directly supported my experimental work. I have a special thanksgiving, particularly, to Mr. Hintsa G. Silassie, whose untiring efforts in facilitating access to and operation of some essential laboratory equipment were crucial for the experimental phase of my research. I am also incredibly grateful to Mr. Tilahun, Mrs. Yeabsira Zenebe, Dr. Molalign Emirie, Mr. Somson Chufemo, and Eng. Dawit Kinfe for their respective assistance, coordination, and individual contributions. Finally, my thanks go to all the voices of encouragement or support that have reached me along the way.

On an institutional level, I extend my heartfelt gratitude to Addis Ababa University, specifically the School of Chemical and Bioengineering and the College of Technology and Built Environment (CTBE). I am deeply indebted to the academic, administrative, and laboratory staff members within these entities for creating an enabling atmosphere for academic excellence and facilitating my research. Additionally, the Ethiopian Pharmaceutical Manufacturing Company, Sc., Ethiopia, deserves a great deal of recognition for providing and identifying the major pharmaceutical pollutants for this study.

LIST OF ACRONYMS AND ABBREVIATIONS

AC	Activated carbon
AC/ZnO-NPs	Activated carbon-zinc oxide nanoparticles
AOPs	Advanced oxidation processes
BBD	Box Behnken Design
BOD	Biological Oxygen Demand
CB	Conduction Band
CCD	Central Composite Design
CECs	Contaminants of Emerging Concerns
COD	Chemical Oxygen Demand
DAF	Dissolved Air Flotation
EPS	Emerging Pollutants
HOMO	Highest Occupied Molecular Orbital
IUPAC	International Union of Pure and Applied Chemistry
LEDs	Light-Emitting Diodes
LUMO	Lowest Unoccupied Molecular Orbital
MBR	Membrane Bioreactor
MoF	Metal-Organic Framework
OTC	Oxytetracycline Hydrochloride
PFO	Pseudo-First-Order
PhACs	Pharmaceuticals Contaminants
PPCPs	Pharmaceuticals and Personal Care Products
PPS	Polytetrafluoroethylene
PSO	Pseudo-Second-Order
ROS	Reactive Oxygen Species
RSM	Response Surface Methodology
SS	Suspended Solids
TC	Tetracycline
TCN	Tetracycline Hydrochloride
TN	Total Nitrogen
TOC	Total Organic Carbon

TP	Total Phosphorus
VB	Valence Band
WWTPS	Wastewater Treatment Plants

TABLE OF CONTENTS

LIST OF FIGURES

LIST OF TABLES

LIST OF PUBLICATIONS

1. **Manyazewal, D.E**., Kiflie, Z., & Kebede, S. Green synthesis and characterization of citrus bergamia leaves-extracted modified zinc oxide nanoparticles impregnated on cassava peel-based activated carbon. *J Sol-Gel Sci Technol* 115, 1180–1194 (2025). https://doi.org/10.1007/s10971-025-06792-8
2. **Manyazewal, D.E**., Kiflie, Z., and Kebede, S. (2025), Machine Learning-Based Process Optimization for Adsorption Removal of Emerging Contaminant (Tetracycline) From Aqueous Solution onto Zinc Chloride Activated Biomass (*Cassava Peels*). Remediation Journal, 35: e70026. https://doi.org/10.1002/rem.70026
3. **Manyazewal, D.E**., Kiflie, Z. & Kassahun, S.K. Parametric Optimization and Kinetics Analysis for Photocatalytic Abatement of Emerging Pollutants (Tetracycline) from Aqueous Solutions Using Citrus bergamia Leaf Extract-Mediated Synthesis of Zinc Oxide Nanoparticles. Water Air Soil Pollut 237, 655 (2026). https://doi.org/10.1007/s11270-026-09318-2
4. **Manyazewal, D.E**., Kiflie, Z., & Kebede, S. Simultaneous Adsorption and Photocatalysis Processes Based on the Synergetic Effect of Composite Materials (Green-based AC/ZnO-NPs) for the removal of pharmaceutical pollutants of (Tetracycline) from Aqueous Solution. Under review

ABSTRACT

The widespread prevalence and ecotoxicological risks posed by the antibiotic tetracycline (TC) in aqueous environments present significant challenges to conventional wastewater treatment plants. This dissertation comprehensively explores the design, characterization, and application of novel, eco-friendly composite materials for eliminating TC from aqueous streams. This research focuses on the sustainable fabrication of a highly efficient material, combining green-synthesized zinc oxide nanoparticles (ZnO-NPs) with low-cost, biomass-derived activated carbon (AC), to leverage the synergistic mechanisms of simultaneous adsorption and photocatalysis.

The study was conducted in three progressive phases. First, a green, sustainable protocol was developed to synthesize ZnO-NPs using *Citrus bergamia* leaf extract as a reducing and capping agent. Concurrently, highly active AC was prepared from cassava peels via chemical activation using $ZnCl_2$. Second, the preparation parameters for both components, including impregnation ratios, carbonization temperatures, and dwell times, were systematically controlled and individually optimized for TC removal using Response Surface Methodology (RSM) coupled with Artificial Neural Networks (ANN). Third, the final composite (AC/ZnO-NPs) was fabricated by impregnating the green-synthesized nanoparticles onto the cassava peel-based carbon matrix. The structural, optical, and morphological properties of all materials were systematically characterized using Fourier-Transform Infrared Spectroscopy (FT-IR), Ultraviolet-Visible Spectroscopy (UV-Vis), X-ray Diffraction (XRD), and Scanning Electron Microscopy (SEM). Subsequently, the composite's treatment performance was optimized using a Box-Behnken Design (BBD) under UV/vis irradiation.

Characterization of the green-synthesized ZnO-NPs confirmed a hexagonal wurtzite structure with an average crystallite size of 13.94 nm, a specific surface area of 371 m^2/g, and a band gap of 3.15 eV. The cassava peel-derived AC exhibited a highly microporous architecture, an extensive surface area of 1250 m^2/g, and an average particle size of approximately 104 nm. In single-component optimization trials, the AC achieved a 97.2% TC removal efficiency under RSM/ANN-optimized conditions (pH 7.49, contact time of 74.15 min, and dosage of 0.059 g/L). Meanwhile, the ZnO-NPs achieved 92.1% TC degradation and 69.47% Total Organic Carbon (TOC) removal under optimized photocatalytic parameters (pH 5.64, irradiation time of 118.96 min, and catalyst

dose of 1.49 g/L). For both individual systems, equilibrium and kinetic profiles were accurately modeled by the Langmuir isotherm and pseudo-second-order kinetics, respectively. For the combined AC/ZnO-NPs composite, RSM-BBD optimization established optimal operational parameters: an AC to ZnO-NPs mass ratio of 3.64:1, a composite dosage of 0.747 g/L, and an initial TC concentration of 5.99 mg/L. Under these specific conditions, the composite achieved a superior TC removal efficiency of 99.83% due to the localized synergy of adsorption and photocatalysis. The predictive quadratic model proved highly accurate, displaying a robust coefficient of determination ($R^2 = 0.9988$) and high statistical significance ($p < 0.0001$).

This dissertation has demonstrated the efficacy of a sustainable, cost-effective, and highly efficient composite material for the abatement of pharmaceutical contaminants in water. By anchoring highly efficient, green-synthesized photocatalytic nanoparticles onto a high-surface-area biomass adsorbent, this research provides a scalable, eco-friendly configuration with substantial potential for integration into advanced industrial water and wastewater treatment systems.

1. INTRODUCTION

1.1 Background of the study

Medical substances like pharmaceutical pollutants (PPS) are a group of emerging anthropogenic hazardous contaminants that contain different groups of human and veterinary medicines that are used widely all over the globe. The broad-spectrum water pollution by these contaminants of emerging concern (CECs) is an environmental health and public well-being issue. (John et al., 2024).

Emerging pharmaceutical pollutants in the aquatic environment commonly include a wide variety of compounds, such as antibiotics, chemotherapy products, hormones, analgesics, antipyretics, antidepressants, anti-inflammatory/antibacterial agents, beta-blockers, steroids, and lipid-lowering drugs. These chemicals are not currently regulated by comprehensive water quality laws, hence their classification as emerging contaminants (Akhter et al., 2024). While antibiotics are typically detected in aquatic systems at sub-inhibitory concentrations ranging from ng/L to µg/L, their chronic presence triggers multiple interconnected long-term risks. Beyond driving the genetic selection of resilient bacteria and accelerating antimicrobial resistance (AMR), persistent, low-level exposure leads to bioaccumulation and subsequent biomagnification through aquatic food webs. This chronic bioaccumulation then triggers significant ecotoxicological impacts in non-target organisms.

These impacts manifest as endocrine disruption, reproductive impairment, and developmental abnormalities in fish and amphibians, broadly observed. In addition, the steady influx of active compounds can alter the composition and functional diversity of natural microbial communities, thereby disrupting key biogeochemical processes such as nutrient cycling and organic matter decomposition. Simultaneously, phytotoxic stress affects primary producers such as microalgae, leading to instability in the entire aquatic ecosystem(Chow et al., 2021).

Among these, TC, the chemical ($C_{22}H_{24}N_2O_8$), and its molecular weight are (444.44 g/mol) is one of the typical pharmaceuticals and personal care products (PPCPs) and occupies a large proportion in the use of antibiotics, and exhibiting activity against infections caused by both Gram-positive and Gram-negative bacteria as well as chlamydia, mycoplasmas, rickettsia, and protozoan parasites (Tsigara et al., 2024). TC, mainly including tetracycline hydrochloride (TCN), oxytetracycline hydrochloride (OTC), and chlortetracycline hydrochloride (CTC), has been widely used for the treatment of infection in animals and humans (Xiong et al., 2018).

It is a widely acknowledged fact that conventional wastewater treatment plants (WWTPs) are ineffective in eliminating persistent pharmaceutical compounds, because of these facility were designed for the removal of bulk organic matter and nutrients, not complex pharmaceutical micro-pollutants including TC (Khasawneh & Palaniandy, 2021). As a result, such contaminants are discharged into receiving water bodies following general treatment arrangements, where they often persist. It is this persistence that speaks to the urgent need for developing new and advanced remediation technologies. The study thus goes ahead to address this area by synthesizing, and optimizing advanced nanocomposite materials for highly effective removal of TC from aqueous environments.

To this imperative need, in this study, a multi-faceted approach to counteract TC contamination was developed by optimizing a novel hybrid water treatment system, which lies in the innovative integration of adsorption and photocatalysis the most promising advanced oxidation methods (D. Wang et al., 2018). This was achieved by the synthesis of a novel composite material from low-cost renewable resources, and the implementation of the principles of green chemistry, process optimization using RSM-BBD and ANN approaches, and synergistic integration among multiple removal pathways (Briche et al., 2020).

The study expedition begins with the initial step of material innovation, and characterization of a novel composite material, where zinc oxide nanoparticles (ZnO-NPs) synthesized using a green extract of *Citrus bergamia* leaves are deposited onto activated carbon from cassava peel waste. This not only supports sustainability by valorizing agricultural residues but also aims to create a material with enhanced properties (Taha et al., 2021).

On this foundation, the research increasingly investigated the adsorption-photocatalysis routes as they are found to be imperative. This innovative approach outperforms traditional single-factor-at-a-time experiments to efficiently model complex interactions and identify optimum conditions for pollutant removal. In parallel, the study conducts a parametric optimization and analysis of the photocatalytic degradation of TC by green-synthesized ZnO-NPs, and the adsorption removal process by cassava peel-derived activated carbon in isolation.

This procedure was essential for the researchers to evaluate the fundamental photocatalytic characteristics and adsorption capacity of the synthesized materials before the composite loading process. AC and ZnO-NPs worked together to enhance the adsorption-photocatalysis process. To improve the photocatalytic degradation of ZnO-NPs, this method employs AC to capture contaminants on their surface (Salah et al., 2024). The consensus was that the AC would adsorb the TC molecules onto its surface and position them close to the ZnO-NPs and considerably enhance their photocatalytic degradation, so that the removal efficiency is greater than the sum of the individual processes.

1.2 Justification of the study

The widespread use in medicine and agriculture, has made it a common water contaminant. It is not uncommon for traditional wastewater treatment plants to fail in removing these persistent compounds, resulting in their presence in aquatic environments. This pollution can be toxic to aquatic life and, more importantly, promote the growth of antibiotic-resistant bacteria, which pose a global health risk. Therefore, there is an urgent need for effective, affordable, and advanced methods to remove these pollutants (TC) from water.

The current study is justified by introducing a new composite material that combines the degradation ability of photocatalysis with the adsorption capacity for improved of activated cassava peel-derived carbon. The green synthesis method for ZnO-NPs, which is environmentally friendly, reduce toxic chemicals. Additionally, activating cassava peel-derived carbon, an easily accessible agricultural waste, transforms what would otherwise be an environmental nuisance into a useful product, making the entire process economical and sustainable.

1.3 Scope of the study

This research focuses on developing a new, environmentally friendly composite material designed to adsorb the antibiotic TC from aqueous solutions. The composite is prepared using green synthesis, incorporating ZnO-NPs with AC derived from waste cassava peel. Its increased efficiency results from the synergistic action of both components.

The ZnO-NPs act as a photocatalyst to degrade TC under UV-Vi's light, while the highly porous AC adsorbs the contaminant onto its surface. This study conducts a comprehensive analysis and optimization of models to examine the kinetics and equilibrium of the removal process. Additionally, RSM-BBD and ANN techniques are used to identify the best operational conditions, including pH, catalyst dose, pollutant concentration, irradiation time, and adsorption time, to maximize removal efficiency. The ultimate goal is to develop a highly effective, sustainable, and cost-efficient method for remediating TC contaminated aqueous solutions. Additionally, the experiment was conducted under laboratory conditions using only model aqueous solutions.

1.4 Limitations of the study

One of the main analytical constraints in this study was its reliance on Total Organic Carbon (TOC) analysis to monitor TC breakdown. While TOC is useful for capturing mineralization, the conversion of organic pollutants into stable inorganic species like CO_2 and H_2O, it does not, by itself, identify specific structural intermediates. Consequently, direct empirical monitoring of short-lived or transient byproducts using Liquid Chromatography-Mass Spectrometry (LC-MS) was not performed within the immediate scope of this work.

As a result, the detailed reaction pathway could not be clearly defined, and the potential toxicity of these short-term intermediates remains untested, leaving a gap in the overall environmental safety assessment of the treatment process.

1.5 Problem statement

Due to their complex chemical structures and low biodegradability, pharmaceutical pollutants, especially antibiotics such as TC, pose a significant threat to public health and environmental sustainability when they contaminate water bodies worldwide. A 2016 global survey detected pharmaceutical residues in 71 countries; by 2020, this number had risen to 89, highlighting an increasing trend in both environmental detection and usage. The most recent global survey, conducted from 2022 to 2024, found active pharmaceutical compounds exceeding safety limits in over 25% of 258 rivers across 104 nations (Wilkinson et al., 2022).

Ethiopia's high demand for veterinary services, combined with inadequate wastewater infrastructure, exacerbates the issue. Regional studies conducted between 2015 and 2017 revealed that oxytetracycline was the most widely used veterinary medication in the country, with over 112 million doses administered. This widespread use has resulted in measurable residues in water sources and food chains (Tegegne et al., 2024). Antibiotic concentrations in wastewater have been found to reach as high as 433 µg/L in recent environmental monitoring conducted across the African continent, greatly exceeding Predicted No-Effect Concentrations (PNEC) (Donkor et al., 2025). Tetracycline residues have been detected in river sediments and biota in Ethiopia, with concentrations ranging from 0.074 to 1161.2 µg/kg.

Standard wastewater treatment methods, such as traditional activated sludge, can effectively reduce biodegradable organic complexes. However, for various reasons, these methods are insufficient to eliminate persistent organic compounds (TC) (Chen et al., 2022). Many pharmaceutically active compounds (PhACs) are highly resistant to microbial biodegradation, primarily due to their thermodynamically stable chemical bonds and complex, heavily functionalized chemical architecture, particularly for aromatic structures. Second, their comparatively low quantities (usually between µg/L and ng/L) are below the threshold required to activate the required degradative enzymes in most biological systems (Zhu et al., 2024).

Third, instead of partitioning into the sludge, many of these substances can stay in the aqueous phase due to their high hydrophilicity. As a result, these partially treated effluents discharge persistent residues into the environment, putting microbial communities under selective pressure and directly promoting the growth of bacteria and antibiotic-resistant genes (ARGs) (ARB) (L. Zhang et al., 2025).

Furthermore, new innovative and energy-efficient technology, which is also sustainable, is needed to mineralize and mitigate these chemicals of emerging concern. Consequently, it is necessary to reach out to another potential and feasible treatment technology that can degrade such types of substances and prevent their accumulation in the environment. Advanced treatment techniques that combine adsorption with photocatalysis are very promising (Farahani, 2024).

Advanced oxidation processes (AOPs) have shown promise for degrading persistent organic pollutants (POPs), and photocatalysis utilizing metallic oxide nanoparticles, such as ZnO-NPs, has recently gained interest in degrading contaminants of emerging concern (CECs) (Semeraro et al., 2020). Although ZnO-NPs are an appealing photocatalyst because they are inexpensive, versatile, exhibit high photocatalytic activity, and are relatively environmentally friendly, their practical application is limited (Karcıoğlu Karakaş & Dönmez, 2025). Issues such as rapid recombination, photocorrosion, agglomeration, recovery after treating water, and bandgap energy limiting activation to only the UV portion of the solar spectrum limit the effectiveness of ZnO-NPs (K. Jia et al., 2022).

To reduce these constraints, immobilization of ZnO-NPs on a porous substrate, AC derived from agricultural waste (cassava peels), can be utilized as a carbon precursor, indicating a suitable, cost-effective, and sustainable method of value-adding waste products (Sağlam et al., 2024). In addition, the green synthesis of ZnO-NPs using plant extracts harbors an even more sustainable and less-harmful alternative to oxidative chemical methods of synthesis (Alshahateet et al., 2024). Using plant extracts, such as extracts from *Citrus bergamia* leaves, can provide ZnO-NPs that can be in line with sustainable engineering's green synthesis principles through the less use of harmful substances.

To provide a solution to limitations associated with any individual adsorption or photocatalytic system, incorporation into single composite materials can be considered. The case of a ZnO-NPs/AC composite is such wherein its very high synergistic effect increases its overall pollutant-removal efficiencies (Albo Hay Allah & Alshamsi, 2023b).

The cassava peels activated carbon (CPAC), with its high surface area acts as an adsorption center, adsorbing and concentrating tetracycline molecules from the bulk solution and bringing them into proximity with the ZnO-NPs photocatalytic sites (Sulaiman et al., 2018). This substrate enrichment dramatically increased the rate of photocatalytic degradation (Rasheed et al., 2025). AC, while an excellent conductor of electrons, serves as a medium to transfer photo-induced electrons in the conduction band of excited ZnO-NPs to itself is the electron sink, providing physical separation between the holes and the electrons, leading to very low rates of recombination. Thus, leaving more holes to generate highly potent $^{\bullet}OH$ radicals, enhancing the photocatalytic activity

The abundance of cassava peels as an agricultural byproduct in Ethiopia makes them a suitable precursor for activated carbon (CPAC) (Parmar et at., 2018). This option features a lignocellulosic structure ideal for creating high porosity and establishing a sustainable waste-to-resource pathway. (Getahun et at., 2026). TC molecules from the bulk solution are concentrated in the resulting AC, which has a large surface area that acts as an adsorption center, drawing them closer to the photocatalytic sites of the ZnO-NPs. This concentration of the substrate significantly accelerates the rate of photocatalytic degradation (Salah et al., 2024).

Citrus bergamia leaves were chosen for the environmentally friendly synthesis of ZnO-NPs due to their rich content of bioactive polyphenols and flavonoids. These compounds serve as effective stabilizing and reducing agents, eliminating the need for hazardous chemical precursors (Chandra et al., 2025). AC plays a dual role in the resultant composite, helping to transfer photo-induced electrons from the conduction band of excited ZnO-NPs since it is a good electron conductor.

1.6 Objective of the study

1.6.1 General objective

The main objective of this research was to study the photocatalytic-adsorptive abatement of TC-an emerging pollutant, using a greenly-synthesized Zinc oxide NPs/Cassava Peel-Activated Carbon.

1.3.2 Specific objectives

The specific objectives were to:

Objective 1: Sustainable Material Synthesis and Multi-Scale Characterization

To synthesize ZnO-NPs using *Citrus bergamia* leaf extract via a green route; produce highly active AC from cassava peel biomass through $ZnCl_2$ chemical activation; and fabricate an integrated AC/ZnO-NPs composite material.

Objective 2**:** Adsorption Performance Optimization via Statistical and Machine Learning Modeling

To model, evaluate, and optimize the batch adsorption removal of TC from aqueous solutions using cassava peel-derived AC by systematically varying operational parameters. This was involved a comparative predictive analysis utilizing RSM-BBD and ANN to model equilibrium isotherms and pseudo-second-order kinetic mechanisms.

Objective 3: Parametric Evaluation and Kinetics of Photocatalytic Abatement

To investigate and optimize the photocatalytic degradation efficiency of the green-synthesized ZnO-NPs for both TC degradation and Total Organic Carbon (TOC) mineralization under UV/vis irradiation.

Objective 4: Evaluation of Synergistic Mechanisms and Multi-Variable Composite Optimization

To investigate, quantify, and optimize the simultaneous adsorption and photocatalytic performance of the combined AC/ZnO-NPs composite material for accelerated TC mitigation. This will involve applying a RSM-BBD to determine the optimal AC to ZnO-NPs mass ratio, composite dosage, and initial pollutant concentration, while statistically validating the localized synergistic treatment index.

1.7 Expected significance and implications of the study

This study lies in formulating a nanocomposite ZnO-NPs/AC derived from waste and describing its synergistic mechanism for water purification. The central novelty of this work resides in associating the adsorption capacity of cassava peel-activated carbon with the photocatalytic activity of green-synthesized ZnO-NPs. It is expected that this synergism would help overcome limitations for both adsorption and photocatalysis, thus allowing for the fast and effective removal of TC by coupling the concentration of the pollutant on the surface of the material with the degradation process.

In addition, the development of machine learning algorithms for the optimization of the process is a substantial methodological turnaround from a heuristic-based engineering to a data-driven intelligent process design in environmental remediation that aims at predictive control. This study has broader implications that are directly targeted at acute environmental and economic challenges. In engineering a suitable technology for the removal of an emerging contaminant, namely TC, this work will, in very tangible ways, contribute towards reducing the global burden of contaminants of emerging concern (CECs) and in the safeguarding of human health and aquatic ecosystems.

The study proposes a circular bioeconomy from an economic standpoint by converting low-value agricultural wastes, cassava peels, and *Citrus bergamia* leaves into high-performance, value-added materials and effectively providing a sustainable, low-cost alternative for conventional, high-cost water treatment systems.

1.8 Organization of the dissertation

This dissertation is structured logically across seven chapters, transitioning from foundational frameworks to specific experimental findings and future directions. It begins in chapter one by defining the research context, the significance of the problem, and the study objectives. Chapter two presents a comprehensive literature review and theoretical framework to identify existing research gaps. The core experimental work includes the green synthesis of ZnO-modified nanoparticles using *Citrus bergamia* leaf extracted and cassava peel in chapter three, the application of machine learning for optimized adsorption of TC in chapter four, and a kinetic study on the photocatalytic degradation of TC in chapter five.

Chapter six explores the synergistic effects of combining simultaneous adsorption and photocatalysis for pollutant removal using a composite material. Finally, chapter seven synthesizes these findings into conclusions, future research avenues, and provides a complete bibliography.

2. LITERATURE REVIEW

2.1 Introduction

TC is recognized as an emerging, toxic, and recalcitrant pollutant (Amangelsin et al., 2023a). The mechanisms and recent developments in the two primary technologies relevant to this study are discussed: semiconductor nanoparticle photocatalysis and waste biomass-based activated carbon adsorption, with a focus on green chemistry concepts. A critical review of the enhancement of photoactivity in composite materials is also presented, along with a detailed explanation of the synergistic adsorption-photocatalysis mechanism. Additionally, this chapter identifies the main research gaps that this study aims to address and offers an overview of the current state of the field.

2.2 Contaminants of Emerging Concern

Emerging contaminants (ECs) are man-made or naturally occurring chemicals not typically of monitoring concern, but with the potential to often not be controlled or monitored in the environment, and are known or suspected to be causing negative ecological and human health impacts (Puri et al., 2023). A diverse array of unregulated pollutants is increasingly prevalent in the environment. This group includes pharmaceuticals, personal care products, endocrine disruptors, and industrial chemicals, all of which can enter the environment through various pathways. These contaminants can persist and accumulate in the food chain, posing risks to both ecosystems and human health. This raises significant concerns due to the unknown long-term adverse effects on the environment and human health. These compounds, which originate from various sources and have diverse chemical natures, have largely gone unnoticed, and remain unregulated in the environment (X. Li et al., 2024).

2.3 Sources of emerging contaminants

Thousands of organic compounds have been identified as contaminants of emerging concern in the last few decades, and, being new, have been largely outside the scope of regulation. Therefore, they can be found in trace concentrations, ranging from a few ng L^{-1} to several µg L^{-1} in water, sediment, soil, and. They show a great diversity of chemical structures, properties, and possible interaction mechanisms with living beings. They may be both natural and synthetic, and most are found in wastewater bio-solids, agriculture and livestock**,** in soils, in groundwater, landfills, and in seawater (F. Wang et al., 2024).

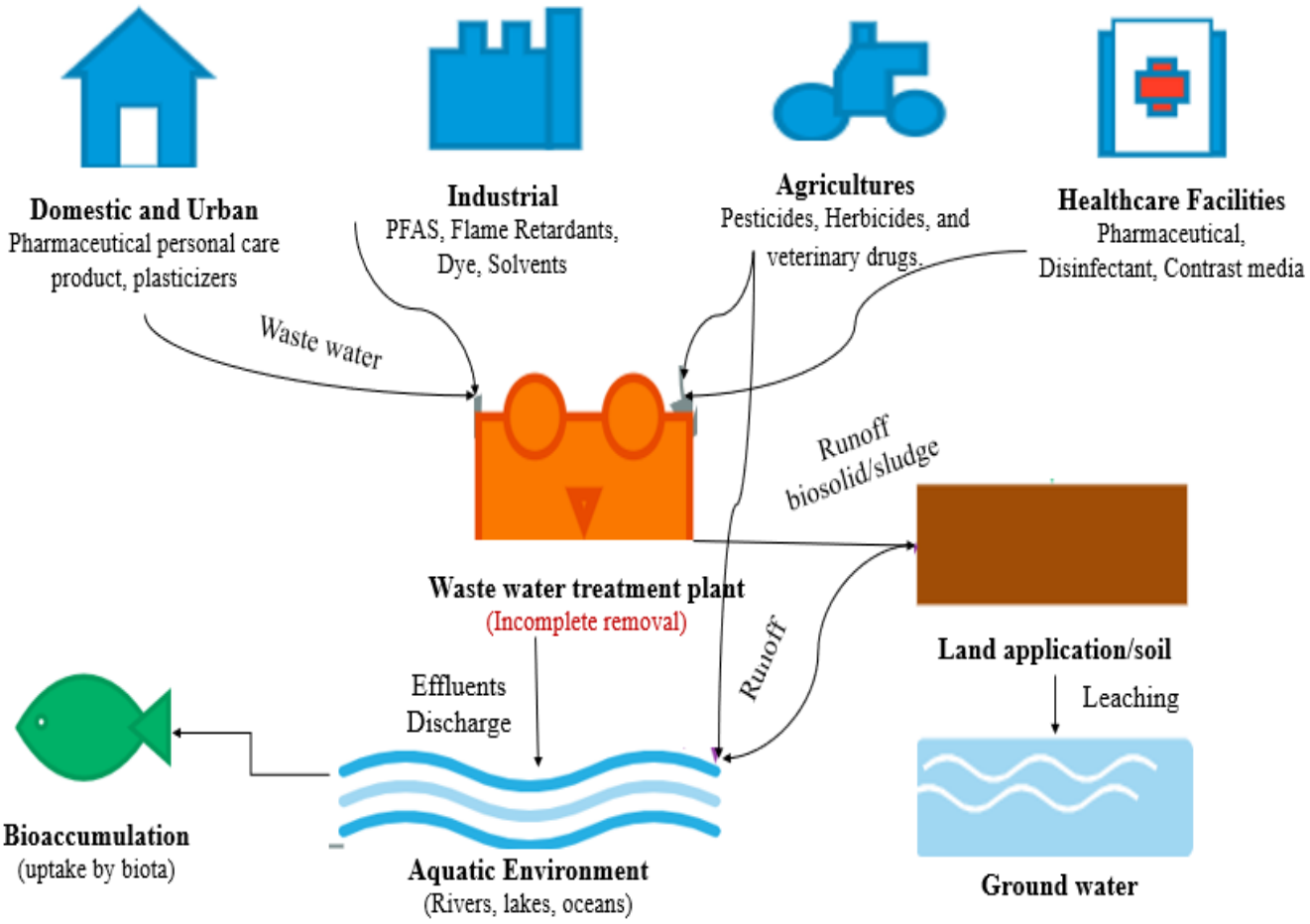

Figure 2-1 Sources and Pathways of Emerging Organic Pollutants

2.4 Tetracycline overview

TC, a broad-spectrum antibiotic, is widely used in human medicine, veterinary medicine, and as a growth promoter for aquaculture and animal production. Due to its extensive use and improper metabolism in humans and animals, it is continuously released into the environment through wastewater effluents, agricultural runoff, and landfill leachate. According to Cheng et al. (2021), the presence of TC in surface water, groundwater, and soil at levels ranging from nanograms per liter (ng/L) to a few micrograms per liter (μg/L).

The presence of constant selective pressure from even sub-lethal concentrations of TC in aquatic environments can build microbial populations that are progressively resistant, which has been indicated by the World Health Organization (WHO) as a key global health issue (Wei et al., 2021). Besides, TC possesses ecotoxicological behavior, having an impact on algal growth, suppressing aquatic plant photosynthesis, and being toxic to other microorganisms and aquatic invertebrates. Its aromatic and stable complexity makes it non-biodegradable by natural processes, hence making it persistent and bio-accumulative (Ebele et al., 2020).

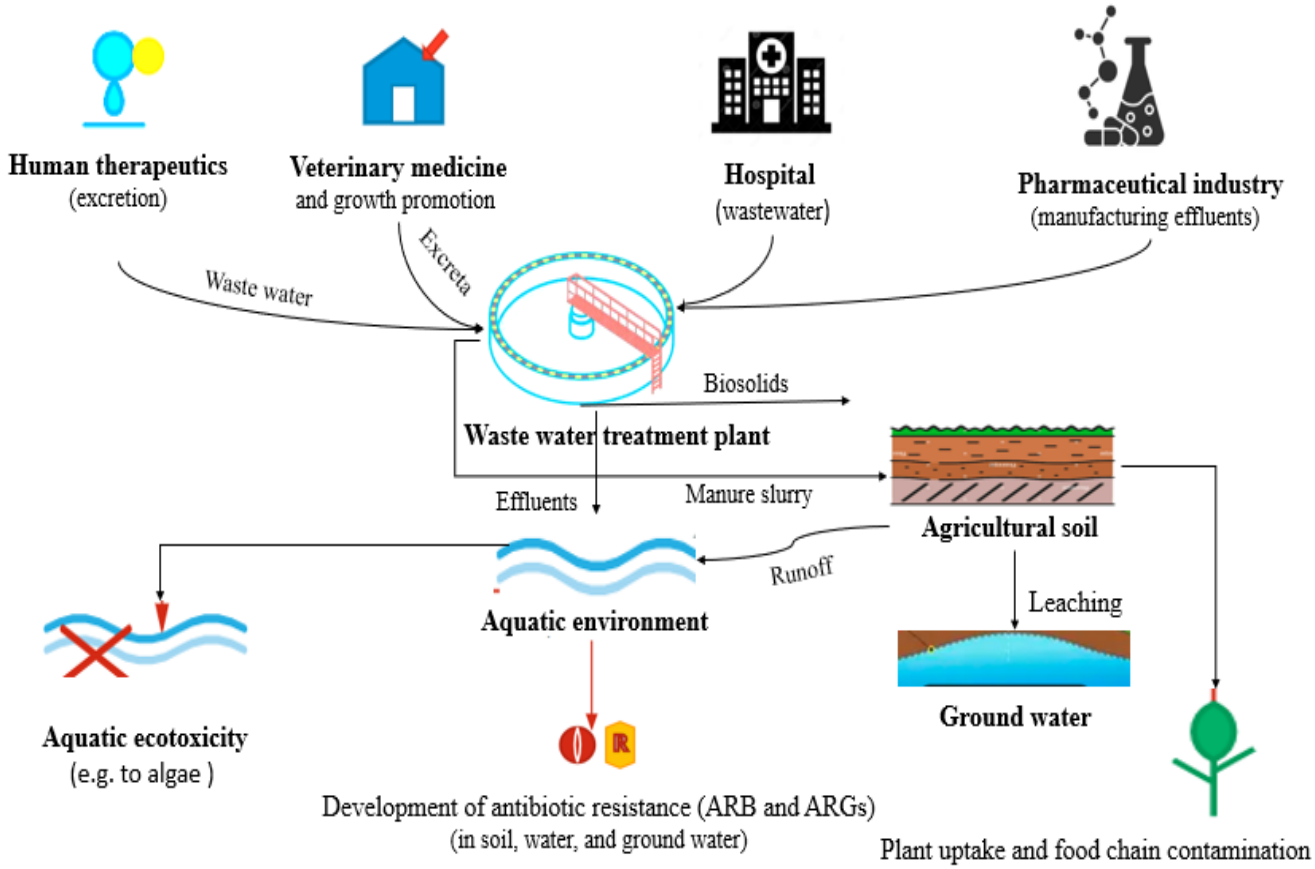

Figure 2-2 Ecological Occurrence and Effects of Tetracycline

Conventional wastewater treatment plants (WWTPs) dominated by biological processes are notoriously inefficient at TC removal and with efficiencies of reported. This inefficiency necessitates the incorporation of next-generation, effective, sustainable tertiary treatment technologies that shall safeguard water resources (Cuetero-Martínez et al., 2023).

2.4.1 Environmental entry pathways of human and veterinary pharmaceuticals

The first generation is ordered only orally, whereas the second generation can be either orally or intravenously, and the third generation, like tetracycline, is administered intravenously by infusion alone (C. Li et al. 2025). The first-generation TC is less lipophilic and therefore has a lower tissue saturation, which is in the range of 25 to 60% (Pearson et al., 2025). Several scholar found the concentration of tetracycline was above the permissible maximum residual limit in livestock, which implies the widespread misappropriation of TCs and the lack of providing the required withdrawal period found the TCs residue in the poultry follows the range, OTC = 124 to 2930 µg/kg, TC = 25

to 311 µg/kg, CTC = 130 to 8148 µg/kg, DC = 127 to 6010 µg/kg with liver as the major deposition site (Uma & Ashenef, 2023).

2.4.1.1 Hospitals

Based on the Kounatidis et al. (2024), TC concentration in hospital effluents is relatively lower than other antibiotics due to the differences in tetracycline practice patterns and medical ingestion compared to the overall antibiotics load from hospitals and households into an urban WWTPs. The lesser contribution of hospitals to the TC load in municipal WWTPs, except in minocycline, the presence of TCs in hospital effluents found in the range of 516 to 1385 ng L^{-1} (Shokouhi et al., 2019).

2.4.1.2 Pharmaceutical industries

TC released from the pharmaceutical industry is rarely studied. In tetracycline manufacturing industries, very high loads are present in the influent of their WWTPs. According to Hameedi (2021) found that the oxytetracycline (OTC) load of 442 ± 9.6 mg/L in the raw wastewater from an OTC manufacturing industry. In a TC manufacturing industry, the influent was found to have a higher concentration of OTC (334.3 mg/L), TC (11.9 mg/L), and CTC (1.8 mg/L) (Hou et al., 2015).

2.4.1.3 Wastewater treatment plants (WWTPs)

According to Scaria et al., (2021), the specific TC analogs present and their corresponding influent concentrations in WWTPs vary significantly depending on the wastewater source and prevailing regional antibiotic consumption patterns. Substantial amounts of TCs are released directly into the receiving aqueous environment. The remaining TCs, removed through these treatments in WWTPs, are merely undergoing phase transfer by bio-sorption and deposition into sludge (Norvill et al., 2017). On WWTPs equipped with activated sludge with chlorination removed TC in 43.5% to 100% and oxidation ditch with UV-light irradiation removed 80% to 100% from aqueous medium, while sorption into sludge is the predominant mechanism (Zhong et al., 2022).

The most significant influence for TC removal is seasonal variations, where during the dry season, up to 20% more removal rate was observed than during the wet season. With the biological process alone, < 40 % of TC and even lower removal rate of its degradation products are described, and the relatively lower elimination rate, along with the possible surface water contamination, urges the need for an advanced tertiary treatment, and tetracycline removal in pharmaceutical wastewater treatment systems is mainly through sorption (Ahmad et al., 2021). The total TC concentration in the influent (1,616 µg/L) and effluent (195 ng/L) from the municipal sewage treatment plant (STP) was also reported by Shao and Wu (2020).

Table 2-1 Concentrations of tetracycline antibiotics detected in WWTP and sludge samples.

Samples		Tetracycline				
		OTC	DOC	CTC	TC	Total
WWTP	Raw influent	22.6 ± 13	741 ± 643.3	51 ± 33.6	314.6 ± 111	1129.2 ± 802
	Pretreatment effluent	16.8 ± 11.8	482.3 ± 433	ND	126 ± 44.5	625 ± 489.6
	Primary effluent	30.2 ± 7	444.2 ± 420	ND	164 ± 69.9	638.4 ± 497.6
	Aeration effluent	22.4 ± 10	457.2 ± 228	ND	153 ± 86.3	632.6 ± 324.6
	Secondary effluent	7.5 ± 1.8	418 ± 511.1	ND	nd	425.5 ± 512.9
	Final effluent	21 ± 5.7	631.6 ± 37.1	ND	nd	652.6 ± 42.8
Sludge	Primary sludge	17.3 ± 1.9	658.9 ± 455	24.8 ± 31.7	nd	701 ± 488.4
	Waste sludge	17.6 ± 7.6	313 ± 306.7	ND	749.6 ± 401	1080.6 ± 715.8
	Dewatered sludge	16.5 ± 9.6	567.6 ± 294	ND	565.9 ± 288.	1150.0 ± 592

Where, ND, Not Detected. OTC, Oxytetracycline. DOC, Doxycycline. CTC, Chlortetracycline. TC, Tetracycline. Antibiotic concentrations in municipal wastewater and sludge samples are given in ng/L and µg/kg dw, respectively (Scaria et al., 2021).

2.4.2 Global usage of TC

The global antibiotic consumption by humans witnessed an upsurge of 65% from 2000 to 2015 (from 21.1 to 34.8 billion daily doses). If the same trend follows, consumption is estimated to rise to 200% by 2030 (Klein et al., 2018). According to, Rodriguez-Mozaz et al. (2020) confirms that tetracycline antibiotics are ranked second in the production and usage of antibiotics worldwide.

National and regional surveillance systems from 71 countries over the past 10 years, antibiotic use is growing steadily worldwide (30%), driven mainly by rising demand in low and middle countries (WHO, 2020). A study by, Fazilati, Nozhat, and Borghei (2018), the annual production volume of drugs has been estimated in several hundred tons, whereas their yearly use has been globally estimated between 100,000 and 200,000 tons. Of these 30,000 to 180,000 tons per year of active antibiotics enter the environment.

After medication, more than 70 to 95 % of TC antibiotics are excreted and released inactive form into the environment via urine (20-55%) and faeces (>70%) from humans and animals. Because most antibiotics are poorly metabolized and absorbed by the treated animal body, large fractions are excreted through urine and faeces as unmodified parent compounds and consequently reach aquatic and soil environments (Qiao et al. 2020a, Amangelsin et al. 2023). TC are considered one of the cheapest classes of antibiotics available today, and it makes them good-looking for use in developing countries with limited health care budgets (Osorio et al., 2021).

2.4.3 Toxicity of TC

The wide use of tetracycline in veterinary and human medicine has led to it becoming a serious environmental contaminant, with serious toxic potential to aquatic environments as well as water bodies. TC finds its way into water bodies primarily by the excretion of unmetabolized antibiotics by humans and animals. A significant percentage, estimated to be 75%, of the tetracycline given is not fully absorbed into the body and is excreted in its active form (Amangelsin et al., 2023b).

TC contamination has numerous adverse effects on sea life, disrupting the ecosystem's balance. Algae and plankton, as producers, form the foundation of aquatic food webs. TC is lethal to algal populations, inhibiting growth in most species at concentrations between 0.25 and 30 mg/L (Amangelsin et al., 2023b). TC affects various primary and secondary producers in the water

ecosystem, and its ecotoxicological effects span multiple trophic levels in aquatic systems. TC is toxic to primary producers, including different species of algae, promoting growth-related cell necrosis. Later, in fish, exposure to tetracycline can cause oxidative stress, hinder embryonic development, alter gut microbiota, and lead to histological changes in gill and liver tissues (Guo et al., 2025).

Perhaps the most significant environmental impact is the spread of antibiotic resistance. The persistent presence of tetracycline in the environment creates selective pressure for the development, spread, and maintenance of tetracycline-resistant bacteria and associated resistance genes in sediment and water. This not only harms various aquatic organisms but also poses a serious risk to humans by potentially transmitting resistance to human pathogens (Long et al., 2020).

2.4.4 Properties of TC

TC's most important physicochemical properties, especially its amphoteric and strong chelating ability, form the basis of its clinical behavior. As an amphoteric compound, it can create salts with both acids and bases, a trait utilized in pharmaceutical products like TC hydrochloride to improve solubility and stability (Rusu & Buta, 2021). Even more crucial clinically, however, is its powerful tendency to undergo chelation, or bind with multivalent metal cations such as calcium, magnesium, iron, and aluminum (Tsigara et al., 2024). This chelation explains the common clinical advice not to take tetracycline with milk, antacids, or iron supplements, as the formation of these insoluble complexes significantly reduces the antibiotic's absorption from the GI tract and decreases its bioavailability (Pearson et al., 2025).

The therapeutic implications of these properties directly affect TC's efficacy and toxicity profile. It is the same chelation process that interferes with absorption, also responsible for the drug's deposition in calcium-containing tissues and its characteristic side effects, such as permanent tooth discoloration and disruption of bone growth in young and unborn individuals. (Manoharan et al., 2023). The same mechanism is also believed to cause the acute hypotension and collapse sometimes seen after rapid intravenous injection, as the drug chelates free calcium ions in the bloodstream.

Moreover, the stability of TC depends on pH, with greater stability in acidic solutions and degradation in alkaline ones, which can influence its effectiveness and formulation needs (Kostrzębska et al., 2024). More recently synthesized derivatives, such as doxycycline, are less calcium-affine, which improves absorption and reduces some side effects, and newer glycylcyclines like tigecycline have been chemically modified to bypass common resistance mechanisms (Katlam et al., 2017). The distinct properties of TCs are provided by the phenolic hydroxyl group (C-OH), dimethyl amino group ($N(CH_3)_2$), acylamino group ($-CONH_2$), and the keto-enol conjugated double bond system (Dai et al., 2020). The TC molecules contain both electron-deficient moieties (amino and enone groups) and electron-rich moieties (phenol ring), and thus possess three distinct acid dissociation constant (pKa) values (Yi et al., 2020).

Table 2-2 The physicochemical properties of major tetracyclines (Azanu et al., 2018).

Compound	Molecular formula	Mol.wt.	Log K_{ow}	pKa_1	pKa_2	pKa_3	Solubility(mg/L)
Tetracycline (TC)	$C_{22}H_{24}O_8N_2$	444.4	-1.18	3.3	7.68	9.69	231
Oxytetracycline (OTC)	$C_{22}H_{24}O_9N_2$	460.4	-0.9	3.27	7.32	9.11	310
Chlortetracycline (CTC)	$C_{22}H_{23}ClN_2O_8$	478.8	-3.6	3.3	7.4	9.3	630
Doxycycline (DC)	$C_{22}H_{24}N_2O_8$	444.4	-0.02	2.2	7.75	-	630

Molar absorption coefficient at $\lambda = 254$ nm.

2.4.5 The challenge of TC pollutants

One major issue with impurities in tetracycline is their significant persistence in the environment and their potential to increase antibiotic resistance (Ahmad et al., 2021). Incomplete metabolic breakdown in humans and animals, combined with widespread use in agriculture and aquaculture, leads to continuous release of these substances into freshwater and land ecosystems (Q. Li et al., 2024). Conventional sewage treatment plants are largely ineffective at removing them, so these substances accumulate in the environment (Matesun et al., 2024). The long-term exposure to these substances at sub-toxic levels creates significant selective pressure, encouraging the development and spread of antibiotic resistance genes (ARGs) within microbial populations.

These ARGs can transfer to human pathogens, posing an increasing threat to global public health by reducing the effectiveness of antibiotics (Shetty et al., 2023). In this study, we identify a significant shortfall in the development of practical, reproducible, and economically feasible remediation methods aimed at removing tetracycline from environmental media. Despite having sophisticated methods like photocatalysis, advanced oxidation processes, and bioremediation that exhibit promising removal efficacies within well-contained laboratory environments, scaling up such methods to bigger applications remains substantially challenged by a host of challenges associated with high expenses, operational complexities, and potential formation of harmful byproducts (Ren et al., 2023).

Additionally, a significant knowledge deficit remains regarding the environmental consequences of long-term exposure to tetracycline, particularly in relation to phenomena associated with the so-called cocktail effect, which involves interactions with other toxic contaminants, including heavy metals and microplastics. Additionally, the life cycle and transmission dynamics of antibiotic resistance genes originating from these pollution sources are poorly understood, thereby hindering our ability to predict and contain their spread.

2.5 Methods of advanced water treatment

Advanced water treatment is a method suite that removes contaminants not effectively eliminated by conventional treatment methods. These processes are important when it comes to purifying water, whether for drinking purposes, industrial use, or safe environmental discharge. This process "cuts across the widest range of pollutants: inorganic, organic, microbes, organic matter, and dissolved solids (Garrido-Cardenas et al., 2020). Main advanced water treatment technologies:

2.5.1 Advanced oxidation processes (AOPs)

AOPs are chemical treatments used to destroy large classes of organic contaminants through the use of highly reactive hydroxyl radicals (•OH). These strong oxidants oxidize many of those persistent pollutants, such as pesticides, pharmaceuticals, and industrial chemicals, down to much less harmful substances like carbon dioxide and water. A lot of common methods for AOP include combining ozone (O_3), hydrogen peroxide (H_2O_2), and/or ultraviolet (UV) light (Pandis et al., 2022).

AOPs can oxidize pollutants by generating free radicals. Common oxidizing agents do not easily degrade these pollutants. Various types of AOPs include wet air oxidation, supercritical water oxidation, Fenton reagent, photocatalytic oxidation, ultrasound oxidation, electrochemical oxidation, and ozonation (Solanki et al., 2020).

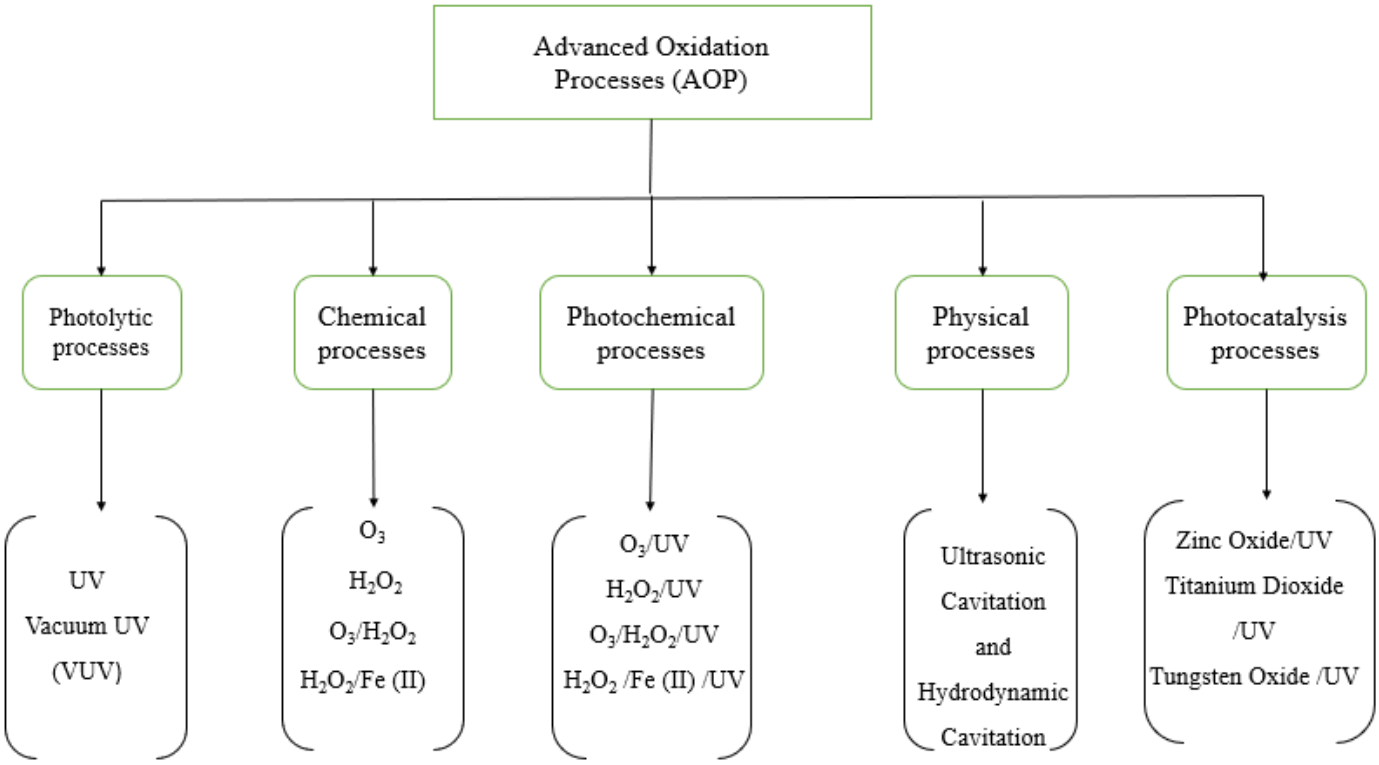

Figure 2-3 General Classification of Advanced Oxidation Processes Methods

2.5.1.1 Photolytic processes

Photolytic processes utilize electromagnetic radiation, typically in the ultraviolet (UV) regime, to initiate the degradation of recalcitrant pollutants (Anisuzzaman et al., 2022). The mechanisms can be by two important pathways: direct photolysis of the target contaminant molecule, where it absorbs a photon directly, moves to an excited state, and then is decomposed through the cleavage of bonds with a high dependence of this pathway on the molar absorption coefficient of the pollutant at the specific wavelength of the applied radiation; and the second, much stronger, pathway using high-energy Vacuum UV (VUV) radiation at around 185 nm (H. Zhang et al., 2024).

At this wavelength, it is the water molecules that directly absorb the photons and are subject to homolytic fission, forming hydroxyl radicals ($H_2O + h\nu \rightarrow {}^{\bullet}OH + H^{\bullet}$) that initiate the oxidation process without the addition of any chemical reagents. Although they are efficient, the main drawbacks of photolytic processes are their high energy consumption and the low quantum yield for many compounds, especially when standard UV light (254 nm) is employed, where direct photolysis is usually inefficient (Miklos et al., 2018).

2.5.1.2 Chemical processes

Chemical AOPs are the reactions of strong chemical oxidants, which lead to the generation of hydroxyl radicals. The most significant examples are ozonation (O_3), hydrogen peroxide (H_2O_2), ozonation and hydrogen peroxide (O_3/H_2O_2), and the Fenton Reaction (H_2O_2/Fe (II)). In ozonation, the ozone can either directly react with organic molecules (through selective electrophilic attack) or decompose in water, particularly at high pH, to form OH (Mahmoodi & Pishbin, 2025).

The combination of H_2O_2 with ozonation greatly speeds up this decomposition and thus enhances ·OH production. The Fenton reaction is the traditional process wherein hydrogen peroxide is reacted with a ferrous iron catalyst (Fe^{2+}) to produce hydroxyl radicals ($Fe^{2+} + H_2O_2 \rightarrow Fe^{3+} + {\bullet}OH + OH^-$). This system works extremely well, but has been confined for the most part to acidic pH ranges (pH 2.5-3.5) to avoid ferric hydroxide precipitation. Such reactions require no light source, though some caveats may limit their efficiency, such as pH, scavenger concentration, and the cost and handling of chemical reagents (Babu et al., 2019).

2.5.1.3 Photochemical processes

Photochemical processes are hybrid AOPs that work synergistically by combining UV irradiation and chemical oxidants such as H_2O_2, O_3, and Fenton reagents. The basic principle of the photochemical processes is that the absorbance of UV photons by the oxidant molecule causes its photolysis and generates hydroxyl radicals at a rate greatly enhanced compared to the other two processes: the mere chemical or photolytic processes (Manna & Sen, 2023). For example, in the H_2O_2/UV process, hydrogen peroxide is fragmented by UV light ($h\nu < 300$ nm) to produce two hydroxyl radicals ($H_2O_2 + h\nu \rightarrow 2{}^{\bullet}OH$). Similarly, the O_3/UV process enhances •OH formation from the decomposition of ozone.

The Photo-Fenton process (H_2O_2/Fe (II)/UV) is very interesting; it allows the generation of •OH from the regular Fenton reaction but also uses the UV light to photoreduce the resulting Fe^{3+} back to the catalytic Fe^{2+} form ($Fe^{3+} + H_2O + h\nu \rightarrow Fe^{2+} + \bullet OH + H^+$) and thus regenerates the catalyst, accelerating the reaction cycle and expanding the effective pH range. This synergy makes photochemical processes some of the most efficient AOPs for water treatment (Bhargava et al., 2023).

2.5.1.4 Physical processes

The physical AOPs employ physical processes to produce hydroxyl radicals. The main processes in this domain are based on acoustic and hydrodynamic cavitation. A cavitation process involves the initiation, growth, and implosion of microbubbles in a liquid. This implosion gives rise to transient, localized "hot spots" at very high temperatures (up to 5000 K) and pressures (up to 1000 atm) (Hübner et al., 2024). Under such extreme conditions, water and oxygen molecules either entrapped within or adjacent to the collapsing bubble undergo thermal dissociation (or pyrolysis) to produce highly reactive species such as •OH, H•, and O• radicals. Ultrasonic cavitation generates such bubbles using high-frequency sound waves (>20 kHz), while hydrodynamic cavitation creates bubbles based on liquid flow through a physical constriction (for example, a venturi or orifice plate) that leads to an abrupt pressure drop. These processes are advantageous in that they are totally chemical-free, but are energy-intensive, and their efficacy is dependent on fluid characteristics and reactor design.

2.5.1.5 Photocatalysis processes.

Heterogeneous photocatalysis stands for an advanced oxidation process under heterogeneous conditions when a solid semiconductor material acts as a catalyst. When the semiconductor (for example, Titanium Dioxide (TiO_2), Zinc Oxide (ZnO), Tungsten Oxide (WO_3)) is illuminated with light energy greater than or equal to the band gap energy, it causes the promotion of an electron (e^-) from the valence band (VB) into the conduction band (CB), leaving a positively charged "hole" (h^+) in the valence band. The redox reactions are mainly driven by these electron-hole pairs. These highly oxidizing valence band holes (h^+) can directly oxidize organic pollutants adsorbed on the catalyst surface or react with water molecules to generate hydroxyl radicals (Constantino et al., 2022).

At the same time, the conduction band electrons (e^-) typically scavenge dissolved oxygen to produce superoxide radical anions ($O_2^{\bullet-}$), which can further participate in the degradation pathway. Because of its higher efficiency, chemical stability, cost-effectiveness, and non-toxic nature, TiO_2 is the most widely studied photocatalyst. Process effectiveness is limited by catalyst recovery, light penetration in turbid solutions, and potentially catalyst deactivation (X. Li et al., 2020).

2.6 Emerging and hybrid technologies

Advanced solutions are often needed to remove persistent pharmaceutical contaminants from water, as typical treatment methods are often ineffective. Ongoing research is focused on emerging and hybrid technologies that combine biological, chemical, and physical processes to address this issue. These integrated systems overcome the limitations of single-process treatments, promising significantly better and more thorough degradation of complex drug compounds (Eniola et al., 2022)

AOPs, along with other technologies, generate highly reactive hydroxyl radicals ($^{\bullet}OH$) that can disrupt and ultimately mineralize relatively persistent organic constituents (Loganathan et al., 2023). Since AOPs can produce byproducts that may be hazardous, they are often combined with other systems. A typical approach is to couple an AOP stage with biological treatment or to use an adsorption step with granular activated carbon (GAC) to remove residual compounds or byproducts. One commercialized example is the combination of UV light with hydrogen peroxide, which generates hydroxyl radicals to "burn" organic pollutants in water (Hasan et al., 2024).

Nanotechnology-based hybrid systems utilize nanomaterials that possess unique properties due to their small dimensions, particularly their high surface area and reactivity, making them effective tools for water purification. Photocatalytic nanomaterials, such as titanium dioxide (TiO_2) and zinc oxide (ZnO), can degrade pharmaceuticals when stimulated by UV or visible light. To address the challenge of retrieving nanoparticle powder after treatment, researchers have begun fixing these particles onto stable supports, such as polymer nanofibers, creating easy-to-handle hybrid materials (Saroa et al., 2023).

Table 2-3 Comparative Analysis of Advanced Methods for Pharmaceutical Pollutant Removal

Method/Category	Material/System	Target Pollutant(s)	Removal Efficiency (%)	Key Conditions & Remarks	Reference
	Commercial Activated Carbon (AC)	Tetracycline (TC), Sulfamethoxazole (SMX)	80 – 95%	Very high surface area but expensive and energy-intensive for regeneration, which may not be complete. Nondestructive; pollutant transfers to another phase	(Y. Xu et al., 2021)
	Biochar (from various biomass)	Ibuprofen (IBP), TC	70 – 92%	Low-cost, renewable source. Tends to vary with pyrolysis temperature and feedstock. Can have an inferior surface area to commercial Acs	(Zhan et al., 2023)
Adsorption	Graphene Oxide (GO)	TC, Ciprofloxacin	>98%	Extremely high surface area and abundant functional groups. The high cost of synthesis is a major barrier to large-scale application.	(Saya et al., 2023)
	Metal-Organic Frameworks (MOFs)	Diclofenac (DCF), TC	90 – 99%	Tunable structure and ultra-high porosity. Stability in aqueous environments can be a concern. Synthesis can be complex and expensive.	(A. Sharma et al., 2024)

Table 2.3 Continued

Photocatalysis (AOP)	Titanium Dioxide (TiO_2)	TC, SMX, DCF	85 – 98%	Benchmark photocatalyst. Highly effective but requires UV light due to its wide bandgap (~3.2 eV). Nanoparticle recovery is a significant challenge.	(Pourkodee et al., 2025)
	Zinc Oxide (ZnO)	TC, Methylene Blue	90 – 99%	Similar bandgap to TiO_2 (~3.3 eV), also requires UV light. Lower cost and potentially higher quantum efficiency. Prone to photocorrosion in acidic/alkaline pH.	(Taie et al., 2021)
	Graphitic Carbon Nitride (g-C_3N_4)	TC, Rhodamine B	80 – 95%	Metal-free photocatalyst, visible-light active (bandgap ~2.7 eV). Lower quantum efficiency compared to metal oxides. Easy to synthesize.	(Ndiaye & Akill, 2025)
	Doped Photocatalysts (e.g., N-doped TiO_2)	IBP, Various Dyes	70 – 90% (under visible light)	Dopants can narrow the bandgap for the absorption of visible light, but they may also introduce recombination centers, thereby decreasing the net efficiency in some cases.	(Natarajan et al., 2021)

Table 2.3 Continued

Other AOPs	Fenton/Photo-Fenton Process	SMX, TC	>95%	Very high oxidation states. Operates within a narrow pH range, factoring in the acidic pH range of between 2-4. It will produce an iron sludge element that would need secondary treatment.	(de Oliveira Cardoso Nascimento et al., 2024)
	Ozonation (O_3)	DCF, Carbamazepine	80 – 99%	Complete effectiveness and rapidity. High operational expenses. The formation of toxic brominated byproducts (such as bromate) from waters rich in bromide is a possibility.	(Topkaya et al., 2021)
Synergistic/Hybrid Methods	AC-TiO_2 Composite	Phenol, DCF, TC	>95%	Adsorption-Photocatalysis Synergy: Activated carbon (AC) adsorbs and concentrates impurities in proximity to the TiO_2 surface to enhance photocatalytic degradation. Prevents agglomeration of catalysts.	(Yue et al., 2024)
	Biochar-ZnO Composite	TC, Methylene Blue	92 – 98%	Combination of low-cost adsorption (biochar) with photocatalysis (ZnO). Biochar works as an electron sink and thus reduces charge recombination in ZnO, and so increases efficiency.	(Eswaran et al., 2025)

	MOF-based Photocatalyst	TC, Cr (VI)	>99%	MOFs serve as adsorbents as well as hosts for photocatalytic species, thus facilitating extraordinary performance. However, cost and stability remain paramount issues.	(L. Wang et al., 2023)
	Proposed System: ZnO-NPs/Cassava Peel-AC	Tetracycline (TC)	Target: 99.83%	It was hypothesized that synergism existed between the green-synthesized AC from cassava peel, providing a sustainable and low-cost adsorbent, and ZnO-NPs offering destructive photocatalytic means. The composite was excellent, showing enhanced TC removals through adsorptive enrichment, followed by photocatalytic degradation.	This Study

2.6.1 Adsorption and photocatalysis

2.6.1.1 The adsorption using the AC derived from low-cost agricultural wastes

Adsorption is a surface phenomenon in which pollutant molecules (adsorbate) get adsorbed on the surface of a solid material (adsorbent). This means that it is considered the most efficient and versatile method for purifying water (Gayathiri et al., 2022). AC happens to be the most common adsorbent because of its exceptionally high surface area, well-developed pore structure, and surface chemistry. The greatest disadvantage of the fact that commercial AC is derived from non-renewable resources like coal is the limited applicability of its use, especially in developing countries (Shah et al., 2023).

Intensive research efforts towards producing AC from abundant, low-cost, and renewable agricultural byproducts have increased. Materials such as coconut husks, rice straw, corn cobs, and palm shells had earlier been converted into effective activated carbons (G et al., 2021). For instance, cassava (Manihot esculenta) peel is a very attractive precursor. With cassava being a major global food crop, processing it results in millions of tons of peel waste generated every year, consequently resulting in a disposal challenge (Sagadevan et al., 2024).

The process of conversion is generally in two stages: Carbonization to produce a char rich in carbon, followed by Activation for the development of the porous structure. Activation may be physical (using steam or CO_2) or chemical (using agents like H_3PO_4, KOH, or $ZnCl_2$) (Amer & Elwardany, 2020). This is because activation has often been preferred over chemical rather than physical, since activation occurs at lower temperatures, and it generally leads to a higher surface area. Several investigations have shown a very high potential that Cassava Peel Activated Carbon (CPAC) can remove dyes, heavy metals, and phenols from water with surface areas mostly over 1000 m^2/g, comparable to commercial grades (Kayiwa et al., 2021).

2.6.1.2 Heterogeneous photocatalysis with ZnO-NPs

The active components of heterogeneous photocatalysis are semiconducting materials used to generate highly reactive oxygen species (ROS) under illumination. When, for example, ZnO-NPs are irradiated with photons having energy values greater than or equal to that of the bandgap (Eg ≈ 3.37 eV) of the semiconductor, an electron (e^-) from the valence band is excited to the conduction band, leaving behind a positive hole (h^+) (Ramos et al., 2025). The charge carriers then move to the surface and initiate redox reactions:

$$h^+ + H_2O \rightarrow \bullet OH + H^+$$

$$e^- + O_2 \rightarrow \bullet O_2^-$$

The hydroxyl radical (•OH) and superoxide radical ($\bullet O_2^-$) generated therein are powerful, unspecific oxidizing agents leading to mineralization of complex organic pollutants such as tetracycline to much simpler and less harmful CO_2, H_2O, and mineral acids (J. Wang & Wang, 2020).

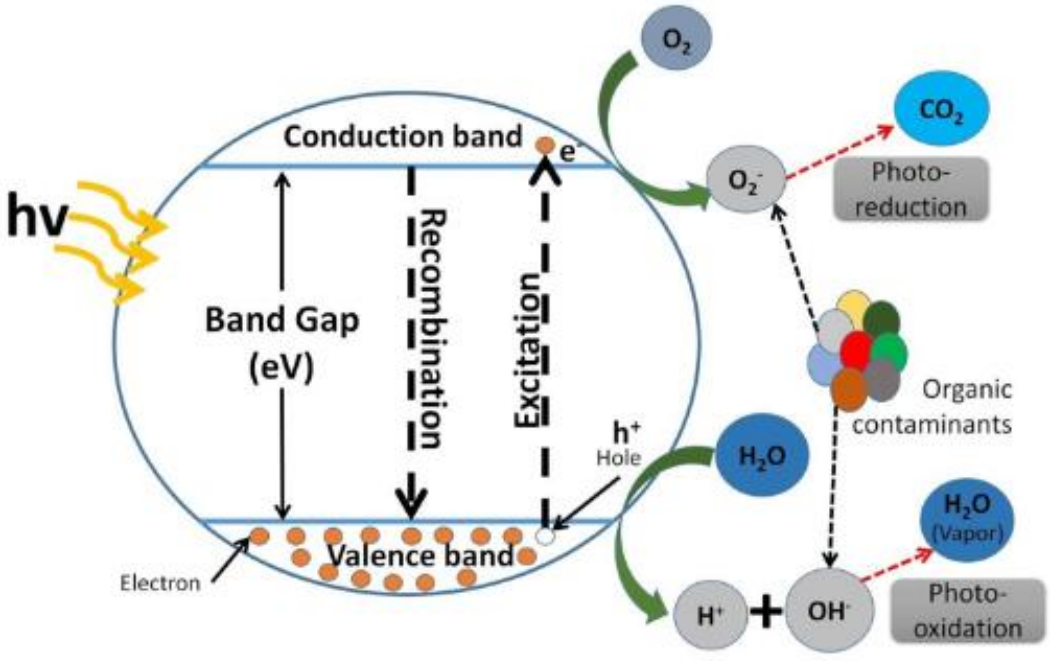

Figure 2-4 Reaction mechanisms of photocatalysis (Morshedy et al., 2024)

Due to its wide band gap, higher quantum efficiencies, lower cost, and proven biocompatibility, ZnO-NPs have emerged as a promising and effective alternative to the extensively researched titanium dioxide (TiO_2) (D. K. Sharma et al., 2022). However, it is the major dispersed phase of ZnO nanoparticles; it generally suffers from the following two disadvantages:

1. Rapid Recombination: The electron-hole pairs can either recombine rapidly, shedding energy in the form of heat, which decreases the total quantum yield of the whole process, or diffuse to the surface for subsequent redox reactions (Morshedy et al., 2024).

2. Photocorrosion: ZnO-NPs are very susceptible to photocorrosion ($ZnO + 2h^+ \rightarrow Zn^{2+} + ½O_2$), which brings a decline in catalytic activity and the release of zinc ions in water under acidic or very alkaline solutions, concerning photocorrosion (Dimitropoulos et al., 2024). These reasons made it necessary the modify ZnO-NPs, which is often achieved by preparing composites expected to enhance charge separation and create better stability.

2.7 The green synthesis of composite materials

Most traditional physical and chemical approaches to synthesizing nanoparticles often require toxic solvents and hazardous reducing/capping agents with high energy input. Green synthesis is now in the limelight as a sustainable, economical, and environmentally friendly method (Gupta et al., 2023). This actually involves the intervention of biological agents, preferably using plant extracts (from leaves, roots, peels, or flowers), which are naturally rich in phytochemicals like polyphenols, flavonoids, and terpenoids, and can act directly in reducing and converting the precursor salt to ZnO-NPs (for example, zinc acetate) (Vinukonda et al., 2025).

Pharmaceutical remediation research is increasingly shifting toward biogenic, green synthesis procedures that utilize biomolecules derived from plants as natural stabilizing and capping agents. These biomolecules help regulate crystal formation and prevent nanoparticle aggregation. Even though these synergistic systems have significant theoretical potential for eliminating resistant medications like TC, a crucial methodological gap remains: most research relies on standard chemical activation of commercial precursors or trial-and-error optimization, overlooking the complex, non-linear interactions between regional biomass properties and metal-oxide loading (Dang et al., 2025).

Additionally, there is a noticeable lack of literature that includes machine learning to shift from descriptive observations to predictive modeling of the dual adsorption-photocatalysis mechanism (Ge et al., 2025).

This study addresses these deficiencies by developing a ZnO-NPs/CPAC composite derived from Ethiopian cassava peels; by bridging the gap between sustainable waste-to-resource pathways and ML-driven multivariate optimization, this research provides a technically robust and economically feasible solution for the complete mineralization of persistent organic pollutants (Rani et al., 2025).

3. GREEN SYNTHESIS AND CHARACTERIZATION OF *CITRUS BERGAMIA* LEAVES EXTRACTED MODIFIED ZINC OXIDE NANOPARTICLES IMPREGNATED ON CASSAVA PEEL-BASED ACTIVATED CARBON

3.1 Introduction

Nanoscience involves the creation of small, unique materials with new properties. These materials offer numerous benefits and increased effectiveness in various technological applications due to their tunable chemical, physical, and mechanical properties, making them ideal for various environmental applications and technological advancements (Maity & Sahoo, 2023). Nanoparticles are widely used due to their properties, including a large surface-to-volume ratio, high dispersion, high penetration, high conductivity, and adsorption characteristics (Ali et al., 2018).

ZnO-NPs are gaining attention due to their exceptional physicochemical properties, including high catalytic and photochemical activities, which have recently attracted significant interest (Sachin et al., 2024), due to their low cost, thermal and chemical stability, non-toxicity, and environmentally-friendly nature (Taha et al., 2020). Recently, sturdies are increasingly using green synthesis methods for synthesizing ZnO-NPs, which are eco-friendly, less toxic, and one-step, compared to conventional methods like alcohol-based reactions, vapor transport, hydrothermal synthesis, and precipitation methods (Santhoshkumar et al., 2017).

Various plant extracts have been proposed for producing ZnO-NPs using a green method, primarily for adsorption, photocatalytic degradation, disinfection, and pollutant removal applications (Santhoshkumar et al., 2017). The NPs are synthesized using naturally extracted plant material, which contains phytochemicals that serve as reducing, stabilizing, and/or capping agents in the synthesis process (Ondijo et al., 2022). On the other hand, several drawbacks must be considered, including particle aggregation, reduction in surface area, and a subsequent decrease in catalytic activity. Additionally, the challenges of nanoparticle separation and the higher cost of recovery are significant drawbacks in practical applications, particularly when using slurry-type reactors (Gowland et al., 2024).

Many studies have focused on process parameters that influence the characteristics of stable ZnO-NPs to overcome these difficulties, and this regard, most researchers have primarily focused on using AC as a support for NPs sorbents. AC is chosen for its abundance, economical value, high surface area, reusability, and unique chemical properties (Kwiatkowski et al., 2019).

In contrast to prior research, this study aims to statistically optimize and investigate the interaction effects of selected parameters (such as temperature, time, and impregnation ratio) on the specific surface area and pore structure of activated carbon prepared from cassava peels. To achieve this, the study applies the RSM-BBD experimental design techniques (Reji & Kumar, 2023). Previous studies have typically used the "one-parameter-at-a-time approach" to investigate the effects of these parameters on AC preparation. However, this approach has limitations in estimating the interaction effects between factors and lacks predictive capabilities (Sitravellu et al., 2023).

By employing statistical experimental design techniques, this study aims to reduce the number of experiments while maximizing the information gathered from the process. The performance of the prepared ZnO-NPs and AC was confirmed using FT-IR, XRD, BET, UV-visible spectroscopy, and SEM analytical techniques. The photocatalytic activity of the catalyst at the optimum condition was also explored using TC as a model pollutant.

3.2 Materials and methods

3.2.1 Materials

After gathering the cassava peel from the Wolaita zone in Ethiopia, NaOH (99.0%) pellets, 35.4% pure HCl, $ZnCl_2$ with a molarity of 136.28 g/mol, and powdered tetracycline hydrochloride ($C_{22}H_{24}O_8N_2$.HCl) were purchased. Citrus bergamia leaves were obtained from the Gullelle Garden in Addis Ababa, Ethiopia. Zinc acetate $(CH_3COO)2Zn\cdot 2H_2O$, with an assay of 98.0%, and absolute ethanol (CH_3CH_2OH, >99%) were used.

3.2.2 Cassava peels proximate analysis

The cassava peels used in this study underwent proximate analysis, following the American Society for Testing and Materials (ASTM) methods. The moisture content was determined using ASTM standard E871-80. The samples were dried (100g) at 105 °C in an oven, and the result was expressed as a percentage of the oven-dry mass. The ash content was determined using ASTM Standard E1755-02, with analysis performed in a muffle furnace. The fixed carbon was obtained using ASTM standard D3174-76.

3.2.3 Activated carbon preparations

Before use, the cassava peels were thoroughly cleaned multiple times with tap water to remove dirt and other inorganic impurities. The samples were then dried for 24 h. at 120 °C to eliminate moisture and ground to a desired particle size of 63–150 μm. To determine the optimal conditions for producing activated carbon with a high surface area from cassava peels, chemical activation with $ZnCl_2$. We used for the experiment, a 10 g/L $ZnCl_2$ solution in a 150 mL volumetric flask was prepared and used varying volumes, as listed in Table 3.1, to obtain $ZnCl_2$ solutions. Each experiment was conducted according to the suggested parameters study by Kwiatkowski et al. (2017).

Table 3-1 Experimental variables with their levels for the BBD-RSM study.

Abbreviation	Levels				
	Variables	Unit	-1 (low)	0 (Medium)	+ (High)
A	Time	hrs.	1	1.5	2
B	Temperature	^{0}C	450	550	650
C	Impregnation ratio ($ZnCl_2$ to CP)	Mass ration	0.75:1	1.625:1	2.5:1

The cassava peel samples were carbonized in a muffle furnace for 60 to 120 min at temperatures ranging from 450 to 650 °C, with an impregnation ratio ($ZnCl_2$ to CP) of 0.75:1 to 2.5:1, before cooling under a nitrogen flow. These conditions significantly influenced the yield of activated carbon (Georgin et al., 2022). Subsequently, a HCl solution was used to wash the activated carbon. The samples were rinsed multiple times with hot distilled water to ensure the complete removal of chloride ions. Finally, the specimens were, and dried at 110 °C for 24 h, and then stored in a desiccator.

3.3 Statistical experimental design with RSM-BBD

The RSM, in conjunction with BBD, was utilized to optimize the synthesis of the ZnO-NPs/CPAC composite. This approach is advantageous because it requires significantly fewer experimental runs than complete factorial designs and is more effective at examining the non-linear relationships between independent variables (Azeez & Jimoh et al., 2022).

In contrast to conventional one-factor-at-a-time methods, RSM-BBD allows for the simultaneous assessment of key synthesis parameter temperature, time, and impregnation ratio, while also identifying intricate interaction effects that significantly impact final porosity and photocatalytic performance (Pais-Chanfrau et al., 2021). To determine the optimal conditions for maximizing TC removal, this multivariate statistical technique was used to accurately model the effects of individual and combined parameters on specific surface area and degradation efficiency. The elements and their study range are listed in Table 3.2.

The variables, namely activation time, activation temperature, and impregnation ratio, were assigned to the letters A, B, and C, respectively. According to BBD, the total number of experiments can be calculated using Eqn. (3.1).

$$N = K^2 + K + C_P \quad \text{.....(3.1)}$$

where K is the number of factors, and Cp is a central replication point. The 17 trial runs that are organized in accordance with RSM-BBD are displayed in Table 3.2

Table 3-2 Experimental runs with actual and predicted responses according to RSM-BBD.

Run	A[a]	B[b]	C[c]	Response			
				S (BET) (m^2/g)		Pore Volume (cm^3/g)	
				Actual	Predicted	Actual	Predicted
1	1.5	550	1.625	1142	1188	0.167	0.185
2	1.5	650	2.5	1373	1312	0.315	0.296
3	1.5	550	1.625	1140	1188	0.196	0.185
4	1.5	450	0.75	936	997	0.112	0.171
5	1.5	450	2.5	963	995	0.114	0.132
6	1	450	1.625	930	923	0.109	0.0914
7	1.5	650	0.75	933	901	0.118	0.140
8	2	650	1.625	1251	1258	0.197	0.197
9	2	550	2.5	1230	1284	0.184	0.219
10	1	550	2.5	1219	1193	0.194	0.209
11	2	450	1.625	1269	1183	0.248	0.211
12	1	550	0.75	909	855	0.148	0.122
13	1	650	1.625	983	1069	0.221	0.240
14	1.5	550	1.625	1220	1188	0.221	0.185
15	1.5	550	1.625	1222	1188	0.239	0.185
16	15.	550	1.625	1218	1188	0.163	0.185
17	2	550	0.75	1188	1213	0.196	0.189

[a] activation time (h), [b] activation temperature (^oC), [C] impregnations $ZnCl_2$ to CP (mass ratio)

To determine the relationship between the independent variables and the response, a second-order polynomial equation shown in equation (3.2) was utilized.

$$Y=\beta_0+\beta_1A+\beta_2B+\beta_3C+\beta_{12}AB+\beta_{13}AC+\beta_{23}BC+\beta_{11}A^2+\beta_{22}B^2+\beta_{33}C^2þ+\varepsilon \ldots\ldots\ldots\ldots\ldots\ldots\ldots\ldots (3.2)$$

where A, B, and C are the independent variables; β_is, β_{ii}s, β_{ij}s, and ε are the coefficients for the linear, cross-product, and quadratic interaction effects, respectively; β_0 is a constant; and ε serves as the random error. Statistical software known as Design-Expert® version 13.0.0 (Stat Ease, Inc.) was utilized to perform regression analysis and estimate coefficients. The suitability of the model equations was evaluated using analysis of variance (ANOVA). To assess the quality of fit and statistical significance of the model equations, the following metrics were employed: coefficient of determination (R^2), correlation coefficient (CV), adjusted coefficient of determination (adj-R^2), prediction coefficient of determination (Pred. R^2), and F-test.

3.4 Green synthesis of ZnO-NPs

3.4.1 Preparation of the extract

Based on Abomuti et al. (2021), the leaves of *C. bergamia* were collected, crushed, and cleaned with distilled water before being dried for 12 h at 40°C in an oven. For the aqueous extract, 100 g of the dried leaves were ground into particles sized between 63 and 150 µm. The ground leaves were then transferred to a 500 mL beaker containing 250 mL of distilled water. The beaker was heated to 60 °C using a heater equipped with a magnetic stirrer, which caused the solution's color to change as the leaf extract developed. The mixture was subsequently stored overnight in an airtight bottle and filtered through Whatman No. 1 filter paper and the samples were kept in refrigerator until analysis.

3.4.2 Mediated synthesis of ZnO-NPs

ZnO-NPs were synthesized using the sol-gel method following (Abomuti et al., 2021). The precursor materials used were $CH_3COO\ Zn.2H_2O$, of the highest purity, and *C. bergamia* leaves obtained in section 2.2. Additionally, NaOH was used (Rafique et al., 2021). Accordingly to (Ramesh et al., 2022), the synthesis of ZnO-NPs commenced with 50 mL of aqueous zinc acetate solution placed in a 250 mL beaker, continuous stirred at 50 °C for 2 h.

The *C. bergamia* leaf aqueous extract (50 mL) was added to the zinc nitrate solution as it was continuously stirred and maintained at the same temperature. The experimental mixture turned light yellow as the phytochemicals present in the extract capped the Zn^{2+} ions and triggered the nucleation of ZnO-NPs (Rupa et al., 2019). In step two, a NaOH solution was added dropwise to the reaction mixture (pH 10-12) at 50 °C under continuous stirring.

The reaction mixture was stirred for the next two hours at 50 °C, which yielded light yellowish precipitation that indicated the synthesis of ZnO-NPs. The reaction mixture was centrifuged for 1 h at 4000 rpm to get the final product (Faisal et al., 2021) . To remove any other contaminants or unreacted components from the surface of the biosynthesized material, the precipitate was repeatedly cleaned with ethanol and distilled water. To ensure total dryness, the synthesized material was placed in an oven set to 80 °C for 24 h in the final step. The dehydrated ZnO-NPs were annealed for 2 h at 450 °C in a muffle furnace. The resulting fine, light-cream-colored ZnO-NPs powder was kept in desiccators used for surface characterization and further study.

3.4.3 Synthesis of ZnO-NPs impregnation on AC

A 0.5 g of ZnO-NPs that had been modified with *C. bergamia* leaves extract was combined with 200 mL of distilled water and subjected to sonication for 30 min to ensure homogenous mixing. Next, 5 g of cassava peel-based activated carbon (as obtained using optimum parameters) was added to the solution, and the mixture was placed on a magnetic stirrer set at 500 rpm for 10 h to complete the impregnation process. Finally, the sample was washed with distilled water and dried in an oven at 95 °C for 10 h, resulting in the production of ZnO impregnated activated carbon and designated as ZnO-NPs/AC.

3.4.4 Characterization

X-ray diffraction (XRD-7000 X-ray Diffractometer) was employed to measure the crystal phase compositions using Cu-Kα radiation (λ = 1.5406 Å), with an accelerating voltage of 40.0 kV and a current of 30.0 mA. The scan rate was set at 3.00 °/min over the 2θ range of 5° to 75°. The Scherrer equation was applied to determine the mean crystallite sizes of the anatase and rutile phases.

The specific surface area, pore volume, and pore size were determined from N_2 adsorption-desorption isotherms using a Quantachrome Instruments Nova 4000E BET machine (NLDFT equilibrium methods). Functional group analysis was performed with a Fourier Transform Infrared (FT-IR) spectrometer (Nicolet iS50, ABX) over a wavenumber range of 4000 to 400 cm^{-1}. The morphology of activated carbon derived from cassava peels was examined using scanning electron microscopy (SEM) (JCM-6000 Plus model, with dimensions of 325 mm (W) × 490 mm (D) × 430 mm (H)). Ultraviolet-visible spectra of the samples were obtained using a UV-VIS-NIR spectrophotometer (JASCO V-770) in the range of 200–800 nm.

3.4.5 Photocatalytic performance test under optimized conditions

The photocatalytic activity was investigated using an aqueous solution of TC in a 250 mL borosilicate glass reactor. The photocatalytic performance was investigated under UV-Vi's light irradiation from Philips UV-C lamps, which had a light intensity of 14.41 W cm^{-2} at the sample. To ensure adsorption equilibrium, the reaction solution was agitated for 30 min in the absence of light.

The concentration of TC before and after the experiment was determined using a UV spectrophotometer at a wavelength of 365 nm (Humancorp X-MA 1200 spectrophotometer). The photocatalytic activity was evaluated through a series of photocatalytic tests by adjusting the catalyst dose concentration (0.5 g/L), maintaining a pH of 6, varying the irradiation time (0 to 120 min), and altering the initial TC concentration from 2.5 to 15 mg/L. The repeated usability of the catalyst was tested to evaluate its stability after separation and drying in the oven following each experimental cycle. After each experiment, the catalyst was filtered and dried in the oven at 105 °C for 1 h before being applied to the next test cycle.

3.5 Results and discussions

3.5.1 Analysis of cassava peels

The various types of cassava peel have a moisture percentage on a dry basis ranging from 9.93% to 11.46%, which is consistent with a previous report (Otache et al., 2017). This variation in moisture content may be attributed to different drying conditions, including higher temperatures and longer drying durations. Additionally, differences in average particle size could have also played a role (Owamah, 2014). Table 3.3 shows the proximate analysis results of cassava peel.

Table 3-3 Proximate analysis of cassava peels

Properties	Experimental value (Wt.%)
Moisture	14.2
Volatile matter	74.2
Fixed carbon	65
Bulk density (kg/m^3)	58.86
Water binding capacity (%)	148.0

According to, De Gisi et al., (2016), conducted an experiment to create activated carbons from cassava peels as a precursor with chemical activation utilizing $ZnCl_2$ as an activating agent. Based on Yang et al., (2025), investigated the effects of different preparation factors on the pore structure and surface area of ZnO and AC-NPs Generally, pre-treating the cassava peel, as shown in Table 3.3, increased the volatile matter and fixed carbon contents. This increase is due to the reduction in ash content. Making, these peel variants more suitable for synthesizing high-surface-area activated carbon (Menya et al., 2018).

3.5.2 Characterization of activated carbon samples prepared under optimum conditions

3.5.2.1 FT-IR analysis

The FT-IR spectra of the CP/$ZnCl_2$ activated carbon sample are presented in Figure 3.1. Analyzing the chemical composition of an adsorbent is essential for understanding its adsorption mechanism. The likely active surface groups include O-H, alkynes, aromatic rings, and carbonyl groups (Kayiwa 2022).

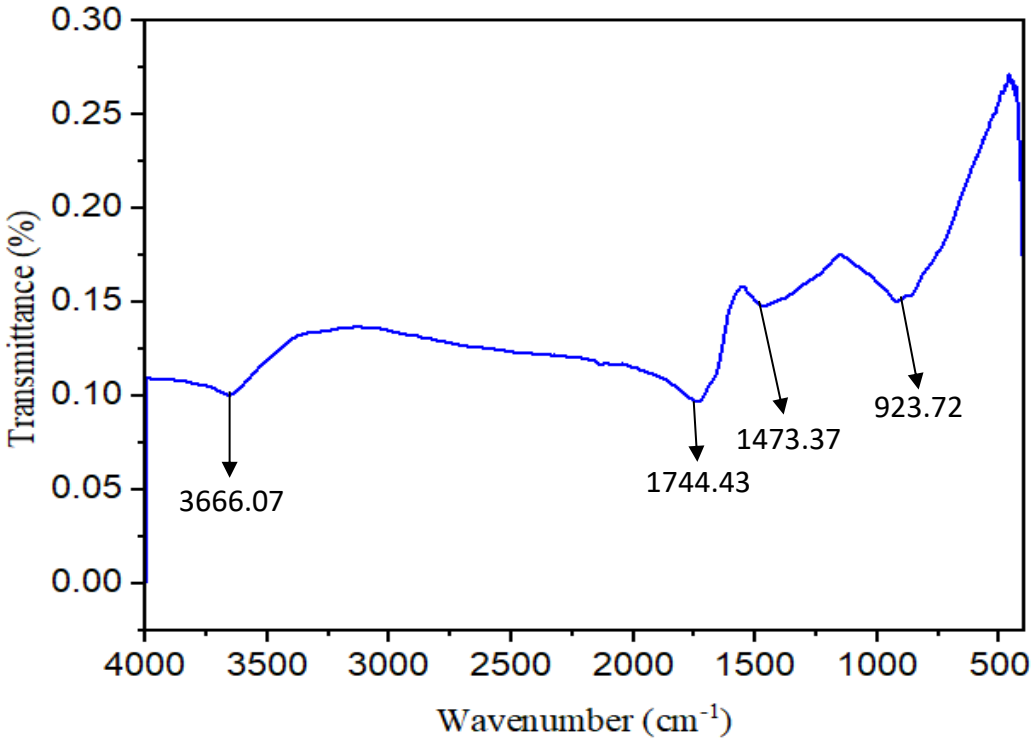

Figure 3-1 FT-IR spectrum for activated carbon from cassava peel at optimized parameters

The FT-IR spectra of the produced activated carbon also displayed a broad band around 3400 cm^{-1}, indicating the presence of hydroxyl groups, which aligns with the results of Kayiwa et al. (2021) who also used $ZnCl_2$ activation for cassava peel. However, the intensity of the C=O stretching around 1700 cm^{-1} was lower in our study compared (Belcaid et al., 2022). The peak at 1744.43 cm^{-1} shows the stretching vibration of the C=C aromatic nucleus (Astuti et al., 2020). Finally, it was determined that the band at 1473.37 cm^{-1} was the aromatic C–H of lignin (Belcaid et al., 2021). All of these factors have a significant impact on the binding of metal ions.

The growth of these bands suggests that surface oxygen functional groups were formed on the activated carbon as a result of surface modification (Kristianto et al., 2016).

3.5.2.2 UV-Vis's analysis

Figure 3.2 presents the UV–Vi's spectra of the CP/$ZnCl_2$ AC, assessed using a UV/Vis/NIR spectrophotometer. A noticeable peak in the spectra at approximately 300 nm indicates high absorption, suggesting successful surface modification, potentially associated with conjugated systems or functional groups created during the activation process (Okiy & Nwabanne et al., 2024).

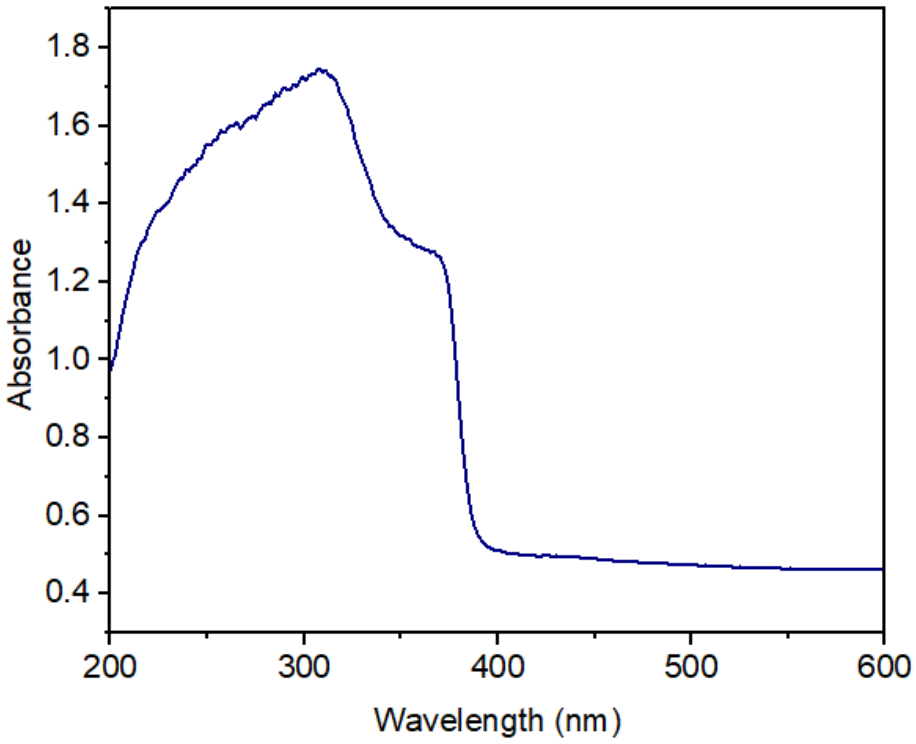

Figure 3-2 UV–Vi's spectra spectrum for activated carbon from cassava peel at optimized parameters

The presence of electronic transitions or functional groups in activated carbon is indicated by the increased absorption in the UV region. The data revealed that, based on UV-visible spectroscopy characterization, the CP/$ZnCl_2$ activated carbon absorbed more light in the UV region than in the visible region.

3.5.2.3 SEM analysis

Figure 3.3 displays the surface morphology of the CP/$ZnCl_2$ activated carbon, as observed through scanning electron microscopy (SEM) at various magnifications. The SEM images clearly illustrate that the pore structure of the material consists of mesopores characteristic of activated carbon (Amakoromo et al., 2022).

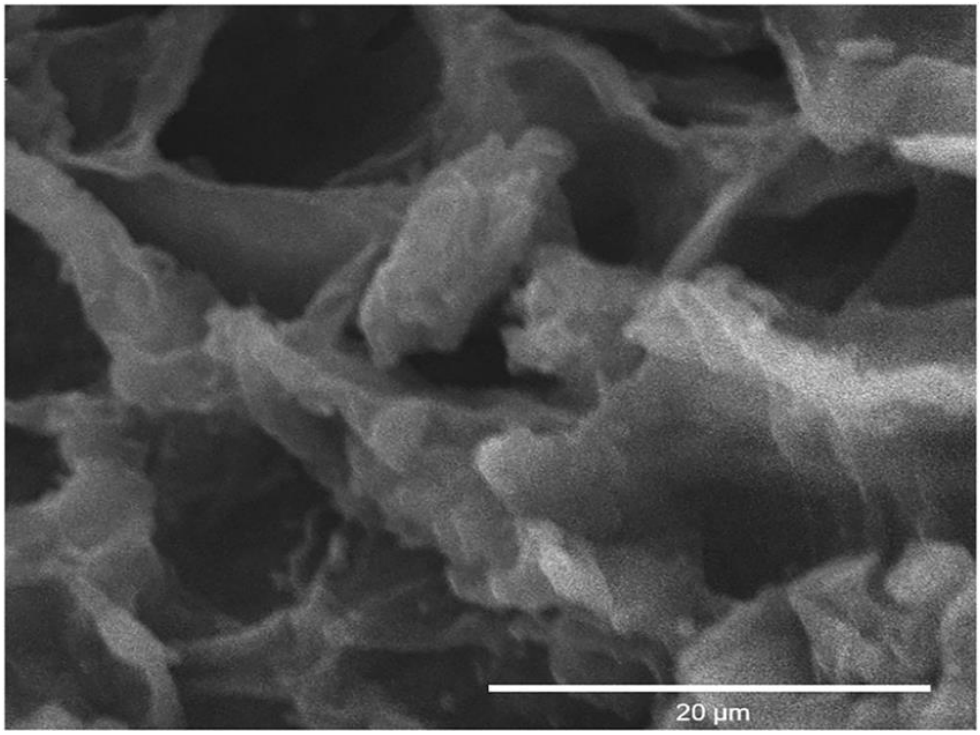

Figure 3-3 SEM micrographs of the prepared activated carbon under optimum conditions

As shown in Figure 3.3, the structure of the CP/$ZnCl_2$ activated carbon consists of amorphous graphite sheets with π–π interlinkages, which function as π-acceptors. According to the theory, the active surface groups in the CP/$ZnCl_2$ activated carbon influence adsorption through hydrogen bonds, potentially including dipole-dipole interactions (Kayiwa 2022). This donor-acceptor electron interaction leads to the adsorption of contaminants, such as TC, from wastewater. The scale bar in Figure 3.3 indicates a size of 20 µm, demonstrating that the particles are micro-sized. Smaller particle sizes typically enhance adsorption efficiency due to their higher surface area-to-volume ratio.

3.5.2.4 XRD analysis

Figure 3.4 presents the XRD analysis conducted to verify the phase composition of the material. The CP/$ZnCl_2$ activated carbon sample used for the XRD investigations was applied to a glass plate, with scanning beginning at 10° and concluding at 80°. The graph reveals multiple peaks at specific 2θ values, indicating that the activated carbon contains crystalline phases. Typically, activated carbons also contain amorphous carbon, as evidenced by a prominent peak around 22°.

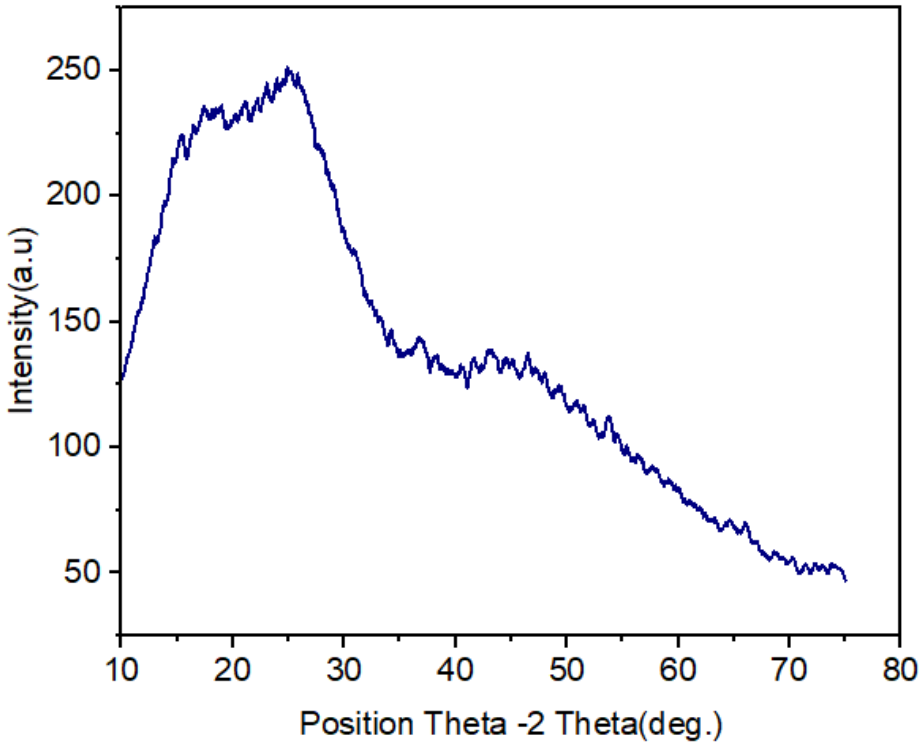

Figure 3-4 Graph showing XRD analysis of cassava peel/$ZnCl_2$ activated carbon at optimized parameters.

The XRD patterns of the CP/$ZnCl_2$ activated carbon samples that were produced were similar, displaying broad diffraction peaks in an amorphous signature at two different 2θ angles: 18–25 and 36–43, which correspond to the (002) and (100) crystallographic planes of the carbon material (Amakoromo et al., 2022). In this study, the amorphous lattice planes of the CP/$ZnCl_2$ activated carbon diffract X-rays at scattered angles that correspond to the obtained diffraction angles. The (002) plane of graphitic carbon is frequently cited as the source of the observed peaks.

While it indicates a significant amorphous characteristic, it also reveals the presence of organized carbon structures. A sharp peak suggests greater crystallinity, while a broad peak indicates a more amorphous structure. The broad peaks observed in Figure 3.4 indicate decreased crystallinity, which is typical of activated carbon (Ekekwe et al., 2018).

3.5.3 Optimization of activated carbon synthesized parameters

A total of 17 experimental runs were carried out using RSM-BBD and the relationships in Table 3.2. This includes the central point that assesses natural variability and process stability. The experimental response was based on the results of characterizations such as BET specific surface area (S_{BET} (m^2/g)) and pore volume (m^3/g). These results indicate that the selected quadratic model is significant.

The BET surface area and pore volume of the prepared activated carbon are significantly influenced by the factors or variables considered in the model. The two responses, S_{BET} and pore volume, were used to further examine the adequacy of the model using the regression coefficient (R^2). The results were 0.89 for S_{BET} and 0.74 for pore volume. The P-value can be used to determine how the test variables interact with one another (K. Vimalashanmugam, 2012).

Furthermore, there was a respectable agreement between the Pred R^2 values and the adj-R^2 of S_{BET} (74.8%) and pore volume (68.2%). The low CV values (6.63 for S_{BET} and 20.3 for pore volume) further help explain the degree of precision and dependability. Moreover, it was discovered that the appropriate precision for the S_{BET} and pore volume responses was 7.99 and 11.3, respectively. Model terms are significant when "Prob > F" values are less than 0.05. By considering all terms, the quadratic model equations for the two responses S_{BET} and pore volume, in terms of actual values, can be described as described by equations (3.3) and (3.4).

$$S_{BET}\left(\frac{m^2}{g}\right) = -1917.08 + 636.6A + 48.2B - 72.7C - 0.35AB - 152.7AC + 1.18BC + 9.6A^2 - 0.008B^2 - 71.07C^2 \quad \text{..... (3.3)}$$

$$\text{Pore volume} = -0.37 + 0.54A + 6.5 * 10^{-4}\,B - 0.22C - 8 * 10^{-4}AB + 5.6 * 10^{-4}AC + 2 * 10^{-3}BC + 0.03A^2 + 2.17 * 10^{-6}B^2 + 0.0134C^2 \quad \text{..... (3.4)}$$

The highest surface area for chemically AC was achieved at 533°C, with an impregnation ratio of 1.6:1, and a carbonization time of 1.82 h. This result of 1250 m^2/g was significantly higher than the previously reported surface areas for chemically activated cassava peel AC found in the literature. These previous reports documented surface areas ranging from 834 to 1567 m^2/g, and 1180 to 1684 m^2/g for chemically AC with impregnation ratios ranging from 2.5:1 to 4:1, respectively (Kayiwa et al., 2022).

Total pore volume (Vt) ranged from 0.109 to 0.315 cm^3/g and increased with temperature in the range of 450 to 650ºC, using an impregnation ratio ($CP/ZnCl_2$) of 0.75:1 to 2.5:1. In this study, the activated carbon material had a substantial pore volume, with a reported value of 0.195 cm^3/g at a temperature of 533ºC, impregnation ratio of 1.6:1, and activation time of 1.82 hours. However, the pore volume was significantly lower than the previously reported value of 0.281 cm^3/g (Kayiwa et al., 2021). Lower pore volumes were also observed in other experiments involving the measurement of pore volume from cassava peels carbonized at temperatures ranging from 450 to 650°C (Amakoromo et al., 2021).

3.5.3.1 Effects of parameters on specific surface area

Figure 3.5 shows that the activation temperature and the $CP/ZnCl_2$ mass ratio have a greater impact on the specific surface areas of the synthesized activated carbon than the activation time. The final activation temperature and impregnation ratio are important variables in the chemical activation process that affect the surface area, pore volume, and pore size distribution of the activated carbon (Bankole et al., 2023). The conventional BET equation (NLDFT method) was used to calculate the BET surface area, pore volume, and pore size distribution within the relative pressure (P/P_0) range of 0.06 to 0.3. The specific surface areas also demonstrate a decreasing trend with a decrease in the impregnation ratio (Fig. 3.5 (a), (b), and (c)).

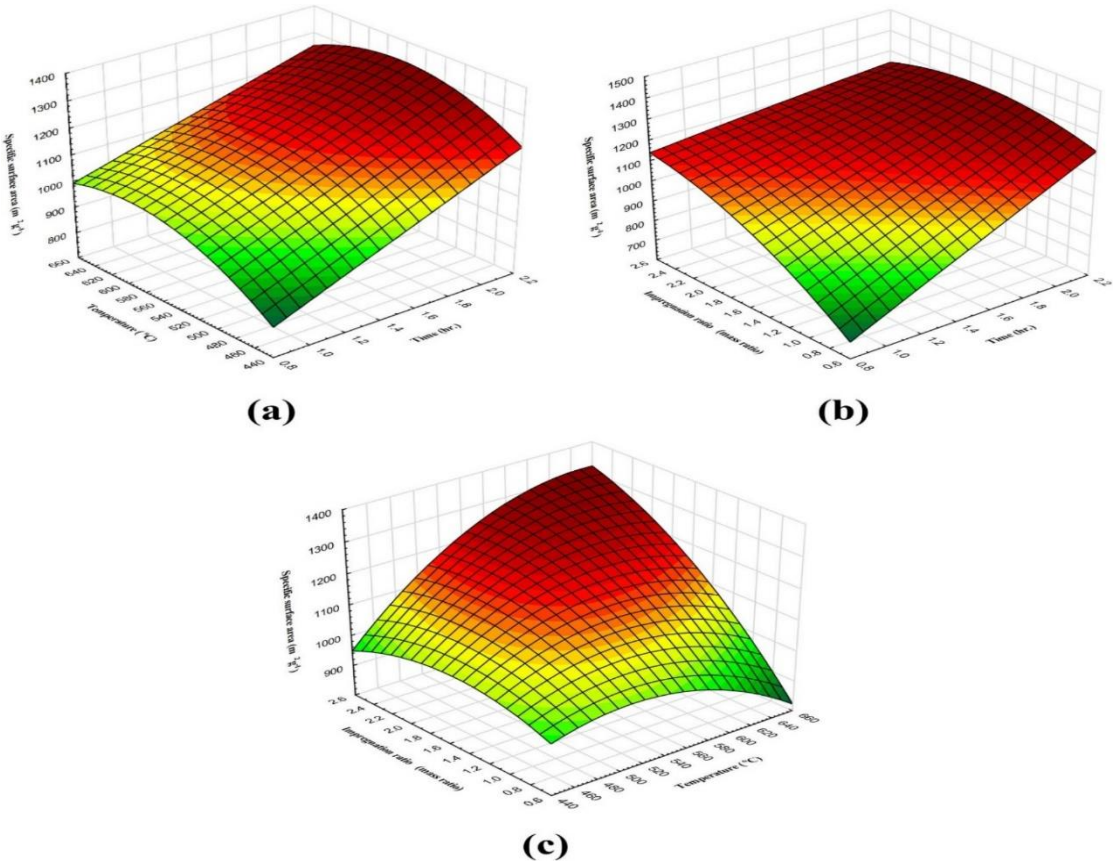

Figure 3-5 Three-dimensional response plots showing interaction effects of temperature and time (a), impregnation ratio and time (b), and temperature and impregnation ratio (mass ratio) on specific surface area (c).

3.5.3.2 Effects of parameters on pore volume

Figure 3.6 describes the effect of time, temperature, and impregnation ratio on the total pore volume ranged from 0.109 to 0.315 cm^3/g and increased with temperature, ranging from 450 to 650 °C, and an impregnation ratio ($ZnCl_2$/CP) of 0.75:1 to 2.5:1. In this investigation, the activated carbon material exhibited a significant pore volume. This was indicated by a reported pore volume and pore size distribution of 0.195 cm^3/g, achieved through optimized parameters such as an activation temperature of 533 °C, an impregnation ratio (mass ratio) of 1.6:1, and an activation time of 1.82 h.

It is important to note that the pore volume observed in this study was slightly smaller than the previously reported value of 0.28 cm^3/g (Kayiwa et al., 2021) for similar carbonization temperature ranges. Additionally, other experiments involving the extraction of cassava peels carbonized at temperatures ranging from 450 to 650°C also yielded lower pore volumes. This discrepancy may be attributed to inherent variations in the raw biomass composition, particularly the inorganic content.

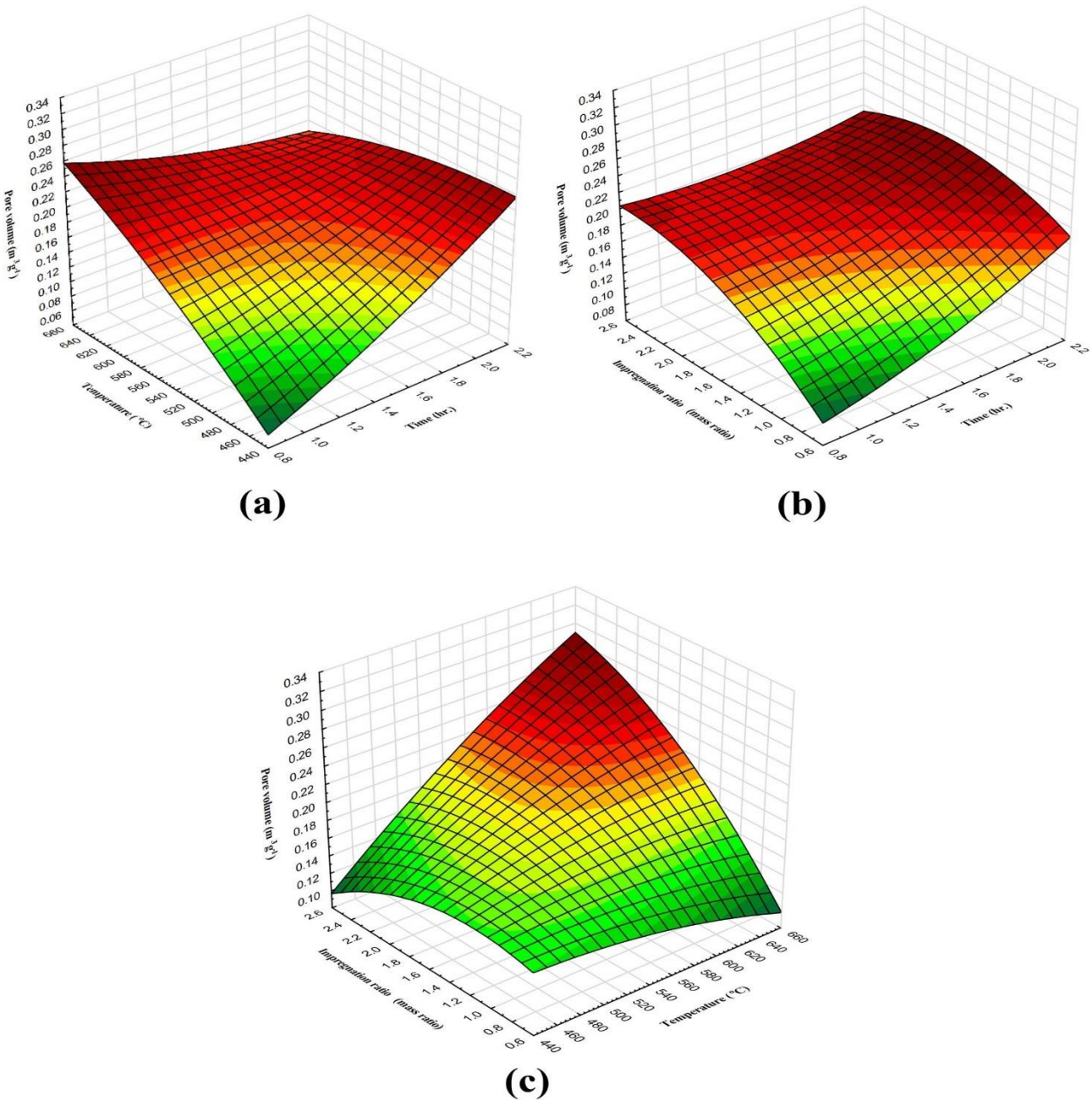

Figure 3-6 Three-dimensional response plots showing interaction effects of temperature and time (a), Impregnation ratio and time (b), and temperature and impregnation ratio (c) on pore volume.

3.5.3.3 Model optimization

The desired set of co-precipitation synthesis of activated carbon parameters was found by optimizing the responses from the two quadratic models. This was achieved using Derringer's desirability function approach for multiple response processes (Equations 3.3 and 4.4). Based on this, the following parameters were chosen to predict the BET surface area of 1250 m^2/g and the pore volume of 0.195 m^3/g, at an activation time of 1.82 h., an activation temperature of 530 ^oC, and an impregnation ratio (mass ratio) of 1.6:1. Using the model equations for each response, it is possible to predict the co-precipitation synthesis of activated carbon parameters along the same preparation routes based on the results obtained.

3.5.3.4 Photocatalytic removal of TC under optimized conditions

Figure 3.7 demonstrates the photocatalytic removal of TC as a function of time using ZnO-NPs/AC. As indicated in the Figure, C/C_o dramatically decreases as irradiation time increases for all initial concentrations of TC. Furthermore, the rate of TC removal appears to be influenced by the initial concentration, with lower concentrations exhibiting a more pronounced decrease in C/C_o over time. This observation suggests that at higher initial concentrations, the saturation of active sites on the photocatalyst hinder the efficiency of both adsorption and degradation processes. Moreover, as the concentration of the TC solution increases, more light is absorbed by the solution itself.

In this particular performance test, the photocatalytic removal efficiency reached almost 99% at an initial TC concentration of 2.5 mg/L, whereas it was about 81% at an initial TC concentration of 15 mg/L. Moreover, the role of the photocatalyst's surface properties cannot be overlooked, as morphology and surface area significantly affect adsorption capacity and subsequent photocatalytic activity. An enhanced surface area facilitates greater interaction between the photocatalyst and TC molecules, thereby promoting more effective degradation.

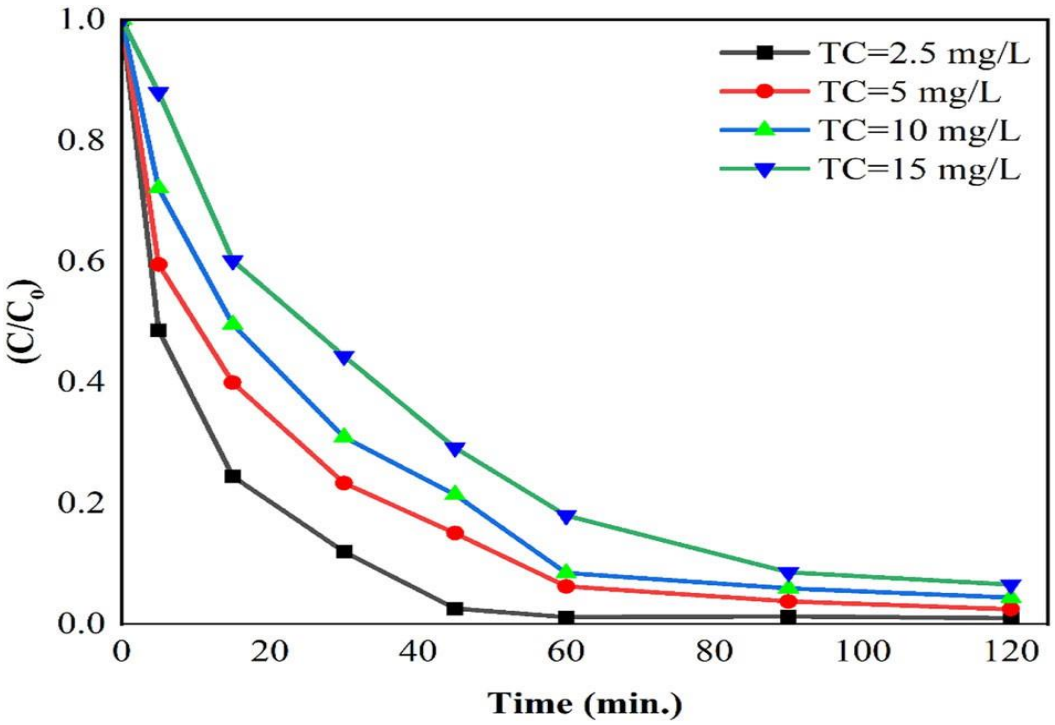

Figure 3-7 The photocatalyst performance of ZnO-NPs impregnated AC for the removal of TC

To investigate the combined effects of adsorption and photocatalysis, bare ZnO and ZnO-NPs impregnated activated carbon were subjected to an initial concentration of TC of 2.5 mg/L and a contact time of 120 min. This was done under UV light (without a catalyst) and in dark conditions (with a catalyst), as shown in Figure 3.8. The results demonstrated only a 13% reduction in TC under UV light (without a catalyst). This could be due to the degradation of TC by UV-C photolysis (M. Xu et al., 2020).

The bare ZnO-NPs were also tested under UV-vis light and demonstrated significant degradation (77%). Similarly, the prepared ZnO-NPs impregnated activated a notable TC removal of 49% under dark conditions after a contact time of 120 min, likely through adsorption, whereas the ZnO-NPs/AC demonstrate almost 99% decomposition under UV-vis light. The findings of nearly complete removal of TC under UV-vis light (with a catalyst) reflect a synergistic effect between adsorption and photocatalytic degradation, as previously reported (Salah et al., 2024; Tran Thi & Lee, 2017a). However, the bare ZnO nanoparticle showed the poorest performance for the removal of TC.

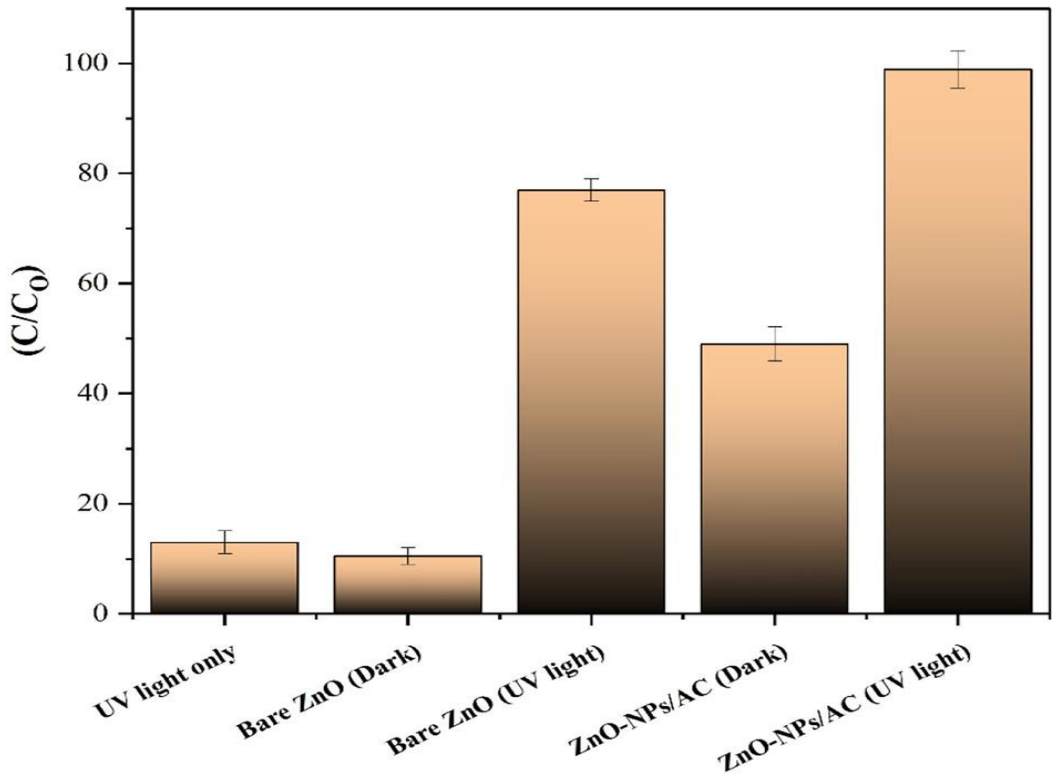

Figure 3-8 The removal performance of bare ZnO and ZnO-NPs impregnated activated carbon, and the removal of TC under different conditions

The composite exhibited excellent reusability, maintaining a TC removal effectiveness of over 80% after five consecutive cycles. The decision to evaluate the material over five cycles was based on established benchmarks in literature for catalyst stability, which provide a reliable indicator of the material's long-term structural integrity and economic feasibility. While a gradual decline in performance is expected after the 5^{th} cycle due to the progressive occupation of active sites and minor photocatalyst leaching, retaining > 80% efficiency at this stage strongly demonstrates the practical applicability of the composite for continuous water treatment. Future scale-up studies will focus on extended life-cycle assessments beyond this benchmark to determine the absolute lifespan of the material (Dubey et al., 2025).

Furthermore, instead of a significant loss of structural integrity, the slight reduction may result from the unavoidable loss of small amounts of the catalyst during the recovery stages (filtering and washing) between cycles (Matei et al., 2023).

Nevertheless, the minimal decrease in activity suggests that the ZnO-NPs are securely bonded to the AC substrate and that the structural framework remains largely intact. This effectively prevents significant leaching and highlights the hybrid's potential for long-term, sustainable environmental cleanup.

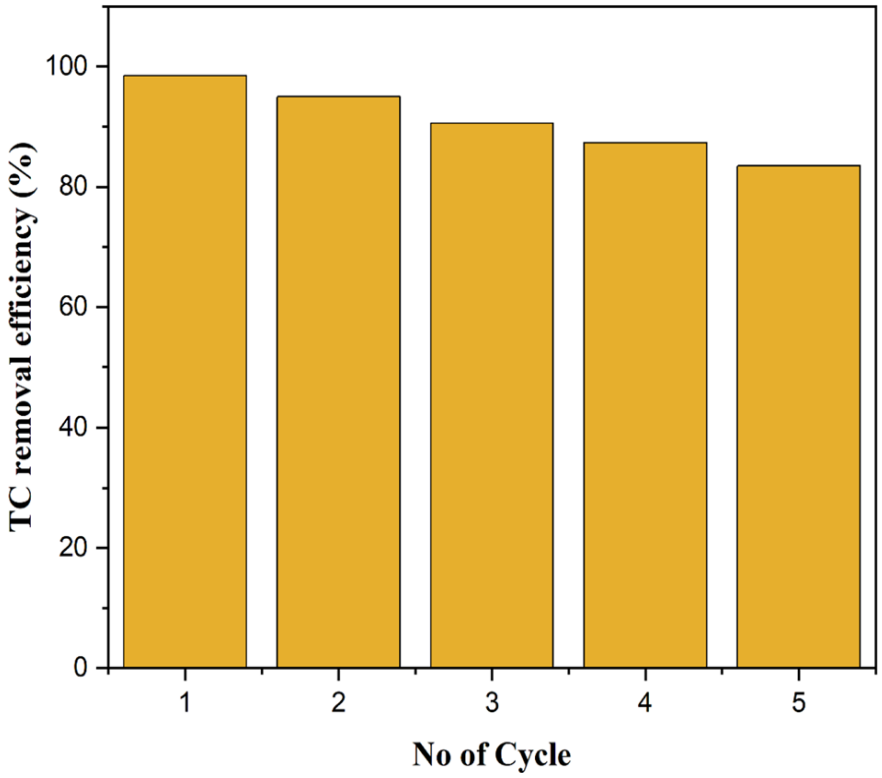

Figure 3-9 The stability of photocatalyst performance of ZnO-NPs impregnated activated carbon at different cycles

3.6 Conclusion

This work demonstrates the successful preparation of activated carbon from cassava peel as a precursor, with chemical activation by $ZnCl_2$. The operational parameters for the preparation of activated carbon were statistically optimized. The results of this study indicate that cassava peel is a good precursor for preparing activated carbon. The carbonization temperature and impregnation ratio both have a significant impact on the pore characteristics of the resulting activated carbons. The use of $ZnCl_2$ in conjunction with the cassava peel enabled the morphology of the activated carbon to be optimized, leading to the development of a highly porous structure.

The synthesis of hexagonal wurtzite ZnO-NPs from $(CH_3COO)_2Zn.2H_2O$) modified by an extract obtained from a *citrus bergamia* leaf sample was also demonstrated. Based on the ZnO-NPs optical properties, the sample's band gap energy was found to be 3.15 eV. The study also successfully demonstrates the impregnation of the synthesized ZnO-NPs on the surface of the prepared activated carbon. The photocatalytic efficiency of the catalyst for decomposition of TC was found to be about 99% under optimized conditions. Therefore, while adsorption initiates the capture, photocatalysis is the major phenomenon responsible for the permanent abatement of TC, continuously regenerating the active sites in situ.

4. MACHINE LEARNING-BASED PROCESS OPTIMIZATION FOR ADSORPTION REMOVAL OF EMERGING CONTAMINANT (TETRACYCLINE) FROM AQUEOUS SOLUTION ONTO ZINC CHLORIDE ACTIVATED BIOMASS (CASSAVA PEELS)

4.1 Introduction

Emerging contaminants (ECs) are a significant global environmental concern. Many harmful organic (Telli et al., 2024a) pollutants, such as pesticides, herbicides, medications, personal hygiene products, surfactants, and other solvents, are released into aquatic ecosystems (Kassahun et al., 2021). Owing to its excellent quality, affordable price, and desired antibacterial action, TC is used extensively in both human medicine and the livestock industry (D. Zhang et al., 2015). It is currently one of the most widely used antibiotics worldwide. However, most residual TC is released into the environment, with only a small portion being digested or absorbed by the body (Qiao et al., 2020).

TC is a broad-spectrum antibiotic with strong activity against a wide range of bacteria. Since TC is inexpensive, it is frequently used to accelerate animal growth and improve feed efficiency. TC has been found in drinking water, groundwater, sediments, wastewater treatment plants, sludge, and surface water (lakes, rivers, and oceans) (Ortiz-Ramos et al., 2022). TC removal from aqueous solutions has been studied using various techniques, including photocatalytic degradation (Gholami et al., 2020), adsorption (Manjunath and Kumar, 2021), and advanced oxidation (Anjali & Shanthakumar, 2019). The primary discrepancies were in the effectiveness of TC removal techniques, ease of use, affordability, and ecological impact. Activated carbon adsorption has attracted considerable attention as a promising and cost-effective method for treating TC-contaminated aqueous effluents.

AC adsorption's qualities include a straightforward and affordable process, high removal efficiency, and the absence of harmful byproducts (Ao et al., 2019, Yan et al., 2024). In addition, the principal adsorption process, involving electrostatic interactions between the carbon surface and the TC species in solution, was a key factor in the granular activated carbon's adsorption capability (C. Ma et al., 2024).

One option in this regard is AC derived from cassava peels, which is an adsorbent with special qualities, including low cost, efficiency, non-toxicity, abundance, biodegradability, and strong adsorption activity for many organic contaminants. This approach not only makes use of abundant waste resources but also enhances environmental sustainability by reducing waste and promoting cleaner water sources.

Several studies describe how specific cassava peels effectively remove TC under certain conditions. However, they do not correlate these removal capacities with typical activated characteristics of cassava peels, such as the BET surface area (Suresh et al., 2024). In this study, AC from cassava peels was synthesized using $ZnCl_2$ as the activating agent, and its effectiveness was investigated adsorbing and removing TC from aqueous solutions. The adsorbent was created using a Sol-gel method, which enhanced its physicochemical properties by increasing surface area, pore volume, and pore size.

While previous studies have utilized RSM and ANN to optimize operational variables like solution pH, contact time, dosage, and initial concentration, a critical gap remains (Kassahun et al., 2021). To address this limitation, this study uniquely customizes the RSM and ANN approaches to model and predict the interactive effects of these key parameters specifically for our synthesized composite system. By pairing the statistical validation of RSM with the high-predictive accuracy of ANN, we precisely map the operational boundaries required to maximize simultaneous adsorption and photocatalytic TC degradation (Rinawati et al., (2024).

4.2 Materials and methods

4.2.1 Materials

After gathering the cassava peel from the Southern Nations Wolaita zone in Ethiopia, pure NaOH (99.0%) pellets, 35.4% pure HCl, $ZnCl_2$ with a molarity of 136.28 g/mol, and powdered tetracycline hydrochloride ($C_{22}H_{24}O_8N_2.HCl$) were purchased.

4.2.2 Activated carbon preparations

Following the preparation procedures detailed in section 3.2.3 of chapter 3, the cassava peels were thoroughly cleaned multiple times with distilled water to remove dirt and other inorganic impurities. With the previous methodology of Manyazewal et al., (2025a), the samples were dried for 24 hours at 120 °C and ground to a particle size of 63–150 µm. Chemical activation with $ZnCl_2$ was then employed to determine the optimal conditions for producing activated carbon with a high surface area. To prepare the varying concentration ranges of $ZnCl_2$ solutions outlined in Table 4.1, appropriate aliquots were measured from a 10 g/L stock solution and diluted using a 150 mL volumetric flask. Each experiment was conducted according to the suggested parameters of (Kwiatkowski et al., 2017).

Following this, the samples were held at the desired temperature for carbonization. A soaking period was implemented to ensure the $ZnCl_2$ solution penetrated deeply into the cells of the cassava peels. The impregnated cassava peels were oven-dried at 105 ^{o}C to gently remove surface moisture without initiating premature chemical activation. Furthermore, maintaining a stable initial pH ensured uniform chemical conditions across all experimental runs.

The cassava peel samples were carbonized in a muffle furnace for 60 to 120 min at temperatures between 450 and 650 °C, with an impregnation ratio of 0.75:1 to 2.5:1 before cooling under nitrogen flow. Subsequently, a HCl solution was used to wash the activated carbon. The samples were rinsed multiple times with hot distilled water to ensure the complete removal of chloride ions. Finally, the specimens were washed with distilled water, dried at 110 °C for 24 h, and then stored in a desiccator (Manyazewal et al., 2025a).

4.2.3 Batch adsorption test

Adsorption removal was conducted using an aqueous solution of TC in a 250 mL borosilicate glass reactor, with the CP/$ZnCl_2$ activated carbon serving as the adsorbent. The procedure conditions, including solution pH, adsorbent dosage, contact time, and initial contaminant concentration (C_o), were varied according to the BBD experimental method, as outlined in Table 4.1. To ensure saturated adsorption and to obtain a sample for determining the initial concentration (C_o), the solution was mixed before each experiment. The borosilicate glass reactor was filled with the

designated adsorbent dosage and continuously stirred with a magnetic stirrer (single phase) to create a homogeneous condition, following single-factor analysis. The measured pH values of the solutions varied.

Table 4-1 Experimental study factors and levels.

Factor	Name	Unit	Study range	
			Minimum	Maximum
A	Initial contaminant concentration	mg/L	2.5	7.5
B	pH	pH	3	9
C	Time	Min	30	90
D	Adsorbent Dosage	gm/L	0.025	0.075

After a specified adsorption time, approximately 5 mL of the solution was withdrawn and filtered to remove the suspended adsorbent. The solution was then centrifuged for 10 min at 500 RPM using a Hettich Zentrifugen Universal 320 R. It was subsequently filtered through a syringe fitted with a 0.2 µm filter to minimize the impact of carbon particles on the aqueous samples. The total TC concentration was measured using a UV/visible spectrophotometer (X-ma 1200) at an absorbance of 350 nm (Hameedi, 2021). The adsorption removal efficiency (R%) and adsorption capacity (qt) at a specific time (t) were subsequently calculated using Equations (4.1) and (4.2).

$$R\ (\%) = \frac{c_o - c_f}{c_o} * 100 \quad \text{(4.1)}$$

$$qt\left(\frac{mg}{g}\right) = \frac{c_o - c_t}{m} * v \quad \text{(4.2)}$$

Where C_o and C_f are the concentrations of TC in solution before adsorption (mg/L) and the final concentration in solution after adsorption (mg/L), respectively. V is the volume of the treatment sample, C_t is the concentration of the adsorbate remaining in the solution at a specific time 't' after the adsorption process has started, and m is the mass of adsorbent material being used in the experiment.

4.2.4 Artificial neural networks (ANNs) and response surface methodology (RSM)

ANNs are algorithmic models that rely on data and are based on independent and dependent process factors (ANN) (Campus, 2018). This model tool is highly significant in the fields of data forecasting, regression, and classification. It has special qualities, including resilience, reliability, and the ability to comprehend complex and nonlinear systems (Ganapathy et al. 2021).

An ANN is structured using multilayer perceptron's (MLPs), which consist of input, hidden, and output layers made up of numerous nodes (Telli et al., 2024b). During the model construction process, a feed-forward neural network was employed, connecting nodes from one layer to nodes in the next. Additionally, the Levenberg-Marquardt (LM) algorithm was utilized to train the neural network (Boutra et al., 2022). The variables used in this investigation included the initial TC concentration (mg/L), adsorbent dose (g/L), adsorption time (min), and solution pH. The ANN analysis was performed using MATLAB R2024b.

The RSM-BBD experimental design, detailed in Tables 4.3, was employed to evaluate each experimental run and the response as continuous inputs and targets. RSM-BBD is a statistical and mathematical modeling technique used to determine the relationship between dependent and independent variables. This model provides prediction capabilities through a sequential experimentation approach for creating and optimizing an empirical model, helping to extract the maximum information from a limited amount of experimental data (Kassahun et al., 2021).

Table 4.2 illustrates the fully randomized design of the tests, featuring one response variable (TC removal efficiency (R%)) and four parameters (solution pH, adsorption time, adsorbent dosage, and initial TC concentration), each at three levels. A second-order polynomial equation was used to establish the relationship between the independent variables and the response. The general equation (4.3) for the four selected experimental factors can be formulated as follows:

$$Y = \beta_O + \sum_{i=1}^{k} \beta_i X_I + \sum_{i=1}^{k} \beta_{ii} X_i^2 + \sum_{1 \le i \le j} \sum \beta_{ij} X_i X_j + \varepsilon \quad \text{.....(4.3)}$$

In this case, Y represents the experimental response, X_i and X_j are experimental variables or factors, β_o is a constant, and the regression coefficients for the linear, quadratic, and cross-product interaction effects are β_i, β_{ii}, and β_{ij}, respectively. Here, ε represents the random error.

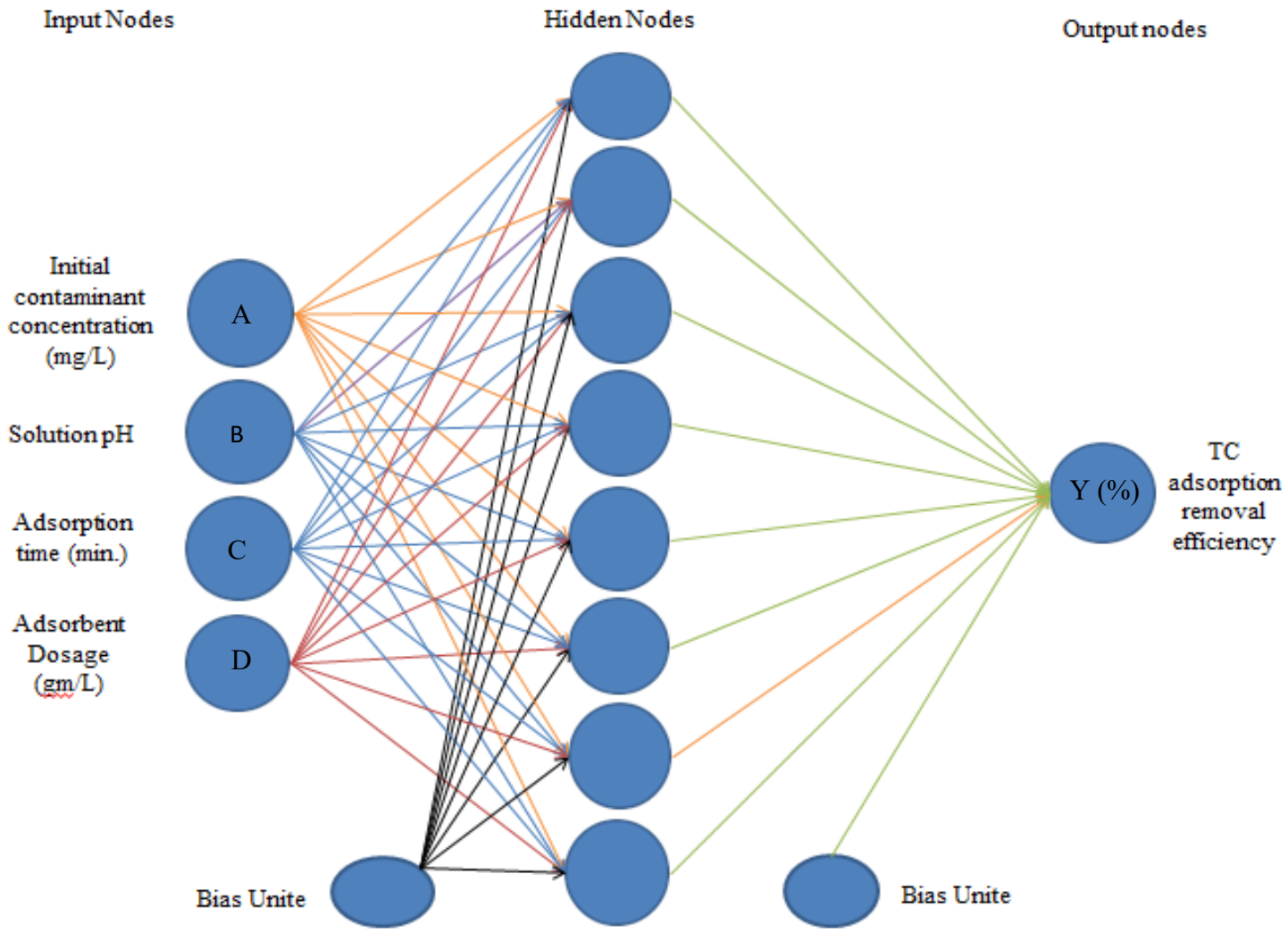

Figure 4-1 Neural Network Architecture for the input and output study variable

Statistical software program, Design-Expert version 13 (Stat-Ease, Inc.), was used to perform the regression analysis and estimate the coefficients (Kassahun et al., 2021).

The quality of fit and statistical significance of the model equations was expressed using the F-test, coefficient of determination (R^2), adjusted coefficient of determination (adj-R^2), prediction coefficient of determination (Pred R^2), and coefficient of variation (CV).

Table 4-2 RSM and ANN removal efficiency response for the input and output study variable

Run	A: Initial Contaminant Concentration (mg/L)	B: Solution pH	C: Adsorption Time (min.)	D: Adsorbent Dosage (g/L)	Removal Efficiency (%)	
					ANN	RSM
1	5	3	60	0.075	74.23	75.33
2	7.5	6	90	0.05	83.1	81.86
3	5	9	30	0.05	57.16	58.71
4	2.5	6	60	0.075	96.92	96.99
5	5	3	90	0.05	71.41	70.92
6	7.5	6	30	0.05	57.71	57.99
7	5	6	90	0.075	95.44	96.81
8	5	6	60	0.05	73.39	74.65
9	7.5	9	60	0.05	59.91	58.42
10	5	6	60	0.05	73.39	74.65
11	5	6	60	0.05	73.39	74.65
12	5	6	60	0.05	73.39	74.65
13	2.5	3	60	0.05	76.13	77.20
14	7.5	6	60	0.025	61.96	63.98
15	7.5	3	60	0.05	65.72	65.44
16	5	6	30	0.025	71.84	70.37
17	5	3	60	0.025	58.21	58.52
18	5	9	90	0.05	76.74	78.35
19	5	6	30	0.075	67.87	67.27
20	2.5	9	60	0.05	88.24	90.01
21	2.5	6	90	0.05	96.62	94.78
22	5	9	60	0.075	74.31	72.75
23	5	9	60	0.025	66.64	66.90
24	2.5	6	60	0.025	89.1	88.81
25	2.5	6	30	0.05	86.86	88.43
26	7.5	6	60	0.075	73.1	78.46
27	5	6	90	0.025	72.16	71.05
28	5	6	60	0.05	76.92	74.65
29	5	3	30	0.05	61.52	60.34

The absolute Average Deviation (AAD) formula is defined as follows Eqn. (4.4), (4.5) and (4.6)

$$R^2 = 1\frac{\sum_{i=1}^{n}(y_{Ai}-y_{Pi})^2}{\sum_{i=1}^{n}(y_m-y_{Pi})^2} \quad \text{..... (4.4)}$$

$$RMSE = \sqrt{\sum_{i=1}^{n}\frac{(y_{Ai}-y_{Pi})^2}{n}} \quad \text{.....(4.5)}$$

$$AAD = \frac{1}{n}\sum_{i=1}^{n}*\frac{|y_{Ai}-y_{Pi}|}{y_{Pi}} \quad \text{.....(4.6)}$$

Where y_A are the actual value, y_P the predicted value, n the number of data points, and y_m the average value.

4.2.5 Results and Discussion

4.2.5.1 FT-IR characterization of activated carbon

The FT-IR spectra of the CP/$ZnCl_2$ activated carbon sample are presented in Figure 4.2. Analyzing the chemical composition of an adsorbent is essential for understanding its adsorption mechanism. The likely active surface groups include O-H, alkynes, aromatic rings, and carbonyl groups (Kayiwa 2022).

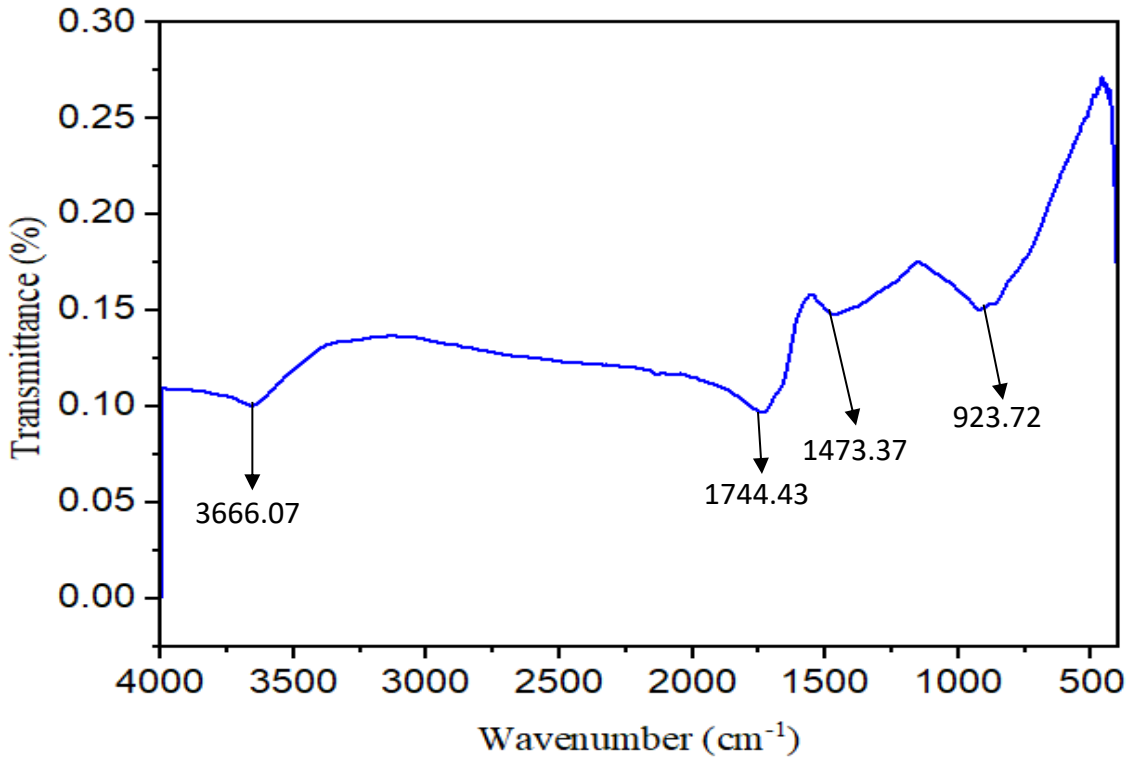

Figure 4-2 FT-IR spectra for activated carbon from cassava peel at optimized parameters

After activating the carbon for 1.14 h at 608.2 °C and impregnating it with a 2.3:1 ratio of ($ZnCl_2$/cassava peel) activated carbon, the surface functional groups of the carbon were examined using FTIR spectroscopy in the mid-infrared range of 4000 to 500 cm^{-1}. The FTIR spectra, shown in Figure 4.2, reveal a peak at 3666.07 cm^{-1}, corresponding to the O-H group found in pectin, cellulose, and lignin in cassava peels, as well as in polymeric substances such as alcohols, phenols, and carboxylic acids (Mohd-Asharuddin et al., 2017).

The FT-IR spectra of the produced activated carbon also displayed a broad band around 3400 cm^{-1}, indicating the presence of hydroxyl groups, which aligns with the results of Kayiwa et al. (2021) who also used $ZnCl_2$ activation for cassava peel. However, the intensity of the C=O stretching around 1700 cm^{-1} was lower in our study compared to theirs (Belcaid et al., 2022). This suggests that the lower activation temperature in our study resulted in a reduced degree of oxidation and fewer carbonyl groups on the carbon surface compared to the higher activation temperature used in research (Y. Zhang et al., 2018). The peak at 1744.43 cm^{-1} shows the stretching vibration of the C=C aromatic nucleus (Astuti et al., 2020). Finally, it was determined that the band at 1473.37 cm^{-1} was the aromatic C–H of lignin (Belcaid et al., 2021). All of these factors have a significant impact on the binding of metal ions. The growth of these bands suggests that surface oxygen functional groups were formed on the activated carbon as a result of surface modification (Kristianto et al., 2016).

4.2.5.2 UV-Vi's characterization of activated carbon

Figure 4.3 presents the UV–Vi's spectra of the ($ZnCl_2$/Cassava peel) AC, assessed using a UV/Vis/NIR spectrophotometer. The figure illustrates that absorbance values are influenced by wavelength; the visible region shows relatively low absorbance values between 400 and 600 nm, while the UV region exhibits significantly higher absorbance values below 400 nm. A noticeable peak in the spectra at approximately 300 nm indicates high absorption, which may suggest successful surface modification, potentially associated with conjugated systems or functional groups created during the activation process (Programme & Plantation, 2024).

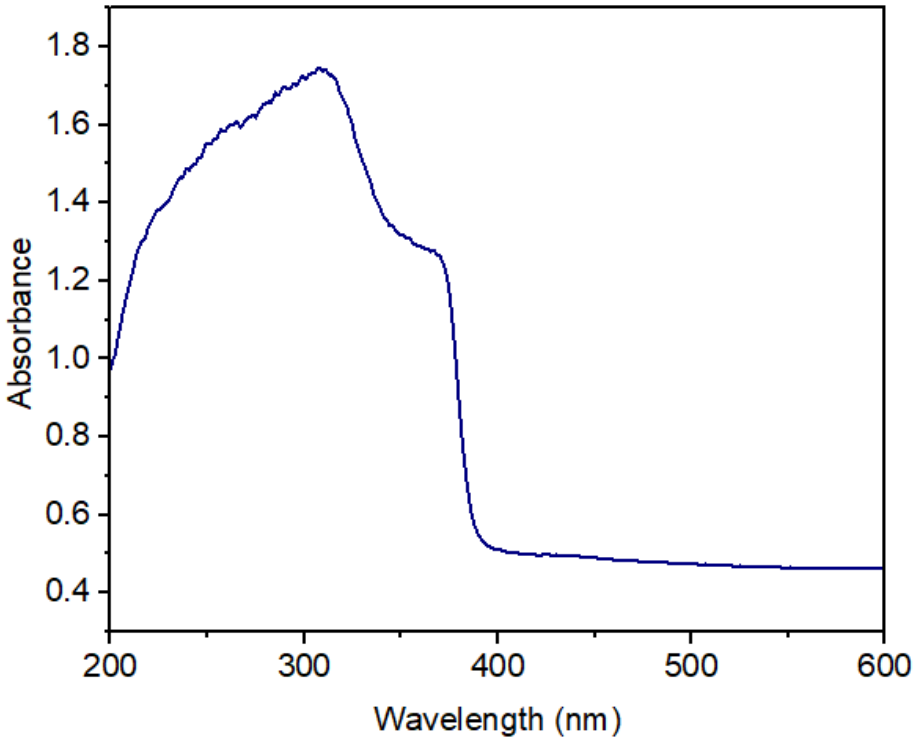

Figure 4-3 UV–Vis spectra of the prepared activated carbon under optimum conditions

The presence of electronic transitions or functional groups in activated carbon is indicated by the increased absorption in the UV region. The data revealed that, based on UV-visible spectroscopy characterization, the ($ZnCl_2$/Cassava peel) AC absorbed more light in the UV region than in the visible region.

4.2.5.3 SEM characterization of activated carbon

Figure 4.4 displays the surface morphology of the ($ZnCl_2$/cassava peel) AC, as observed through scanning electron microscopy (SEM) at various magnifications. Typically, activated carbon features a rough surface, irregularly shaped particles, and a porous structure. The SEM images clearly illustrate that the pore structure of the material consists of mesopores characteristic of activated carbon (Amakoromo et al., 2022).

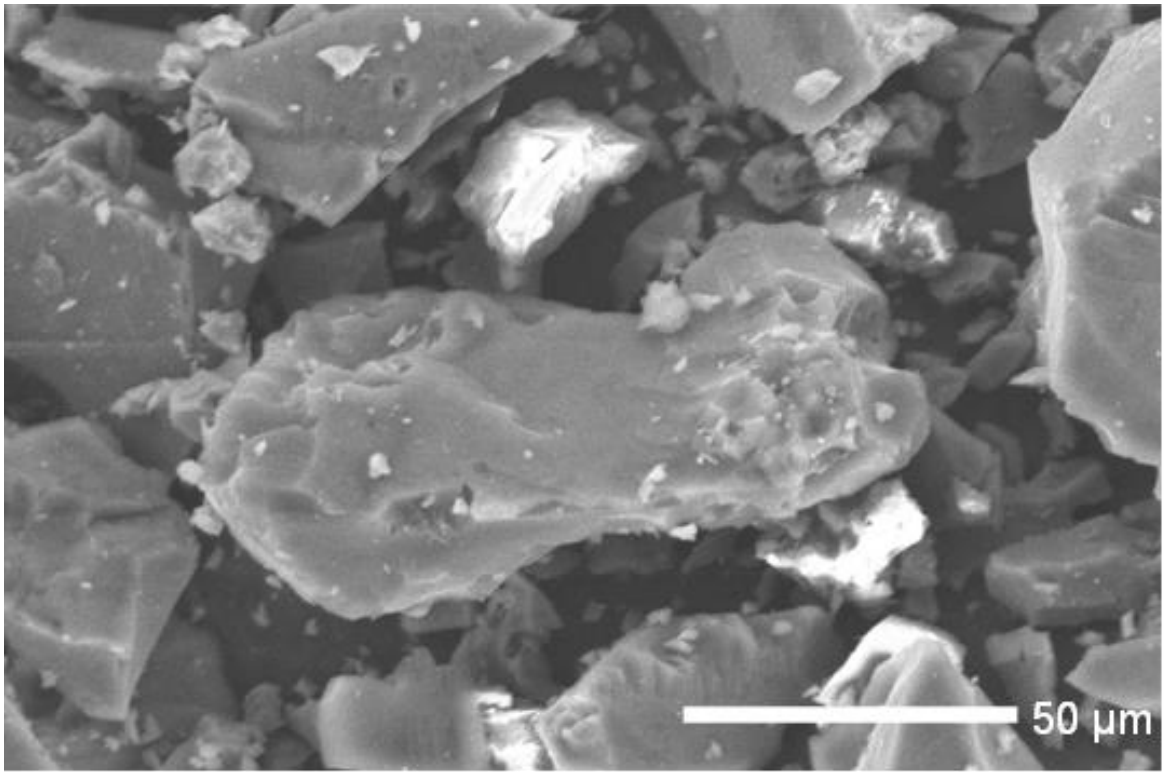

Figure 4-4 SEM micrographs of ($ZnCl_2$/cassava peel) activated carbon

As shown in Figure 4.4, the structure of the $ZnCl_2$/ cassava peel AC consists of amorphous graphite sheets. According to the theory, the active surface groups in the $ZnCl_2$/Cassava peel AC influence adsorption through hydrogen bonds, potentially including dipole-dipole interactions (Kayiwa, 2022). This donor-acceptor electron interaction leads to the adsorption of contaminants, such as TC, from wastewater.

The scale bar in Figure 4.4 indicates a size of 50 µm, demonstrating that the particles are micro-sized. Smaller particle sizes typically enhance adsorption efficiency due to their higher surface area-to-volume ratio. The identified morphological features of AC support their use in industrial processes and environmental remediation by enhancing efficient adsorption. A comprehensive assessment of their performance will require further research, including surface area analysis and adsorption capacity tests (Sanz-Santos et al., 2022). Because some contaminants, such as TC, have large molecular sizes, mesopores are preferred over micropores for the adsorption of pollutants (Zietzschmann et al., 2016), and the mesopore volume ratio of activated carbon determines how well it can adsorb pharmaceutical pollutants such as TC (Kayiwa et al., 2022).

4.2.5.4 XRD characterization of activated carbon

Figure 4.5 presents the XRD analysis conducted to verify the phase composition of the material. The CP/$ZnCl_2$ activated carbon sample used for the XRD investigations was applied to a glass plate, with scanning beginning at 10° and concluding at 80°. The graph reveals multiple peaks at specific 2θ values, indicating that the activated carbon contains crystalline phases. Typically, activated carbons also contain amorphous carbon, as evidenced by a prominent peak around 22°.

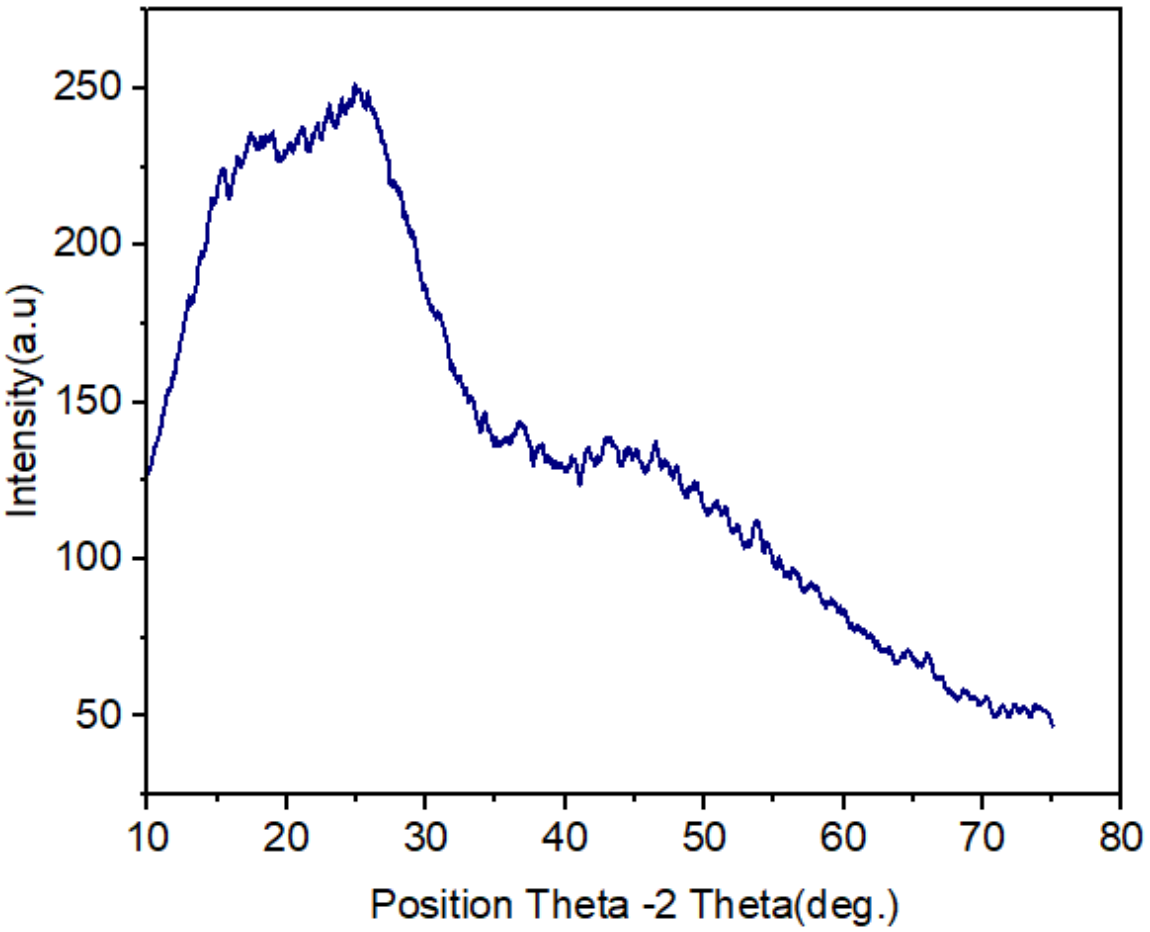

Figure 4-5 Graph showing XRD analysis of activated carbon at optimized parameters

The XRD patterns of the activated carbon samples that were produced were similar, displaying broad diffraction peaks in an amorphous signature at two different 2θ angles: 18–25 and 36–43, which correspond to the (002) and (100) crystallographic planes of the carbon material (Amakoromo et al., 2022). In this study, the amorphous lattice planes of the cassava peel/$ZnCl_2$ activated carbon diffract X-rays at scattered angles that correspond to the obtained diffraction angles. The (002) plane of graphitic carbon is frequently cited as the source of the observed peaks. While it indicates a significant amorphous characteristic, it also reveals the presence of organized carbon structures. A sharp peak suggests greater crystallinity, while a broad peak indicates a more amorphous structure. The broad peaks observed in Figure 4.5 may indicate decreased crystallinity, which is typical of activated carbon (Ekekwe et al., 2018).

4.2.6 RSM statistical analysis

Table 4.3 presents the ANOVA for the removal of TC by adsorption. The models demonstrate substantial effectiveness in TC adsorption removal, indicated by their F-value of 98.02. In the ANOVA table, model terms were considered significant if their p-values were less than 0.05. As a result, the significant model terms for TC adsorption removal efficiency include A, B, C, D, AB, AC, BC, BD, CD, A^2, B^2, and D^2. The model's inability to accurately represent the data in the experimental domain at points excluded from the regression was assessed through the lack-of-fit test (Wiens, 2019). As shown in Table 4.4, the TC adsorption removal F value and P value for the lack of fit test were 98.02 and <0.0001, respectively. This suggests that there was no statistically significant lack of fit and that the model equations were sufficient to anticipate a response falling within the study range.

According to the RSM-BBD, the coefficient of determination (R^2) for the regression models of TC adsorption removal was 0.9899, indicating that the models explained 98.99% of the variability within the experimental range. Predictions of TC adsorption removal can be made using the model equations, even when the study factors fall outside the experimental range, as evidenced by the predicted R^2 value of 0.9568. The values of R^2 and forecast R^2 for a decent model should generally be near 1 (Chicco et al., 2021). Following the removal of the inconsequential variables, the model equations that connect the responses to the process variables in terms of the actual values are provided in Eqn. (4.7).

$$\text{TC Adsorption Removal Efficiency } (\%) = 97.36 - 14.58A + 14.48B - 0.7C - 499.9D - 0.66AB + 0.058AC + 25.2AD + 0.025BC - 36.5BD + 9.62CD + 0.94A^2 - 0.86B^2 + 0.0024C^2 + 2421.3D^2 \quad (4.7)$$

Table 4-3 Analysis of variance (ANOVA) of the response surface model for TC adsorption.

Source	Sum of Squares	df	Mean Square	F-value	p-value	
Model	3731.07	14	266.50	98.02	< 0.0001	significant
A-contaminant concentration	1409.85	1	1409.85	518.55	< 0.0001	
B-pH	25.20	1	25.20	9.27	0.0087	
C-Time	684.94	1	684.94	251.92	< 0.0001	
D-Adsorbent	385.11	1	385.11	141.64	< 0.0001	
AB	98.31	1	98.31	36.16	< 0.0001	
AC	76.74	1	76.74	28.22	0.0001	
AD	9.92	1	9.92	3.65	0.0768	
BC	20.48	1	20.48	7.53	0.0158	
BD	29.98	1	29.98	11.03	0.0051	
CD	208.37	1	208.37	76.64	< 0.0001	
A^2	226.15	1	226.15	83.18	< 0.0001	
B^2	392.91	1	392.91	144.51	< 0.0001	
C^2	0.3092	1	0.3092	0.1137	0.7409	
D^2	14.86	1	14.86	5.46	0.0348	
Residual	38.06	14	2.72			
Lack of Fit	25.08	10	2.51	0.7729	0.6638	Not significant
Pure Error	12.98	4	3.25			
Cor Total	3769.13	28				

4.2.7 ANN analysis

Additionally, the ANN effectively correlates with the input-output relationship. The optimal topologies for the modeling technique, which reduces training, test, and validation errors, were found to be three-layer perceptron networks with configurations of 4-8-1 for TC adsorption removal. As illustrated in Figures 4.6 (a-c), the ANN's outputs were compared with the actual experimental data to assess these errors.

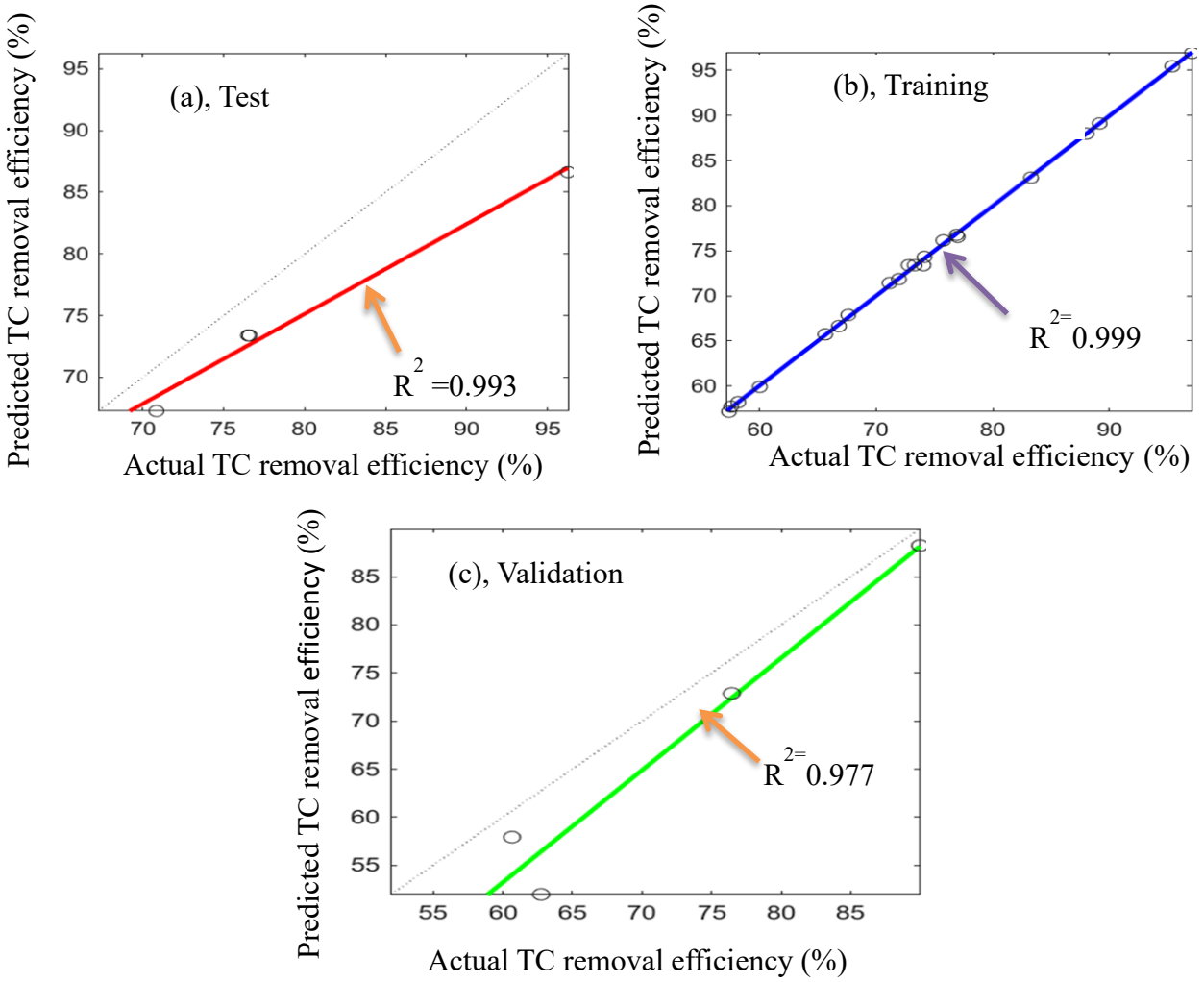

Figure 4-6 The scatter plots of (a) testing, (b) training, and (c) validation datasets show the predicted ANN output values compared to the actual experimental values for TC adsorption removal efficiency at the optimized topology.

As shown in Figures 4.6 (a), (b), and (c), the R^2 values for TC adsorption removal efficiency were 0.9907 for the test data, 0.99971 for the training data, and 0.97728 for the validation data. When comparing the ANN and RSM-BBD estimates for TC removal efficiency, Figure 4.7 demonstrate that the two predictions are quite similar. Generally, the ANN values are higher than the RSM-BBD values, suggesting that the ANN model may be more sensitive or better at identifying specific patterns in the data compared to the RSM-BBD model.

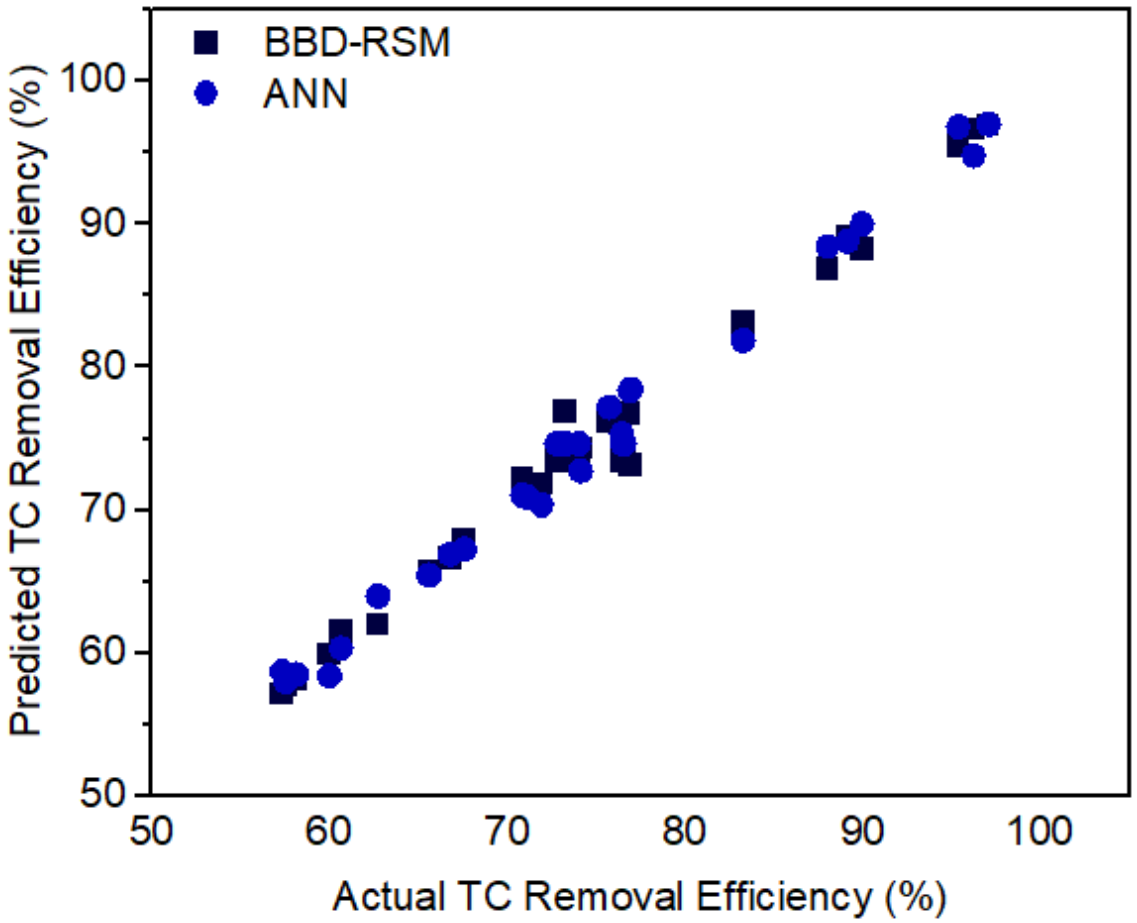

Figure 4-7 Comparison of predicted and actual values between RSM and ANN for TC adsorption removal efficiency.

Table 4-4 Performance indicators for the RSM-BBD and ANN model approach on TC adsorption removal efficiency

Statistical Parameter	BBD-RSM TC adsorption removal efficiency	ANN TC adsorption removal efficiency
R^2	0.9899	0.9997
AAD	0.027	0.0358
RMSE	0.99	1.52

Table 4.4 further demonstrates that the ANN effectively captures the relationship between input and output variables, as indicated by the computed values of absolute average deviation (AAD), root mean square error (RMSE), and the coefficient of determination (R^2). Additionally, prior research has shown that both ANN and RSM-BBD techniques can assess multiple responses within a single procedure (Kassahun et al. 2021).

4.2.8 Effects of single operational parameters on TC adsorption removal efficiency

Figure 4.8 (a–d) illustrates the single-factor analysis of operational parameters as a function of the TC concentration ratio (C/C_o), focusing on various factors, including adsorption time, pH, adsorbent dosage, and initial TC concentration. In this context, C represents the concentration of TC in the solution after adsorption (mg/L), while C_o refers to the initial concentration of TC in the solution before adsorption (mg/L). The C/C_0 ratio indicates the fraction of TC that remains in the solution after adsorption; effective adsorption is indicated by a significant drop in this ratio, suggesting that a substantial amount of TC is being adsorbed (Delgado et al., 2019). TC can be effectively removed by the adsorbent when there is strong adsorption; lower C/C_o values at greater starting concentrations show this in Figure 4.8 (a-d).

As shown in Figure 4.8 (a), the adsorption removal efficiency over time (min) and the residual concentration (C/C_o) were evaluated at a constant adsorbent dosage of 0.75 g/L, a pH of 6, and a TC concentration of 2.5 mg/L. The residual concentration ratio was 0.53762 at 5 min, corresponding to a removal efficiency of approximately 46.2%.

However, these values decreased to 0.01919 at 90 min, with a removal efficiency of approximately 98.08%, which is similar to a removal efficiency of 97.2% reported in another study by Zhai et al., (2022). After 90 min, the removal efficiency approaches a steady state, indicating that the adsorption process is nearly complete, as measured using a UV/Vis spectrophotometer. Figure 4.8 (b) presents the results of an investigation into the impact of the initial pH value on TC adsorption removal efficiency. In this study, the maximum TC removal efficiency was achieved at a pH of 5 to 7 after 90 min, with an adsorbent dosage of 0.05 g/L and a TC concentration of 2.5 mg/L. Another study also reported maximum removal efficiency at a pH of 6 to 8 (Xiang et al., 2022).

TC's solubility and charge, which influence its adsorption, are significantly affected by solutions pH. Figure 4.8 (b) shows that the contaminant concentration (C/C_o) at pH 2 was 0.3089, corresponding to an adsorption removal efficiency of approximately 69.11%. As the pH increased to 6, the C/C_o value dramatically decreased to 0.00732, resulting in an adsorption removal efficiency of approximately 96.25%. However, at a pH of 12, the C/C_o value rose to 0.29821, indicating a significant drop in removal efficiency (70.17%). According to this investigation, TC may have a repellent effect due to the cationic nature of the adsorbent surface and varying pH levels. Additionally, TC can exist in solution as different species, as it is classified as an amphoteric molecule with multiple ionizable functional groups (Chang et al., 2020). C/C_o rapidly decreases at pH 6, indicating more efficient adsorption (Z. Li et al., 2023).

To examine the impact of the adsorbate on adsorption behavior, the adsorbent concentration was varied from 0.25 to 1.5 g/L. The amount of adsorbent used is a crucial experimental factor that can influence adsorption efficiency. As demonstrated in Figure 4.8 I, the removal percentage increased with the activated carbon dosage; the residual concentration ratio (C/C_o) decreased from 0.5 to 0.05 while keeping other factors constant: time at 90 min, pH at 6, and TC at 2.5 mg/L. At an initial adsorbent dosage of 0.25 g/L, the ratio (C/C_o) was 0.427, resulting in a removal efficiency of approximately 57.3%. In contrast, at an adsorbent dosage of 1.5 g/L, the ratio (C/C_o) decreased to 0.021, yielding a removal efficiency of approximately 97.9%. This indicates that removal efficiency improved proportionally as the adsorbent dosage increased, providing more reactive sites in the solution (Rizkallah et al., 2023).

One of the key factors influencing the effectiveness of adsorption removal is the contaminant concentration. TC can be adsorbed by various adsorbents to a certain extent, and the elimination efficiency is often high at low concentrations. However, as the concentration increases, the adsorption sites become saturated (Mohammed & Kareem, 2019). Figure 4.8 (d) illustrates how adsorption is affected by the TC concentration, ranging from 2.5 to 15 mg/L, at a time of 90 min, with an adsorbent dosage of 1.5 g/L and a pH of 6. It shows that, as the initial concentration of TC increases, the residual concentration ratio (C/C_o) also rises, while the TC adsorption removal efficiencies decrease significantly. At an initial concentration of 2.5 mg/L, the ratio (C/C_o) was 0.014, corresponding to a removal efficiency of approximately 98.6%. However, at a TC concentration of 15 mg/L, the ratio increased to 0.187, resulting in a removal efficiency of approximately 81.3%.

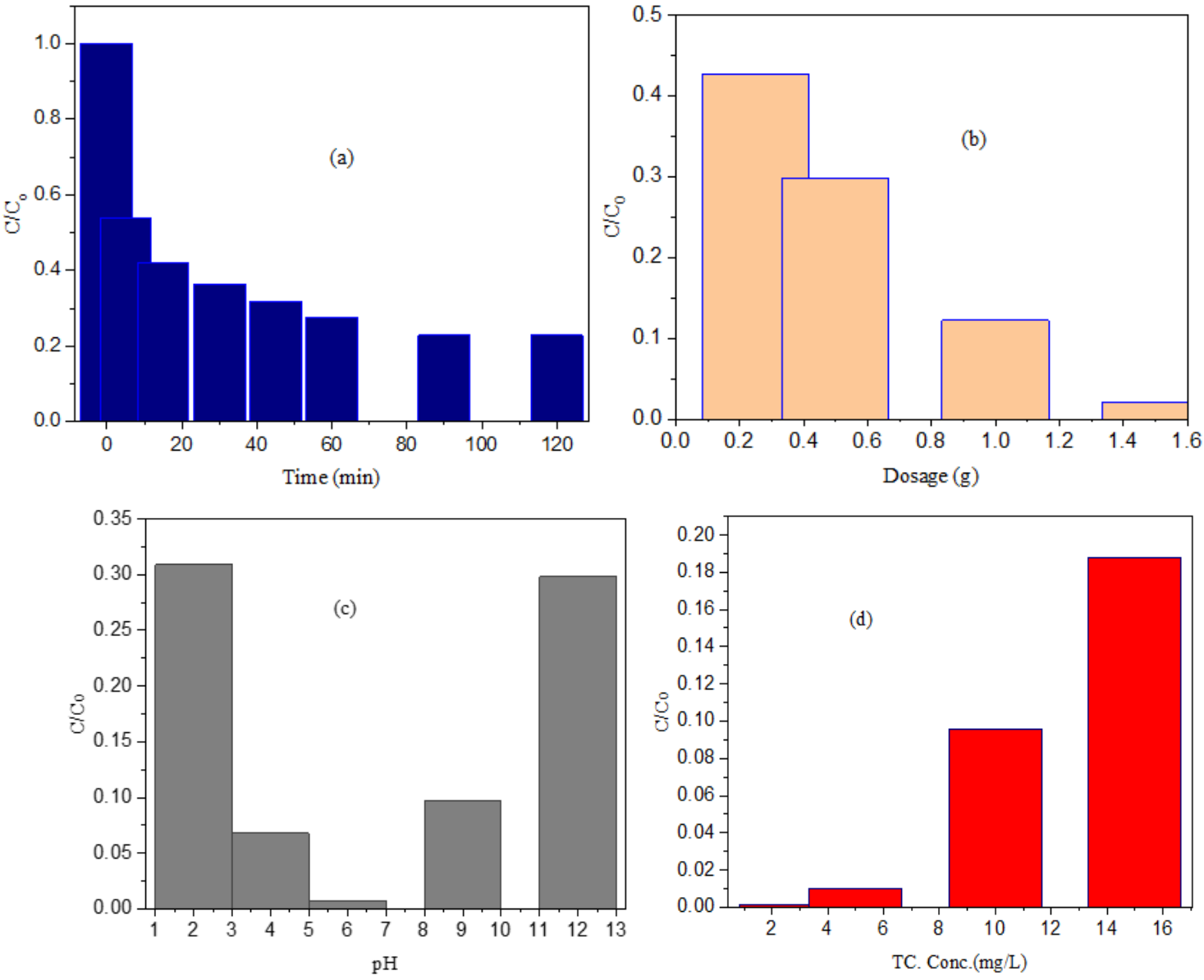

Figure 4-8 Plot of TC adsorption removal efficiency as a function of concentration ratio (C/Co) for (a) adsorption time, (b) solution pH, (c) adsorbent dosage, and (d) initial TC conc. (mg/L)

4.2.9 Effects of interaction parameters on TC adsorption removal efficiency

Figure 4.9 (a–f) illustrates the interplay between operating parameters and TC adsorption removal efficiency, considering solution pH, adsorption time, adsorbent dosage, and initial contaminant (TC) concentration.

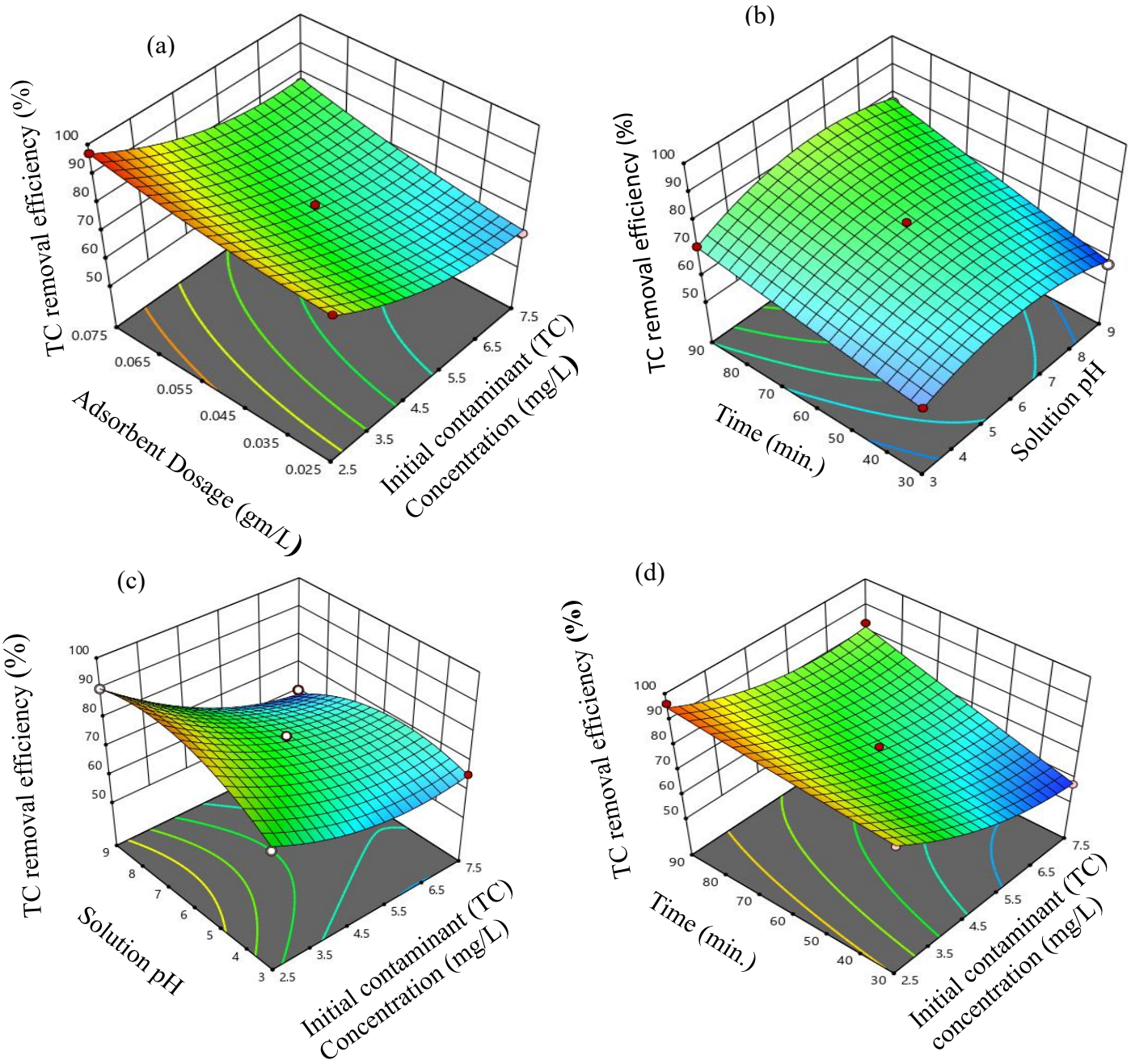

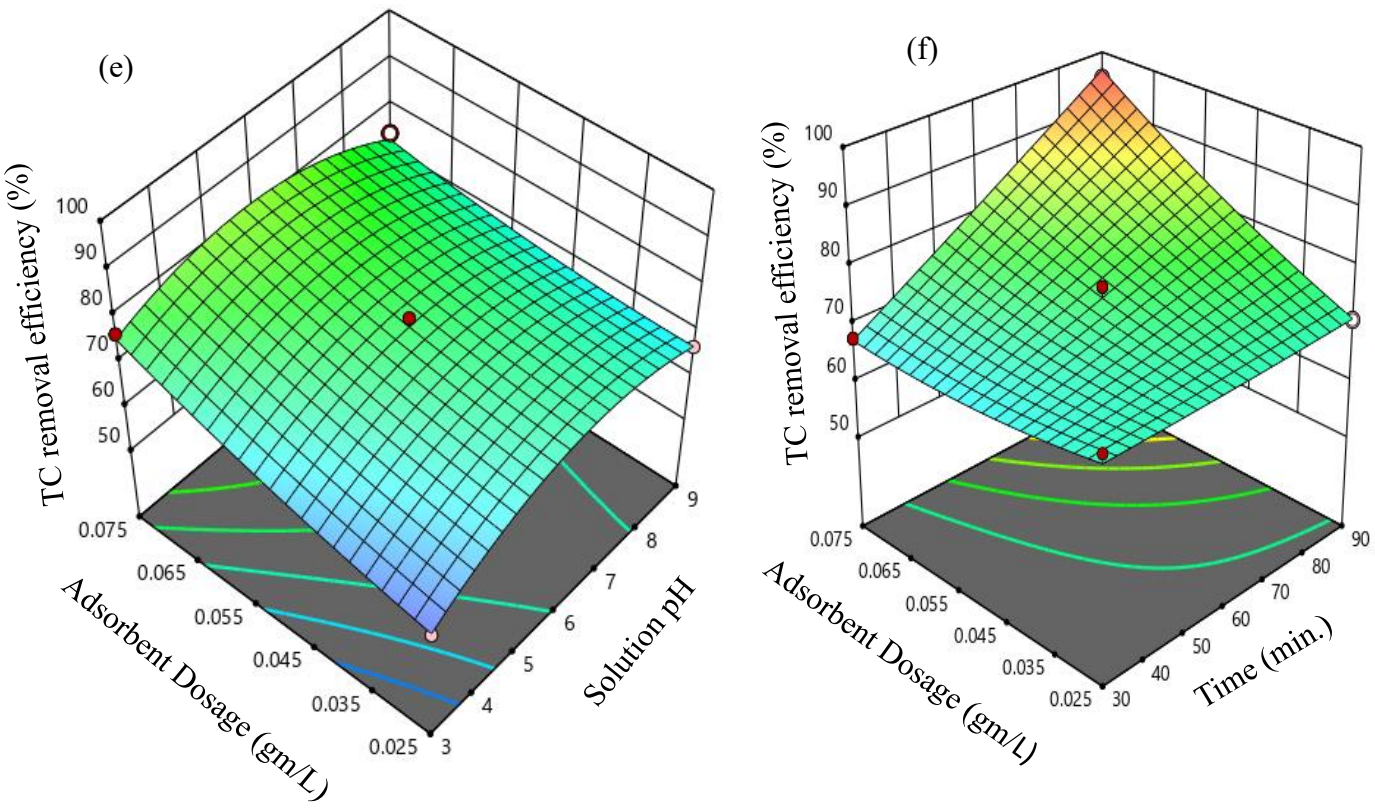

Figure 4-9 3D surface plot of TC removal efficiency as a function of (a) adsorbent dosage and initial TC concentration, (b) initial TC concentration and time, (c) solution pH and initial TC concentration, (d) time and initial TC concentration, (e) adsorbent dosage and solution pH and, (f) adsorbent dosage and time.

TC removal efficiency is influenced by complex interdependencies rather than isolated parameter effects, as demonstrated by the 3D response surface plots in Figure 4.9 (a–f). Figure 4.9 (a) illustrates the interaction between adsorbent dosage and initial TC concentration. While increasing the dosage enhances the number of active sites available for removal, this effect diminishes at higher initial concentrations, as the available sites quickly become saturated, resulting in a competitive environment for adsorption (Padmavathy et al., 2016). The interaction between solution pH and other factors (b, c, e) illustrates the sensitivity of the adsorption process to the electrostatic environment. As concentration increases, removal efficiency becomes more sensitive to pH changes. This indicates that to maximize attraction, the surface charge of the carbon derived from cassava must be precisely aligned with the molecular speciation of TC.

Additionally, Figure 4.9 (d, f) illustrates a synergistic relationship between adsorbent dosage and contact duration. A larger dosage can partially compensate for shorter contact times by increasing the number of collisions between the adsorbent and the contaminant. The curvature of these surfaces indicates that to achieve maximum removal, it is essential to optimize parameters in a synchronized manner. Specifically, maintaining a high dosage and sufficient contact time at a mid-range pH is crucial to overcoming the mass transfer resistance present at higher initial TC concentrations (Ngoc et al., 2023).

4.2.10 Optimizing and validating the model

Using a numerical optimization technique based on RSM-BBD, we determined the ideal process conditions for the adsorption removal of TC using CP/$ZnCl_2$ activated carbon. The primary goal was to estimate the maximum adsorption efficiency for TC removal. We employed Derringer's desired function approach (Luis Pérez, 2021), which ranges from 0 to 1, to assess the optimum conditions identified through RSM-BBD and evaluate how well these conditions fulfill the response's ultimate purpose.

To maximize TC removal efficiency, we conducted a single-factor analysis to establish the parameter ranges for solution pH, adsorption time, TC concentration, and adsorbent dosage. These parameters were maintained within the following ranges: pH 3 to 9, adsorption time 30 to 90 min, TC concentration 2.5 to 7.5 mg/L, and adsorbent dosage 0.025 to 0.075 g/L. Consequently, an optimal TC removal efficiency of 97.2% was projected for the ideal operating parameters: solution pH 6.45, adsorption time of 74.15 min, adsorbent dosage of 0.0592 g/L, and an initial TC concentration of 2.5 mg/L.

4.2.10.1 Adsorption isotherm studies

Models of isotherms can be used to study the adsorption of TC onto CP/$ZnCl_2$ activated carbon. Adsorption isotherm models enable an understanding of the interaction between liquid-phase adsorbate concentrations and solid-phase adsorption quantities. These models provide insight into the adsorption mechanism (Abumelha et al., 2023) by correlating the adsorption process using theoretical equations (Shokoohi et al., 2020).

In the current investigation, two well-known isotherm models, Freundlich and Langmuir, were examined using the optimal synthetic parameters to assess the adsorption properties of the CP/$ZnCl_2$ activated carbon particles. The isotherm constant parameters for both models were determined using the corresponding linearized equations (4.8) and (4.9).

$$\frac{C_e}{q_e} = \frac{1}{q_m k_L} + \frac{C_e}{q_m} \quad \text{.....(4.8)}$$

$$lnq_e = lnK_f + \frac{1}{n} lnC_e \quad \text{.....(4.9)}$$

Where C_e is the contaminant equilibrium concentration (mg/L), q_e is the equilibrium amount of contaminant adsorbed (mg/g), K_L and K_F are the Langmuir and Freundlich constants (L/mg), q_m is the maximum adsorbed quantity, and n is the Freundlich adsorption intensity constant. By plotting C_e/q_e versus C_e and ln (C_e) versus ln(q_e), the values of K_L, K_F, q_m, and n were calculated from the slopes and intercepts of the two equations Figure 4. 10 (a) and 4.10 (b). As shown in Table 4.6, the higher correlation coefficient value (R^2 = 0.9921) indicates that the Langmuir isotherm model fits the experimental data better the Freundlich isotherm model. The two models were selected as they represent the foundational standards for establishing baseline surface uniformity. The superior Langmuir fit physically indicates a homogeneous monolayer adsorption phenomenon, meaning that the composite features evenly distributed active sites that accommodate only a single layer of TC molecules.

Table 4-5 Isotherm models parameters for TC adsorption onto cassava peel-activated carbon

Isotherm Models	Constant parameters				Correlation coefficient
	q_m	K_L	K_F	n	R^2
Langmuir	5.71	5.72	-	-	0.9921
Freundlich	-	-	16.0	19.6	0.7376

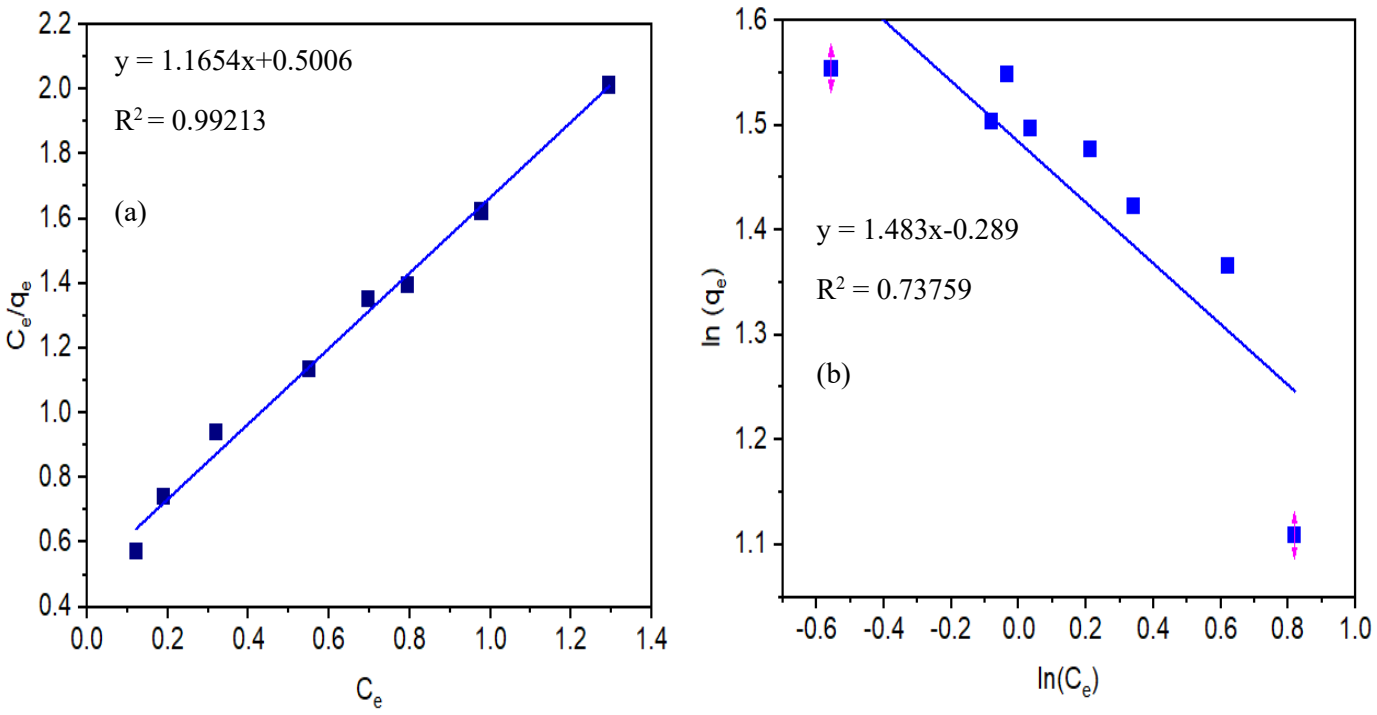

Figure 4-10 Adsorption isotherm models: (a) Langmuir and (b) Freundlich

4.2.10.2 Adsorption kinetics models

Since kinetics provides essential information about the rate of contaminant uptake, the design of adsorbents greatly benefits from studying the kinetics of the adsorption process (Zaher et al., 2020). In the kinetics investigation, interparticle diffusion, pseudo-first-order, and pseudo-second-order kinetic models (eqn. (4.10), (4.11), and (4.12)) were considered.

$$\mathrm{Log}(q_e - q_t) = \log q_e - \frac{K_1}{2.303} t \quad \text{(4.10)}$$

$$\frac{t}{q_t} = \frac{1}{k_2 q_e^2} + \frac{t}{q_e} \quad \text{(4.11)}$$

$$q_e = k_i t^2 + C_i \quad \text{(4.12)}$$

Where q_e is the TC adsorption removal amount at equilibrium, q_t is the degradation amount at any time t, C_i is the interparticle diffusion boundary layer thickness, and K_1, K_2, and K_i are the rate constants for pseudo-first-order, pseudo-second-order, and interparticle diffusion kinetic models.

Table 4-6 Table Pseudo-first-order, pseudo-second-order, and interparticle diffusion kinetic model parameters

Kinetics Model	Parameters	TC Concentration (mg/L)			
		2.5	5	10	15
Pseudo-first-order	k_1 (per min.)	0.311	0.0235	0.0215	0.020
	$q_{e\ cal}$ (mg/L)	2.484	3.77	7.58	12.57
	$q_{e\ exp}$ (mg/L)	2.28	4.99	8.933	14.64
	R^2	0.984	0.994	0.9617	0.976
Pseudo-second-order	K_2 (per min.)	0.329	0.019	0.016	0.013
	$q_{e\ cal}$ (mg/L)	2.21	3.56	4.21	4.24
	$q_{e\ exp}$ (mg/L)	2.43	2.53	5.33	5.32
	R^2	0.992	0.997	0.987	0.996
Interparticle diffusion	K_i	0.104	0.13	0.85	1.27
	C_i	0.8	2.06	4.33	7.10
	R^2	0.9435	0.817	0.9545	0.848

Table 4.6 demonstrates that a pseudo-second-order kinetic model best explains the reaction mechanism of TC adsorption removal on the adsorbent surface. The pseudo-second-order kinetic model provides crucial information regarding the nature of the binding forces. Its superior fit statistically approves that the rate-limiting step is chemosorption rather than physical tricking. According to this model, the quantity of TC removed at equilibrium (q_e) is nearly equal to the amount of TC adsorbed at any given time (q_t). The regulating step appears to be a chemical process involving valence forces through electron sharing or exchange between the adsorbent and TC ions, as indicated by the pseudo-second-order kinetic model.

Figure 4.11 shows that the constant K_1 for the pseudo-first-order model equation was determined from the straight-line plot of $\ln(q_e - q_t)$ versus time (Figure 4.11a). Plotting t/q_t against time allowed for the calculation of K_2 for the pseudo-second-order model (Figure 4.11b). Additionally, the interparticle diffusion kinetic parameter was calculated based on $t^{0.5}$ versus q_e (Figure 4.11c). The optimal reaction kinetic model was selected using the values of the correlation coefficient R^2. The kinetic parameters of the chosen models are presented in Table 4.7

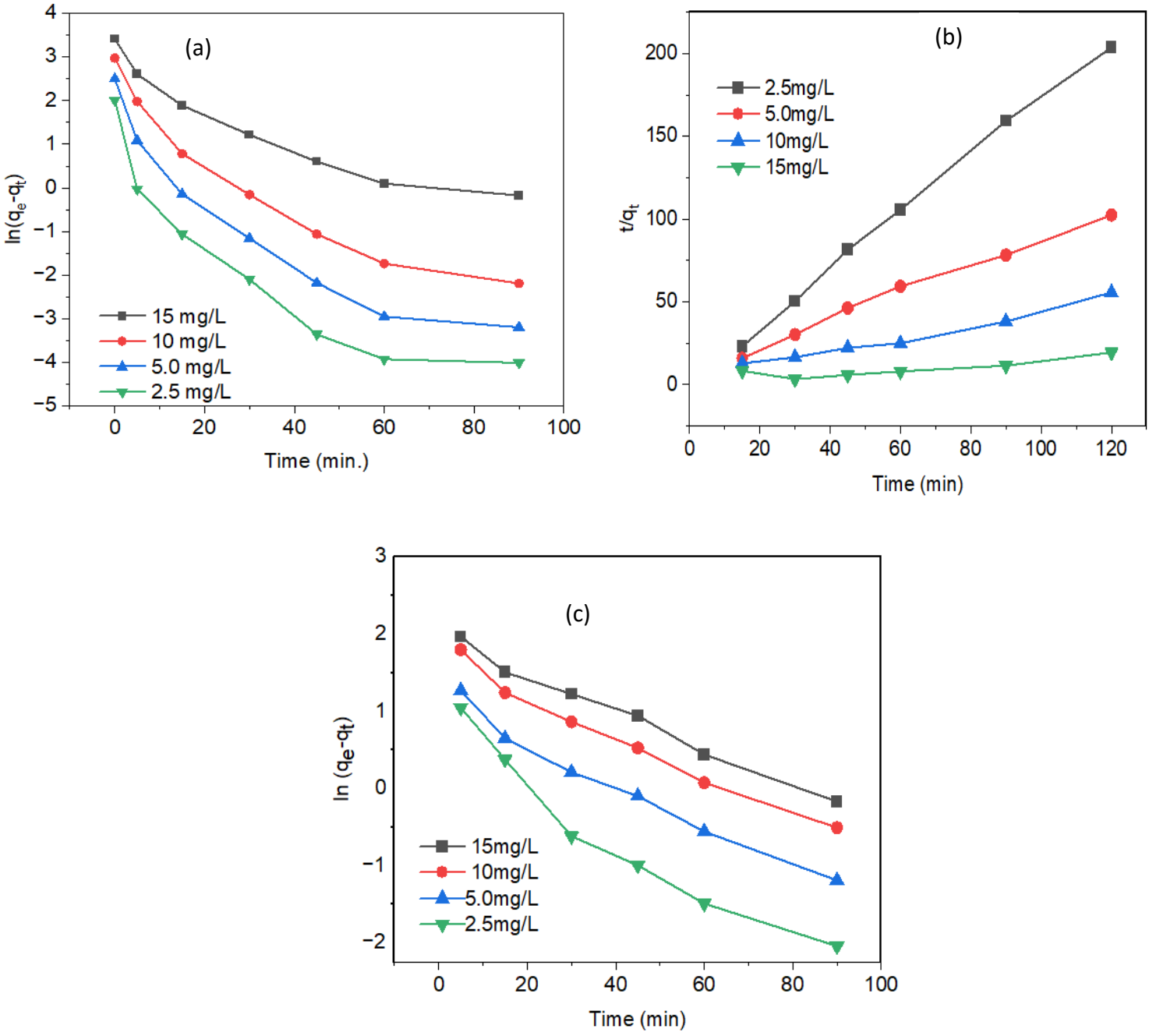

Figure 4-11 Reaction kinetics models of (a) pseudo-first-order, (b) pseudo-second-order, and (c) interparticle diffusion

In Figure 4.11, As the concentration gradient changes, the dominance of mass transfer and surface contact processes shifts, influencing the transition through various adsorption stages. A steep concentration gradient promotes rapid film diffusion and immediate occupancy of the most accessible, high-energy active sites on the adsorbent surface. This steep gradient is the primary

factor driving the rapid adsorption phase at low starting concentrations (0–2.5 mg/L) (W. Jia et al., 2025). The mechanism shifts to moderate and slow adsorption as the starting concentration increases (2.5–10 mg/L). During these phases, the external surface sites become saturated, prompting TC molecules to diffuse through intra-particle pathways into the internal micropores of the carbon produced from cassava.(H. O. Singh et al., 2025). This phase is characterized by higher mass transfer resistance and increasing electrostatic repulsion between zwitterionic TC molecules that have already been adsorbed and those still in the bulk phase. Under dynamic conditions, where the rate of adsorption equals the rate of desorption, the system ultimately reaches adsorption equilibrium at concentrations greater than 15 mg/L. This occurs as the chemical potential gradient decreases and the available surface area becomes fully saturated (Yao et al., 2026).

Additionally, to identify the best-fitting adsorption isotherm and kinetic models, several error function studies, such as sum square error (SSE), average relative error (ARE), sum of absolute error (SAE), and hybrid fractional error function (HFEF) are conducted using the following eqn. (4.13), (4.14), (4.15), and (4.16).

$$SSE = \sum_{i=1}^{n} \left(q_{e,i,(exp.)} - q_{e,i,(\,pred.)}\right)^2 \quad \text{.....(4.13)}$$

$$ARE = \sum_{n=1}^{n} \left(\left| \frac{q_{e,i\,(\exp.)} - q_{e,i\,(pred.)}}{q_{e,i\,(exp.)}} \right| * 100 \right) \quad \text{.....(4.14)}$$

$$SAE = \sum_{i=1}^{n} \left| q_{e,i,(\exp.)} - q_{e,i\,(pred.)} \right| \quad \text{.....(4.15)}$$

$$HFEF = \frac{1}{n} \sum_{i=1}^{n} \left(\frac{\left| q_{e,i\,(exp.)} - q_{e,i,(pred.)} \right|}{q_{e,i\,(exp.)} + q_{e,i,(pred.)}} \right) \quad \text{.....(4.16)}$$

Where $q_{e,\,I\,(exp)}$ is the actual measured adsorption value, $q_{e,\,i(pred.)}$ is the predicted adsorption value, and n is the number of data points.

Table 4-7 Error function analyses for model selection

	Error function			
Kinetics Models	SSE	ARE	SAE	HFEF
Pseudo-first-order	0.38	10.6	0.48	0.34
Pseudo-second-order	0.26	7.25	0.32	0.24

Table 4.7 indicates that the pseudo-second-order model best fits the data when compared to the pseudo-first-order model based on the TC concentration difference, as evidenced by its lower SSE, ARE, SAE, and HFEF values.

The statistical superiority of the pseudo-second-order (PSO) model over the pseudo-first-order model is confirmed by the error function analysis presented in Table 4.7. The PSO model demonstrates greater effectiveness in reducing the variation between experimental data and theoretical predictions, as indicated by consistently lower values for SSE (0.26), ARE (7.25), SAE (0.32), and HFEF (0.24). This improved fit suggests that chemisorption, characterized by valence forces through electron sharing or exchange between the contaminant molecules and the functional groups on the carbon surface derived from cassava, is the primary mechanism governing the rate-limiting phase of TC adsorption (Beltrán et al., 2025).

4.3 Conclusions

The current investigation utilized activated carbon produced from cassava peels using the sol-gel method to examine the adsorption of TC. The efficiency of TC adsorption removal was optimized through the use of BBD-RSM and ANN, focusing on selected significant ranges of operational parameters derived from single-factor analysis. These parameters included solution pH (3 to 9), adsorption time (30 to 90 min), adsorbent dosage (0.025 to 0.075 g/L), and initial TC concentration (2.5 to 7.5 mg/L). The findings revealed that the optimal parameters were as follows: a maximum TC adsorption removal efficiency of 97.45%, a solution pH of 7.49, an adsorption time of 74.15 min, an adsorbent dosage of 0.059 g/L, and an initial TC concentration of 2.5 mg/L.

The ANN predicts a 96.92% effectiveness in TC adsorption removal under ideal conditions. Both the RSM and ANN approaches demonstrated stronger correlation coefficients in predicting the process conditions. The optimal topology for the ANN modeling technique was identified as a three-layer perceptron network (4-8-1 configuration for TC adsorption removal), which exhibited very low test, training, and validation errors. Furthermore, the characteristics of the synthesized adsorbent were accurately represented using pseudo-second-order kinetic models and the Langmuir adsorption isotherm. In addition to improving the understanding of the adsorption process, the machine learning method outperformed the best optimization techniques in both accuracy and speed (Ullah et al., 2023).

5. PARAMETRIC OPTIMIZATION AND KINETICS OF PHOTOCATALYTIC TETRACYCLINE ABATEMENT FROM AQUEOUS SOLUTION USING *CITRUS BERGAMIA* LEAF EXTRACT-MEDIATED ZnO-NPS

5.1 Introduction

The increasing frequency of drugs in sewage has become a critical environmental concern, since residues of pharmaceuticals like TC can cause unwanted effects on human health and aquatic life (Aljeboree et al., 2020). TC antibiotics are a class of broad-spectrum antibiotics containing phenanthrene cores that have been extensively used to treat infections caused by most Gram-positive and Gram-negative bacteria since the 1940s (Wu et al., 2020a). These residues have been detected in various water sources; therefore, effective treatment methods must be employed to mitigate their impact.

Thus, the development of highly efficient, cost-effective, and environmentally friendly methods for mineralizing TC from wastewater is crucial to conserve water resources and achieve sustainable development goals. AOP utilize heterogeneous photocatalysis to oxidize organic and inorganic compounds fully (X. Li et al., 2023). Photocatalysis, which is based on light-activated semiconductors, is the most environmentally benign and promising method for treating wastewater (Rana et al., 2024). Although ZnO-NPs have shown incredible effectiveness in photo-catalytic degradation of TC and other pharmaceutical contaminants, particle agglomeration, surface area, and lack of stability in aqueous medium may limit their efficiency (Fouda et al., 2023).

In this study, ZnO-NPs were modified, and the photocatalytic efficiency and stability in solution were enhanced using *Citrus bergamia* leaf extract, which not only improved the physicochemical properties of ZnO-NPs but also stabilized the nanoparticles (Mahlaule-Glory & Hintsho-Mbita, 2022). Previous studies have explored the photocatalytic degradation of TC using ZnO-NPs. However, there is a notable lack of comprehensive analyses that incorporate process optimization through RSM-BBD approaches, specifically for ZnO-NPs synthesized with *C.bergamia* leaf extract (Alshahateet et al., 2024).

Furthermore, the degradation process using these modified ZnO-NPs has not been fully examined, and this disparity presents a substantial opportunity to enhance operational circumstances for greater effectiveness and expand our understanding of the mechanisms underlying photodegradation.

The application of RSM-BBD has the potential to determine the optimal conditions for TC mineralization and study complex relationships between analysis of variables (ANOVA). RSM-BBD provides an excellent basis for optimizing unknowns of catalyst dose, initial TC concentration, solution pH, and irradiation time, and producing better predictive abilities and optimizations for future photocatalytic processes (Kassahun et al., 2021). The scope of this study combines both approaches to assess the photocatalytic degradation of TC and TOC removal efficiency, providing a more sustainable and efficient wastewater treatment approach using *C. bergamia* leaf extract-modified ZnO-NPs.

5.2 Materials and methods

5.2.1 Materials

C. bergamia leaves were obtained from the Gullelle botanic garden in Addis Ababa, Ethiopia. NaOH pellets with a purity of 99.0 %, zinc acetate (CH_3COO) $2Zn \cdot 2H_2O$ with an assay of 98.0 %, and powdered TC hydrochloride ($C_{22}H_{24}O_8N_2.HCl$) with a purity of 98 %, absolute ethanol (CH_3CH_2OH, > 99 %) and hydrochloric acid (HCl, 34.5 %) were purchased from market.

5.2.2 Preparation of the extract

Based on Abomuti et al. (2021), the leaves of *C.bergamia* were collected, crushed, and cleaned with distill water before being dried for 12 hours at 40°C in an oven. For the aqueous extract, 100 g of the dried leaves were ground into particles sized between 63 and 150 µm. The ground leaves were then transferred to a 500 mL beaker containing 250 mL of distilled water. The beaker was heated to 60°C using a heater equipped with a magnetic stirrer, which caused the solution's color to change as the leaf extract developed. The mixture was subsequently stored overnight in an airtight bottle and filtered through Whatman No. 1 filter paper (Manyazewal et al., 2025a).

5.2.3 Mediated synthesis of ZnO-NPs

ZnO-NPs were synthesized using the sol-gel method following (Abomuti et al., 2021). The precursor materials used were zinc acetate dihydrate $(CH_3COO).2Zn.2H_2O$, of the highest purity, and C. bergamia leaves obtained. Additionally, sodium hydroxide (NaOH) was used (Rafique et al., 2021). Accordingly to (Ramesh et al., 2022), the synthesis of ZnO-NPs commenced with 50 mL of aqueous zinc nitrate solution (0.2 M) placed in a 250 mL beaker, then continuously stirred at 50 °C for 2 hrs. The C. bergamia leaf aqueous extract (50 mL) was added to the zinc nitrate solution as it was continuously stirred and maintained at the same temperature. The experimental mixture turned light yellow as the phytochemicals present in the extract capped the Zn^{2+} ions and triggered the nucleation of ZnO-NPs (Rupa et al., 2019). In step two, a new NaOH (2.0 M) solution was added dropwise to the reaction mixture (pH 10-12) at 50 °C under continuous stirring.

Based on the Faisal et al., (2021) ,the reaction mixture was stirred for the next 2 h at 50 °C, which yielded light yellowish precipitation that indicated the synthesis of ZnO-NPs. The reaction mixture was centrifuged for 1 h at 4000 rpm to collect the final product. To remove any other contaminants or unreacted components from the surface of the biosynthesized material, the precipitate was repeatedly cleaned with ethanol and distilled water. To ensure total dryness, the synthesized material was placed in an oven set to 80 °C for 24 h in the final step (as shown in Figure 1). The dehydrated ZnO-NPs were annealed for 2 h at 450 °C in a muffle furnace. The resulting fine, light-cream-colored ZnO-NP powder was used for surface characterization and further study.

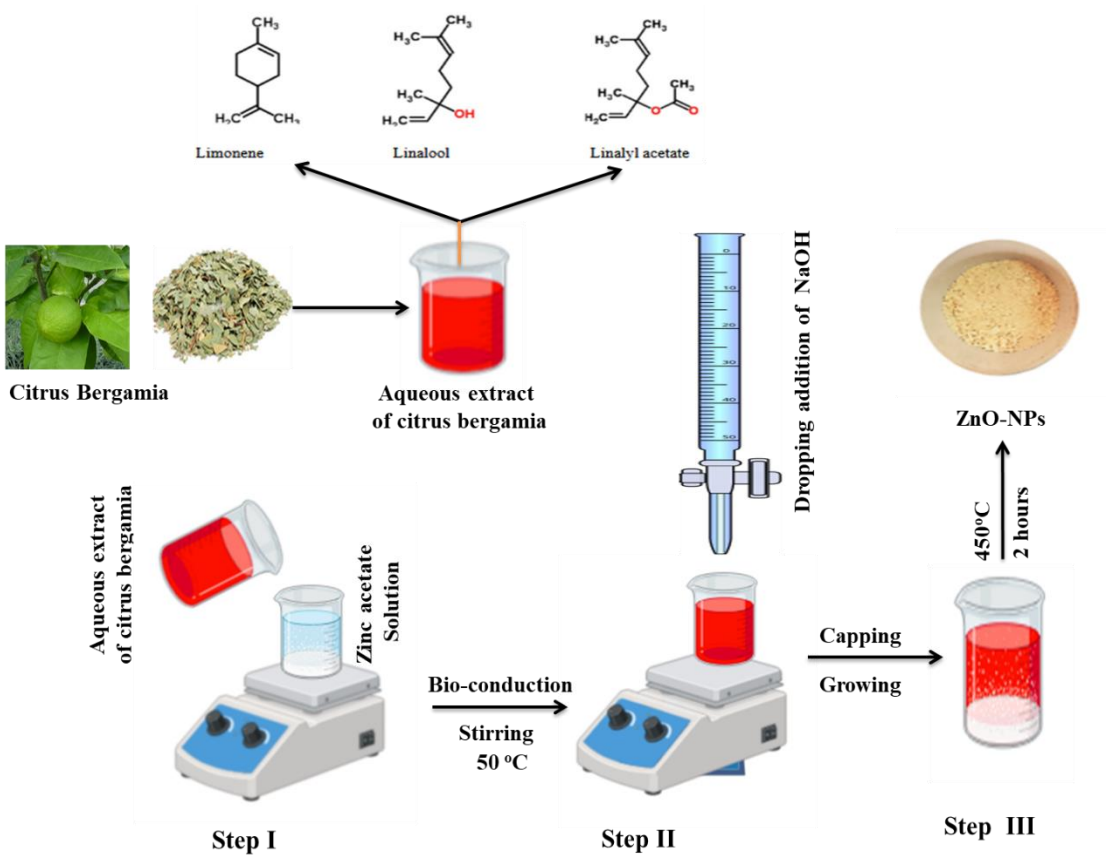

Figure 5-1 Diagrammatic illustration of the *Citrus bergamia* leaf extract-based fabrication of ZnO-NPs.

5.3 Photocatalytic test of TC

There is theoretical evidence that the UV light absorbed by the ZnO photocatalyst can produce pairs of a positive hole and a negative electron (Morshedy et al., 2024). While the negative electrons in ZnO react with the oxygen molecules to form superoxide radicals, the positive holes in ZnO break the water molecules to produce hydrogen ions and hydroxyl radicals. Organic substance is quickly oxidized by superoxide and hydroxyl radicals (Gurylev & Perng, 2021). TC is thus photocatalyzed into low-molecular-weight intermediates when UV/vis is shone on the reaction system (Mohmad Ameran et al., 2025).

The photocatalytic activity of the modified ZnO-NPs catalysts was evaluated in a 250 mL borosilicate glass slurry-type reactor while being exposed to visible light (at a light intensity of 14.41 mW/cm^2) using a radiometer (Analytikjena, UVX-25Sensor Probe Assy 254 nm). Irradiation was performed at the top of the reactor (10 cm from the light source) using a Sankyo Denki (BESTEC model, BJ2015M11CGL 1800) with a 14.5 W UV/vis.

Before each experiment, the solution was mixed in the dark for 30 min and oscillated to guarantee adsorption equilibrium (Manju et al., 2025). After the specified irradiation time, approximately 3.5 mL of solution was taken and filtered from the suspended catalyst using a 0.2 μm syringe filter. The TC concentration was determined using a UV/visible spectrophotometer (V-730 UV/visible/NIR spectrophotometer) at a wavelength of 360 nm. The photocatalytic efficiency at adsorption capacity (q_t) at time (t) was calculated from Eqn. (5.1) and (5.2) (L. Ma et al., 2023).

$$E\ \% = \frac{C_i - C_f}{C_i} * 100 \quad \text{.....(5.1)}$$

$$q_t\left(\frac{mg}{g}\right) = \frac{C_i - C_t}{m} * V \quad \text{.....(5.2)}$$

where C_i and C_f are the concentrations of TC at the initial and final irradiation times, respectively. V is the volume of the treatment sample, C_t is the concentration of the adsorbate remaining in the solution at a specific time after the adsorption process has started, and m is the mass of the adsorbent material used in the experiment. The experimental design method known as the response surface method RSM-BBD was used to modify the chosen process parameters, which included irradiation time, catalyst load, initial contaminant concentration, and solution pH, as shown in Table 5.1 (Kassahun et al., 2021).

Table 5-1 Factors and stages of experimental investigations

Factor	Name	Unit	Study range	
			Minimum	Maximum
A	Initial TC concentration	mg/L	5	15
B	pH	pH	5	7
C	Time	Min	30	120
D	Catalyst Dose	gm/L	0.5	1.5

Designated process parameters, including irradiation duration, catalyst load, and solution pH, were adjusted using the RSM-BBD experimental design method, as shown in Table 5.1. The studies were conducted using a completely randomized design with four parameters (solution pH, irradiation time, catalyst dose, and initial TC concentration) at three levels of response and two responses (TC degradation and TOC removal efficiency), as indicated in Table 5.2. The relationship between the independent variables and the responses was determined using second-order polynomial equations (Ryu & Jeong, 2020). The general equation for the three experimental elements that were chosen is as follows Eqn. (5.3).

$$Y = \beta_{\circ} + \sum_{i=1}^{k} \beta_i X_i + \sum_{i=1}^{k} \beta_{ii} X_i^2 + \sum_{1 \leq i \leq j} \sum \beta_{ij} X_I X_j + \varepsilon \quad (5.3)$$

where Y is the experimental response, X_i and X_j are the experimental variables or factors, β_o is a constant, β_i,β_{ii}, and β_{ij} are the regression coefficients for linear interaction effects, quadratic interaction effects, and cross-product interaction effects, respectively, and ε is the random error. Regression analysis and coefficient estimation were conducted using Design-Expert version 13.0.1.0 (Stat-Ease, Inc.) (Kassahun et al., 2021).

The performed an analysis of variance (ANOVA) to evaluate the adequacy of the model equations (X. Li et al., 2022). Assessed the quality of fit and statistical significance of the model equations using the F-test, coefficient of determination (R^2), prediction coefficient of determination (Pred R^2), adjusted coefficient of determination (adj-R^2), and coefficient of variation.

Table 5-2 Experimental runs arranged according to BBD-RSM

Run	Factors				Responses	
	A: Initial TC. Concentration (mg/L)	B: solution pH	C: Irradiation Time (min.)	D: Catalyst dosage (g/L)	TC Degradation efficiency (%)	TOC Removal efficiency (%)
1	10	5	120	1	92.17	70.17
2	5	6	75	0.5	66.38	45.66
3	10	6	75	1	78.86	57.89
4	5	6	120	1	87.19	64.91
5	5	6	75	1.5	85.56	63.45
6	10	5	30	1	60.47	42.75
7	15	6	75	1.5	50.78	37.19
8	10	6	75	1	78.79	61.54
9	10	6	30	1.5	80.32	59.65
10	10	6	120	0.5	91.06	68.28
11	10	5	75	1.5	83.87	61.59
12	15	6	120	1	59.81	40.85
13	10	5	75	0.5	70.13	52.63
14	10	6	75	1	81.08	62.47
15	10	7	30	1	74.94	57.32
16	10	6	75	1	80.53	61.01
17	5	6	30	1	63.97	46.97
18	5	5	75	1	54.99	38.88
19	15	6	30	1	48.44	32.67
20	5	7	75	1	85.20	64.01
21	15	6	75	0.5	58.34	41.95
22	10	6	75	1	80.18	60.99
23	15	7	75	1	32.39	27.72
24	15	5	75	1	*64.61*	47.08
25	10	6	30	0.5	65.73	48.17
26	10	7	75	0.5	75.02	59.07
27	10	6	120	1.5	*82.63*	63.11
28	10	7	75	1.5	68.71	50.96
29	10	7	120	1	70.21	53.64

The following eqn. (5.4), (5.5), and (5.6), metrics necessary to critically assess model predictive ability and as well as reliability. The coefficient of determination (R^2) indicates how well the model describes the experimental data. The model accurately represents the real process when the value is closer to 1.0. RMSE and AAD are metrics that evaluate the discrepancy between the actual lab results and the model's predictions. Values closer to zero indicate greater accuracy and reliability in the model's predictions (Chicco et al., 2021). These hold a promise for strong statistical validation of model accuracy and robustness: a high R^2 value with low AAD and RMSE values. The model is confirmed to be appropriate to predict and optimize the photocatalytic degradation of TC using Citrus bergamia leaf extract-amended ZnO NPs under various operating conditions (Chicco et al., 2021).

$$R^2 = 1\frac{\sum_{i=1}^{n}(y_{Ai}-y_{Pi})^2}{\sum_{i=1}^{n}(y_m-y_{Pi})^2} \quad \text{.....(5.4)}$$

$$\text{RMSE} = \sqrt{\sum_{i=1}^{n}\frac{(y_{Ai}-y_{Pi})^2}{n}} \quad \text{.....(5.5)}$$

$$\text{AAD} = \frac{1}{n}\sum_{i=1}^{n}*\frac{|y_{Ai}-y_{Pi}|}{y_{Pi}} \quad \text{..... (5.6)}$$

Where y_A is the actual value, y_P is the predicted value, n is the number of data points, and y_m is the average value.

5.4 Reusability

According to Nuraishah et al. (2025), the reusability and stability of *C. bergamia* extract-synthesized ZnO-NPs were, therefore, tested in five steps post-photocatalysis, where the samples were scanned using a UV-VIS-NIR Spectrophotometer over the wavelength range of 360 nm. In every run, the degradation test was carried out by constant illumination for 2 h. After every run, the photocatalyst was centrifuged from the aqueous solution. Subsequently, the respective pellets were washed with deionized water, and excess water removal was done by centrifugation at 6000 RPM for 10 min. Further purification was made by washing the pellet with excess distilled water and subsequently an ethanol wash to remove any probably adsorbed TC or intermediate reaction species.

For cleaning, the sample was kept in an oven for 2 h. at 105 °C and then placed in a fresh TC solution to carry out the second degradation run, similar to the first. The TC degradation efficiencies were recorded after each of the five cycles, thus proving the stability and sustained activity of the ZnO-NPs (Abdullahi Ari et al., 2023a).

5.5 Results and discussion

5.5.1 Characterization of *C. bergamia* leaf extract and modified ZnO-NPs

Table 5.3 shows the factors of *C. bergamia* leaf extract in the surface area, pore volume, and pore size distribution in a previous study (Manyazewal et al., 2025a).

Table 5-3 Effect of *C. bergamia* leaf extract and zinc acetate precursor on the BET surface area of ZnO-NPs.

No.	Sample	Calcination		S_{BET} (m^2/g)
		Time (hrs.)	Temperature (°C)	
1	ZnO-NPs precursor (Zinc acetate)	2	450	362.251
2	ZnO-NPs modified with *C. bergamia* leaves extract	2	450	371.213

According to Maziarka et al. (2021), BET analysis of the specific surface area, pore volume, and pore size distribution, which relied on the normal BET equation (NLDFT method), was measured by N_2 adsorption in the relative pressure (P/P_0) range of 0.06 to 0.3. The specific surface area of the green-modified ZnO-NPs was slightly larger than that of the ZnO precursor, despite unchanged conditions; this could be attributed to the different characteristics of the *C. bergamia* leaf extract used. This method produces highly stable ZnO-NPs; no noticeable changes were observed even after several months (Storage & Applications, 2023). The data presented in Table 5.3 provide a high surface area (BET) value of 371.213 m^2/g, corresponding to quasi-spherical particles derived from the citrus bergamia leaf extract and the $CH_3COO.2Zn\cdot 2H_2O$, which was obtained at a calcination temperature of 450 °C for 2 h.

This value is greatly more than the previous recorded model at 101.32 m^2/g (Shamhari et al., 2018), indicating the availability of interactions with active sites for chemical reactions with the nanoparticles or other compounds (Barzinjy & Azeez, 2020).

5.5.1.1 FT-IR analysis of *C. bergamia,* leaf ZnO-NPs, and modified ZnO-NPs.

FT-IR spectra help in validating the synthesis and surface modification of ZnO-NPs with *C. bergamia* extract Figure 5.2. There was a prominent broad band at 3320 cm^{-1} corresponding to phenolic compounds, alcohols, and absorbed water O-H stretching vibrations (Alamdari et al., 2020). The peak at 2920 cm^{-1} is due to the C-H stretching of aliphatic groups present in several organic molecules. Furthermore, the absorption at 1735 cm^{-1} indicates C=O (carbonyl) stretching from aldehydes, ketones, or carboxylic acids, whereas the peak at 1050 cm^{-1} can be assigned to C-O stretching (Benaiche et al., 2025). These functional groups are characteristic of flavonoids, terpenoids, and other polyphenols commonly found in citrus extracts, which are effective reducing and capping agents in nanoparticle synthesis (Gruca et al., 2024).

The FT-IR spectrum, Figure 5.2, shows that unmodified ZnO-NPs have a distinctive profile, characterized by a sharp and intense absorption peak at about 400 – 455 cm^{-1}range. This peak corresponds to the vibrational mode associated with the Zn-O bond in the wurtzite crystal structure of zinc oxide, confirming the successful synthesis of inorganic nanoparticles (K et al., 2025). The lack of other significant peaks relative to the extract indicates the purity of the synthesized ZnO-NPs material before modification. The simplicity of this spectrum provides a clear baseline for detecting changes during surface modification with the plant extract (Jayachandran et al., 2021).

A comparative analysis of all these spectra confirmed the successful functionalization of the ZnO-NPs. Significant overlaps are observed in both the plant extract and the bare nanoparticles, with the broad absorption in the 400-600 cm^{-1} range capturing the essential Zn-O vibration, thus confirming the integrity of the ZnO-NPs core (K et al., 2025). Most importantly, the characteristic peaks of the *C. bergamia* extract are retained in the modified ZnO-NPs spectrum, in Figure 5.2, including the broad O-H band around 3430 cm^{-1}, the C-H stretch at 2920 cm^{-1}, and the C=O peak at 1735 cm^{-1} (Alamdari et al., 2020).

The presence of these organic functional groups indicates that phytochemicals from the extract are effectively adsorbed or chemically bonded to the surface of the ZnO-NPs and serve as capping agents. As this surface modification enhances colloidal stability for the nanoparticles, more photocatalytic efficiency is expected from it in degrading TC through improved adsorption and facilitated charge transfer processes (Karam & Abdulrahman, 2022).

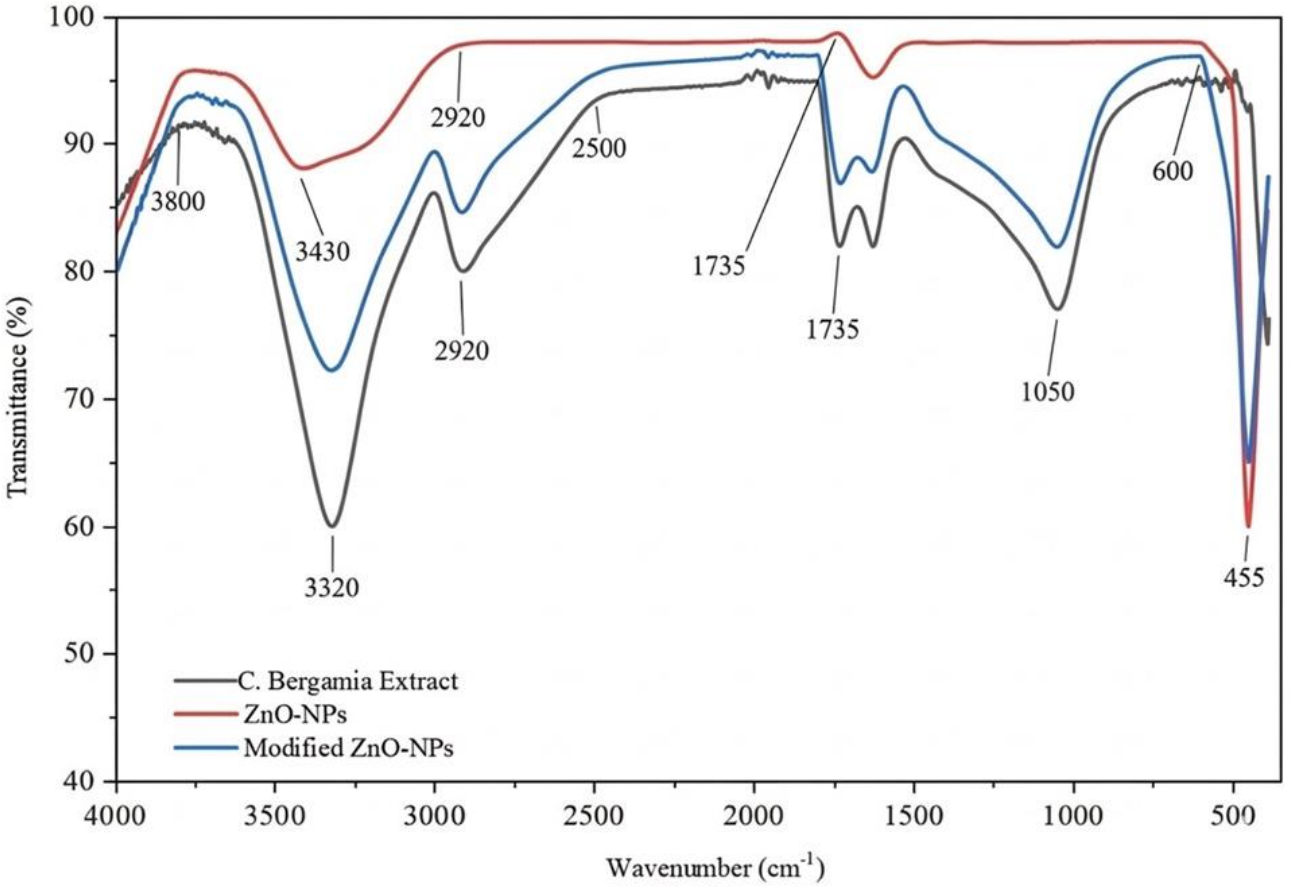

Figure 5-2 FT-IR spectrum of *C. bergamia* leaf extract, Pure ZnO-NPs, and modified ZnO-NPs

5.5.1.2 UV-Vi's analysis of *C. bergamia* ZnO-NPs, and modified ZnO-NPs

In Figure 5.3, spectra in the UV-vis range reveal the optical properties of the synthesized materials and confirm the modification of ZnO-NPs with *C. bergamia* extract. The absorption spectrum of the aqueous C. bergamia extract exhibits a broad peak centered at approximately 250 and 350 nm (Dattola & Gullo, 2024), and between 340 and 370 nm, indicating the presence of flavonoid peaks (Mapuranga et al., 2023). This broad absorption range is common with the rich phytochemical profile of *citrus* extracts, which includes phenolic acids and aromatic compounds (Formisano et al., 2019). These compounds contain chromophoric groups that absorb UV light and play a role in reducing zinc precursors and stabilizing or capping the formed nanoparticles (Pierdomenico et al., 2023).

The unmodified and modified ZnO-NPs demonstrate the successful synthesis and surface functionalization, as evidenced by their optical properties. ZnO-NPs exhibit a sharp, well-defined excitonic absorption peak at 378 nm, which is characteristic of the wurtzite hexagonal structure of crystalline ZnO-NPs (Tiwari et al., 2024). On the contrary, ZnO-NPs modified with *C. bergamia* extract show a peak of absorption largely shifted to 370 nm. This shift of the absorption maximum toward a shorter wavelength (higher energy) is referred to as a blueshift (Dey et al., 2025). By adhering to the surfaces of nucleated particles, several phytochemicals found in *C. bergamia* extract, primarily polyphenols and flavonoids such as limonene and linalool, function as capping agents. This steric barrier prevents agglomeration and halts further crystal formation. As a result, the extract produces smaller, more homogeneous nanoparticles by interrupting the development phase early (Muhammad et al., 2019).

However, the modified ZnO-NPs will be preferred for photocatalysis for another reason, leading to a smaller particle size. Smaller particles provide a higher surface-area-to-volume ratio, offering more active sites for adsorption and degradation of TC molecules (Rasheed et al., 2025). Additionally, the organic capping layer from the *C. bergamia* extract on the NPs' surface may also boost photocatalytic efficiency by trapping photogenerated electrons, preventing quick recombination of electron-hole pairs, and encouraging the formation of highly reactive oxygen species (ROS) such as hydroxyl and superoxide, which are crucial for breaking down stubborn organic pollutants like TC (Rodríguez-Flores et al., 2025).

Therefore, using *C. bergamia* extract not only offers an environmentally friendly synthesis method but also alters the nanoparticles toward improved structural and electronic qualities, indicating enhanced photocatalytic performance in degrading TC compared to their unmodified versions (Abdullahi Ari et al., 2023b).

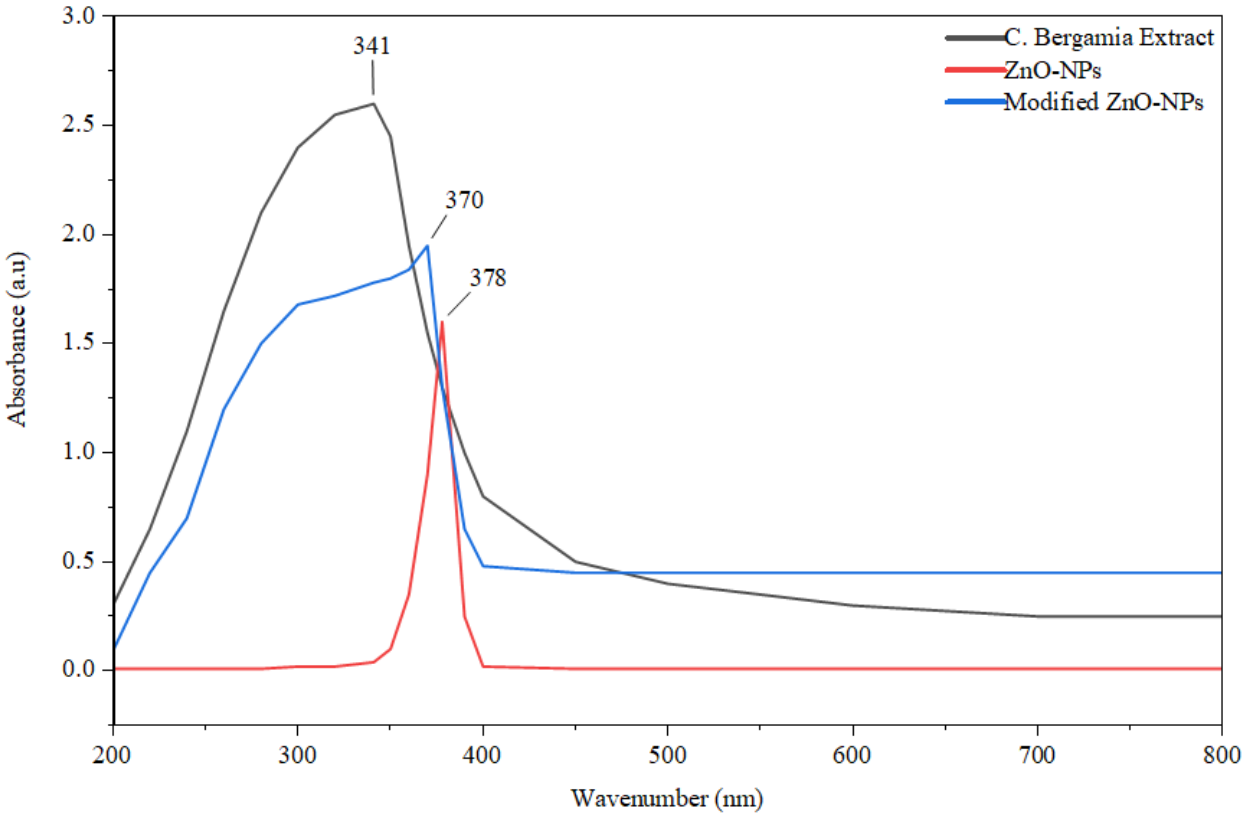

Figure 5-3 UV-Vis's absorption spectra of *C.bergamia,* ZnO-NPs, and modified ZnO-NPs

5.5.1.3 Band gap energy of modified ZnO-NPs

Figure 5.4 provides a Tauc plot; the energy band gap (Eg) is estimated by projecting the linear part of the curve to the energy axis, where $(\alpha h\nu)^2$ is equal to zero. The tangent line drawn on the diagram intersects the x-axis (Energy) at around 3.15 eV. This value is consistent with the frequently reported band gap energy for ZnO-NPs synthesized using green methods (Umamaheswari et al., 2021).

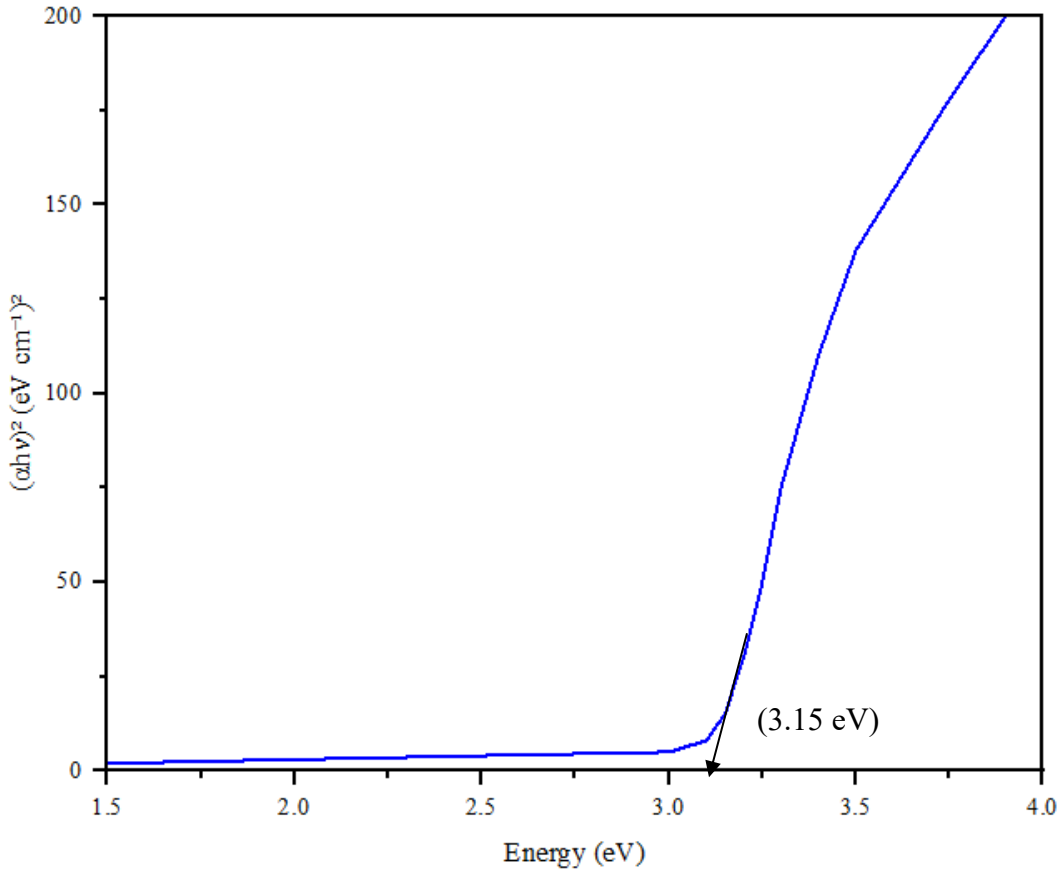

Figure 5-4 Tauc plot of ZnO-NPs for calculating the optical band gap energy (eV).

Based on the, Karam and Abdulrahman (2022), the Tauc plot method was used to determine the band gap energy of the modified *C. bergamia* ZnO-NPs prepared at a calcination temperature of 450 °C, and the calcination time was 2 h based on the provided wavelength (nm) and absorbance (%) data. The Tauc plot relates the absorption coefficient (α) to the photon energy (hν) as shown in the following Eqn. (5.7).

$$(\alpha h\nu)^2 = A(h\nu - E_x) \quad \text{.....(5.7)}$$

Where $(\alpha h\nu)^2$ = (absorbance × hν)², A = constant, h is Planck's constant ($6.626*10^{-34}$ J.s), n is dependent on the transition; for direct, n = ½, and indirect, n = 2, and E_x is the band gap energy.

To determine the band gap energy, plotted $(\alpha hv)^2$ as a function of photon energy (hv) and determined the intercept on the x-axis, which corresponds to the band gap energy (E_x). Calculated $(\alpha hv)^2$ using the provided data in Figure 5.4.

In this study, the data provided were lower than the reported value of 3.37 eV elsewhere (Meena et al., 2022). Plant extracts (*C. bergamia* leaves) consist of a variety of phytochemicals (such as flavonoids, terpenes, and polyphenols) that introduce more organic molecules into the reaction. These organic materials serve as natural capping and reducing agents to facilitate nanoparticle growth; however, they also introduce surface defects or strain at the surface of the crystal lattice (Motelica et al., 2023). These structural changes and surface defects can create additional energy levels within the band gap, thereby decreasing the optical band gap and lowering the overall band gap. Therefore, in Figure 5.4, a band gap of 3.15 eV was useful because these ZnO-NPs were able to be used for photocatalytic applications (Adnan et al., 2024).

5.5.1.4 Analyzing X-ray diffraction (XRD) of ZnO-NPs

In the 2Θ range of 10° to 75°, where diffractogram patterns were recorded by X-ray diffraction (XRD), the ZnO-NPs were found free of impurities (Figure 5.5). The standard X-ray diffraction (XRD) data for ZnO-NPs reveal that the peaks in the pattern conform well to the hexagonal wurtzite crystal structure, as per the standard reference data from the Joint Committee on Powder Diffraction Standards (JCPDS) card no. (36-1451) (Rahat Al Hassan et al., 2021). As widely referred to as the standard of ZnO-NPs, the peaks in the pattern are specific to particular crystal planes associated with the Miller indices (hkl) (S. Singh et al., 2024).

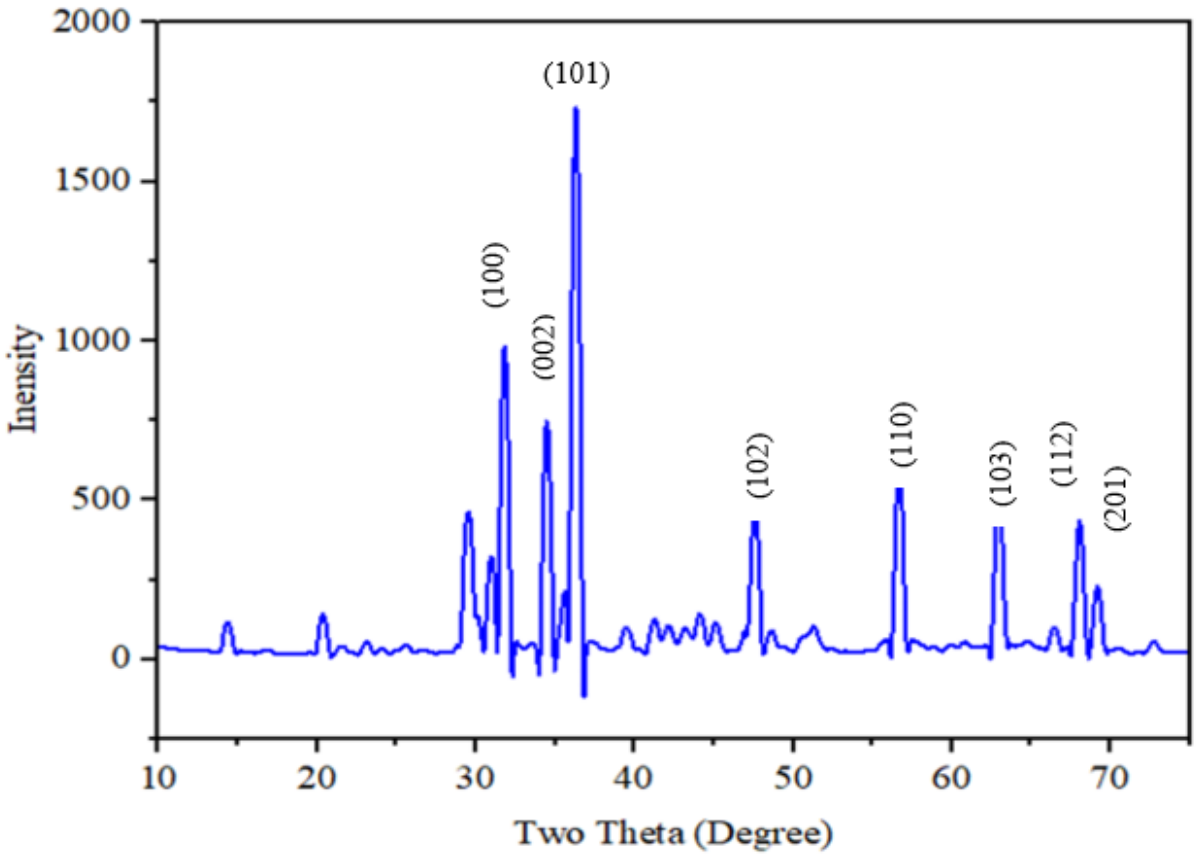

Figure 5-5 The XRD pattern of modified ZnO-NPs

In this study, the XRD shown in Figure 5.5 displayed the most notable peaks, identified and indexed in the following order: 100, 002, 101, 102, 110, 103, 112, and 201 planes, corresponding to 31.8°, 34.4°, 36.3°, 47.5°, 56.6°, 62.8°, 67.9°, and 69.1° respectively. Therefore, the X-ray diffraction pattern confirms that pure green modified ZnO-NPs were produced (Sánchez-Pérez et al., 2023). The average crystalline particle size (D) and average crystalline size were determined from the full width at half maximum (FWHM) of the diffraction peaks using Scherrer's Eqn. (5.8).

$$D = \frac{K*\lambda}{\beta*\cos\theta} \quad \text{.....(5.8)}$$

Where *D* is the crystalline size, *K* is the Scherrer constant (typically taken as 0.9), λ is the wavelength of the X-ray used for diffraction (typically taken as 1.5406 Å for Cu Kα radiation), β is the FWHM of the diffraction peak in radians, and θ is the diffraction angle in radians.

The ZnO-NPs average crystalline particle size (D_{avg}) was calculated as D = 13.94 nm, which is less than the previously reported value of 31.04 nm (Mohamed Isa et al., 2021).

5.5.1.5 Morphological analysis of ZnO-NPs

The surface morphology and microstructure of the ZnO-NPs synthesized using *C. bergamia* extract were examined using Scanning Electron Microscopy (SEM) at various magnifications, Figure 5.6. At lower magnifications, it is evident that the ZnO-NPs were not individually disbursed but were instead highly agglomerated and transformed into interlinked porous structures (Tymoszuk & Wojnarowicz, 2020). Irregularly shaped agglomerates, with different size distributions, created an interconnected sponge-like network. With higher magnification, Figure 5.6, it was further observed that these larger micro-scale clusters are formed due to dense packing of the very much smaller primary nanoparticles. Surfaces of the agglomerates appear to be coarse, confirming that they are built from these fundamental nano crystallites that appear to be quasi-spherical, closely packed, and fuse (Pedroza Toscano et al., 2022).

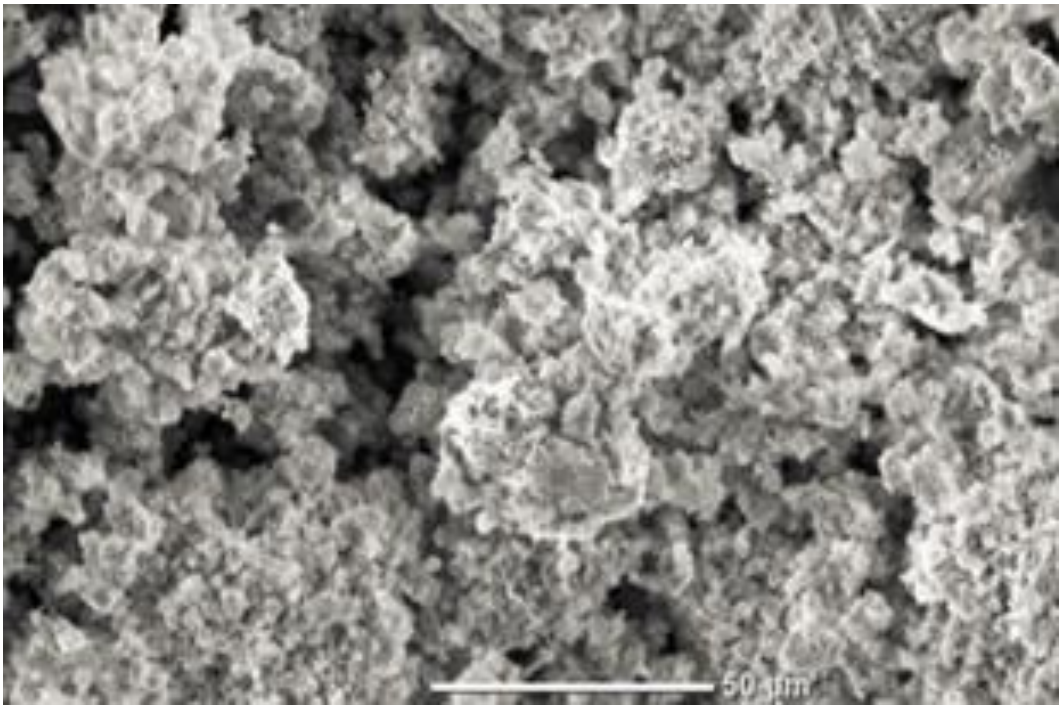

Figure 5-6 SEM images of ZnO-NPs synthesized at a calcination temperature of 450 °C and a calcination time of 2 hrs.

This hierarchical morphology was characteristic of green synthesis protocols in which the biomolecules within the *C. bergamia* extract may play a dual role as reducing and capping/stabilizing agents (Kazemi et al., 2023). However, the high surface energy of these primary nanoparticles, together with the functional groups of the capping biomolecules, promotes their self-assembly and agglomeration to produce the stable porous micro-sized secondary structures characterized in the images (Shrestha et al., 2020). Such a high-surface-area morphology is very beneficial for potential applications in photocatalysis/adsorption.

5.5.2 RSM-BBD statistical analysis

Tables 5.4 and 5.5 show the outcomes of the ANOVA for TC degradation and the TOC removal, respectively. Both models were statistically significant, with a model F value of 209.94 for TC degradation and 54.41 for TOC removal. Both values were relatively high in this study, and the models were capable of predicting TOC removal and TC degradation efficiency (Asgharian et al., 2020). The study indicates that the P values were below 0.05 in both ANOVA tables, suggesting the model terms are significant. Therefore, the model terms to be considered for TOC removal efficiency and TC degradation are: A, B, C, D, AB, BC, A^2, B^2, C^2, and D^2. The lack of fit was not significant in Tables 5.4 and 5.5, as shown; thus, the model equations were adequate to predict both responses for the study of each parameter within the study range (Kassahun et al., 2021).

Based on RSM-BBD analysis, the regression models for TC deterioration and TOC removal proved to have R^2 values of 0.995 and 0.982, respectively. This means that the regression models explain 99.5 % and 98.2 % of the variance in the experimental range. Even when the study elements of interest are outside the experimental range, the model equations provided useful predictions of the responses TC degradation and TOC removal, with predicted R^2 values of 0.9905 and 0.9102. In summary, if both R^2 and predicted R^2 values are close to 1, it shows that the statistical model has excellent quality, it is consistent, and it can provide reasonable predictions (Abewaa et al., 2023). The model equations that relate the responses to the process variables, after excluding the insignificant ones, are presented in Eqns. (5.9) and (5.10).

$$\text{TC Degradation Removal Efficiency (\%)} = -558.9977 + 1.7693A + 121.49467B + 108.937C + 32.19503D - 0.202389AB - 0.255778AC - 0.013167AD - 10.025BC - 3.1215BD - 2.67400CD - 0.000016A^2 - 5.56025B^2 + 0.669C^2 - 0.597660D^2 \quad (5.9)$$

$$\text{TOC Removal Efficiency (\%)} = -436.48255 + 1.53575A + 88.99667B + 95.30333C + 25.27567D - 0.172778AB - 0.185000AC - 0.010844AD - 8.53500BC - 2.2245BD - 2.25500CD - 0.000464A^2 - 3.77417B^2 - 2.15167C^2 - 0.523367D^2 \quad (5.10)$$

Table 5-4 Analysis of variance (ANOVA) of the response surface model for TC degradation

Source	Sum of Squares	df	Mean Square	F-value	p-value	
Model	5519.70	14	394.26	209.94	< 0.0001	Significant
A-Irradation Time	663.05	1	663.05	353.07	< 0.0001	
B-Solution pH	32.57	1	32.57	17.34	0.0010	
C-Catalyst Doasge	52.96	1	52.96	28.20	0.0001	
D-Initial Contaminant concentration	1385.03	1	1385.03	737.51	< 0.0001	
AB	331.79	1	331.79	176.67	< 0.0001	
AC	132.48	1	132.48	70.54	< 0.0001	
AD	35.11	1	35.11	18.69	0.0007	
BC	100.50	1	100.50	53.52	< 0.0001	
BD	974.38	1	974.38	518.84	< 0.0001	
CD	178.76	1	178.76	95.19	< 0.0001	
A^2	0.0064	1	0.0064	0.0034	0.9541	
B^2	200.54	1	200.54	106.78	< 0.0001	
C^2	0.1814	1	0.1814	0.0966	0.7605	
D^2	1448.10	1	1448.10	771.09	< 0.0001	
Residual	26.29	14	1.88			
Lack of Fit	22.11	10	2.21	2.12	0.2449	Not significant
Pure Error	4.18	4	1.05			
Cor Total	5545.99	28				

Table 5-5 Analysis of variance (ANOVA) of the response surface model for TOC removal.

Source	Sum of squares	Df	Mean square	F- value	P-value	
Model	3456.05	14	246.86	54.41	< 0.0001	Significant
A-irradiation time	449.33	1	449.33	99.04	< 0.0001	
B-solution pH	0.0120	1	0.0120	0.0027	0.9597	
C-catalyst dosage	33.97	1	33.97	7.49	0.0161	
D-initial TC. Concentration	774.73	1	774.73	170.77	< 0.0001	
AB	241.80	1	241.80	53.30	< 0.0001	
AC	69.31	1	69.31	15.28	0.0016	
AD	23.81	1	23.81	5.25	0.0380	
BC	72.85	1	72.85	16.06	0.0013	
BD	494.84	1	494.84	109.07	< 0.0001	
CD	127.13	1	127.13	28.02	0.0001	
A^2	5.74	1	5.74	1.26	0.2797	
B^2	92.40	1	92.40	20.37	0.0005	
C^2	1.88	1	1.88	0.4137	0.5305	
D^2	1110.46	1	1110.46	244.77	< 0.0001	
Residual	63.51	14	4.54			
Lack of fit	51.63	10	5.16	1.74	0.3129	Not significant
Pure error	11.88	4	2.97			
Cor total	3519.56	28				

Figure 5.7 (a) and (b) demonstrate that both models are exact, as the actual points closely align with the ideal y = x line. This means the models' outputs are very close to the actual experimental results in the real world (Foroughi et al., 2020). The model for TC degradation efficiency, Figure 7 (a), seems to be slightly more accurate than the model for TOC removal efficiency, Figure 5.7 (b) (Wu et al., 2020b). This is visually evident in Figure 5.7 (a), where the data points are more tightly clustered around the trend line, compared to the slightly more dispersed points in Figure 5.7 (b). The high relationship designates that the input variables used in the models are important forecasters of these consequences (Sjah et al., 2023).

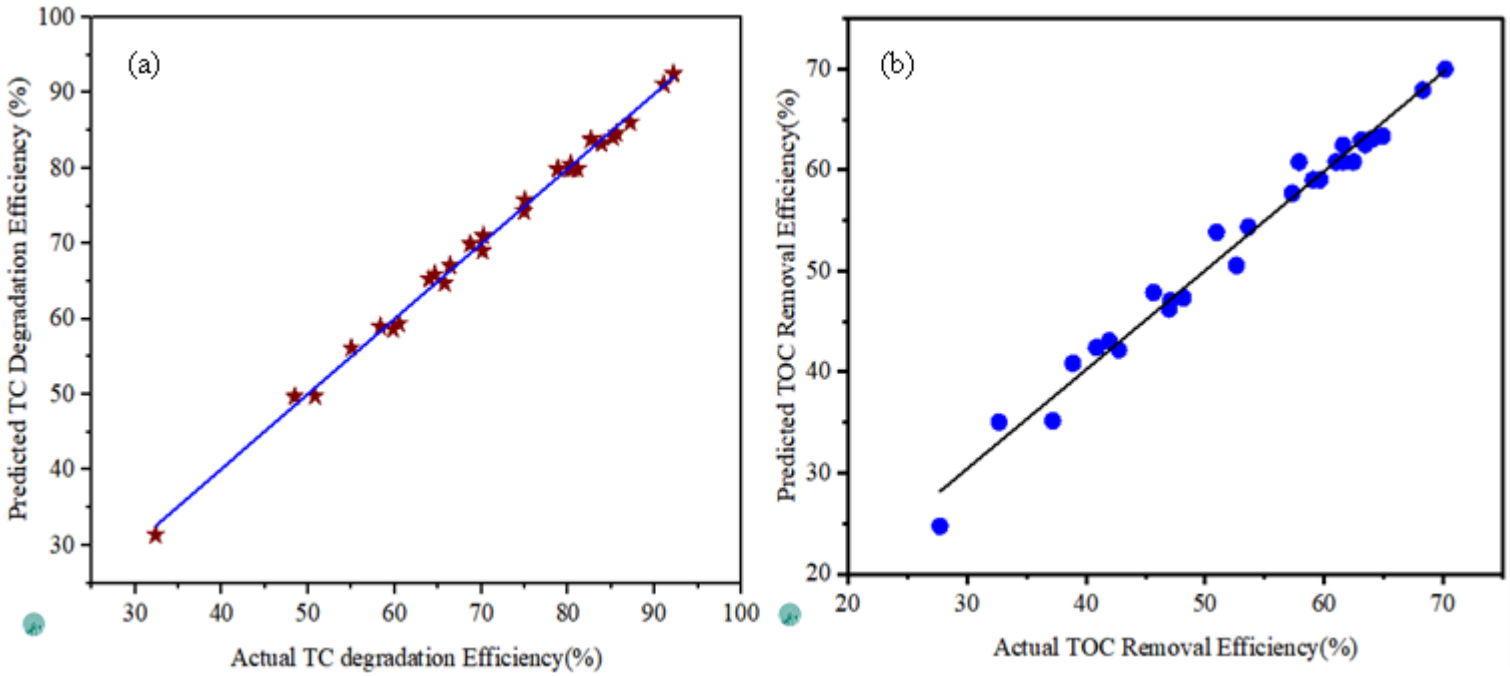

Figure 5-7 Comparison of predicted and actual values (a) for TC degradation efficiency, and (b) for TOC removal efficiency

.

Table 5-6 Performance indicators for the RSM model approach related to TC degradation and TOC removal.

Statistical Parameter	BBD-RSM	
	TC Degradation Efficiency (%)	TOC Removal Efficiency (%)
R^2	0.995	0.982
AAD	0.845	1.348
RMS	0.944	1.684

Table 5.6 presents low AAD and RMS values and a high R^2 value of 0.995 for TC degradation efficiency, suggesting that the RSM-BBD model showed a very high level of accuracy and good correlation with the experimental data (Abdullahi Ari et al., 2023a). Additionally, the results of AAD and RMS for TOC, paired with an R^2 value of 0.982, confirm that the model for TOC removal efficiency was also a strong predictor. The higher values of the experimental outcomes, supported by the low error metrics presented in previous work, endorse the use of green-synthesized ZnO-NPs in photocatalysis, optimized with RSM-BBD as an established and effective method for the degradation of TC. The high R^2 values observed for both TC degradation and TOC removal are comparable to those reported in the scientific literature (Lu et al., 2024).

5.5.3 Effect of operational parameters on TC photocatalytic degradation

Figures 5.8 (a-f) illustrate the combined effects of various variable pairs on the percentage of TC degradation. The curved surfaces in the plots indicate significant interactive effects between the variables. Irradiation time was a critical factor influencing TC degradation efficiency, as consistently demonstrated in Figures 5.8 (a), (b), and (c). Prolonged radiation time allows for more time for TC molecules to interact with energetic sites on the catalyst. The pH of the solution also significantly affected the degradation process, as indicated by the consistent data presented in Figures 5.8 (a), (d), and I. In each case, the greatest efficiency was achieved in the more acidic environment (pH 5.5).

The pH alters the surface charge of the catalyst; under acidic conditions (low pH), the catalyst surface tends to acquire a positive charge, enhancing the electrostatic interaction and adsorption of TC molecules, particularly when they are in an anionic or zwitterionic form (Kosmulski, 2021). TC exists in different ionic forms (cationic, zwitterionic, anionic) at varying pH levels.

The quantity of the catalyst was another important factor for the TC degradation (Gheytanzadeh et al., 2022), but the effect of this is explained in Figures 5.8 (b), (d), and (f). Initially, at a higher catalyst dose, more active sites are present and available for the reaction; hence, the degradation rate is higher, resulting in greater efficiency. However, once an optimal dosage is reached, adding more catalyst may not improve performance and could even be detrimental. This is often due to particle agglomeration at high concentrations, which reduces the total effective surface area (Shrestha et al., 2020). As clearly illustrated in Figures 5.8 (c), and (f), the initial concentration of TC consistently has an inverse effect on removal efficiency. The number of active sites on the catalyst is finite for a given dosage; therefore, with a fixed number of sites, only a limited amount of TC can be processed within a specific time frame.

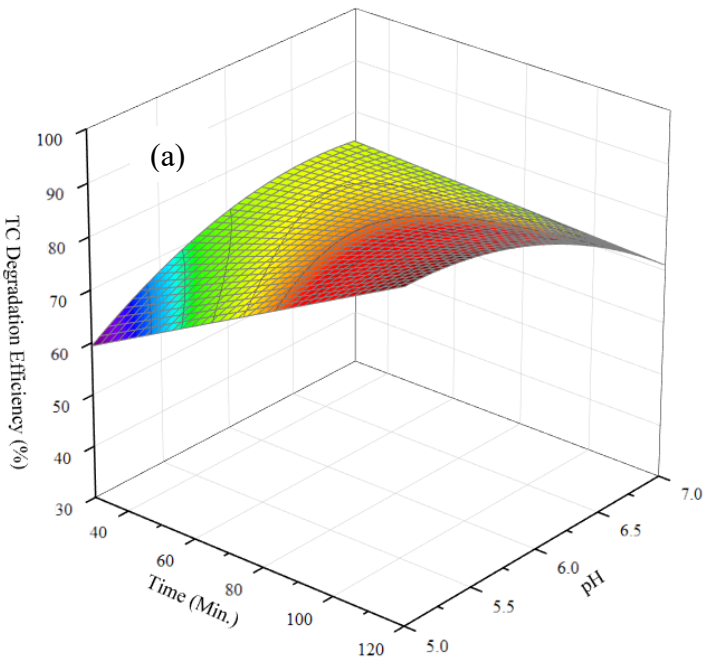
(a)
TC Degradation Efficiency (%)
100
90
80
70
60
50
40
30
Time (Min.)
40
60
80
100
120
pH
5.0
5.5
6.0
6.5
7.0

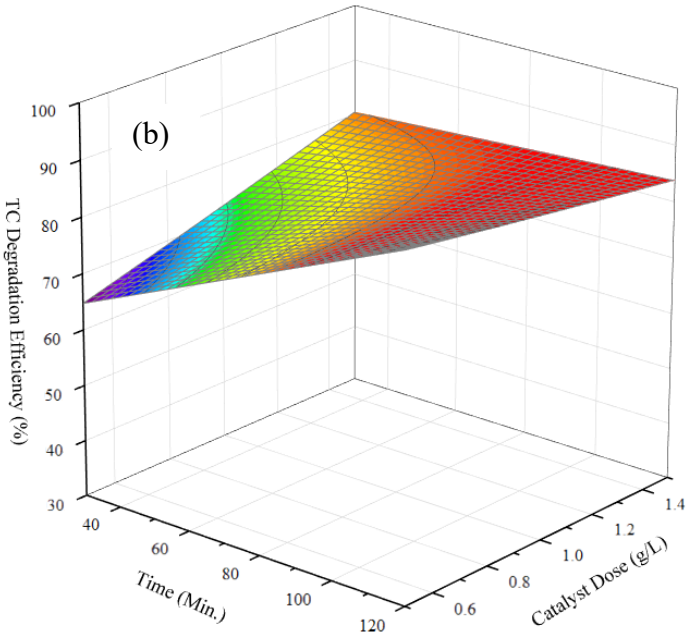
(b)
TC Degradation Efficiency (%)
100
90
80
70
60
50
40
30
Time (Min.)
40
60
80
100
120
Catalyst Dose (g/L)
0.6
0.8
1.0
1.2
1.4

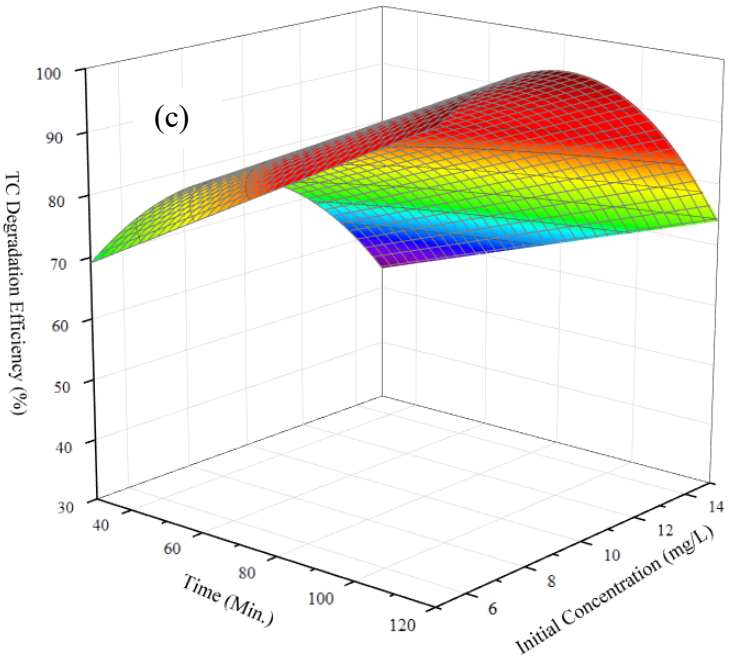
(c)
TC Degradation Efficiency (%)
100
90
80
70
60
50
40
30
Time (Min.)
40
60
80
100
120
Initial Concentration (mg/L)
6
8
10
12
14

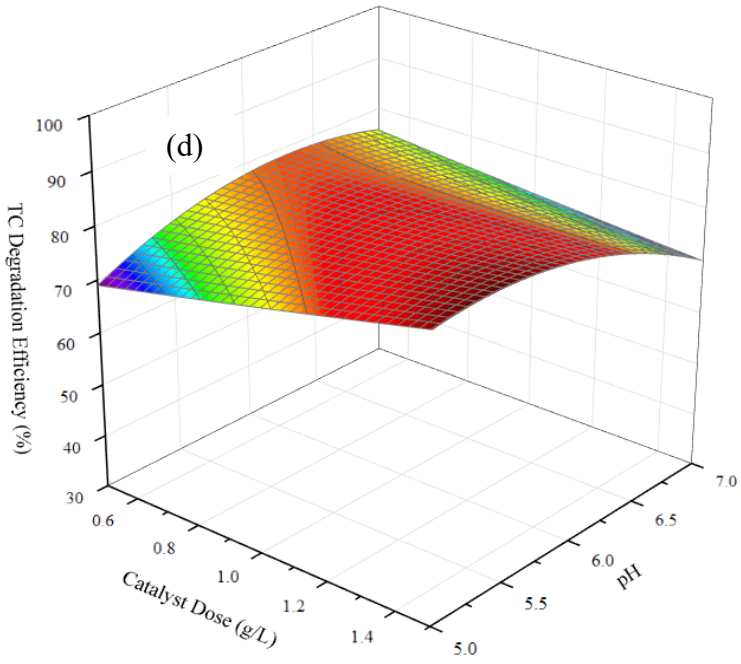
(d)
TC Degradation Efficiency (%)
100
90
80
70
60
50
40
30
Catalyst Dose (g/L)
0.6
0.8
1.0
1.2
1.4
pH
5.0
5.5
6.0
6.5
7.0

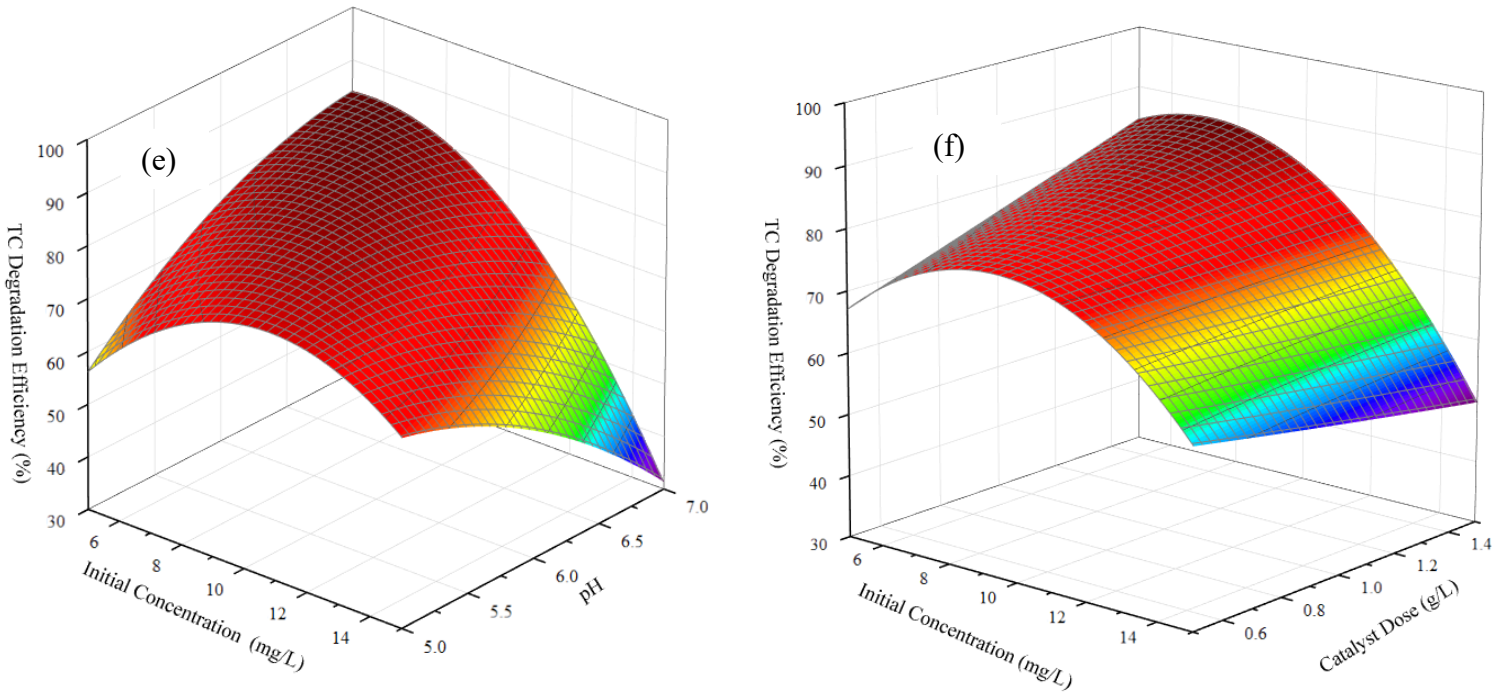

Figure 5-8 Interaction Effects of parameters on the TC degradation efficiency (%)

Figures 5.9 (a-f) are graphical representations of a mathematical model, developed using RSM-BBD. Figure 5.9 (a) indicates a strong interaction effect of irradiation time and pH on TOC removal efficiency. The positive effect of increasing the irradiation time was more pronounced at a lower pH. The highest TOC removal efficiency (over 70%) is achieved at the combination of a long irradiation time and a low pH. Figure 5.9 (b) shows a synergistic interaction between catalyst dosage and irradiation time. The combination of a high catalyst dosage and a long irradiation time results in the highest removal efficiency. Figure 5.9 (c) shows that achieving high removal efficiency for higher initial TC concentration requires significantly longer irradiation times.

Figure 5.9 (d) highlights the critical interplay between catalyst dosage and pH. The effect of the catalyst dosage was much more pronounced at low pH. Efficiencies were only marginally affected by increased dosages of catalysts at pH 7, while under a pH of 5, there was a major increase in terms of TOC removal for the same increase in catalyst dosages. From this, we conclude that catalyst activity was very pH dependent.

The peak efficiency was found at high catalyst dosage (1.5 g/L) and low pH (5). Figure 5.9 (e), shows the relationship between the initial TC concentration and pH. The negative impact of a high initial TC concentration is exacerbated at non-optimal (higher) pH values. Conversely, operating at the optimal low pH helps to mitigate the drop in efficiency when treating higher concentrations of TC. The best results are obtained at low TC concentration (5 mg/L) and low pH (5), and Figure 5.9 (f) clearly shows that a higher catalyst dosage was necessary to effectively treat higher concentrations of the TC (Kassahun et al., 2021).

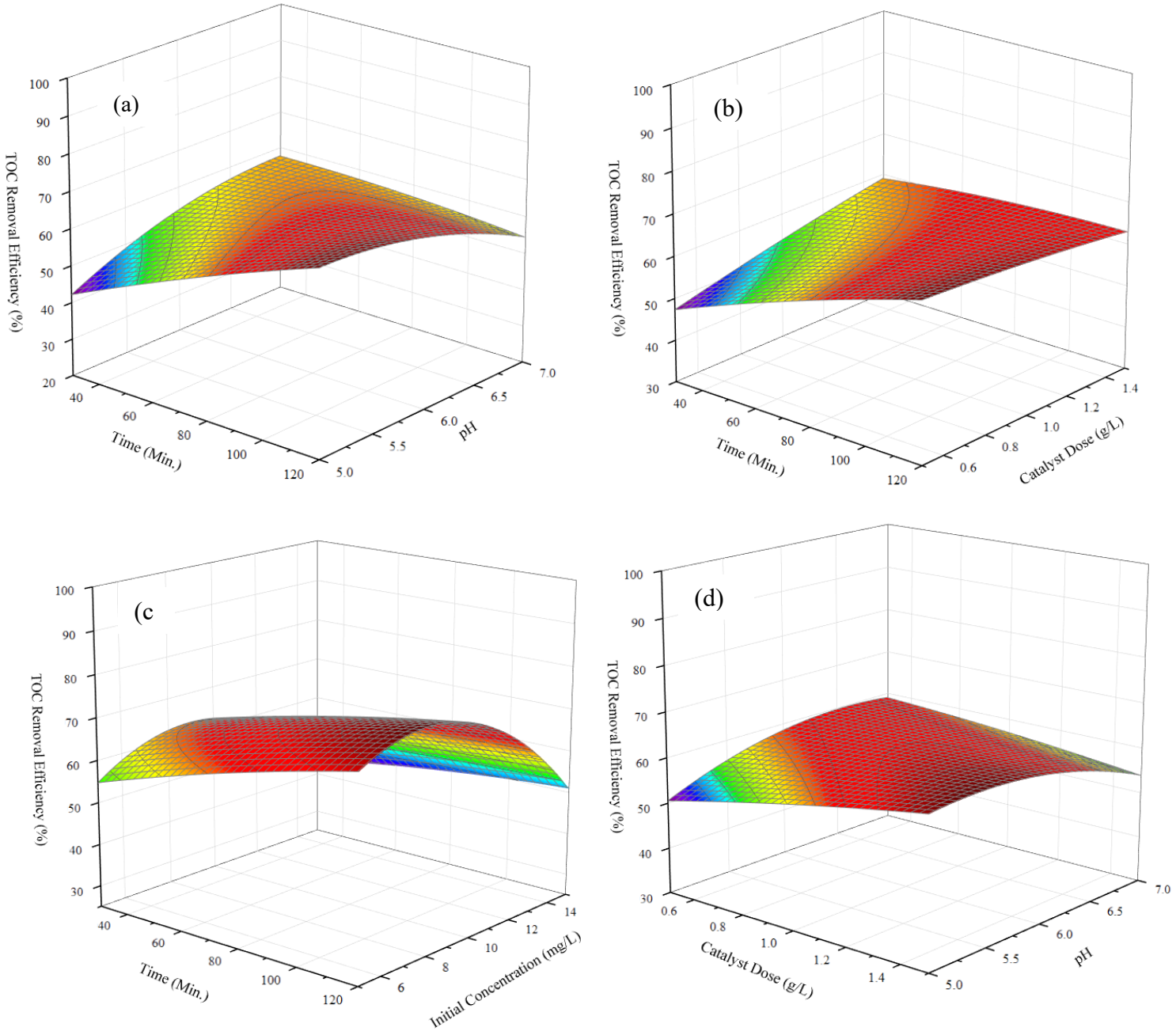

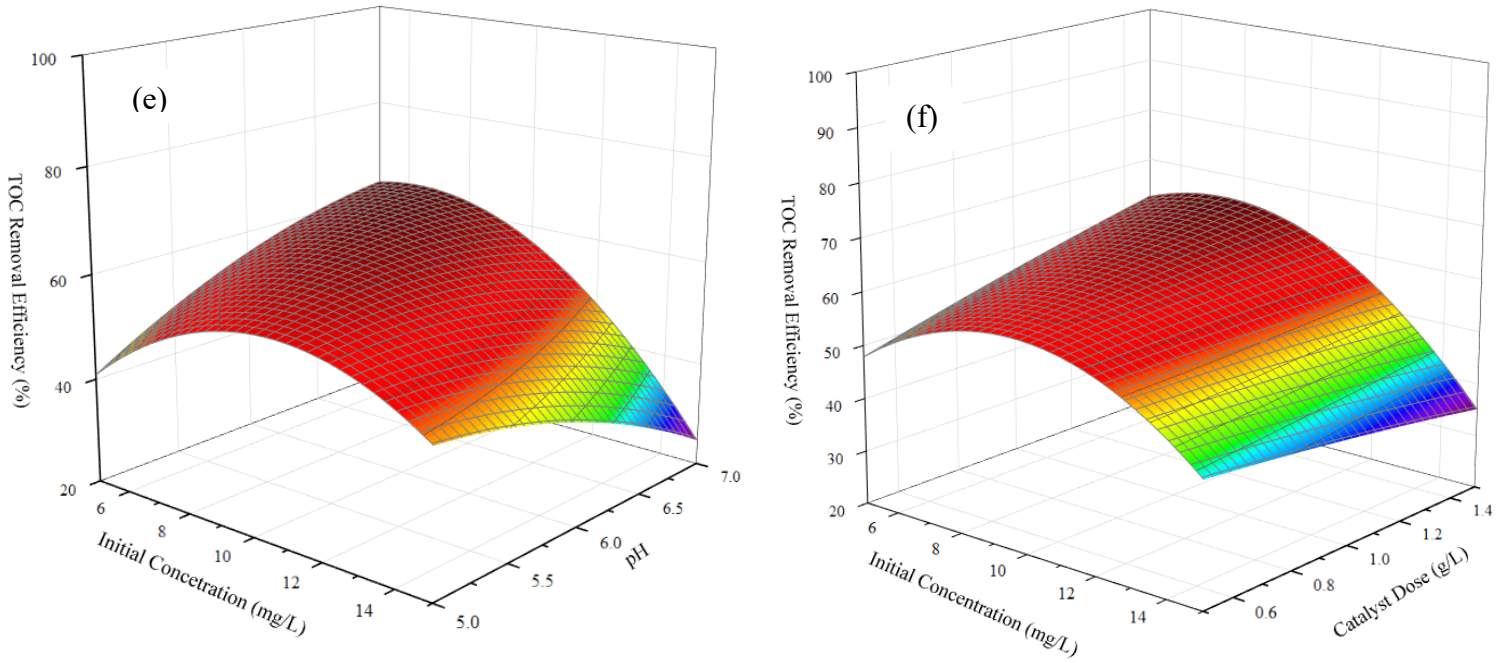

Figure 5-9 Interaction effects of parameters on the TOC removal Efficiency

5.5.4 Model optimization and validation

The RSM, along with BBD, is a very powerful statistical technique that is being more widely used by environmental engineers and scientists to help promote the optimization of chemical processes for the treatment of water, and it is effective for optimally degrading persistent pollutants like the antibiotic TC and for maximizing the removal of a critical measure of water quality, TOC (Juyal & Sharma, 2023).

For the optimum conditions discussed above, the RSM-BBD was analyzed using Derringer's desired function method, in which values from 0 to 1 are assigned to determine how well the optimum conditions achieve the ultimate response goal (Meenu et al., 2023). To achieve maximum TC degradation and TOC removal efficacy, the pH of the solution, irradiation time, and catalyst dose were kept in the ranges of 5 – 7, 30 – 120 min, and 1 – 1.5 g/L, respectively. At the outset, the target contaminant concentration was 5 – 15 mg/L. Accordingly, the maximum TC degradation and TOC removal efficiencies of 92.18 % and 69.47%, respectively, were observed at the optimum operating condition of solution pH of 5.64, irradiation time of 118.96 min, catalyst dose of 1.49 g/L, and initial contaminant concentration of 7.82 mg/L, with a desirability of 1.000.

A meaningful note was that attention was drawn to there was a separation between TC degradation efficiency (92.1%) and TOC removal efficiency (69.47%).

5.5.5 Adsorption isotherm studies

Adsorption isotherm models offer valuable insights into the adsorption mechanism by illustrating the relationship between liquid-phase adsorbate concentrations and the amount of adsorption on the solid phase, and the models relate theoretical equations to how adsorption occurs (Kassahun et al., 2021). In the present work, the following Figures 5.10 (a) and (b) display that Langmuir and Freundlich's models were investigated under the optimal conditions of synthesis, used to describe the equilibrium between the TC adsorbed onto the ZnO-NPs and the remaining in the solution (Pereira et al., 2022). The isotherm constant parameters for both models were determined using the corresponding linearized equations (5.11) and (5.12).

$$\frac{C_e}{q_e} = \frac{1}{q_m k_L} + \frac{C_e}{q_m} \quad \text{(5.11)}$$

$$\ln q_e = \ln K_f + \frac{1}{n} \ln C_e \quad \text{(5.12)}$$

Where C_e is the contaminant equilibrium concentration (mg/L), q_e is the equilibrium amount of contaminant adsorbed (mg/g), K_L and K_F are the Langmuir and Freundlich constants (L/mg), q_m is the maximum adsorbed quantity, and n is the Freundlich adsorption intensity constant. By plotting C_e/q_e versus C_e and $\ln(C_e)$ versus $\ln(q_e)$, were able to calculate the values of K_L, K_F, qm, and n from the slopes and intercepts of the two equations (Figure 10a and b) (Rizkallah et al., 2023). As shown in Table 5.7, the high R^2 value of 0.9914 shows that the experimental results back up the Langmuir model idea. This model's main idea was that stuff sticks to specific equal spots on the surface of what is absorbing it, and this points to a smooth, non-porous surface. So, this model, fitting the data, tells us that the ZnO-NPs remove TC by forming a single layer on a flat surface (Tran et al., 2021).

Table 5-7 Isotherm models parameters for TC adsorption onto C. bergamia extract ZnO-NPs

Isotherm Models	Constant parameters				Correlation coefficient
	q_m	K_L	K_F	n	R^2
Langmuir	30.21	0.507	-	-	0.9914
Freundlich	-	-	0.878	0.357	0.8224

In the previous study, the value of n in Table 5.7 was usually between 1 and 10 (Kalam et al., 2021). Therefore, as shown in Table 5.7, the value of n was 0.357, indicating that the adsorption process did not meet the expectations of the Freundlich model.

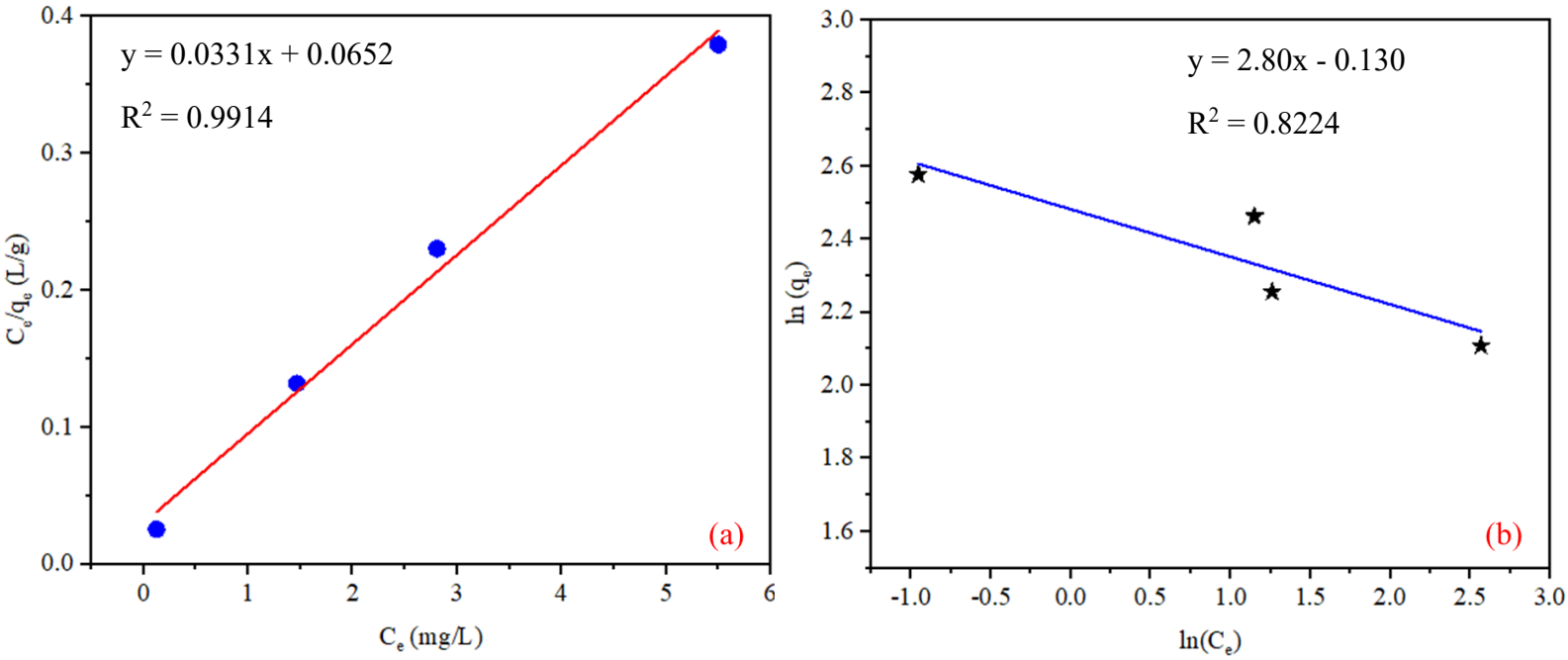

Figure 5-10 Adsorption isotherm models: (a) Langmuir and (b) Freundlich

The interaction between TC and the modified ZnO-NPs was assessed using the Langmuir and the Freundlich adsorption isotherm models (Figure 5.10). The Langmuir model demonstrated a better fit (R^2 = 0.9914) compared to the Freundlich model (R^2 = 0.8224). This indicates that TC adsorption occurs on a limited number of homogeneous active sites via a monolayer mechanism. Therefore, it can be tentatively concluded that the modification of ZnO effectively created consistent surface sites that facilitate strong TC-catalyst contact.

5.5.6 Reaction kinetics models

These studies go beyond simple observation to offer a quantitative and mechanistic understanding of photocatalytic reaction in the degradation of the TC process, as shown by the following equations (5.13) ,(5.14), and (5.15) (Taylor et al., 2021).

$$\mathrm{Log}(q_e - q_t) = \log q_e - \frac{K_1}{2.303} t \quad (5.13)$$

$$\frac{t}{q_t} = \frac{1}{k_2 q_e^2} + \frac{t}{q_e} \quad (5.14)$$

$$q_e = k_i t^2 + C_I \quad (5.15)$$

Where q_e is the TC adsorption removal amount at equilibrium, q_t is the degradation amount at any time t, C_i is the interparticle diffusion boundary layer thickness, and K_1, K_2, and K_i are the rate constants for pseudo-first-order, pseudo-second-order, and interparticle diffusion kinetic models.

Table 5-8 Pseudo-first-order, pseudo-second-order, and interparticle diffusion kinetic model parameters.

Kinetics Model	Parameters	TC Concentration (mg/L)			
		5	10	15	20
Pseudo-first-order	k_1 (per min.)	0.0266	0.0188	0.0068	0.0105
	$q_{e\ cal}$ (mg/L)	4.212	7.861	11.223	14.083
	$q_{e\ exp}$ (mg/L)	4.876	8.534	12.196	14.501
	R^2	0.938	0.931	0.903	0.941
Pseudo-second-order	K_2 (per min.)	0.3340	0.044	0.0125	0.00798
	$q_{e\ cal}$ (mg/L)	4.2615	8.870	12.643	19.275
	$q_{e\ exp}$ (mg/L)	4.2468	9.925	12.708	18.871
	R^2	0.985	0.957	0.996	0.994
Interparticle diffusion	K_i	0.328	0.615	1.181	1.4972
	C_i	0.573	0.283	1.413	1.931
	R^2	0.920	0.987	0.879	0.946

Table 5.8 illustrated, it was found that a pseudo-second-order kinetic model most satisfactorily describes the mechanism of the reaction for TC adsorption removal on the surface of the adsorbent. The model demonstrates that the quantity of TC removed at equilibrium (qe) is in close correlation with the amount of TC adsorbed at any given moment (q_t) (Kassahun et al., 2021). Table 5.8 shows that the adsorption of TC attains the best fit for pseudo-second-order kinetics. This assumption was further strengthened by the very high values of the coefficients of determination (R^2=0.985, 0.957, 0.996, 0.994) for all the other possible models, along with a good correlation between the calculated ($q_{e\ cal}$) and experimental ($q_{e\ exp}$) values of equilibrium adsorption capacities (Tran, 2023). The intraparticle diffusion model shows that diffusion is also involved in the process, but with the nonzero intercepts (C_i), it is established that this is not the only rate-determining step, further validating the notion that surface reaction controls the overall kinetics (Zhao et al., 2024).

Figure 5.11 (a,b,c) demonstrates the adsorption mechanism and rate-controlling steps during TC degradation, which were investigated by fitting the experimental data with pseudo-first-order, pseudo-second-order, and intraparticle diffusion kinetic models. The linearized plots for these models at varying initial TC concentrations (5,10,15, and 20 mg/L) are presented in Figure 5.11(a), (b), and (c) (Zamri et al., 2021) . For the pseudo-first-order model ln(q_e - q_t) vs. time) in Figure 5.11(a) shows moderate linearity interspersed with substantial scatter, indicating that this model does not adequately represent the entire adsorption process (Revellame et al., 2020). In direct contrast to this, Figure 5.11(b) presents the linearized plot for the pseudo-second-order model (t/q_t vs. time) with excellent linearity for all concentrations tested.

Figure 5.11, looking at diffusion, shows that the linear plots did not go through the origin. A non-zero intercept in the Weber-Morris model of intraparticle diffusion (q_t vs. $t^{0.5}$) suggests that intraparticle diffusion alone does not constitute the rate-limiting step (Chu et al., 2025). This corroborates the theory that the overall adsorption process is, therefore, a multi-step process, probably initially dictated by boundary-layer diffusion, followed by surface reaction chemisorption. Thus, kinetic analyses taken together support that the adsorption of TC is best described by a pseudo-second-order model, with the chemisorption reaction as the main rate-controlling step (J. Wang & Guo, 2020).

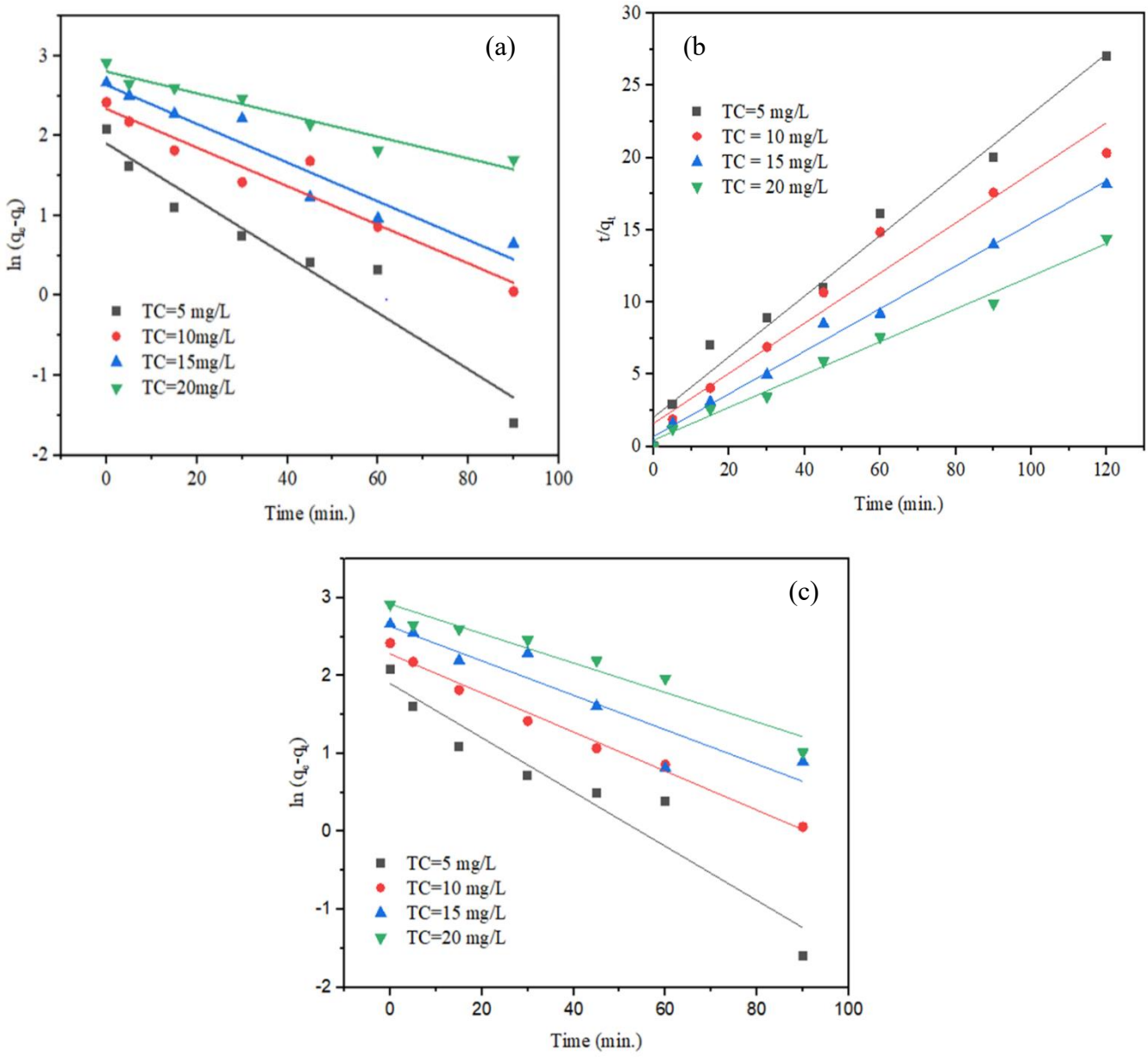

Figure 5-11 Reaction kinetics models of (a) pseudo-first-order, (b) pseudo-second-order, and (c) interparticle diffusion.

To identify the best-fitting adsorption isotherm and kinetic models, several error function studies were conducted, including sum square error (SSE), average relative error (ARE), sum of absolute error (SAE), and hybrid fractional error function (HFEF), using the following equations (5.16), (5.17), (5.18), and (5.19) (Kanagalakshmi et al., 2024).

$$\mathrm{SSE} = \sum_{i=1}^{n} \left(q_{e,I,(exp.)} - q_{e,I,(\,pred.)}\right)^2 \quad \text{(5.16)}$$

$$\mathrm{ARE} = \sum_{n=1}^{n} \left(\left| \frac{q_{e,I\,(exp.)} - q_{e,I\,(pred.)}}{q_{e,I\,(exp.)}} \right| * 100 \right) \quad \text{(5.17)}$$

$$\mathrm{SAE} = \sum_{i=1}^{n} \left| q_{e,i,(exp.)} - q_{e,i\,(pred.)} \right| \quad \text{(5.18)}$$

$$\mathrm{HFEF} = \frac{1}{n} \sum_{i=1}^{n} \left(\frac{\left| q_{e,I\,(exp.)} - q_{e,I,(pred.)} \right|}{q_{e,I\,(exp.)} + q_{e,I,(pred.)}} \right) \quad \text{(5.19)}$$

Where $q_{e,\,I\,(exp)}$ is the actual measured adsorption value, $q_{e,\,i(pred.)}$ is the predicted adsorption value, and n is the number of data points.

Table 5-9 Error function analyses for model selection

	Error function			
Kinetics Models	SSE	ARE	SAE	HFEF
Pseudo-first-order	29.906	0.5699	14.929	1.643
Pseudo-second-order	3.010	0.147	4.243	0.141

Table 5.9 shows that the pseudo-second-order model yielded a superior fit the data better than the pseudo-first-order model, as indicated by lower values of SSE, ARE, SAE, and HFEF, which are based on the TC concentration difference (Manyazewal et al., 2025b).

5.5.7 Reusability

The *C. bergamia* extract-synthesized ZnO-NPs demonstrated outstanding reusability, maintaining a TC degradation efficiency of approximately 80.8% after five consecutive cycles (Figure 5.12), which compares favorably to the 80.95% achieved after only three cycles in other reported studies (Abdullahi Ari et al., 2023a). This high stability is attributed to the strong capping and stabilizing effect of the phytoconstituents within the *C. bergamia* extract, which effectively anchored the active species and minimized the photocorrosion typically associated with bare ZnO. The limited leaching of active species and the retention of photocatalytic activity suggest that the biosynthesized NPs possess a robust chemical resistance to the aqueous environment, preventing the dissolution of Zn ions and maintaining the surface-active sites throughout the recycling process

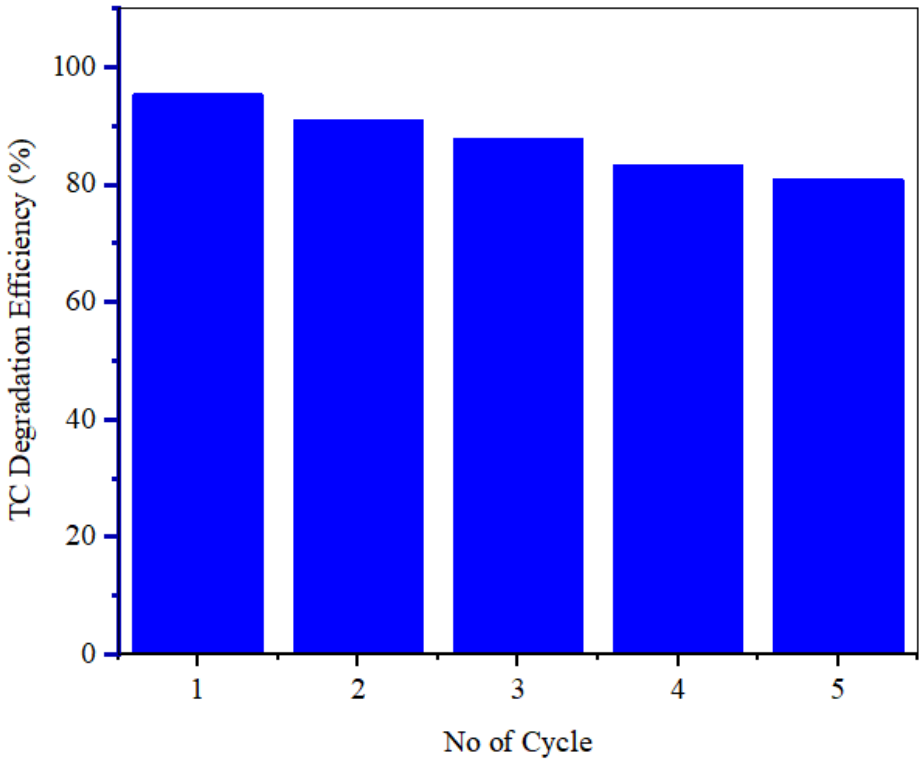

Figure 5-12 Recyclability of green-synthesized ZnO-NPs for TC degradation efficiency at optimized parameters (pH =5.64, time =120 min, dose =1.49 g/L, and TC =7.82 mg/L).

The *C. bergamia* leaf extract-modified ZnO-NPs demonstrate significant potential as a stable and reusable photocatalyst for the degradation of TC, as indicated by the recycling data in Figure 5.12. Over five runs, the degradation efficiency only slightly declined, reaching approximately 80.8% in the final cycle. This minor performance drop is attributed to the gradual accumulation of intermediate degradation products on the catalyst surface and the minimal loss of fine catalyst particles during washing and recovery procedures, rather than structural instability (Villagrán et al., 2024).

5.6 Conclusions

Rather than merely presenting a standard green synthesis, this study demonstrates an advanced Sol-gel modification that significantly suppresses electron-hole recombination, thereby maximizing the visible-light photocatalytic efficiency of the ZnO-NPs. It also details steps for optimizing the process needed to efficiently remove TC from water. The research examined and optimized how various operational parameters affect TC degradation and TOC removal efficiency using RSM-BBD. The parameters included solution pH (from 5 to 7), irradiation time (30 to 120 min), catalyst dose (1 to 1.5 g/L), and initial TC concentration (5 to 15 mg/L).

The optimal conditions identified for the process were a solution pH of 5.64, an irradiation time of 118.96 min, a catalyst dose of 1.49 g/L, and an initial TC concentration of 7.82 mg/L. Under these conditions, the maximum degradation efficiency of TC reached 92.1%, and the TOC removal efficiency was 69.47%. The RSM-BBD method proved highly effective for predicting process conditions, resulting in even stronger correlation coefficients. The optimization stage identified conditions where the synthesized ZnO-NPs exhibited excellent photocatalytic activity in degrading a high percentage of TC under UV/vis irradiation, along with TOC removal. This improvement was due to the generation of reactive oxygen species that enhanced surface production and catalyzed the breakdown of the complex antibiotic molecule. These findings provide a strong foundation for developing effective and sustainable water remediation technologies to protect the environment. The characteristics of the ZnO-NPs synthesized using *C. bergamia* leaf extract aligned well with the Langmuir adsorption isotherm and pseudo-second-order kinetic models.

6. SIMULTANEOUS ADSORPTION AND PHOTOCATALYSIS BASED ON SYNERGETIC EFFECT OF GREEN-BASED AC/ZnO-NPS COMPOSITE FOR TETRACYCLINE REMOVAL FROM AQUEOUS SOLUTION

6.1 Introduction

Large amounts of pharmaceuticals are released into water systems, causing significant contamination issues. These substances, which include antibiotics, anticonvulsants, antipyretics, cytostatic drugs, and hormones, have been detected in wastewater worldwide. Their presence raises serious concerns about potential physiological toxicity to both ecosystems and human health. In recent decades, the widespread use of TC has increased the risk of environmental contamination due to both accidental releases and intentional discharges (Tran Thi & Lee, 2017b).

As a result, there is a strong search for new pollutant removal technologies that are effective, cost-efficient, and environmentally friendly (Długosz et al., 2022). Among advanced oxidation processes (AOPs), using metal oxide semiconductors is a promising technique for removing various harmful pollutants from wastewater. They produce highly reactive hydroxyl radicals that can efficiently break down harmful substances into harmless byproducts, providing a comprehensive solution for wastewater treatment (Hama Aziz et al., 2025).

The synthesis of ZnO-NPs using a green method with *C. bergamia* leaf extracts has become a promising technique for wastewater treatment. To develop a reliable and detailed synthesis process, it is crucial to thoroughly examine the factors that affect the properties of these green-synthesized ZnO-NPs (Lu et al., 2024). Various materials have been explored to support photocatalyst particles, including alumina, zeolite, silica gel, quartz, stainless steel, clays, and AC (Shintre et al., 2022). Recently, AC derived from cassava peels has gained notable attention as an excellent substrate for photocatalysts, due to its high BET surface area (1250 m^2/g), micropore volume, and its abundance, affordability, reusability, and unique chemical properties (Manyazewal et al., 2025a).

6.2 Materials and methods

6.2.1 Material preparation

C. bergamia were collected from the Gullele Garden in Addis Ababa, and cassava peel was obtained from the, Wolaita, Ethiopia. NaOH pellets with 99.0% purity, $CH_3COO2Zn.2H_2O$ with an assay of 98.0%, and powdered $C_{22}H_{24}O_8N_2 \cdot HCl$ with 98% purity were purchased, along with absolute CH_3CH_2OH, (> 99%), HCl, (34.5%), and $ZnCl_2$ with a molar mass of 136.28 g/mol.

6.2.2 Activated carbon preparations

Before use, the cassava peels were thoroughly cleaned multiple times with distilled water to remove dirt and other inorganic impurities. The samples were then dried for 24 h at 120 °C to eliminate moisture and ground to a desired particle size of 63–150 µm. To determine the optimal conditions for producing AC with a high surface area from cassava peels, and chemical activation with $ZnCl_2$.

The cassava peel samples were carbonized in a muffle furnace for 60 to 120 min at temperatures ranging from 450 to 650 °C, with an impregnation ratio of 0.75:1 to 2.5:1 before cooling under nitrogen flow. Subsequently, a HCl solution was used to wash the activated carbon. The samples were rinsed multiple times with hot distilled water to ensure the complete removal of chloride ions. Finally, the specimens were washed with cold distilled water, dried at 110 °C for 24 h, and then stored in a desiccator (Manyazewal et al., 2025a).

6.2.3 Green synthesis of ZnO-NPs

The ZnO-NPs were synthesized using an environmentally friendly method based on the sol-gel process described by Abomuti et al. (2021). The initial materials included $CH_3COO)2Zn \cdot 2H_2O$, *C. bergamia* leaves extract, and NaO. According to Ramesh et al. (2022), the synthesis of ZnO-NPs started with 50 mL of an aqueous Zn(NO3)2 solution in a 250 mL beaker, which was stirred continuously for 2 h at 50 °C. During this process, 50 mL of *C. bergamia* leaf extract was added while stirring and maintaining the same temperature. The mixture's color changed to light yellow as the phytochemicals in the extract capped the Zn^{2+} ions and initiated the nucleation of ZnO-NPs (Mohamed Isa et al., 2021).

In step two, a freshly prepared NaOH solution was slowly added dropwise to the reaction mixture (pH 10-12) at 50 °C while continuously stirring. The mixture was stirred for the next 2 h at 50 °C, producing a light yellowish precipitate that indicated the formation of ZnO-NPs (Abomuti et al., 2021). The dehydrated ZnO-NPs were then annealed for 2 h at 450 °C in a muffle furnace. The resulting fine, light-cream-colored ZnO-NP powder was used for surface characterization and further research.

6.2.4 Preparation of AC/ZnO-NPs Composite Materials

Research studies, such as that by Cruz-Quesada et al. (2025), examining this composite for comparable applications typically test numerous ratios to optimize the adsorption capacity of AC in conjunction with the photocatalytic activity of zinc oxide nanoparticles (ZnO-NP). The objective is often to create a synergistic effect, where the adsorption of TC onto the AC surface brings it closer to the ZnO-NP, thereby improving photocatalytic degradation, and recommended testing ratios include higher proportions of AC (2:1, 3:1, and 4:1) AC to ZnO-NPs, as described in Table 6.1 (Wardah et al., 2024).

Table 6-1 Preparation of composite materials requires 10 g of each component in the specified ratio.

AC: ZnO-NPs	AC	ZnO-NPs	Zinc Acetate Dihydrate
2:1	6.67 g	3.33 g	0.89 g
3:1	7.50 g	2.50 g	0.67 g
4:1	8.00 g	2.00 g	0.54 g

Then, calculate the small amount of zinc acetate dihydrate needed to form the ZnO binder mass, which was roughly 10% of the ZnO-NP.

In this study, composites of activated carbon and pre-synthesized ZnO nanoparticles (AC/ZnO-NPs) were prepared using a Sol-gel method based on mass ratios of 2:1, 3:1, and 4:1, with each synthesis aiming for a final yield of 10 g, as shown in Table 6.1. For the synthesis of the 2:1 ratio composite, 6.67 g of AC and 3.33 g of ZnO-NPs were dispersed in 100 mL of ethanol in a 500 mL beaker.

Then, a small amount of zinc acetate dihydrate (0.89 g) was added to the suspension as a binding agent. Next, a NaOH solution was added dropwise to induce the formation of zinc hydroxide gel, which anchored the ZnO-NPs onto the surface of the AC and was vigorously stirred with a magnetic stirrer. The resulting slurry was matured for 2 h with continuous magnetic stirring at room temperature. To ensure uniform dispersion, the mixture was ultrasonicated for 30 min. The product was then recovered by centrifugation and thoroughly washed with deionized water, followed by drying in an oven at 105 °C for 12 h. Finally, the dried powder was calcined in a muffle furnace at 450 °C for 2 h to produce the final composite AC/ZnO-NPs. The same procedure was applied for the 3:1 and 4:1 ratio.

6.2.5 Integrated adsorption-photocatalysis test

This method involves conducting both processes simultaneously within a single experiment, leveraging the potential synergy between adsorption and photocatalysis from the outset. This is often referred to as “simultaneously integrating (Amir et al., 2022). The experimental procedure was designed to evaluate the combined effect of adsorption and photocatalysis on TC removal

Based on Liu et al. (2024), simultaneous adsorption and photocatalysis experiments were performed in a 250 mL beaker acting as a batch photoreactor. The reactor was exposed to UV/visible light at an intensity of 14.41 mW/cm², measured with a radiometer (Analytikjena, UVX-25 Sensor Probe Assy 254 nm). The light source was positioned at the top of the reactor, 10 cm from the sample, and was a Sankyo Denki (BESTEC model, BJ2015M11CGL 1800) equipped with a 14.5 W UV/vis. The process started by turning on the lamp after an optimized time of 2 h and 30 min, with a pH of 5.5 as determined in previous work (Manyazewal et al., 2025b).

In this study, different ratios of composites (AC/ZnO-NPs), TC concentrations, and composite dosages were tested, as shown in Table 6.2. Afterward, the samples were collected, centrifuged at 6000 rpm for 10 min, and filtered through a 0.45 µm syringe filter. This method ensures that adsorption and photocatalytic degradation occur simultaneously from the beginning of the experiment (Chen et al., 2022). The general removal of tetracycline via the composite materials was presented in Figure 6.1.

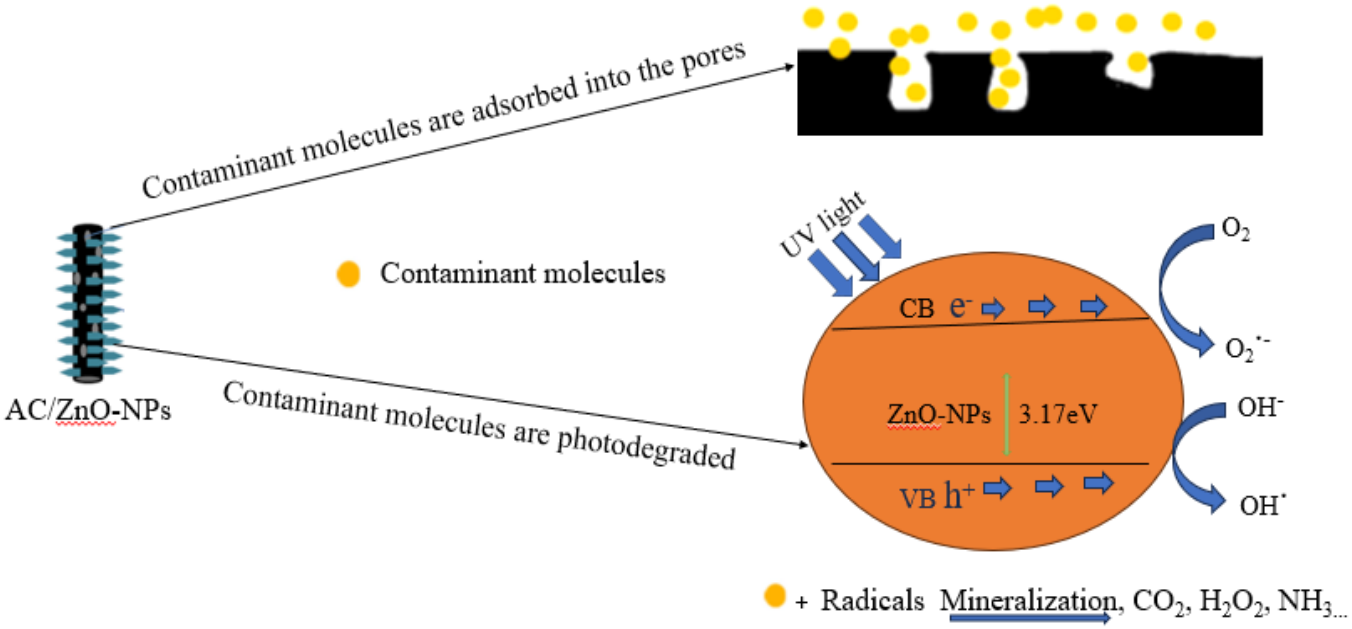

Figure 6-1 Removal mechanism of tetracycline by using the AC/ZnO-NPs composite

6.2.6 Analytical methods

The TC concentration in the aqueous samples was measured using a UV-VIS-NIR Spectrophotometer in the wavelength range of 200 to 800 nm. The absorbance was measured at the maximum wavelength of TC, which is at 360 nm (Deng et al., 2020). A calibration curve from previously prepared stock solutions of TC with known concentrations (0.5 to 10 mg/L) was established in order to quantify the results. The removal efficiency (%) of TC was calculated using the following equations (6.1), and (6.2).

$$E\ \% = \frac{C_i - C_f}{C_i} * 100 \quad (6.1)$$

$$q_t\left(\frac{mg}{g}\right) = \frac{C_i - C_t}{m} * V \quad (6.2)$$

Where C_i and C_f are the concentrations of TC at the initial and final irradiation times, respectively. V is the volume of the treatment sample, C_t is the concentration of the adsorbate remaining in the solution at a specific time 't' after the adsorption process has started, and m is the mass of the adsorbent material used in the experiment (Manyazewal et al., 2025b).

6.2.7 RSM-BBD for process optimization

The RSM-BBD with a three-level, three-factor to identify and optimize the best process parameters for removing TC. The three independent variables selected were the initial TC concentration (A, mg/L), the composite dosage amount (B, g/L), and the ZnO-NPs/AC ratio at the start. For all optimization experiments, the total reaction time and solution pH were fixed at 150 min and 5.5, respectively, as shown in Table 6.2.

Table 6-2 Factors and stages of experimental investigations

Factor	Name	Unit	Study range	
			Minimum	Maximum
A	Initial contaminant concentration	mg/L	5	15
B	Composite Dosage	gm/L	0.5	1.5
C	ZnO-NPs/AC Ratio	-	2:1	4:1

The key process parameters specifically the ratio ZnO-NPs/AC, composite dosage, and initial solution concentration were optimized using a RSM-BBD, as detailed in Table 6.3. It provides predictive capabilities through a structured experimental approach, helping to develop and refine empirical models (Kassahun et al., 2021).

The relationship between the independent variables and the answer was determined using a second-order polynomial equation. The general equation for the three experimental elements that were chosen is as follows Eqn. (6.3):

$$Y = \beta_\circ + \sum_{i=1}^{k} \beta_i X_i + \sum_{i=1}^{k} \beta_{ii} X_i^2 + \sum_{1 \le i \le j} \sum \beta_{ij} X_I X_j + \varepsilon \quad (6.3)$$

Where Y is the experimental response, X_i and X_j are the experimental variables or factors, β_o is a constant, β_i,β_{ii}, and β_{ij} are the regression coefficients for linear interaction effects, quadratic interaction effects, and cross-product interaction effects, respectively, and ε is the random error. Regression analysis and coefficient estimation were conducted using Design-Expert version 13.0.1.0 (Stat-Ease, Inc.) (Kassahun et al., 2021).

Table 6-3 Independent Variables and Their Levels for the Box-Behnken Design

Run	Parameters			Response
	ZnO-NPs/AC Ratio	Initial (TC) Conc. (mg/L)	Composite Dosage (g/L)	Removal Efficiency (%)
1	2:1	5	1	92.12
2	4:1	5	1	80.92
3	2:1	15	1	83.65
4	4:1	15	1	79.36
5	2:1	10	0.5	80.98
6	4:1	10	0.5	77.75
7	2:1	10	1.5	95.41
8	4:1	10	1.5	81.93
9	3:1	5	1.5	93.02
10	3:1	15	0.5	73.31
11	3:1	5	1.5	99.41
12	3:1	15	1.5	86.94
13	3:1	10	1	98.70

The following eqn. (6.4), (6.5), and (6.6), metrics necessary to critically assess model predictive ability and as well as reliability: coefficient of determination (R^2), absolute average deviation (AAD), and root mean square error (RMSE). The amount of goodness-of-fit R^2 value denotes the percentage of variation of TC degradation efficiency that the model can specify, while AAD and RMSE show the extent of the average error between predicted and experimental values.

These hold a promise for strong statistical validation of model accuracy and robustness: a high R^2 value with low AAD and RMSE values. The model was confirmed to be appropriate for predicting and optimizing the photocatalytic degradation of TC using the green-synthesized ZnO-NPs under various operating conditions (Chicco et al., 2021). These measures are defined as follows.

$$R^2 = 1\frac{\sum_{i=1}^{n}(y_{Ai}-y_{Pi})^2}{\sum_{i=1}^{n}(y_m-y_{Pi})^2} \quad (6.4)$$

$$RMSE = \sqrt{\sum_{i=1}^{n}\frac{(y_{Ai}-y_{Pi})^2}{n}} \quad (6.5)$$

$$AAD = \frac{1}{n}\sum_{i=1}^{n}*\frac{|y_{Ai}-y_{Pi}|}{y_{Pi}} \quad (6.6)$$

Where y_A, y_P are the actual value, and the predicted value, respectively, n is the number of data points, and y_m is the average value.

6.3 Results and Discussions

6.3.1 Statistical analysis of RSM-BBD

The ANOVA results shown in Table 6.4, in a statistically way, confirm the validity of the quadratic model made up for optimizing TC removal from aqueous solutions, too. The global weight of the model is very significant, as evidenced by an F-value of 695.54 and a P-value of less than 0.0001 (Zhao et al., 2023). This means that the model is sound and dependable to explain the relationship between input variables as well as TC removal efficiency. Considering the overall significance of the model, it may be said that it has certainly been surpassed by an F-value of 695.54 and a P-value of less than 0.0001. Then it means that the model builds solidly and indeed describes the relationship between input variables and TC removal efficiency.

All specific linear terms, like the AC/ZnO-NPs ratio and also the initial TC concentration, plus composite dosage, are highly significant with p-values. This indicates that each individual factor plays a critical role on its own in the degradation process (Albo Hay Allah & Alshamsi, 2023b). The contribution of the quadratic terms A, B, C, A^2, B^2, and C^2, as well as the interaction terms AB, AC, and BC, indicates significance values. One of the main positive outcomes is that the Lack of Fit test recorded a P-value (0.7127) of an insignificant nature.

This is a highly favorable result because it shows good agreement between the experimental data and the model's predictions, which is suitable for exploring the design space without systematic deviations (Sureiman & Mangera, 2020). Analyses using RSM-BBD indicated that the regression models developed for TC removal exhibited an R^2 of 0.9988. This indicates that 99.88% of the variance in the experimental range is explained by the regression models. The model equations forecasted useful predictions on the outcome (TC degradation) based on values of predicted R^2 of 0.993, even in instances where the mentioned study elements are outside the experimental range. In conclusion, the proximity of both R^2 and predicted R^2 values to the unit indicates that the statistical model is of superior quality, consistent, and can provide reasonably accurate predictions (When, 2024). The model equations that correlate the responses to the process variables after removal of the insignificant ones are presented in Eqn. (6.7).

$$\text{Removal Efficiency (\%)} = -22.8 + 49.7A + 3.135B + 131.72C + 0.345AB - 8.65AC - 1.934BC - 8.77A^2 - 0.186B^2 - 64.74C^2 \quad \text{.....(6.7)}$$

Table 6-4 Analysis of variance (ANOVA) of the response surface model for TC removal

Source	Sum of Squares	Df	Mean Square	F-value	P-value	
Model	991.61	9	110.18	695.54	< 0.0001	Significant
A-Ratio (AC/ZnO-NPs)	117.04	1	117.04	738.89	< 0.0001	
B-Initial concentration (TC)	53.35	1	53.35	336.82	< 0.0001	
C-Catalyst Dosage	235.23	1	235.23	1484.96	< 0.0001	
AB	11.94	1	11.94	75.36	< 0.0001	
AC	18.71	1	18.71	118.09	< 0.0001	
BC	23.38	1	23.38	147.58	< 0.0001	
A^2	324.31	1	324.31	2047.29	< 0.0001	
B^2	91.09	1	91.09	575.04	< 0.0001	
C^2	68.94	1	68.94	435.18	< 0.0001	
Residual	1.11	7	0.1584			
Lack of Fit	0.2943	3	0.0981	0.4816	0.7127	Not significant
Pure Error	0.8146	4	0.2036			
Cor Total	992.71	16				

6.4 Effect of operational parameters on TC photocatalytic-adsorption removal

Figures 6.2 (a-c) illustrate the combined effects of various variable pairs on the percentage of TC degradation. The interactive impact of initial TC concentration and the dose of AC/ZnO-NPs on the removal efficiency is illustrated as shown in Figure 6.2 (a). The plot reveals strong quadratic relations among the variables and process output. Improved removal efficiency is demonstrated upon raising the nanocomposite from 0.3 g/L, at which point it reaches an optimal plateau at around 0.5-0.6 g/L. This initial increase is due to a greater number of active sites available for both adsorption on the AC surface and photocatalysis held on the ZnO-NPs.

The curvature of the surface suggests that any increased dosage beyond the optimal will not lead to a commensurate increase in efficiency, possibly due to aggregation of the particles, which reduces effective surface area and increases turbidity in the solution, which scatters the incident light to inhibit photocatalytic activity (M. Sharma et al., 2022). Peak removal is achieved when the TC concentration is intermediate at about 10 mg/L and decreased when moving toward higher concentrations (15 mg/L). This happens because the number of active sites, when fixed in the adsorbent/catalyst dosage, is finite. As the initial TC concentration increases, these sites become progressively saturated, leading to lower percentages of removal for the entire contaminant load (Zheng et al., 2025) .

Figure 6.2 (b) demonstrates the integrated effect between mass ratios of AC/ZnO-NPs and the dose of nanocomposite on TC removal efficiency. Similar to the observations made previously, there is an increase in efficiency under the increasing dosage up to an optimal point (~0.5-0.6 g/L), as more material is now available for the reaction (Salah et al., 2024). More critically, the ratio AC/ZnO-NPs has a different optimal range from that at which the highest removal efficiency occurs, which was approximately 3:1. This is core for the design of the composite (Akmal et al., 2024). A high ratio (4:1), which is rich in AC, may enhance initial adsorption but simultaneously inhibits overall performance by blocking light from reaching the ZnO-NPs catalyst phenomenon known as the inner filter or light-shading effect, on the other hand, a low ratio (2:1), rich in ZnO-NPs, may not leverage much the adsorptive capacity of AC, which serves to pre-concentrate TC molecules near the photocatalytic surfaces, thereby enhancing degradation kinetics (Albo Hay Allah & Alshamsi, 2023a).

Figure 6.2 further explains the interaction between the AC/ZnO-NPs ratio and initial TC concentration; the dose being held constant at the optimum level. Since an apparent peak was found in the removal efficiency of approximately 10 mg/L TC for moderate initial concentrations and an optimal composite ratio of about 3.64, the graph corroborates the earlier conclusions (Doosti et al., 2022). The curved topology of the surface indicates a strong interaction between these two parameters. At initially low TC concentrations, removal across a wider range of ratios is generally high since the service is not yet limited by either active sites or light penetration (Aljeboree et al., 2020).

When the initial TC concentration rises, sensitivity to the formulation of the composite increases. High TC concentrations (15 mg/L) show a considerable drop in efficiency since the fixed active sites (determined by the constant dose) reach saturation irrespective of the AC/ZnO-NPs ratio (Rizkallah et al., 2023). This shows powerfully that for a given contaminant load, there is a unique composite formulation that provides such performance (Tran Thi & Lee, 2017b).

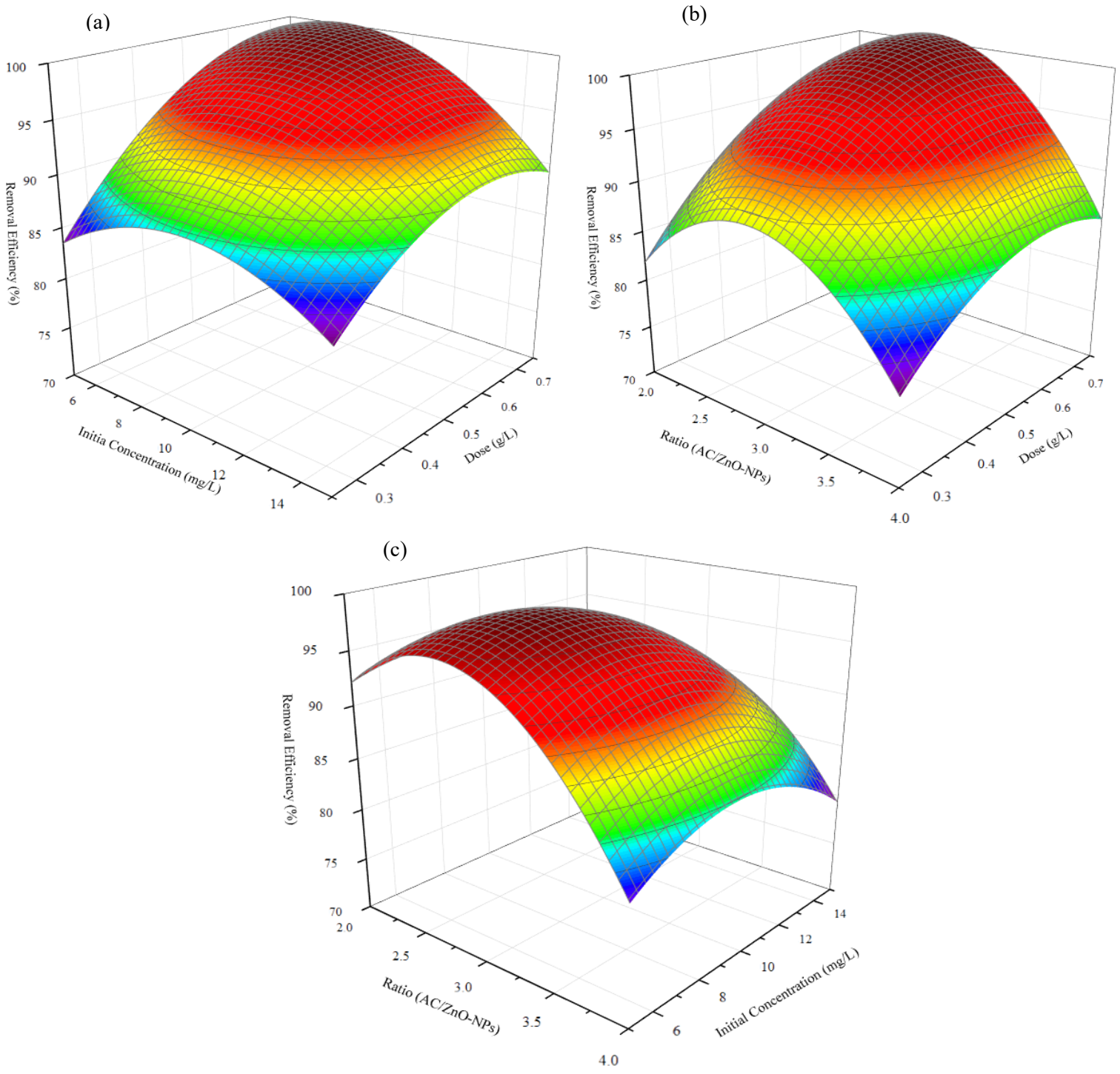

Figure 6-2 D interaction effects of parameters on the TC removal efficiency (%)

In Figure 6.3, a strong correlation is evident, with the data points clustered tightly around the diagonal regression line, visually representing the congruence between the predicted and actual outcomes. This relationship is quantified, however, by an exceptionally high coefficient of determination (R^2) value of 0.99888, indicating that this model can explain 99.888% of the variance in the responses. The correlation between predicted and experimental data strongly validates the developed model, establishing it was adequacy and reliability in navigating design space and accurately predicting TC removal efficiency using the AC/ZnO-NPs composite material through hybrid adsorption-photocatalysis technology within this experimental domain.

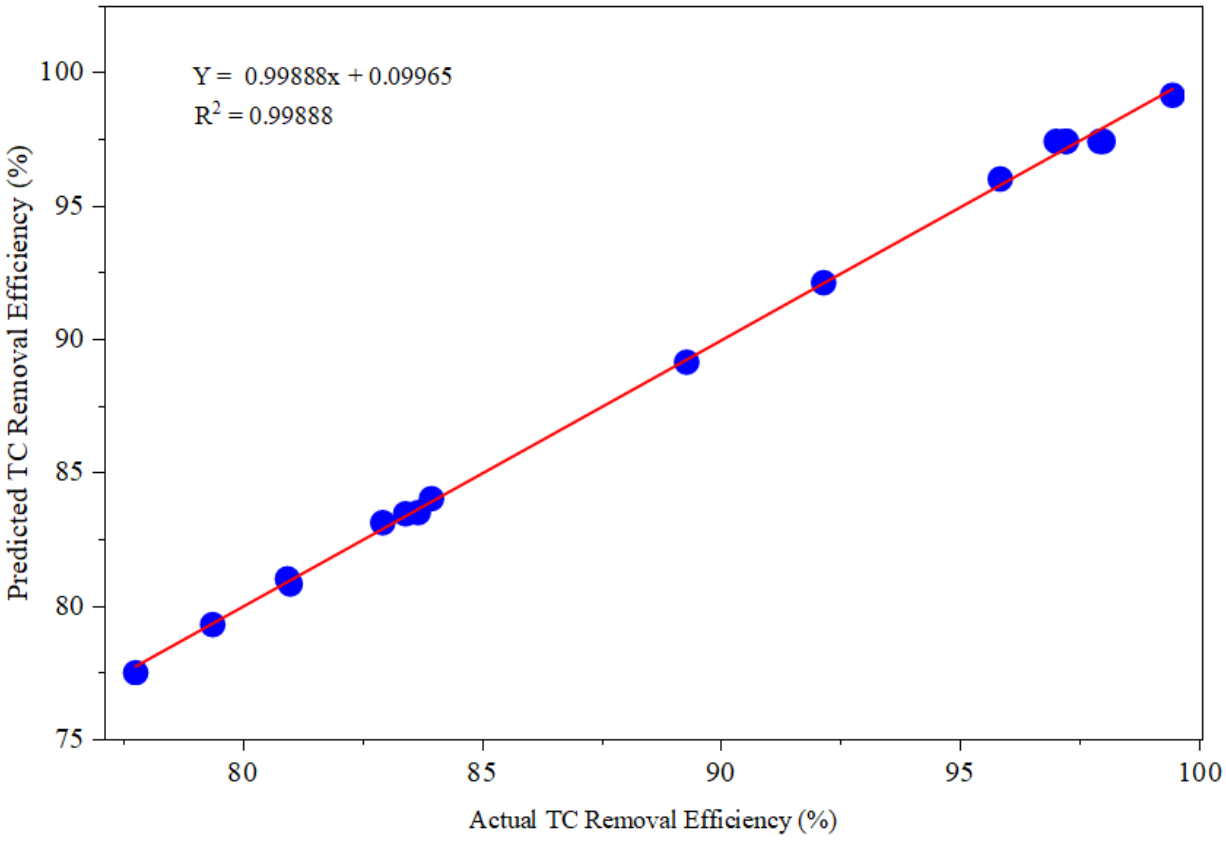

Figure 6-3 Comparison of predicted and actual values for TC removal efficiency

Table 6.5 shows all three statistical measures presented here-R^2, AAD, and RMS- support the arguments for the models' strong accuracy and reliability. R^2 is very close to 1.0, at 0.9988, thus indicating almost perfect correlation with respect to TC removal efficiency between experimental data and its prediction by the model. It means that the model accounts for 99.88% of the variation caused within TC removal efficiency, hence proving its wonderful goodness of fit. Support for such high correlation comes from the error metrics that measure how much width of error there is in the prediction.

The Average Absolute Deviation (AAD) indicates that, on average, the difference between a predicted value and its corresponding actual experimental value is just 0.171 percentage points: such a small deviation points towards a very high accuracy in general, while the RMS too is low at 0.289 and thus, very sensitive to larger errors, further confirming the absence of significant outliers and affirming the constant integrity of the model across the range of data. Hence, convergence around a near-unity value of R^2 and with places of minimal errors in AAD and RMS provides a good deal of evidence to be held in support of the robustness, accuracy, and predictability of the TC removal process, as articulated by the RSM developed.(Lu et al., 2024).

Table 6-5 Performance indicators for the RSM model approach related to TC removal efficiency.

Statistical Parameter	TC Removal Efficiency (%)
R^2	0.9988
AAD	0.171
RMS	0.289

6.5 Model optimization and validation

The RSM, along with BBD, is a very powerful statistical technique that is being more widely used by environmental engineers and scientists to help promote the optimization of chemical processes for the treatment of water, and it is effective for optimally degrading persistent pollutants like the antibiotic TC and for maximizing the removal of a critical measure of water quality. (Juyal & Sharma, 2023).

For the optimum conditions discussed above, the RSM-BBD was analyzed using Derringer's desired function method, in which values from 0 to 1 are assigned to determine how well the optimum conditions achieve the ultimate response goal (Meenu et al., 2023). To achieve maximum TC removal efficacy, the mass ratio of (AC/ZnO-NPs) 2:1 to 4:1, the composition dose 0.025 to 0.75 g/L, and the initial TC concentration was 5 to 15 mg/L were held constant at pH 5.5, and a time of 120 min. Accordingly, the maximum TC removal efficiencies of 99.83 % were observed at the optimum operating condition of mass ratio of 3.64, AC/ZnO-NPs dose of 0.747 g/L, and initial TC concentration of 5.99 mg/L, with a desirability of 1.000.

6.6 Degree of mineralization

Figure 6.4 illustrates the potential for removing TC by an augmented process of adsorption and photocatalysis on the AC/ZnO-NP composite under optimized conditions. An initial 60 min dark phase allowed for the adsorption-desorption equilibrium and gave rise to 8% reduction in TOC due to the physical adsorption on the surface of the catalyst. The very fast photocatalytic breakup of the TC molecule was observed immediately after UV light switching at t=0, as indicated by the C/C_0 curve, which suddenly drops to show that nearly 100% of the initial TC was degraded in the first 60 min of illumination, corroborating the rapid photocatalytic activity of the ZnO-NP component.

The comparison of the C/C_0 and TOC/TOC_0 curves clearly showed that TC degradation is distinctly different from its total mineralization. A very rapid drop in the parent TC concentration was observed even in a very short time frame, while the TOC removal was very slow. This observation indicates that the formation of intermediate organic by-products was taking place simultaneously with the photocatalytic conversion, signifying their gradual mineralization into

inorganic products like CO_2 and H_2O that resulted in this slower drop in the TOC/TOC_0 curve. After a total reaction time of 120 min, the TOC/TOC_0 value settled down, which corresponds to a total organic carbon removal efficiency of 93.1%, illustrating significantly high mineralization and reflecting on the effectiveness of the AC/ZnO-NP composite and, thus, 6.9 % of TOC remained and mineralization was not completely converted to water or carbon dioxide, which indicated the formation of long-lived by-products (Tran Thi & Lee, 2017a).

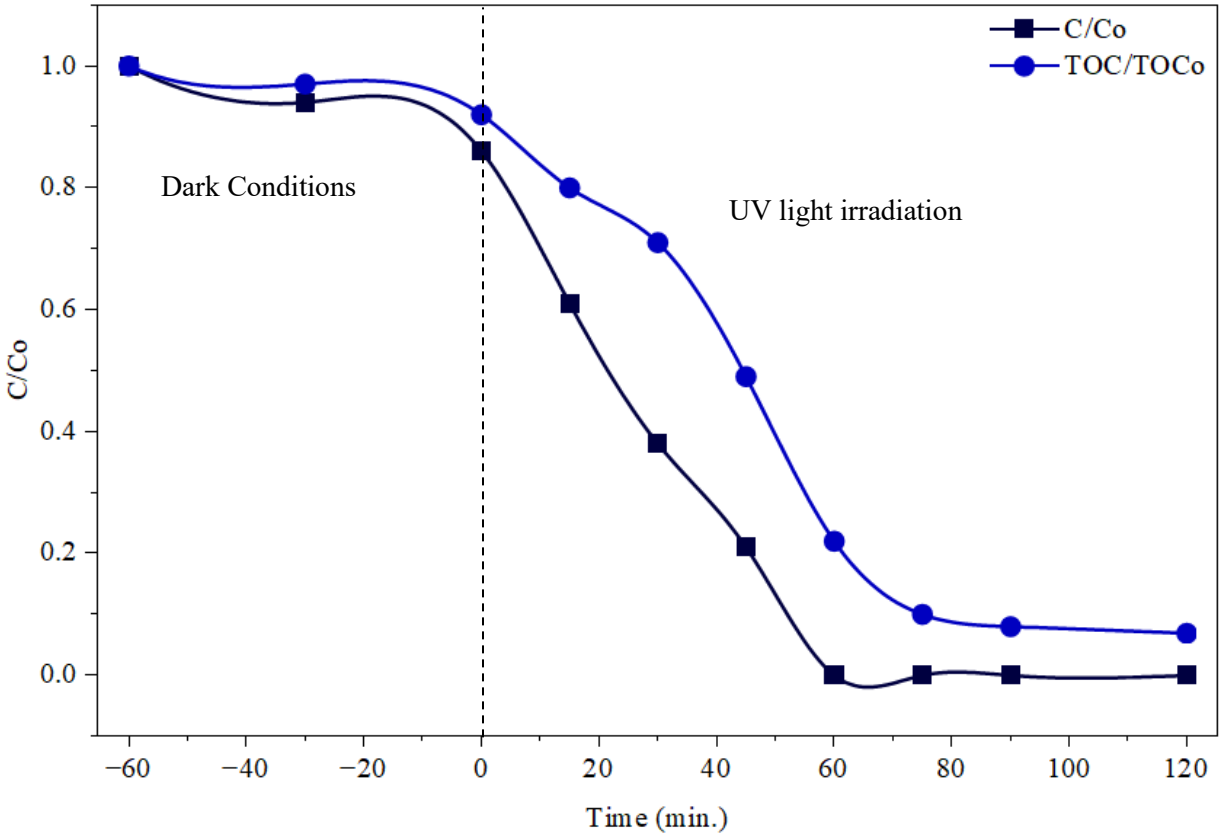

Figure 6-4 Removal of tetracycline at optimized conditions and TOC by using the Composite materials (AC/ZnO-NPs).

6.7 Stability and reusability of composite materials (AC/ZnO-NPs)

In water treatment, the reusability of adsorbents and operational stability are among the paramount factors determining the practical and economic value of a given adsorbent (Baskar et al., 2022). Figure 6.5 demonstrated that the AC/ZnO-NPs composite underwent performance testing for the removal of tetracycline (TC) over five consecutive cycles of adsorption-photocatalysis was caried out. The experimental runs were conducted under conditions determined as being optimal, namely, with a composite dosage of 0.747 g/L, an initial TC concentration of 5.99 mg/L, and a mass ratio of AC: ZnO-NPs of 3.64:1. As illustrated in Figure 6.5, the composite performed excellently in the first cycle, with a TC removal efficiency of 99.83%. A slight and gradual decline in efficiency was noted in the subsequent cycles.

For the second, third, fourth, and fifth cycles, the corresponding removal efficiencies were 98.46%, 97.05%, 95.61%, and 93.18%. The AC/ZnO-NPs composite demonstrates exceptional structural stability, evidenced by a minimal cumulative loss of only 6.65%. This high retention of efficacy is likely due to the strong anchoring of ZnO onto the carbonaceous matrix, which reduces leaching and prevents active site agglomeration during multiple regeneration cycles. Such stability is essential for future industrial applications where material longevity and cost-effectiveness are critical (Albo Hay Allah & Alshamsi, 2023b).

Several factors are causing reduced TC removal rates: obviously, the first is probably incomplete desorption of TC molecules from the active sites of the adsorbent during the regeneration procedure, causing gradual saturation and blockage of these sites (L. Zhang et al., 2025). Occasionally, there might be some losses of the composite between cycles during recovery and washing, ascribed to the minor decline. Such high reusability is very desirable as it sharply reduces the operation cost for adsorbent replacement and the secondary pollution due to spent adsorbent disposal. Therefore, the above findings support the notion of using the AC/ZnO-NPs composite as an efficient, stable, and economically feasible adsorbent for the remediation of tetracycline from aqueous solutions.(Gkika et al., 2022).

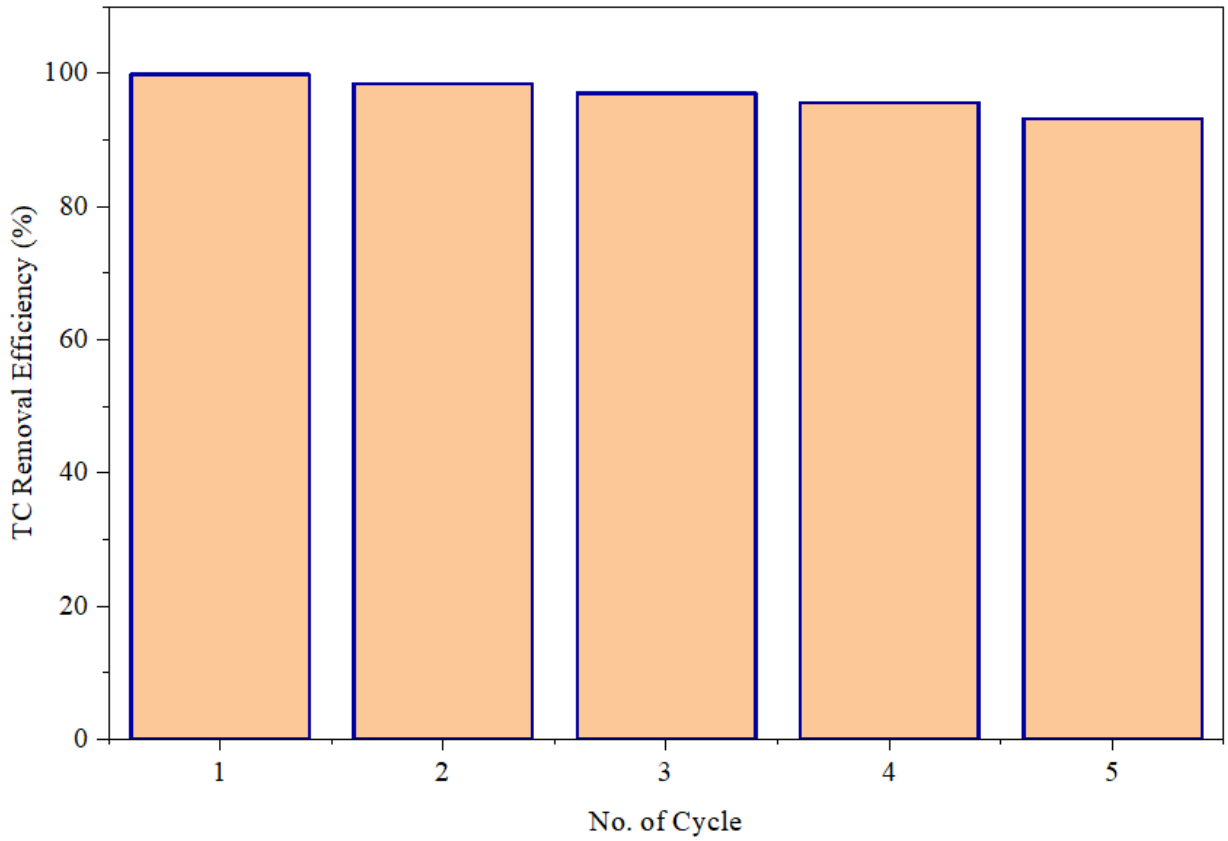

Figure 6-5 Recyclability of green-synthesized AC/ZnO-NPs for TC removal efficiency

6.8 Conclusion

This study carried out has successfully established the synthesis, characterization, and application of an innovative green-based composite material (AC/ZnO-NPs) for the efficient removal of TC from aqueous solutions through a simultaneous adsorption and photocatalysis process. This solution utilizes activated carbon derived from a sustainable biomass source (cassava peels) that has been green-synthesized into zinc oxide nanoparticles using *C. bergamia* leaf extract.

RSM BBD, the process optimization was able to identify the best operational parameters. The resulting quadratic model proved to be statistically robust and predictive enough, $R^2 = 0.9988$; the Lack of Fit test was insignificant at $P = 0.7127$. The analysis of variance (ANOVA) confirmed that all three independent variables-the AC: ZnO-NPs ratio, initial TC concentration, and composite dosage-as well as their interactions, were significant factors influencing TC removal efficiency. The optimal conditions were determined to be an AC: ZnO-NPs mass ratio of 3.64:1, a composite dosage of 0.747 g/L, and an initial TC concentration of 5.99 mg/L. Under the best conditions, 99.83% removal efficiency has been achieved, confirming the model predictions.

Such excellent performance is attributed to the strong synergistic effect between the two components. The high-surface-area AC acts as a very efficient adsorbent, concentrating TC molecules from the solution and surrounding them close to the photocatalytically reacting ZnO-NPs, thus enhancing the degradation process, as ZnO-NPs produce reactive oxygen species under light irradiation that can efficiently decompose the adsorbed TC molecules. This study thus not only introduces a highly potent material for improving water quality but also embodies the rich ground for sustainable material synthesis toward the good statistical optimization against the challenge of emerging contaminants in wastewater.

7. CONCLUSIONS AND RECOMMENDATIONS

7.1 Conclusions

The urgent environmental issue of pharmaceutical pollution has been addressed through the design, optimization, and testing of innovative and sustainable adsorbents for the removal of TC from aqueous solutions. The major contribution of this study was a holistic improvement from the green synthesis of the individual components to their assembly in a hugely effective hybrid composite material, displaying a strong synergy between these morphologies, mentioned adsorption, and photocatalysis.

This initial phase of the research led to the successful green synthesis of the materials required. Activated carbon (AC), having a well-developed and hierarchical porosity construction, was a low-cost and sustainable renewable biomass precursor made with cassava peels by $ZnCl_2$ chemical activation. At the same time, hexagonally structured wurtzite zinc oxide nanoparticles (ZnO-NPs) of bandgap energy of 3.17 eV were produced through a novel green sol-gel method, with Citrus bergamia leaf extracts being used as a modifying agent. The final output of this objective was the impregnation of these ZnO-NPs into the surface of the AC to obtain the evolved composite material (AC/ZnO-NPs).

The effectiveness of the individual components in succession was evaluated. The adsorptive ability of cassava peel AC alone was highly optimized using a rigorous Response Surface Methodology (RSM) and having an Artificial Neural Network (ANN)-based prediction tools facility, obtaining a notable removal effectiveness of 97.45% for TC. The result shows that the prepared AC is indeed a promising adsorbent. Similarly, the photocatalytic performance of green-synthesized ZnO-NPs alone was optimized to give a TC degradation efficiency of 92.1% under visible light irradiation.

The composite material (AC/ZnO-NPs) was put to the test under the objective of a combined adsorption- photocatalysis system, which was indeed the crowning achievement of the research. Resulting from this hybrid process was its highest removal, 99.83%. This result could be defined by the very powerful sharing learned from the two components.

The adsorbent, which has a high specific surface area, works excellently to enrich TC molecules from the solution toward its surface. This pre-concentration brings the pollutant close enough to hit from inside the photocatalytically active ZnO-NPs. Upon exposure to irradiation, the ZnO-NPs produce highly reactive oxygen species (ROS) that readily degrade the adsorbed TC within the same area. To this extent, synergism overcomes the limitations of individual processes.

7.2 Recommendations and future outlooks

This dissertation provides ample evidence for the intervention prospects of green-synthesized composite materials in environmental remediation. The following recommendations are given from this work to future researchers:

Performance in Real Wastewaters Matrices: The synthesized aqueous solutions were used in this study. Emphasis must be placed on the effectiveness, durability of the composite in real-effluent wastewater disposal from hospitals, the pharmaceutical industry, and the local municipal site with complicated combinations of organic matter, inorganic ions, and competing pollutants that can influence the material's performance.

Material Reusability and Regeneration: Long-term stability and reusability of the catalyst are vital aspects that reveal its economic viability. Research work should diagnose how many adsorption–photocatalysis cycles with the AC/ZnO-NPs composite can resist before an evident decrease in activity is detected. Simultaneously, more thorough progress toward much-improved economic regeneration methods, such as thermal application and solvent washing, should be prioritized.

Mechanistic Elucidation and Degradation Pathway: Advanced characterizations in addition to the synergistic demonstration would, capitalization-wise, contribute toward an even deeper understanding of the charge transfer mechanisms at the AC-ZnO interface, for instance, in situ spectroscopy, transient photocurrent response, etc. In addition, elucidation of the degradation pathway (reaction mechanisms) with respect to intermediate TC degradation byproducts and toxicity assessment should be done to ensure full mineralization and environmental safety of the process.

Widening the Scope of Pollutants: The applicability of the AC/ZnO-NPs composite needs to be evaluated against even a greater range of emerging contaminants, including other classes of antibiotics, pesticides, endocrine-disrupting chemicals, and personal care products.

In summary, this research was introduced a very efficient material in water purification but also preaches an environmentally sustainable “waste to resource” ideology, transforming biomass waste into a high-value environmental solution. The proven synergy of the AC-ZnO-NPs composite represents a powerful pathway toward developing next-generation technologies to mitigate the global challenge of emerging contaminants in water.

Pilot Scale and Continuous Flow Studies: Building upon those gained through laboratory batch tests, a pilot scale set-up modeled after the continuous flow of the AC/ZnO-NPs composite reactor system design and evaluation may then be considered for carrying on further investigations, which simulate real-life conditions by which these subjects would be subjected in an industrial or municipal wastewater treatment plant.

8. REFERENCES

Abdullahi Ari, H., Adewole, A. O., Ugya, A. Y., Asipita, O. H., Musa, M. A., & Feng, W. (2023b). Biogenic fabrication and enhanced photocatalytic degradation of tetracycline by bio structured ZnO nanoparticles. *Environmental Technology*, *44*(9), 1351–1366. https://doi.org/10.1080/09593330.2021.2001049

Abewaa, M., Mengistu, A., Takele, T., Fito, J., & Nkambule, T. (2023). Adsorptive removal of malachite green dye from aqueous solution using Rumex abyssinicus derived activated carbon. *Scientific Reports*, *13*(1), 14701. https://doi.org/10.1038/s41598-023-41957-x

Abomuti, M. A., Danish, E. Y., Firoz, A., Hasan, N., & Malik, M. A. (2021). Green synthesis of zinc oxide nanoparticles using salvia officinalis leaf extract and their photocatalytic and antifungal activities. *Biology*, *10*(11). https://doi.org/10.3390/biology10111075

Abumelha, H. M., Alzahrani, S. O., Alrefaee, S. H., Al-bonayan, A. M., Alkhatib, F., Saad, F. A., & El-Metwaly, N. M. (2023). Evaluation of tetracycline removal by magnetic metal organic framework from aqueous solutions: Adsorption isotherm, kinetics, thermodynamics, and Box-Behnken design optimization. *Journal of Saudi Chemical Society*, *27*(5), 101706. https://doi.org/https://doi.org/10.1016/j.jscs.2023.101706

Adnan, Nisar, Shah, R., Zada, F. M., Khan, B., Aziz, S., Rehman, N. U., Soonmin, H., Ahmad, N., Khan, M., & Hanzala. (2024). Novel Ni/ZnO Nanocomposites for the Effective Photocatalytic Degradation of Malachite Green Dye. *Civil Engineering Journal (Iran)*, *10*(8), 2601–2614. https://doi.org/10.28991/CEJ-2024-010-08-011

Ahmad, F., Zhu, D., & Sun, J. (2021). Environmental fate of tetracycline antibiotics: degradation pathway mechanisms, challenges, and perspectives. *Environmental Sciences Europe*, *33*. https://doi.org/10.1186/s12302-021-00511-0

Akhter, S., Bhat, M. A., Ahmed, S., & Siddiqui, W. A. (2024). Antibiotic residue contamination in the aquatic environment, sources and associated potential health risks. *Environmental Geochemistry and Health*, *46*(10), 387. https://doi.org/10.1007/s10653-024-02146-5

Akmal, A., Tahir, D., Heryanto, H., Akouibaa, A., & Rahmat, R. (2024). Synthesis and characterisation of superior AC/ZnO NPs biocomposite for hexavalent chromium Cr(VI) adsorption. *Physica Scripta*, *99*. https://doi.org/10.1088/1402-4896/ad74b7

Alamdari, S., Ghamsari, M. S., Lee, C., Han, W., Park, H., Tafreshi, M. J., & Afarideh, H. (2020). Applsci-10-03620.Pdf. *Applied Sciences*, *10*(3620), 1–19. doi:10.3390/app10103620

Albo Hay Allah, M. A., & Alshamsi, H. A. (2023a). Facile green synthesis of ZnO/AC nanocomposites using Pontederia crassipes leaf extract and their photocatalytic properties based on visible light activation. *Journal of Materials Science: Materials in Electronics*, *34*(16), 1263. https://doi.org/10.1007/s10854-023-10636-y

Albo Hay Allah, M. A., & Alshamsi, H. A. (2023b). Green synthesis of AC/ZnO nanocomposites for adsorptive removal of organic dyes from aqueous solution. *Inorganic Chemistry Communications*, *157*, 111415. https://doi.org/https://doi.org/10.1016/j.inoche.2023.111415

Ali, J., Irshad, R., Li, B., Tahir, K., Ahmad, A., Shakeel, M., Khan, N. U., & Khan, Z. U. H. (2018). Synthesis and characterization of phytochemical fabricated zinc oxide nanoparticles with enhanced antibacterial and catalytic applications. *Journal of Photochemistry and Photobiology. B, Biology*, *183*, 349–356. https://doi.org/10.1016/j.jphotobiol.2018.05.006

Aljeboree, A. M., Abdulrazzak, F. H., Alqaragoly, M. B., Karam, F. F., Alkaim, A. F., & Hussein, F. H. (2020). Photocatalytic of pharmaceutical tetracycline (TCS) by zinc oxide (ZnO). *Journal of Critical Reviews*, *7*(7), 960–962. https://doi.org/10.31838/jcr.07.07.174

Alshahateet, S. F., Al-Trawneh, S. A., Er-rajy, M., Zerrouk, M., Azzaoui, K., Al-Tawarh, W. M., Hammouti, B., Salghi, R., Sabbahi, R., Alanazi, M. M., & Rhazi, L. (2024). Green Synthesis of Zinc Oxide Nanoparticles for Tetracycline Adsorption: Experimental Insights and DFT Study. *Plants*, *13*(23). https://doi.org/10.3390/plants13233386

Amakoromo, T. E., Abumere, O. E., & Amusan, J. A. (2022). Synthesis and characterization of a high surface area activated carbon derived from cassava peels waste by KOH activation.

Scientia Africana, *20*(3), 141–148. https://doi.org/10.4314/sa.v20i3.12

Amakoromo, T. E., Abumere, O. E., Amusan, J. A., Anye, V., & Bello, A. (2021). Porous carbon from Manihot Esculenta (cassava) peels waste for charge storage applications. *Current Research in Green and Sustainable Chemistry*, *4*(February), 100098. https://doi.org/10.1016/j.crgsc.2021.100098

Amangelsin, Y., Semenova, Y., Dadar, M., Aljofan, M., & Bjørklund, G. (2023a). The Impact of Tetracycline Pollution on the Aquatic Environment and Removal Strategies. *Antibiotics (Basel, Switzerland)*, *12*(3). https://doi.org/10.3390/antibiotics12030440

Amir, M., Fazal, T., Iqbal, J., Din, A. A., Ahmed, A., Ali, A., Razzaq, A., Ali, Z., Rehman, M. S. U., & Park, Y.-K. (2022). Integrated adsorptive and photocatalytic degradation of pharmaceutical micropollutant, ciprofloxacin employing biochar-ZnO composite photocatalysts. *Journal of Industrial and Engineering Chemistry*, *115*, 171–182. https://doi.org/https://doi.org/10.1016/j.jiec.2022.07.050

Anisuzzaman, S. M., Joseph, C. G., Pang, C. K., Affandi, N. A., Maruja, S. N., & Vijayan, V. (2022). *Current Trends in the Utilization of Photolysis and Photocatalysis Treatment Processes for the Remediation of Dye Wastewater : A Short Review*.

Anjali, R., & Shanthakumar, S. (2019). Insights on the current status of occurrence and removal of antibiotics in wastewater by advanced oxidation processes. *Journal of Environmental Management*, *246*, 51–62. https://doi.org/https://doi.org/10.1016/j.jenvman.2019.05.090

Ao, X., Sun, W., Li, S., Yang, C., Li, C., & Lu, Z. (2019). Degradation of tetracycline by medium pressure UV-activated peroxymonosulfate process: Influencing factors, degradation pathways, and toxicity evaluation. *Chemical Engineering Journal*, *361*, 1053–1062. https://doi.org/10.1016/j.cej.2018.12.133

Asgharian, M., Mehdipourghazi, M., Khoshandam, B., & Keramati, N. (2020). Experimental design and rsm modeling of tetracycline photocatalytic degradation using rgo/zno/cu. *Desalination and Water Treatment*, *195*, 177–185. https://doi.org/10.5004/dwt.2020.25878

Astuti, W., Hidayah, M., Fitriana, L., Mahardhika, M. A., & Irchamsyah, E. F. (2020).

Preparation of activated carbon from cassava peel by microwave-induced H3PO4 activation for naphthol blue-black removal. *AIP Conference Proceedings*, *2243*. https://doi.org/10.1063/5.0001464

Azanu, D., Styrishave, B., Darko, G., Juhl, J., & Clement, R. (2018). Science of the Total Environment Occurrence and risk assessment of antibiotics in water and lettuce in Ghana. *Science of the Total Environment*, *622–623*, 293–305. https://doi.org/10.1016/j.scitotenv.2017.11.287

Azeez, S. O., & Jimoh, A. A. (2022). *Box Behnken Design in the Optimization of Rhodamine B Adsorption onto Activated Carbon Prepared from Delonix regia Seeds and Pods*. *9*(1), 205–222.

Babu, D. S., Srivastava, V., Nidheesh, P. V, & Kumar, M. S. (2019). Detoxification of water and wastewater by advanced oxidation processes. *Science of The Total Environment*, *696*, 133961. https://doi.org/https://doi.org/10.1016/j.scitotenv.2019.133961

Bankole, D. T., Oluyori, A. P., & Inyinbor, A. A. (2023). The removal of pharmaceutical pollutants from aqueous solution by Agro-waste. *Arabian Journal of Chemistry*, *16*(5), 104699. https://doi.org/https://doi.org/10.1016/j.arabjc.2023.104699

Barzinjy, A. A., & Azeez, H. H. (2020). Green synthesis and characterization of zinc oxide nanoparticles using Eucalyptus globulus Labill. leaf extract and zinc nitrate hexahydrate salt. *SN Applied Sciences*, *2*(5), 1–14. https://doi.org/10.1007/s42452-020-2813-1

Baskar, A. V, Bolan, N., Hoang, S. A., Sooriyakumar, P., Kumar, M., Singh, L., Jasemizad, T., Padhye, L. P., Singh, G., Vinu, A., Sarkar, B., Kirkham, M. B., Rinklebe, J., Wang, S., Wang, H., Balasubramanian, R., & Siddique, K. H. M. (2022). Recovery, regeneration and sustainable management of spent adsorbents from wastewater treatment streams: A review. *The Science of the Total Environment*, *822*, 153555. https://doi.org/10.1016/j.scitotenv.2022.153555

Belcaid, A., Beakou, B. H., Bouhsina, S., & Anouar, A. (2022). Insight into adsorptive removal of methylene blue, malachite green, and rhodamine B dyes by cassava peel biochar (Manihot esculenta Crantz) in single, binary, and ternary systems: competitive adsorption

study and theoretical calculations. *Biomass Conversion and Biorefinery*, *0123456789*. https://doi.org/10.1007/s13399-022-02928-w

Belcaid, A., Beakou, B. H., El Hassani, K., Bouhsina, S., & Anouar, A. (2021). Efficient removal of Cr (VI) and Co (II) from aqueous solution by activated carbon from Manihot esculenta Crantz agricultural bio-waste. *Water Science and Technology*, *83*(3), 556–566. https://doi.org/10.2166/wst.2020.585

Beltrán, S. D., Piña, G. M., Efrén, E., Gutiérrez, G., Eleuterio, R. A., Luis, J., Rivas, G., & García, A. R. (2025). *ANN-Based Prediction of Tartrazine Adsorption on Chitosan – Polyvinyl Alcohol Hydrogel Beads : A Comparison with Kinetic Models*. 1–15.

Benaiche, G., Belhaddad, O. E., Djaidja, S., & Mechegueg, L. (2025). Eco-Friendly Synthesis of Zinc Oxide Nanoparticles Using Camellia Sinensis Leaf Extracts. *Asian Journal of Green Chemistry*, *9*(2), 220–230. https://doi.org/10.48309/AJGC.2025.492527.1608

Bhargava, N., Bahadur, N., & Kansal, A. (2023). Techno-economic assessment of integrated photochemical AOPs for sustainable treatment of textile and dyeing wastewater. *Journal of Water Process Engineering*, *56*, 104302. https://doi.org/https://doi.org/10.1016/j.jwpe.2023.104302

Boutra, B., Sebti, A., & Trari, M. (2022). Response surface methodology and artificial neural network for optimization and modeling the photodegradation of organic pollutants in water. *International Journal of Environmental Science and Technology*, *19*(11), 11263–11278. https://doi.org/10.1007/s13762-021-03875-1

Briche, S., Derqaoui, M., Belaiche, M., El Mouchtari, E. M., Wong-Wah-Chung, P., & Rafqah, S. (2020). Nanocomposite material from TiO2 and activated carbon for the removal of pharmaceutical product sulfamethazine by combined adsorption/photocatalysis in aqueous media. *Environmental Science and Pollution Research*, *27*(20), 25523–25534. https://doi.org/10.1007/s11356-020-08939-2

Campus, O. (2018). *Modeling Performance of Response Surface Methodology and Artificial Neural Network DOI : https://dx.doi.org/10.4314/jasem.v22i6.6*.

Chandra, N., Prabhakar, J., Debasis, S., Prateek, M., & Silver, A. (2025). A mini review on the synthesis , antimicrobial , and anticancer activities of Pd NPs. *Discover Chemistry*. https://doi.org/10.1007/s44371-025-00101-6

Chang, J., Shen, Z., Hu, X., Schulman, E., Cui, C., Guo, Q., & Tian, H. (2020). Adsorption of Tetracycline by Shrimp Shell Waste from Aqueous Solutions: Adsorption Isotherm, Kinetics Modeling, and Mechanism. *ACS Omega*, *5*(7), 3467–3477. https://doi.org/10.1021/acsomega.9b03781

Cheng, N., Wang, B., Wu, P., Lee, X., Xing, Y., Chen, M., & Gao, B. (2021). Adsorption of emerging contaminants from water and wastewater by modified biochar: A review. *Environmental Pollution*, *273*, 116448. https://doi.org/https://doi.org/10.1016/j.envpol.2021.116448

Chicco, D., Warrens, M. J., & Jurman, G. (2021). The coefficient of determination R-squared is more informative than SMAPE, MAE, MAPE, MSE and RMSE in regression analysis evaluation. *PeerJ Computer Science*, *7*, 1–24. https://doi.org/10.7717/PEERJ-CS.623

Chow, L. K. M., Ghaly, T. M., & Gillings, M. R. (2021). A survey of sub-inhibitory concentrations of antibiotics in the environment. *Journal of Environmental Sciences*, *99*, 21–27. https://doi.org/https://doi.org/10.1016/j.jes.2020.05.030

Chu, K. H., Hashim, M. A., Zawawi, M. H., & Bollinger, J.-C. (2025). The Weber–Morris model in water contaminant adsorption: Shattering long-standing misconceptions. *Journal of Environmental Chemical Engineering*, *13*(4), 117266. https://doi.org/https://doi.org/10.1016/j.jece.2025.117266

Constantino, D. S. M., Dias, M. M., Silva, A. M. T., Faria, J. L., & Silva, C. G. (2022). Intensification strategies for improving the performance of photocatalytic processes: A review. *Journal of Cleaner Production*, *340*, 130800. https://doi.org/https://doi.org/10.1016/j.jclepro.2022.130800

Cruz-Quesada, G., García-Ruíz, C., López-Ramón, M. V., Fernández-Poyatos, M. del P., & Velo-Gala, I. (2025). Carbon-based metal oxide nanocomposites for water treatment by photocatalytic processes. *Environmental Research*, *279*, 121724. https://doi.org/https://doi.org/10.1016/j.envres.2025.121724

Cuetero-Martínez, Y., de los Cobos-Vasconcelos, D., Aguirre-Garrido, J. F., Lopez-Vidal, Y., & Noyola, A. (2023). Next-generation Sequencing for Surveillance of Antimicrobial Resistance and Pathogenicity in Municipal Wastewater Treatment Plants. *Current Medicinal Chemistry*, *30*(1), 5–29. https://doi.org/https://doi.org/10.2174/0929867329666220802093415

Dai, Y., Liu, M., Li, J., Yang, S., Sun, Y., Sun, Q., Wang, W., Lu, L., Zhang, K., Xu, J., Zheng, W., Hu, Z., Yang, Y., Gao, Y., & Liu, Z. (2020). A review on pollution situation and treatment methods of tetracycline in groundwater. *Separation Science and Technology (Philadelphia)*, *55*(5), 1005–1021. https://doi.org/10.1080/01496395.2019.1577445

Dang, V. D., Nguyen, H.-H. T., Nguyen, X. C., & Truong, H. B. (2025). Green Synthesis of Zinc Oxide Nanomaterials for Water Remediation: A Review. *International Journal of Environmental Research*, *19*(5), 197. https://doi.org/10.1007/s41742-025-00872-x

Dattola, A., & Gullo, G. (2024). Effect of two reflective materials on the physiological and production behaviour of bergamot (Citrus bergamia Risso et Poiteau) plants. *Scientia Horticulturae*, *338*, 113636. https://doi.org/https://doi.org/10.1016/j.scienta.2024.113636

De Gisi, S., Lofrano, G., Grassi, M., & Notarnicola, M. (2016). Characteristics and adsorption capacities of low-cost sorbents for wastewater treatment: A review. *Sustainable Materials and Technologies*, *9*, 10–40. https://doi.org/10.1016/j.susmat.2016.06.002

de Oliveira Cardoso Nascimento, C., Palácio, S. M., Veit, M. T., Borba, F. H., Zorzo, C. F., & Amado, D. V. (2024). Degradation of antibiotic sulphamethoxazole by application of modified photo-Fenton processes: kinetics, degradation pathways and toxicity. *International Journal of Environmental Studies*, *81*(2), 693–723. https://doi.org/10.1080/00207233.2024.2322896

Delgado, N., Capparelli, A., Navarro, A., & Marino, D. (2019). Pharmaceutical emerging pollutants removal from water using powdered activated carbon : Study of kinetics and adsorption equilibrium. *Journal of Environmental Management*, *236*(September 2018), 301–308. https://doi.org/10.1016/j.jenvman.2019.01.116

Deng, H., Wang, X., Wang, L., Li, Z., Liang, P., Ou, J., Liu, K., Yuan, L., Jiang, Z., Zheng, L., Chai, Z., & Shi, W. (2020). Enhanced photocatalytic reduction of aqueous Re(VII) in ambient air by amorphous TiO2/g-C3N4 photocatalysts: Implications for Tc(VII) elimination. *Chemical Engineering Journal*, *401*, 125977. https://doi.org/https://doi.org/10.1016/j.cej.2020.125977

Dey, S., Mohanty, D. lochan, Divya, N., Bakshi, V., Mohanty, A., Rath, D., Das, S., Mondal, A., Roy, S., & Sabui, R. (2025). A critical review on zinc oxide nanoparticles: Synthesis, properties and biomedical applications. *Intelligent Pharmacy*, *3*(1), 53–70. https://doi.org/https://doi.org/10.1016/j.ipha.2024.08.004

Dimitropoulos, M., Aggelopoulos, C. A., Sygellou, L., Tsantis, S. T., Koutsoukos, P. G., & Yannopoulos, S. N. (2024). Unveiling the photocorrosion mechanism of zinc oxide photocatalyst: Interplay between surface corrosion and regeneration. *Journal of Environmental Chemical Engineering*, *12*(2), 112102. https://doi.org/https://doi.org/10.1016/j.jece.2024.112102

Długosz, O., Staroń, A., Brzoza, P., & Banach, M. (2022). Synergistic effect of sorption and photocatalysis on the degree of dye removal in single and multicomponent systems on ZnO-SnO2. *Environmental Science and Pollution Research*, *29*(18), 27042–27050. https://doi.org/10.1007/s11356-021-18044-7

Donkor, E. S., Odoom, A., & Hotor, P. (2025). *Antibiotic Concentrations in Aquatic Environments of the African Continent : A Systematic Review and Predicted No-Effect Concentration (PNEC) Assessment*. https://doi.org/10.1177/11786302251391299

Doosti, M., Jahanshahi, R., Laleh, S., Sobhani, S., & Sansano, J. M. (2022). Solar light induced photocatalytic degradation of tetracycline in the presence of ZnO/NiFe2O4/Co3O4 as a new

and highly efficient magnetically separable photocatalyst. *Frontiers in Chemistry*, *10*(October), 1–17. https://doi.org/10.3389/fchem.2022.1013349

Dubey, M., Pandey, S., & Tyagi, M. (2025). *Carbon-Based Nanocomposites for Pharmaceutical Contaminants Degradation in Water Sources BT - Carbon-Based Nanocomposites for Sustainable Applications, Volume II: Energy and Environmental Innovations* (V. Khanna (ed.); pp. 343–369). Springer Nature Switzerland. https://doi.org/10.1007/978-3-031-96895-2_16

Ebele, A. J., Oluseyi, T., Drage, D. S., Harrad, S., & Abou-Elwafa Abdallah, M. (2020). Occurrence, seasonal variation and human exposure to pharmaceuticals and personal care products in surface water, groundwater and drinking water in Lagos State, Nigeria. *Emerging Contaminants*, *6*, 124–132. https://doi.org/https://doi.org/10.1016/j.emcon.2020.02.004

Ekekwe, E. D., Nnabuike, C. C., & Chibuzo, C. K. (2018). Adsorption of Zinc on Cassava Peels Activated Carbon and Kaolin Clay: Kinetics, Thermodynamics and Optimization Studies. *International Journal of Advances in Scientific Research and Engineering*, *January*. https://doi.org/10.7324/ijasre.2018.32619

Eniola, J., Kumar, R., Barakat, M., & Rashid, J. (2022). A review on conventional and advanced hybrid technologies for pharmaceutical wastewater treatment. *Journal of Cleaner Production*, *356*, 131826. https://doi.org/10.1016/j.jclepro.2022.131826

Eswaran, P., Madasamy, P. D., Pillay, K., & Brink, H. (2025). Sunlight-driven photocatalytic degradation of methylene blue using ZnO/biochar nanocomposite derived from banana peels. *Biomass Conversion and Biorefinery*, *15*(8), 12347–12367. https://doi.org/10.1007/s13399-024-05999-z

Faisal, S., Jan, H., Shah, S. A., Shah, S., Khan, A., Akbar, M. T., Rizwan, M., Jan, F., Wajidullah, Akhtar, N., Khattak, A., & Syed, S. (2021). Green Synthesis of Zinc Oxide (ZnO) Nanoparticles Using Aqueous Fruit Extracts of Myristica fragrans: Their Characterizations and Biological and Environmental Applications. *ACS Omega*, *6*(14), 9709–9722. https://doi.org/10.1021/acsomega.1c00310

Farahani, R. (2024). Adsorptive and Photocatalytic Removal of Methylene Blue and Tetracyline Residue By Covalent Organic Framework Functionalized With Titanium Dioxide Nanosheets Adsorbent From Water. *Journal CleanWAS*, *8*(1), 11–16. https://doi.org/10.26480/jcleanwas.01.2024.11.16

Formisano, C., Rigano, D., Lopatriello, A., Sirignano, C., Ramaschi, G., Arnoldi, L., Riva, A., Sardone, N., & Taglialatela-Scafati, O. (2019). Detailed Phytochemical Characterization of Bergamot Polyphenolic Fraction (BPF) by UPLC-DAD-MS and LC-NMR. *Journal of Agricultural and Food Chemistry*, *67*. https://doi.org/10.1021/acs.jafc.8b06591

Foroughi, M., Rahmani, A. R., Asgari, G., Nematollahi, D., Yetilmezsoy, K., & Samarghandi, M. R. (2020). Optimization and Modeling of Tetracycline Removal from Wastewater by Three-Dimensional Electrochemical System: Application of Response Surface Methodology and Least Squares Support Vector Machine. *Environmental Modeling & Assessment*, *25*(3), 327–341. https://doi.org/10.1007/s10666-019-09675-9

Fouda, A., Saied, E., Eid, A. M., Kouadri, F., Alemam, A. M., Hamza, M. F., Alharbi, M., Elkelish, A., & Hassan, S. E. D. (2023). Green Synthesis of Zinc Oxide Nanoparticles Using an Aqueous Extract of Punica granatum for Antimicrobial and Catalytic Activity. *Journal of Functional Biomaterials*, *14*(4). https://doi.org/10.3390/jfb14040205

G, G., S, K., R, Y. K., Bhatia, S. K., S, A. K., M, R., Kumar, G., Pugazhendhi, A., Chi, N. T. L., & J, R. B. (2021). Valorization of agricultural residues: Different biorefinery routes. *Journal of Environmental Chemical Engineering*, *9*(4), 105435. https://doi.org/https://doi.org/10.1016/j.jece.2021.105435

Ganapathy, S., Balasubramanian, P., Vasanth, B., & Thulasiraman, S. (2021). Comparative investigation of Artificial Neural Network (ANN) and Response Surface Methodology (RSM) expectation in EDM parameters. *Materials Today: Proceedings*, *46*, 9592–9596. https://doi.org/https://doi.org/10.1016/j.matpr.2020.05.499

Garrido-Cardenas, J. A., Esteban-García, B., Agüera, A., Sánchez-Pérez, J. A., & Manzano-Agugliaro, F. (2020). Wastewater treatment by advanced oxidation process and their worldwide research trends. *International Journal of Environmental Research and Public Health*, *17*(1). https://doi.org/10.3390/ijerph17010170

Gayathiri, M., Pulingam, T., Lee, K. T., & Sudesh, K. (2022). Activated carbon from biomass waste precursors: Factors affecting production and adsorption mechanism. *Chemosphere*, *294*, 133764. https://doi.org/https://doi.org/10.1016/j.chemosphere.2022.133764

Ge, Y., Ying, K., Yu, G., Ali, M. U., Idris, A. M., Shahab, A., & Ullah, H. (2025). *A systematic review on machine learning-aided design of engineered biochar for soil and water contaminant removal*. *July*. https://doi.org/10.3389/fsoil.2025.1623083

Georgin, J., Pinto, D., Franco, D. S. P., Netto, M. S., Lazarotto, J. S., Allasia, D. G., Tassi, R., Silva, L. F. O., & Dotto, G. L. (2022). *Improved Adsorption of the Toxic Herbicide Diuron Using Activated Carbon Obtained from Residual Cassava Biomass*.

Getahun, A. (2026). *Fruit and Vegetable Peels as Alternative Feed for Sustainable Poultry Production : A Solution for Small-Scale Farms in Central and Southern Ethiopia*. https://doi.org/10.1002/vms3.70791

Gheytanzadeh, M., Baghban, A., Habibzadeh, S., Jabbour, K., Esmaeili, A., Mohaddespour, A., & Abida, O. (2022). An insight into tetracycline photocatalytic degradation by MOFs using the artificial intelligence technique. *Scientific Reports*, *12*(1), 6615. https://doi.org/10.1038/s41598-022-10563-8

Gholami, P., Khataee, A., Soltani, R. D. C., Dinpazhoh, L., & Bhatnagar, A. (2020). Photocatalytic degradation of gemifloxacin antibiotic using Zn-Co-LDH@biochar nanocomposite. *Journal of Hazardous Materials*, *382*, 121070. https://doi.org/https://doi.org/10.1016/j.jhazmat.2019.121070

Gkika, D. A., Mitropoulos, A. C., & Kyzas, G. Z. (2022). Why reuse spent adsorbents? The latest challenges and limitations. *Science of The Total Environment*, *822*, 153612.

https://doi.org/https://doi.org/10.1016/j.scitotenv.2022.153612

Gowland, D., Robertson, N., & Chatzisymeon, E. (2024). Life Cycle Assessment of Immobilised and Slurry Photocatalytic Systems for Removal of Natural Organic Matter in Water. *Environments*, *11*, 114. https://doi.org/10.3390/environments11060114

Gruca, D., Wais, M., Zając, M., Zalewski, P., Wróblewski, W., & Raabe, A. (2024). Bergamot Polyphenols: Promising Agents for Health and Wellness. *Journal of Education, Health and Sport*, *65*, 49852. https://doi.org/10.12775/JEHS.2024.65.009

Guo, Z., Zhang, T., Yang, H., Zhu, X., Lu, S., Chen, A., Fan, M., & Qu, J. (2025). Unraveling tetracycline and its degradation product: Induction mechanisms of antibiotic resistance in Escherichia coli. *Science of The Total Environment*, *970*, 178959. https://doi.org/https://doi.org/10.1016/j.scitotenv.2025.178959

Gupta, D., Boora, A., Thakur, A., & Gupta, T. K. (2023). Green and sustainable synthesis of nanomaterials: Recent advancements and limitations. *Environmental Research*, *231*, 116316. https://doi.org/https://doi.org/10.1016/j.envres.2023.116316

Gurylev, V., & Perng, T. P. (2021). Defect engineering of ZnO: Review on oxygen and zinc vacancies. *Journal of the European Ceramic Society*, *41*(10), 4977–4996. https://doi.org/https://doi.org/10.1016/j.jeurceramsoc.2021.03.031

Hama Aziz, K. H., Mustafa, F. S., Karim, M. A. H., & Hama, S. (2025). Pharmaceutical pollution in the aquatic environment: advanced oxidation processes as efficient treatment approaches: a review. *Materials Advances*. https://doi.org/10.1039/d4ma01122h

Hameedi, I. T. (2021). Determination of tetracycline hydrochloride in pure and pharmaceutical samples via oxidative coupling reaction. *Materials Today: Proceedings*, *42*(xxxx), 2953–2958. https://doi.org/10.1016/j.matpr.2020.12.802

Hasan, M., Islam, M. D., & Mondal, B. (2024). *Nanomaterials for the removal of pollutants from pharmaceutical wastewater* (pp. 171–193). https://doi.org/10.1016/B978-0-323-99278-7.00012-2

Hou, J., Wang, C., Mao, D., & Luo, Y. (2015). *The occurrence and fate of tetracyclines in two pharmaceutical wastewater treatment plants of Northern China*. https://doi.org/10.1007/s11356-015-5431-5

Hübner, U., Spahr, S., Lutze, H., Wieland, A., Rüting, S., Gernjak, W., & Wenk, J. (2024). Advanced oxidation processes for water and wastewater treatment – Guidance for systematic future research. *Heliyon*, *10*(9), e30402. https://doi.org/https://doi.org/10.1016/j.heliyon.2024.e30402

Jayachandran, A., T R, A., & Nair, A. S. (2021). Green synthesis and characterization of zinc oxide nanoparticles using Cayratia pedata leaf extract. *Biochemistry and Biophysics Reports*, *26*, 100995. https://doi.org/10.1016/j.bbrep.2021.100995

Jia, K., Liu, G., Lang, D.-N., Chen, S.-F., Yang, C., Wu, R.-L., Wang, W., & Wang, J.-D. (2022). Degradation of tetracycline by visible light over ZnO nanophotocatalyst. *Journal of the Taiwan Institute of Chemical Engineers*, *136*, 104422. https://doi.org/10.1016/j.jtice.2022.104422

Jia, W., Sun, L., Li, H., & Lv, T. (2025). *Adsorption of oxytetracycline hydrochloride by magnetic activated carbon : kinetics , mechanism and site energy distribution analysis*. *September*, 1–16. https://doi.org/10.3389/fmars.2025.1542584

John, K. I., Issa, T. B., Ho, G., Nikoloski, A. N., & Li, D. (2024). Enhanced Visible-Light-Assisted Photocatalytic Removal of Tetracycline Using Co/La@g-C3N4 Ternary Nanocomposite and Underlying Reaction Mechanisms. *Water (Switzerland)*, *16*(18). https://doi.org/10.3390/w16182563

JUYAL, J., & SHARMA, S. K. (2023). Optimization of Process Parameters for Dye Removal Through Chitinous Waste By Response Surface Methodology. *Pollution Research*, *42*(01), 80–87. https://doi.org/10.53550/pr.2023.v42i01.013

K. Vimalashanmugam, T. V. (2012). Response Surface Methodology Optimization of Process Parameters for Silage Production by Effective Microorganisms using Central Composite

Design. *International Journal of Engineering Research and Applications (IJERA)*, *2*(6), 277–287.

K, F. N., Tiwari, A., Shaik, A. H., P, I., Brianna, B., Anwar, A., & Chandan, M. R. (2025). Anti-cancer and antimicrobial efficacy of ZnO nanoparticles synthesized via green route using Amaranthus dubius (Spleen Amaranth) leaves extract. *Green Chemistry Letters and Reviews*, *18*(1), 2453532. https://doi.org/10.1080/17518253.2025.2453532

Kalam, S., Abu-Khamsin, S. A., Kamal, M. S., & Patil, S. (2021). Surfactant Adsorption Isotherms: A Review. *ACS Omega*, *6*(48), 32342–32348. https://doi.org/10.1021/acsomega.1c04661

Kanagalakshmi, M., Devi, S. G., Ananthi, P., & Pius, A. (2024). *Adsorption Isotherms and Kinetic Models BT - Carbon Nanomaterials and their Composites as Adsorbents* (J. Tharini & S. Thomas (eds.); pp. 135–154). Springer International Publishing. https://doi.org/10.1007/978-3-031-48719-4_8

Karam, S. T., & Abdulrahman, A. F. (2022). Green Synthesis and Characterization of ZnO Nanoparticles by Using Thyme Plant Leaf Extract. *Photonics*, *9*(8). https://doi.org/10.3390/photonics9080594

Karcıoğlu Karakaş, Z., & Dönmez, Z. (2025). A Sustainable Approach in the Removal of Pharmaceuticals: The Effects of Operational Parameters in the Photocatalytic Degradation of Tetracycline with MXene/ZnO Photocatalysts. *Sustainability (Switzerland)*, *17*(5). https://doi.org/10.3390/su17051904

Kassahun, S. K., Kiflie, Z., Kim, H., & Baye, A. F. (2021). Process optimization and kinetics analysis for photocatalytic degradation of emerging contaminant using N-doped TiO2-SiO2 nanoparticle: Artificial Neural Network and Surface Response Methodology approach. *Environmental Technology and Innovation*, *23*, 101761. https://doi.org/10.1016/j.eti.2021.101761

Katlam, S., Deshmukh, Y. A., & Jadhav, P. R. (2017). *IJBCP International Journal of Basic & Clinical Pharmacology Original Research Article Comparative study of oxytetracycline and doxycycline on calcium chelation : in-vitro assay*. *6*(5), 1160–1164.

Kayiwa, R., Kasedde, H., Lubwama, M., & Kirabira, J. B. (2021). Mesoporous activated carbon yielded from pre-leached cassava peels. *Bioresources and Bioprocessing*, *8*(1). https://doi.org/10.1186/s40643-021-00407-0

Kayiwa, R., Kasedde, H., Lubwama, M., & Kirabira, J. B. (2022). Active Pharmaceutical Ingredients Sequestrated from Water Using Novel Mesoporous Activated Carbon Optimally Prepared from Cassava Peels. *Water (Switzerland)*, *14*(21). https://doi.org/10.3390/w14213371

kazemi, S., Hosseingholian, A., Gohari, S. D., Feirahi, F., Moammeri, F., Mesbahian, G., Moghaddam, Z. S., & Ren, Q. (2023). Recent advances in green synthesized nanoparticles: from production to application. *Materials Today Sustainability*, *24*, 100500. https://doi.org/https://doi.org/10.1016/j.mtsust.2023.100500

Khasawneh, O. F. S., & Palaniandy, P. (2021). Occurrence and removal of pharmaceuticals in wastewater treatment plants. *Process Safety and Environmental Protection*, *150*, 532–556. https://doi.org/https://doi.org/10.1016/j.psep.2021.04.045

Klein, E. Y., Van Boeckel, T. P., Martinez, E. M., Pant, S., Gandra, S., Levin, S. A., Goossens, H., & Laxminarayan, R. (2018). Global increase and geographic convergence in antibiotic consumption between 2000 and 2015. *Proceedings of the National Academy of Sciences of the United States of America*, *115*(15), E3463–E3470. https://doi.org/10.1073/pnas.1717295115

Kosmulski, M. (2021). The pH dependent surface charging and points of zero charge. IX. Update. *Advances in Colloid and Interface Science*, *296*, 102519. https://doi.org/https://doi.org/10.1016/j.cis.2021.102519

Kostrzębska, A., Junka, A., Brożyna, M., & Musiał, W. (2024). The Assessment of Physicochemical and Antimicrobial Properties of Hydrophilic Gels Containing Tetracycline Hydrochloride and Various Concentrations of Ethanol. *Pharmaceutics*, *16*(6). https://doi.org/10.3390/pharmaceutics16060830

Kounatidis, D., Dalamaga, M., Grivakou, E., Karampela, I., Koufopoulos, P., Dalopoulos, V., Adamidis, N., Mylona, E., Kaziani, A., & Vallianou, N. G. (2024). Third-Generation Tetracyclines: Current Knowledge and Therapeutic Potential. *Biomolecules*, *14*(7). https://doi.org/10.3390/biom14070783

Kristianto, H., Arie, A. A., Susanti, R. F., Halim, M., & Lee, J. K. (2016). The effect of activated carbon support surface modification on characteristics of carbon nanospheres prepared by deposition precipitation of Fe-catalyst. *IOP Conference Series: Materials Science and Engineering*, *162*(1). https://doi.org/10.1088/1757-899X/162/1/012034

Kwiatkowski, M., Fierro, V., & Celzard, A. (2019). Confrontation of various adsorption models for assessing the porous structure of activated carbons. *Adsorption*, *25*(8), 1673–1682. https://doi.org/10.1007/s10450-019-00129-y

Kwiatkowski, M., Sreńscek-Nazzal, J., & Michalkiewicz, B. (2017). An analysis of the effect of the additional activation process on the formation of the porous structure and pore size distribution of the commercial activated carbon WG-12. *Adsorption*, *23*(4), 551–561. https://doi.org/10.1007/s10450-017-9867-4

Li, C., Awasthi, M. K., Liu, J., & Yao, T. (2025). Veterinary tetracycline residues: Environmental occurrence, ecotoxicity, and degradation mechanism. *Environmental Research*, *266*, 120417. https://doi.org/https://doi.org/10.1016/j.envres.2024.120417

Li, Q., Zheng, Y., Guo, L., Xiao, Y., Li, H., Yang, P., Xia, L., Liu, X., Chen, Z., Li, L., & Zhang, H. (2024). Microbial Degradation of Tetracycline Antibiotics: Mechanisms and Environmental Implications. *Journal of Agricultural and Food Chemistry*, *72*(24), 13523–13536. https://doi.org/10.1021/acs.jafc.4c02677

Li, X., Shen, X., Jiang, W., Xi, Y., & Li, S. (2024). Comprehensive review of emerging contaminants: Detection technologies, environmental impact, and management strategies. *Ecotoxicology and Environmental Safety*, *278*, 116420. https://doi.org/https://doi.org/10.1016/j.ecoenv.2024.116420

Li, X., Wang, H., Wang, B., & Guan, Y. (2022). Machine learning methods for prediction analyses of 4H–SiC microfabrication via femtosecond laser processing. *Journal of Materials Research and Technology*, *18*, 2152–2165. https://doi.org/https://doi.org/10.1016/j.jmrt.2022.03.124

Li, X., Wei, H., Song, T., Lu, H., & Wang, X. (2023). A review of the photocatalytic degradation of organic pollutants in water by modified TiO2. *Water Science and Technology*, *88*(6), 1495–1507. https://doi.org/10.2166/wst.2023.288

Li, X., Yu, J., & Jiang, C. (2020). Chapter 1 - Principle and surface science of photocatalysis. In J. Yu, M. Jaroniec, & C. B. T.-I. S. and T. Jiang (Eds.), *Surface Science of Photocatalysis* (Vol. 31, pp. 1–38). Elsevier. https://doi.org/https://doi.org/10.1016/B978-0-08-102890-2.00001-4

Li, Z., Jiang, H., Wang, X., Wang, C., & Wei, X. (2023). Effect of pH on Adsorption of Tetracycline Antibiotics on Graphene Oxide. *International Journal of Environmental Research and Public Health*, *20*(3). https://doi.org/10.3390/ijerph20032448

Loganathan, P., Vigneswaran, S., Kandasamy, J., Cuprys, A. K., Maletskyi, Z., & Ratnaweera, H. (2023). Treatment Trends and Combined Methods in Removing Pharmaceuticals and Personal Care Products from Wastewater-A Review. *Membranes*, *13*(2). https://doi.org/10.3390/membranes13020158

Long, S., Yang, Y., Pavlostathis, S. G., Xiang, F., Sun, P., Li, N., & Zhao, L. (2020). Toxicity of tetracycline and its transformation products to a phosphorus removing Shewanella strain. *Chemosphere*, *246*, 125681. https://doi.org/https://doi.org/10.1016/j.chemosphere.2019.125681

Lu, G., Li, X., Lu, P., Guo, H., Wang, Z., Zhang, Q., Li, Y., Sun, W., An, J., & Zhang, Z. (2024). Z-Type Heterojunction MnO2@g-C3N4 Photocatalyst-Activated Peroxymonosulfate for the Removal of Tetracycline Hydrochloride in Water. *Toxics*, *12*(1). https://doi.org/10.3390/toxics12010070

Ma, C., Aryee, A. A., Zhu, K., Wang, R., & Han, R. (2024). Adsorption and catalytic degradation of tetracycline hydrochloride by HCNTs /MnFe2O4. *Journal of Environmental Chemical Engineering*, *12*(4), 113156. https://doi.org/https://doi.org/10.1016/j.jece.2024.113156

Ma, L., Cai, Q., Ong, S. L., Yang, Z., Zhao, W., Duan, J., & Hu, J. (2023). Photonic efficiency optimization-oriented dependence model of characteristic coupling spectrum on catalytic absorbance in photocatalytic degradation of tetracycline hydrochloride. *Chemical Engineering Journal*, *451*, 138623. https://doi.org/https://doi.org/10.1016/j.cej.2022.138623

Mahlaule-Glory, L. M., & Hintsho-Mbita, N. C. (2022). Green Derived Zinc Oxide (ZnO) for the Degradation of Dyes from Wastewater and Their Antimicrobial Activity: A Review. *Catalysts*, *12*(8). https://doi.org/10.3390/catal12080833

Mahmoodi, M., & Pishbin, E. (2025). Ozone-based advanced oxidation processes in water treatment: recent advances, challenges, and perspective. *Environmental Science and Pollution Research*, *32*(7), 3531–3570. https://doi.org/10.1007/s11356-024-35835-w

Maity, D., & Sahoo, S. (2023). *Synthesis and Characterization of Nanomaterials for Electrochemical Sensors* (pp. 193–222). https://doi.org/10.1021/bk-2023-1437.ch009

Manju, R., Samraj, J. J., & Neppolian, B. (2025). Real sample analysis of persistent contaminant abatement via synergistic adsorption and visible-light catalysis in continuous flow reactors. *Separation and Purification Technology*, *360*, 131050. https://doi.org/https://doi.org/10.1016/j.seppur.2024.131050

Manjunath, S. V, & Kumar, M. (2021). Simultaneous removal of antibiotic and nutrients via Prosopis juliflora activated carbon column: Performance evaluation, effect of operational parameters and breakthrough modeling. *Chemosphere*, *262*, 127820. https://doi.org/https://doi.org/10.1016/j.chemosphere.2020.127820

Manna, M., & Sen, S. (2023). Advanced oxidation process: a sustainable technology for treating refractory organic compounds present in industrial wastewater. *Environmental Science and*

Pollution Research, *30*(10), 25477–25505. https://doi.org/10.1007/s11356-022-19435-0

Manoharan, D., Srinivasan, S., Vignesh, N. R., & Senthilvel, A. (2023). Tetracyclines: The Old, the New and the Improved - A Short Review. *Biomedical and Pharmacology Journal*, *16*(3), 1441–1450. https://doi.org/10.13005/bpj/2722

Manyazewal, D. E., Kiflie, Z., & Kebede, S. (2025a). Green synthesis and characterization of citrus bergamia leaves extracted modified zinc oxide nanoparticles impregnated on cassava peel-based activated carbon. *Journal of Sol-Gel Science and Technology*. https://doi.org/10.1007/s10971-025-06792-8

Manyazewal, D. E., Kiflie, Z., & Kebede, S. (2025b). Machine Learning-Based Process Optimization for Adsorption Removal of Emerging Contaminant (Tetracycline) From Aqueous Solution Onto Zinc Chloride Activated Biomass (Cassava Peels). *Remediation Journal*, *35*(4), e70026. https://doi.org/https://doi.org/10.1002/rem.70026

Mapuranga, J., Chang, J., Zhao, J., Liang, M., Li, R., Wu, Y., Zhang, N., Zhang, L., & Yang, W. (2023). The Underexplored Mechanisms of Wheat Resistance to Leaf Rust. *Plants*, *12*(23). https://doi.org/10.3390/plants12233996

Matei, E., Andreea, A., Maria, Ș ăulean, Alexandra, R., Andra, C., Predescu, M., Coman, G., Constantin, A., & Cristian, B. (2023). ZnO nanostructured matrix as nexus catalysts for the removal of emerging pollutants. In *Environmental Science and Pollution Research* (Vol. 30, Issue 54). Springer Berlin Heidelberg. https://doi.org/10.1007/s11356-023-30713-3

Matesun, J., Petrik, L., Musvoto, E., Ayinde, W., & Ikumi, D. (2024). Limitations of wastewater treatment plants in removing trace anthropogenic biomarkers and future directions: A review. *Ecotoxicology and Environmental Safety*, *281*, 116610. https://doi.org/https://doi.org/10.1016/j.ecoenv.2024.116610

Maziarka, P., Wurzer, C., Arauzo, P. J., Dieguez-Alonso, A., Mašek, O., & Ronsse, F. (2021). Do you BET on routine? The reliability of N2 physisorption for the quantitative assessment of biochar's surface area. *Chemical Engineering Journal*, *418*. https://doi.org/10.1016/j.cej.2021.129234

Meena, P. L., Poswal, K., & Surela, A. K. (2022). Facile synthesis of ZnO nanoparticles for the effective photodegradation of malachite green dye in aqueous solution. *Water and Environment Journal*, *36*(3), 513–524. https://doi.org/10.1111/wej.12783

Meenu, Vashishtha, M., & Meena, S. O. (2023). Determination of optimized process variables using RSM-BBD for the production of biochar derived from mustard straws. *Biomass Conversion and Biorefinery*. https://doi.org/10.1007/s13399-023-04981-5

Menya, E., Olupot, P. W., Storz, H., Lubwama, M., & Kiros, Y. (2018). Characterization and alkaline pretreatment of rice husk varieties in Uganda for potential utilization as precursors in the production of activated carbon and other value-added products. *Waste Management*, *81*, 104–116. https://doi.org/10.1016/j.wasman.2018.09.050

Miklos, D. B., Remy, C., Jekel, M., Linden, K. G., Drewes, J. E., & Hübner, U. (2018). Evaluation of advanced oxidation processes for water and wastewater treatment – A critical review. *Water Research*, *139*, 118–131. https://doi.org/https://doi.org/10.1016/j.watres.2018.03.042

Mohamed Isa, E. D., Shameli, K., Ch'ng, H. J., Che Jusoh, N. W., & Hazan, R. (2021). Photocatalytic degradation of selected pharmaceuticals using green fabricated zinc oxide nanoparticles. *Advanced Powder Technology*, *32*(7), 2398–2409. https://doi.org/10.1016/j.apt.2021.05.021

Mohammed, A. A., & Kareem, S. L. (2019). Adsorption of tetracycline fom wastewater by using Pistachio shell coated with ZnO nanoparticles: Equilibrium, kinetic and isotherm studies. *Alexandria Engineering Journal*, *58*(3), 917–928. https://doi.org/10.1016/j.aej.2019.08.006

Mohd-Asharuddin, S., Othman, N., Mohd Zin, N. S., & Tajarudin, H. A. (2017). A Chemical and Morphological Study of Cassava Peel: A Potential Waste as Coagulant Aid. *MATEC Web of Conferences*, *103*, 1–8. https://doi.org/10.1051/matecconf/201710306012

Mohmad Ameran, H., Abdullah, A. H., Tan, Y. P., Muhamad, E. N., Ohno, T., & Ando, Y. (2025). Photocatalytic degradation of tetracycline by TiO2/PVDF film photocatalyst:

degradation mechanism and intermediates analysis. *Discover Nano*, *20*(1), 206. https://doi.org/10.1186/s11671-025-04384-7

Moreno-Piraján, J. C., & Giraldo, L. (2010). Study of activated carbons by pyrolysis of cassava peel in the presence of chloride zinc. *Journal of Analytical and Applied Pyrolysis*, *87*(2), 288–290. https://doi.org/10.1016/j.jaap.2009.12.003

Morshedy, A. S., El-Fawal, E. M., Zaki, T., El-Zahhar, A. A., Alghamdi, M. M., & El Naggar, A. M. A. (2024). A review on heterogeneous photocatalytic materials: Mechanism, perspectives, and environmental and energy sustainability applications. *Inorganic Chemistry Communications*, *163*, 112307. https://doi.org/https://doi.org/10.1016/j.inoche.2024.112307

Motelica, L., Vasile, B.-S., Ficai, A., Surdu, A.-V., Ficai, D., Oprea, O.-C., Andronescu, E., Mustățea, G., Ungureanu, E. L., & Dobre, A. A. (2023). Antibacterial Activity of Zinc Oxide Nanoparticles Loaded with Essential Oils. *Pharmaceutics*, *15*(10). https://doi.org/10.3390/pharmaceutics15102470

Muhammad, W., Ullah, N., Haroon, M., & Abbasi, B. H. (2019). Optical, morphological and biological analysis of zinc oxide nanoparticles (ZnO NPs) using: Papaver somniferum L. *RSC Advances*, *9*(51), 29541–29548. https://doi.org/10.1039/c9ra04424h

Natarajan, T. S., Mozhiarasi, V., & Tayade, R. J. (2021). *Nitrogen Doped Titanium Dioxide (N-TiO 2): Synopsis of Synthesis Methodologies , Doping Mechanisms , Property Evaluation and Visible Light Photocatalytic Applications*. 371–410.

Ndiaye, D., & Akill, A. (2025). A critical review on g-C_3N_4 for environmental remediation: synthesis, properties, and pollutant photodegradation. *Rendiconti Lincei. Scienze Fisiche e Naturali*. https://doi.org/10.1007/s12210-025-01371-z

Ngoc, D. M., Hieu, N. C., Trung, N. H., Chien, H. H., & Thi, N. Q. (2023). *Tetracycline Removal from Water by Adsorption on Hydrochar and Hydrochar-Derived Activated Carbon : Performance , Mechanism , and Cost Calculation*.

Norvill, Z. N., Toledo-cervantes, A., Blanco, S., Shilton, A., & Muñoz, R. (2017). Department of

Chemical Engineering and Environmental Technology , University of School of Engineering and Advanced Technology , Massey University , Private Bag 11. *Bioresource Technology*. https://doi.org/10.1016/j.biortech.2017.02.011

Nuraishah, W., Ishak, W., & Tan, H. L. (2025). *Hydrothermal ZnO Photocatalysis for Efficient Removal of Tetracycline from Wastewater*. *25*(1), 184–197. https://doi.org/10.22146/ajche.16598

Ondijo, C., Kengara, F., & K'Owino, I. (2022). Synthesis, Characterization, and Evaluation of the Remediation Activity of Cissus quadrangularis Zinc Oxide Nanoparticle-Activated Carbon Composite on Dieldrin in Aqueous Solution. *Journal of Nanotechnology*, *2022*. https://doi.org/10.1155/2022/2055024

Ortiz-Ramos, U., Leyva-Ramos, R., Mendoza-Mendoza, E., & Aragón-Piña, A. (2022). Removal of tetracycline from aqueous solutions by adsorption on raw Ca-bentonite. Effect of operating conditions and adsorption mechanism. *Chemical Engineering Journal*, *432*, 134428. https://doi.org/https://doi.org/10.1016/j.cej.2021.134428

Osorio, C., Garzón, L., Jaimes, D., Silva, E., & Bustos, R. H. (2021). Impact on antibiotic resistance, therapeutic success, and control of side effects in therapeutic drug monitoring (Tdm) of daptomycin: A scoping review. *Antibiotics*, *10*(3), 1–22. https://doi.org/10.3390/antibiotics10030263

Otache, M., Ubwa, S., & Godwin, A. (2017). Proximate Analysis and Mineral Composition of Peels of Three Sweet Cassava Cultivars. *Asian Journal of Physical and Chemical Sciences*, *3*(4), 1–10. https://doi.org/10.9734/ajopacs/2017/36502

Owamah, H. I. (2014). Biosorptive removal of Pb(II) and Cu(II) from wastewater using activated carbon from cassava peels. *Journal of Material Cycles and Waste Management*, *16*(2), 347–358. https://doi.org/10.1007/s10163-013-0192-z

Padmavathy, K. S., Madhu, G., & Haseena, P. V. (2016). A study on Effects of pH, Adsorbent Dosage, Time, Initial Concentration and Adsorption Isotherm Study for the Removal of Hexavalent Chromium (Cr (VI)) from Wastewater by Magnetite Nanoparticles. *Procedia Technology*, *24*, 585–594. https://doi.org/https://doi.org/10.1016/j.protcy.2016.05.127

Pais-Chanfrau, J. M., Núñez Pérez, J., Espín-Valladares, R. del C., Lara-Fiallos, M. V., & Trujillo-Toledo, L. E. (2021). *Uses of the Response Surface Methodology for the Optimization of Agro-Industrial Processes* (P. Kayaroganam (ed.)). IntechOpen. https://doi.org/10.5772/intechopen.98283

Pandis, P. K., Kalogirou, C., Kanellou, E., Vaitsis, C., Savvidou, M. G., Sourkouni, G., Zorpas, A. A., & Argirusis, C. (2022). Key Points of Advanced Oxidation Processes (AOPs) for Wastewater, Organic Pollutants and Pharmaceutical Waste Treatment: A Mini Review. *ChemEngineering*, *6*(1). https://doi.org/10.3390/chemengineering6010008

Pearson, J. C., Gillett, E., Gadri, N. D., & Dionne, B. (2025). Tetracyclines, the old and the new: A narrative review. *CMI Communications*, *2*(1), 105059. https://doi.org/https://doi.org/10.1016/j.cmicom.2025.105059

Pedroza Toscano, M. A., Peña, R. S., Velasco, M. R., Ibarra Montalvo, J. J., Aréchiga Guzmán, J. A., & Cuenca, S. L. (2022). Effect of Reaction Conditions on Particle Size of Zno Nanoparticles Via Controlled Precipitation Method and in-Vitro Antibacterial Capacity. *Quimica Nova*, *45*(8), 901–905. https://doi.org/10.21577/0100-4042.20170881

Pereira, S. K., Kini, S., Prabhu, B., & Jeppu, G. P. (2022). A simplified modeling procedure for adsorption at varying pH conditions using the modified Langmuir–Freundlich isotherm. *Applied Water Science*, *13*(1), 29. https://doi.org/10.1007/s13201-022-01800-6

Pierdomenico, M., Cicero, A. F. G., Veronesi, M., Fogacci, F., Riccioni, C., & Benassi, B. (2023). Effect of Citrus bergamia extract on lipid profile: A combined in vitro and human study. *Phytotherapy Research : PTR*, *37*(9), 4185–4195. https://doi.org/10.1002/ptr.7897

Pourkodee, D., Renuka Devee, D., Pavithra, M., Muthukrishnan, R. M., Sridevi, D., Renganayaki, V., Uthra, D., & Sailatha, E. (2025). Pharmaceutical Pollution (DCF, PARA & TC) Treatment and Remediation Via AOP-enhanced HB-TiO2 Catalyst With Antimicrobial Activity. *Journal of Inorganic and Organometallic Polymers and Materials*, *35*(8), 6918–6939. https://doi.org/10.1007/s10904-025-03703-w

Programme, W. M., & Plantation, M. (2024). *Characterization and Adsorption Capacity Evaluation of ZnCl 2 Impregnated Cassava Peel Carbon for Removal of Fe , Ca , Mg and*

Zn ions in Wastewater from Cassava processing Industry.

Puri, M., Gandhi, K., & Kumar, M. S. (2023). Emerging environmental contaminants: A global perspective on policies and regulations. *Journal of Environmental Management*, *332*, 117344. https://doi.org/https://doi.org/10.1016/j.jenvman.2023.117344

Qiao, D., Li, Z., Duan, J., & He, X. (2020). Adsorption and photocatalytic degradation mechanism of magnetic graphene oxide/ZnO nanocomposites for tetracycline contaminants. *Chemical Engineering Journal*, *400*(June), 125952. https://doi.org/10.1016/j.cej.2020.125952

Rafique, M., Sohaib, M., Tahir, R., Tahir, M. B., Khalid, N. R., Shakil, M., Gillani, S. S. A., Khan, M. I., Alrobei, H., Shahzad, K., Ali, A. M., & Muhammad, S. (2021). Novel, facile and first time synthesis of zinc oxide nanoparticles using leaves extract of Citrus reticulata for photocatalytic and antibacterial activity. *Optik*, *243*(June), 167495. https://doi.org/10.1016/j.ijleo.2021.167495

Rahat Al Hassan, M., Sen, A., Khalid Hasan, M., & Abdul Matin, M. (2021). Structural, Morphological and Optical Properties of Spray Deposited Multi-doped (Ba, Sr, Mn, Fe and Ni) Compositionally Complex ZnO Thin Films. *American Journal of Nanosciences*, *7*(1), 6. https://doi.org/10.11648/j.ajn.20210701.12

Ramesh, P., Rajendran, A., & Ashokkumar, M. (2022). Biosynthesis of zinc oxide nanoparticles from Phyllanthus Niruri plant extract for photocatalytic and antioxidant activities. *International Journal of Environmental Analytical Chemistry*, *00*(00), 1–12. https://doi.org/10.1080/03067319.2022.2041004

Ramos, P., Sánchez, L., & Rodríguez, J. (2025). *Mechanisms of ZnO Photocatalysis BT - Enhancing Photocatalytic Water Decontamination: Exploring the Efficacy of ZnO Nanorods in Advanced Treatment Processes* (P. Ramos, L. Sánchez, & J. Rodríguez (eds.); pp. 15–16). Springer Nature Switzerland. https://doi.org/10.1007/978-3-031-82506-4_3

Rana, G., Dhiman, P., Kumar, A., Chauhan, A., & Sharma, G. (2024). Recent advances in

photocatalytic removal of antiviral drugs by Z-scheme and S-scheme heterojunction. *Environmental Science and Pollution Research*, *31*(28), 40851–40872. https://doi.org/10.1007/s11356-024-33876-9

Rani, N., Sagar, N. A., Chauhan, A., & Mondal, A. (2025). Green synthesis of ZnO nanoparticles: Characterization and emerging applications in sustainable agriculture. *Industrial Crops and Products*, *233*, 121393. https://doi.org/https://doi.org/10.1016/j.indcrop.2025.121393

Rasheed, H. M., Aroosh, K., Meng, D., Ruan, X., Akhter, M., & Cui, X. (2025). A review on modified ZnO to address environmental challenges through photocatalysis: Photodegradation of organic pollutants. *Materials Today Energy*, *48*, 101774. https://doi.org/https://doi.org/10.1016/j.mtener.2024.101774

Reji, M., & Kumar, R. (2023). Response surface methodology (RSM): An overview to analyze multivariate data. *Indian Journal of Microbiology Research*, *9*, 241–248. https://doi.org/10.18231/j.ijmr.2022.042

Ren, S., Wang, S., Liu, Y., Wang, Y., Gao, F., & Dai, Y. (2023). A review on current pollution and removal methods of tetracycline in soil. *Separation Science and Technology*, *58*(14), 2578–2602. https://doi.org/10.1080/01496395.2023.2259079

Revellame, E. D., Fortela, D. L., Sharp, W., Hernandez, R., & Zappi, M. E. (2020). Adsorption kinetic modeling using pseudo-first order and pseudo-second order rate laws: A review. *Cleaner Engineering and Technology*, *1*, 100032. https://doi.org/https://doi.org/10.1016/j.clet.2020.100032

Rinawati, R., Buhani, B., Widiarti, W., Isro, A., Fitrianingsih, E., Rahmawati, A., Kiswandono, A. A., & Nitti, F. (2024). Enhancing Ciprofloxacin Removal: Unveiling the Potential of Graphene Oxide Synthesized from Cassava Peels through Box-Behnken Design Optimization. *Journal of Sustainable Development of Energy, Water and Environment Systems*, *12*(4), 1120516.

Rizkallah, B. M., Galal, M. M., & Matta, M. E. (2023). Characteristics of Tetracycline Adsorption on Commercial Biochar from Synthetic and Real Wastewater in Batch and Continuous Operations: Study of Removal Mechanisms, Isotherms, Kinetics, Thermodynamics, and Desorption. *Sustainability (Switzerland)*, *15*(10). https://doi.org/10.3390/su15108249

Rodríguez-Flores, T., Hernández-Pérez, I., de la Huerta-Hernández, G. E., Ayala-Parada, Y., Cadena-Silva, J. G., & Haro-Pérez, C. (2025). Comparison of Photocatalytic Performance of Sonochemically Synthesized ZnO with Different Capping Agents. *ACS Omega*, *10*(28), 30181–30193. https://doi.org/10.1021/acsomega.5c00929

Rodriguez-Mozaz, S., Vaz-Moreira, I., Varela Della Giustina, S., Llorca, M., Barceló, D., Schubert, S., Berendonk, T. U., Michael-Kordatou, I., Fatta-Kassinos, D., Martinez, J. L., Elpers, C., Henriques, I., Jaeger, T., Schwartz, T., Paulshus, E., O'Sullivan, K., Pärnänen, K. M. M., Virta, M., Do, T. T., … Manaia, C. M. (2020). Antibiotic residues in final effluents of European wastewater treatment plants and their impact on the aquatic environment. *Environment International*, *140*(March), 105733. https://doi.org/10.1016/j.envint.2020.105733

Rupa, E. J., Kaliraj, L., Abid, S., Yang, D. C., & Jung, S. K. (2019). Synthesis of a zinc oxide nanoflower photocatalyst from sea buckthorn fruit for degradation of industrial dyes in wastewater treatment. *Nanomaterials*, *9*(12). https://doi.org/10.3390/nano9121692

Rusu, A., & Buta, E. L. (2021). The development of third-generation tetracycline antibiotics and new perspectives. *Pharmaceutics*, *13*(12). https://doi.org/10.3390/pharmaceutics13122085

Sachin, S., Sundaram, S. J., Franklin, J. B., Raj, A. D., Kumar, J. V., & Alam, M. W. (2024). Synthesis of Zinc Oxide nano bars incorporated with activated Carbon (ZnO NBs/AC) nanocomposites for high specific capacitance value. *Journal of Sol-Gel Science and Technology*, *109*(3), 896–904. https://doi.org/10.1007/s10971-024-06334-8

Sagadevan, S., Balakrishnan, T., Rahman, M. Z., Soga, T., Randriamahazaka, H., Kakavandi, B., & Johan, M. R. (2024). Agricultural biomass-based activated carbons for efficient and sustainable supercapacitors. *Journal of Energy Storage*, *97*, 112878.

https://doi.org/https://doi.org/10.1016/j.est.2024.112878

Sağlam, S., Türk, F. N., & Arslanoğlu, H. (2024). Tetracycline (TC) removal from wastewater with activated carbon (AC) obtained from waste grape marc: activated carbon characterization and adsorption mechanism. *Environmental Science and Pollution Research International*, *31*(23), 33904–33923. https://doi.org/10.1007/s11356-024-33493-6

Salah, W., Djeridi, W., Houas, A., & Elsellami, L. (2024). Synergy between activated carbon and ZnO: a powerful combination for selective adsorption and photocatalytic degradation. *Materials Advances*, *5*(4), 1667–1675. https://doi.org/10.1039/d3ma01171b

Sánchez-Pérez, D. M., Flores-Loyola, E., Márquez-Guerrero, S. Y., Galindo-Guzman, M., & Marszalek, J. E. (2023). Green Synthesis and Characterization of Zinc Oxide Nanoparticles Using Larrea tridentata Extract and Their Impact on the In-Vitro Germination and Seedling Growth of Capsicum annuum. *Sustainability (Switzerland)*, *15*(4). https://doi.org/10.3390/su15043080

Santhoshkumar, J., Kumar, S. V., & Rajeshkumar, S. (2017). Synthesis of zinc oxide nanoparticles using plant leaf extract against urinary tract infection pathogen. *Resource-Efficient Technologies*, *3*(4), 459–465. https://doi.org/https://doi.org/10.1016/j.reffit.2017.05.001

Sanz-Santos, E., Alvarez Torrellas, S., Larriba, M., & Garcia, J. (2022). *Activated carbons derived from biomass for the removal by adsorption of several pesticides from water* (pp. 565–583). https://doi.org/10.1016/B978-0-323-90485-8.00020-5

Saroa, A., Singh, A., Jindal, N., Kumar, R., Singh, K., Guleria, P., Boopathy, R., & Kumar, V. (2023). Nanotechnology-assisted treatment of pharmaceuticals contaminated water. *Bioengineered*, *14*(1), 2260919. https://doi.org/10.1080/21655979.2023.2260919

Saya, L., Rameshwor Singh, W., & Hooda, S. (2023). Adsorptive removal of ciprofloxacin from aqueous medium by magnetic guar gum grafted graphene oxide nano composite. *Journal of Environmental Chemical Engineering*, *11*(5), 110766. https://doi.org/https://doi.org/10.1016/j.jece.2023.110766

Scaria, J., Anupama, K. V., & Nidheesh, P. V. (2021). Tetracyclines in the environment: An overview on the occurrence, fate, toxicity, detection, removal methods, and sludge management. *Science of the Total Environment*, *771*, 145291. https://doi.org/10.1016/j.scitotenv.2021.145291

Semeraro, P., Bettini, S., Sawalha, S., Pal, S., Licciulli, A., Marzo, F., Lovergine, N., Valli, L., & Giancane, G. (2020). Photocatalytic degradation of tetracycline by zno/γ-fe2o3 paramagnetic nanocomposite material. *Nanomaterials*, *10*(8), 1–12. https://doi.org/10.3390/nano10081458

Shah, H. H., Amin, M., Pepe, F., Mancusi, E., & Fareed, A. G. (2023). Overview of environmental and economic viability of activated carbons derived from waste biomass for adsorptive water treatment applications. *Environmental Science and Pollution Research*. https://doi.org/10.1007/s11356-023-30540-6

Shamhari, N. M., Wee, B. S., Chin, S. F., & Kok, K. Y. (2018). Synthesis and characterization of zinc oxide nanoparticles with small particle size distribution. *Acta Chimica Slovenica*, *65*(3), 578–585. https://doi.org/10.17344/acsi.2018.4213

Shao, S., & Wu, X. (2020). Microbial degradation of tetracycline in the aquatic environment: a review. *Critical Reviews in Biotechnology*, *40*(7), 1010–1018. https://doi.org/10.1080/07388551.2020.1805585

Sharma, A., Rathore, V. K., & Chakraborty, M. (2024). Adsorptive removal of diclofenac sodium from aqueous solution by highly efficient metal organic framework (UiO-66)/multi-walled carbon nanotube composite. *Environmental Science and Pollution Research*, *31*(28), 40142–40155. https://doi.org/10.1007/s11356-023-28789-y

Sharma, D. K., Shukla, S., Sharma, K. K., & Kumar, V. (2022). A review on ZnO: Fundamental properties and applications. *Materials Today: Proceedings*, *49*, 3028–3035. https://doi.org/https://doi.org/10.1016/j.matpr.2020.10.238

Sharma, M., Mandal, M. K., Pandey, S., Kumar, R., & Dubey, K. K. (2022). Visible-Light-Driven Photocatalytic Degradation of Tetracycline Using Heterostructured Cu(2)O-TiO(2) Nanotubes, Kinetics, and Toxicity Evaluation of Degraded Products on Cell Lines. *ACS*

Omega, *7*(37), 33572–33586. https://doi.org/10.1021/acsomega.2c04576

Shetty, S. S., D, D., S, H., Sonkusare, S., Naik, P. B., Kumari N, S., & Madhyastha, H. (2023). Environmental pollutants and their effects on human health. *Heliyon*, *9*(9), e19496. https://doi.org/https://doi.org/10.1016/j.heliyon.2023.e19496

Shokoohi, R., Salari, M., Molla Mahmoudi, M., Azizi, S., Ghiasian, S. A., Faradmal, J., & Faraji, H. (2020). The sorption of cationic and anionic heavy metal species on the biosorbent of Aspergillus terreus: Isotherm, kinetics studies. *Environmental Progress and Sustainable Energy*, *39*(2), 1–9. https://doi.org/10.1002/ep.13309

Shokouhi, R., Ghobadi, N., Godini, K., Hadi, M., & Atashzaban, Z. (2019). Jo ur na l P re. *Process Safety and Environmental Protection*. https://doi.org/10.1016/j.psep.2019.10.020

Shrestha, S., Wang, B., & Dutta, P. (2020). Nanoparticle processing: Understanding and controlling aggregation. *Advances in Colloid and Interface Science*, *279*, 102162. https://doi.org/https://doi.org/10.1016/j.cis.2020.102162

Singh, H. O., Murugesan, G., Selvaraj, R., Varadavenkatesan, T., & Vinayagam, R. (2025). Sustainable activated carbon from copper pod tree leaves for efficient tetracycline removal and regeneration. *Scientific Reports*, *15*(1), 17312. https://doi.org/10.1038/s41598-025-02213-6

Singh, S., Gade, J. V, Verma, D. K., Elyor, B., & Jain, B. (2024). Exploring ZnO nanoparticles: UV–visible analysis and different size estimation methods. *Optical Materials*, *152*, 115422. https://doi.org/https://doi.org/10.1016/j.optmat.2024.115422

Sitravellu, B. R., Yagoub, S. A. M., Aulia, A., Hasiholan, B., & Mukhtar, Y. M. F. (2023). *Comparative Study of Variance-Based and One-Parameter-At-A-Time Sensitivity Analysis Method for Polymer Flood Performance History Matching BT - Proceedings of the International Field Exploration and Development Conference 2022* (J. Lin (ed.); pp. 5179–5193). Springer Nature Singapore.

Sjah, W., Rahman, B., Hindarto, D., & Wedha, B. (2023). Diagnostic on Car Internal Combustion Engine through Noise. *SinkrOn*, *8*, 1128–1139. https://doi.org/10.33395/sinkron.v8i2.12392

Solanki, V. S., Pare, B., Gupta, P., Jonnalagadda, S. B., & Shrivastava, R. (2020). A review on advanced oxidation processes (AOPs) for wastewater remediation. *Asian Journal of Chemistry*, *32*(11), 2677–2684. https://doi.org/10.14233/ajchem.2020.22806

Sulaiman, N. S., Hashim, R., Mohamad Amini, M. H., Danish, M., & Sulaiman, O. (2018). Optimization of activated carbon preparation from cassava stem using response surface methodology on surface area and yield. *Journal of Cleaner Production*, *198*, 1422–1430. https://doi.org/10.1016/j.jclepro.2018.07.061

Sureiman, O., & Mangera, C. (2020). F-test of overall significance in regression analysis simplified. *Journal of the Practice of Cardiovascular Sciences*, *6*(2), 116. https://doi.org/10.4103/jpcs.jpcs_18_20

Suresh, R., Rajendran, S., & Ponce, L. C. (2024). *Chapter 10 - Waste-based adsorbents for the removal of emerging pollutants and their adsorption mechanisms* (M. Hadi Dehghani, R. R. Karri, & I. B. T.-S. R. T. for E. P. in A. E. Tyagi (eds.); pp. 203–221). Elsevier. https://doi.org/https://doi.org/10.1016/B978-0-443-18618-9.00024-3

Taha, A., Ben Aissa, M., & Da'na, E. (2020). Green Synthesis of an Activated Carbon-Supported Ag and ZnO Nanocomposite for Photocatalytic Degradation and Its Antibacterial Activities. *Molecules (Basel, Switzerland)*, *25*(7). https://doi.org/10.3390/molecules25071586

Taie, M., Fadaei, A., Sadeghi, M., Hemati, S., & Mardani, G. (2021). *Comparison of the Efficiency of Ultraviolet / Zinc Oxide (UV / ZnO) and Ozone / Zinc Oxide (O 3 / ZnO) Techniques as Advanced Oxidation Processes in the Removal of Trimethoprim from Aqueous Solutions*. *2021*. https://doi.org/10.1155/2021/9640918

Taylor, C. J., Booth, M., Manson, J. A., Willis, M. J., Clemens, G., Taylor, B. A., Chamberlain, T. W., & Bourne, R. A. (2021). Rapid, automated determination of reaction models and kinetic parameters. *Chemical Engineering Journal*, *413*, 127017.

https://doi.org/https://doi.org/10.1016/j.cej.2020.127017

Tegegne, A. A., Mekasha, Y. T., Ayu, A. A., Hasen, G., & Suleman, S. (2024). *A review on emerging pharmaceutical residues in Ethiopia : occurrence , ecotoxicological aspects , and regulatory concerns*. *December*, 1–14. https://doi.org/10.3389/fmicb.2024.1499487

Telli, S., Ghodbane, H., Laouissi, A., Zamouche, M., & Kadmi, Y. (2024a). Remediation of cationic dye from wastewater using a new environmentally friendly adsorbent: A response surface methodology and artificial neural network modeling study. *International Journal of Chemical Kinetics*, *June 2024*, 16–39. https://doi.org/10.1002/kin.21756

Telli, S., Ghodbane, H., Laouissi, A., Zamouche, M., & Kadmi, Y. (2024b). Remediation of cationic dye from wastewater using a new environmentally friendly adsorbent: A response surface methodology and artificial neural network modeling study. *International Journal of Chemical Kinetics*, *June*, 1–24. https://doi.org/10.1002/kin.21756

Tiwari, A. K., Jha, S., Tripathi, S. K., Shukla, R., Awasthi, R. R., Bhardwaj, A. K., Singh, A. K., & Dikshit, A. (2024). Spectroscopic investigations of green synthesized zinc oxide nanoparticles (ZnO NPs): antioxidant and antibacterial activity. *Discover Applied Sciences*, *6*(8), 399. https://doi.org/10.1007/s42452-024-06049-z

Topkaya, E., Arslan, A., & Yatmaz, H. C. (2021). Diclofenac Degradation by Ozone-Based Oxidation Processes: PROMETHEE Method, Kinetic and Cost-Effectiveness Study. *Ozone: Science & Engineering*, *43*(2), 136–146. https://doi.org/10.1080/01919512.2020.1765737

Tran, H. N. (2023). Applying Linear Forms of Pseudo-Second-Order Kinetic Model for Feasibly Identifying Errors in the Initial Periods of Time-Dependent Adsorption Datasets. *Water (Switzerland)*, *15*(6). https://doi.org/10.3390/w15061231

Tran, H. N., Lima, E. C., Juang, R.-S., Bollinger, J.-C., & Chao, H.-P. (2021). Thermodynamic parameters of liquid–phase adsorption process calculated from different equilibrium constants related to adsorption isotherms: A comparison study. *Journal of Environmental Chemical Engineering*, *9*(6), 106674. https://doi.org/https://doi.org/10.1016/j.jece.2021.106674

Tran Thi, V. H., & Lee, B.-K. (2017a). Great improvement on tetracycline removal using ZnO rod-activated carbon fiber composite prepared with a facile microwave method. *Journal of Hazardous Materials*, *324*(Pt B), 329–339. https://doi.org/10.1016/j.jhazmat.2016.10.066

Tsigara, A. S., Banti, C. N., Hatzidimitriou, A., & Hadjikakou, S. K. (2024). Tetracycline: structural characterization and antimicrobial properties of its water-soluble di-anionic bi-sodium salt. *Dalton Transactions (Cambridge, England : 2003)*, *53*(29), 12080–12089. https://doi.org/10.1039/d4dt01384k

Tymoszuk, A., & Wojnarowicz, J. (2020). Zinc Oxide and Zinc Oxide Nanoparticles Impact on In Vitro Germination and Seedling Growth in Allium cepa L. *Materials*, *13*, 2784. https://doi.org/10.3390/ma13122784

Ullah, H., Khan, S., Chen, B., Shahab, A., Riaz, L., Lun, L., & Wu, N. (2023). Machine learning approach to predict adsorption capacity of Fe-modified biochar for selenium. *Carbon Research*, *2*(1). https://doi.org/10.1007/s44246-023-00061-5

Uma, G., & Ashenef, A. (2023). Determination of some antibiotic residues (tetracycline, oxytetracycline and penicillin-G) in beef sold for public consumption at Dukem and Bishoftu (Debre Zeyit) towns, central Ethiopia by LC/MS/MS. *Cogent Food & Agriculture*, *9*(1), 2242633. https://doi.org/10.1080/23311932.2023.2242633

Umamaheswari, A., Prabu, S. L., John, S. A., & Puratchikody, A. (2021). Green synthesis of zinc oxide nanoparticles using leaf extracts of Raphanus sativus var. Longipinnatus and evaluation of their anticancer property in A549 cell lines. *Biotechnology Reports (Amsterdam, Netherlands)*, *29*, e00595. https://doi.org/10.1016/j.btre.2021.e00595

Villagrán, Z., Anaya-Esparza, L. M., Velázquez-Carriles, C. A., Silva-Jara, J. M., Ruvalcaba-Gómez, J. M., Aurora-Vigo, E. F., Rodríguez-Lafitte, E., Rodríguez-Barajas, N., Balderas-León, I., & Martínez-Esquivias, F. (2024). Plant-Based Extracts as Reducing, Capping, and Stabilizing Agents for the Green Synthesis of Inorganic Nanoparticles. *Resources*, *13*(6). https://doi.org/10.3390/resources13060070

Vinukonda, A., Bolledla, N., Jadi, R. K., Chinthala, R., & Devadasu, V. R. (2025). Synthesis of nanoparticles using advanced techniques. *Next Nanotechnology*, *8*, 100169.

https://doi.org/https://doi.org/10.1016/j.nxnano.2025.100169

Wang, D., Jia, F., Wang, H., Chen, F., Fang, Y., & Dong, W. (2018). Journal of Colloid and Interface Science Simultaneously efficient adsorption and photocatalytic degradation of tetracycline by Fe-based MOFs. *Journal of Colloid And Interface Science*, *519*, 273–284. https://doi.org/10.1016/j.jcis.2018.02.067

Wang, F., Xiang, L., Sze-Yin Leung, K., Elsner, M., Zhang, Y., Guo, Y., Pan, B., Sun, H., An, T., Ying, G., Brooks, B. W., Hou, D., Helbling, D. E., Sun, J., Qiu, H., Vogel, T. M., Zhang, W., Gao, Y., Simpson, M. J., … Tiedje, J. M. (2024). Emerging contaminants: A One Health perspective. *The Innovation*, *5*(4), 100612. https://doi.org/https://doi.org/10.1016/j.xinn.2024.100612

Wang, J., & Guo, X. (2020). Adsorption kinetic models: Physical meanings, applications, and solving methods. *Journal of Hazardous Materials*, *390*, 122156. https://doi.org/https://doi.org/10.1016/j.jhazmat.2020.122156

Wang, J., & Wang, S. (2020). Reactive species in advanced oxidation processes: Formation, identification and reaction mechanism. *Chemical Engineering Journal*, *401*, 126158. https://doi.org/https://doi.org/10.1016/j.cej.2020.126158

Wang, L., Zhang, K., Qian, J., Qiu, M., Li, N., Du, H., Hu, X., Fu, Y., Tan, M., Hao, D., & Wang, Q. (2023). S-scheme MOF-on-MOF heterojunctions for enhanced photo-Fenton Cr(VI) reduction and antibacterial effects. *Chemosphere*, *344*, 140277. https://doi.org/https://doi.org/10.1016/j.chemosphere.2023.140277

Wardah, J., Winardi, S., Madhania, S., Rozy, M. I. F., & Kusdianto, K. (2024). Effect of Doping ZnO on Activated Carbon Prepared from Waste Paper for Photocatalytic Applications. *Engineering Chemistry*, *7*, 79–88. https://doi.org/10.4028/p-thtn4c

Wei, L., Li, H., & Lu, J. (2021). Algae-induced photodegradation of antibiotics: A review. *Environmental Pollution*, *272*, 115589.

https://doi.org/https://doi.org/10.1016/j.envpol.2020.115589

WHO. (2020). Global Antimicrobial Resistance and Use Surveillance System (GLASS) Report. In *Who*. https://apps.who.int/iris/bitstream/handle/10665/332081/9789240005587-eng.pdf?ua=1%0Ahttp://www.who.int/glass/resources/publications/early-implementation-report-2020/en/%0Ahttp://apps.who.int/iris/bitstream/10665/188783/1/9789241549400_eng.pdf?ua=1

Wiens, D. P. (2019). Maximin power designs in testing lack of fit. *Journal of Statistical Planning and Inference*, *199*, 311–317. https://doi.org/10.1016/j.jspi.2018.07.007

Wilkinson, J. L., Boxall, A. B. A., Kolpin, D. W., Leung, K. M. Y., Lai, R. W. S., Wong, D., Ntchantcho, R., Pizarro, J., Mart, J., Echeverr, S., Garric, J., Chaumot, A., Gibba, P., Kunchulia, I., Seidensticker, S., Lyberatos, G., Morales-salda, J. M., & Kang, H. (2022). *Pharmaceutical pollution of the world ' s rivers*. *119*(8), 1–10. https://doi.org/10.1073/pnas.2113947119/-/DCSupplemental.Published

Wu, S., Hu, H., Lin, Y., Zhang, J., & Hu, Y. H. (2020a). Visible light photocatalytic degradation of tetracycline over TiO2. *Chemical Engineering Journal*, *382*(June 2019), 122842. https://doi.org/10.1016/j.cej.2019.122842

Xiang, W., Zhang, X., Luo, J., Li, Y., Guo, T., & Gao, B. (2022). Performance of lignin impregnated biochar on tetracycline hydrochloride adsorption: Governing factors and mechanisms. *Environmental Research*, *215*. https://doi.org/10.1016/j.envres.2022.114339

Xiong, W., Zeng, G., Yang, Z., Zhou, Y., Zhang, C., Cheng, M., Liu, Y., Hu, L., Wan, J., Zhou, C., Xu, R., & Li, X. (2018). Adsorption of tetracycline antibiotics from aqueous solutions on nanocomposite multi-walled carbon nanotube functionalized MIL-53(Fe) as new adsorbent. *Science of the Total Environment*, *627*, 235–244. https://doi.org/10.1016/j.scitotenv.2018.01.249

Xu, M., Deng, J., Cai, A., Ma, X., Li, J., Li, Q., & Li, X. (2020). Comparison of UVC and

UVC/persulfate processes for tetracycline removal in water. *Chemical Engineering Journal*, *384*(October), 123320. https://doi.org/10.1016/j.cej.2019.123320

Xu, Y., Liu, Y., Zhang, B., Bu, C., Wang, Y., Zhang, D., Xi, M., & Qin, Q. (2021). Enhanced removal of sulfamethoxazole and tetracycline in bioretention cells amended with activated carbon and zero-valent iron: System performance and microbial community. *Science of The Total Environment*, *797*, 148992. https://doi.org/https://doi.org/10.1016/j.scitotenv.2021.148992

Yan, L., Song, X., Miao, J., Ma, Y., Zhao, T., & Yin, M. (2024). Removal of tetracycline from water by adsorption with biochar: A review. *Journal of Water Process Engineering*, *60*, 105215. https://doi.org/https://doi.org/10.1016/j.jwpe.2024.105215

Yang, N., Xiong, S., Zhang, S., Lv, F., Zhang, Y., Wang, X., Li, Z., Wang, H., & Xu, J. (2025). Influence of pre-oxidization on the surface condition, pore structure and capacitance performance of activated carbon derived from coal gasification fine slag. *Colloids and Surfaces A: Physicochemical and Engineering Aspects*, *709*, 136078. https://doi.org/https://doi.org/10.1016/j.colsurfa.2024.136078

Yi, L., Zuo, L., Wei, C., Fu, H., Qu, X., Zheng, S., Xu, Z., Guo, Y., Li, H., & Zhu, D. (2020). Science of the Total Environment Enhanced adsorption of bisphenol A , tylosin , and tetracycline from aqueous solution to nitrogen-doped multiwall carbon nanotubes via cation- π and π - π electron-donor-acceptor (EDA) interactions. *Science of the Total Environment*, *719*, 137389. https://doi.org/10.1016/j.scitotenv.2020.137389

Yue, Y., Yue, X., Tang, X., Han, L., Wang, J., Wang, S., & Du, C. (2024). Synergistic adsorption and photocatalysis study of TiO2 and activated carbon composite. *Heliyon*, *10*(10), e30817. https://doi.org/10.1016/j.heliyon.2024.e30817

Zamri, N. I. I., Zulmajdi, S. L. N., Daud, N. Z. A., Mahadi, A. H., Kusrini, E., & Usman, A. (2021). Insight into the adsorption kinetics, mechanism, and thermodynamics of methylene blue from aqueous solution onto pectin-alginate-titania composite microparticles. *SN Applied Sciences*, *3*(2). https://doi.org/10.1007/s42452-021-04245-9

Zhai, W., He, J., Han, P., Zeng, M., Gao, X., & He, Q. (2022). Adsorption mechanism for

tetracycline onto magnetic Fe3O4 nanoparticles: Adsorption isotherm and dynamic behavior, location of adsorption sites and interaction bonds. *Vacuum*, *195*, 110634. https://doi.org/https://doi.org/10.1016/j.vacuum.2021.110634

Zhan, D., Ye, A., & Hou, T. (2023). *Research progress on biochar-based material adsorption and removal of ibuprofen*. *December*, 1–14. https://doi.org/10.3389/fenvs.2023.1327000

Zhang, D., Yin, J., Zhao, J., Zhu, H., & Wang, C. (2015). Adsorption and removal of tetracycline from water by petroleum coke-derived highly porous activated carbon. *Journal of Environmental Chemical Engineering*, *3*(3), 1504–1512. https://doi.org/10.1016/j.jece.2015.05.014

Zhang, H., Sun, W., Zhang, J., & Ma, J. (2024). Vacuum-ultraviolet based advanced oxidation and reduction processes for water treatment. *Journal of Hazardous Materials*, *471*, 134432. https://doi.org/https://doi.org/10.1016/j.jhazmat.2024.134432

Zhang, L., Yang, W., Chen, Y., & Yang, L. (2025). Removal of Tetracycline from Water by Biochar: Mechanisms, Challenges, and Future Perspectives. *Water (Switzerland)*, *17*(13), 1–24. https://doi.org/10.3390/w17131960

Zhang, Y., Cong, Y., Zhang, J., Li, X., Li, Y., Dong, Z., Yuan, G., Zhang, J., & Cui, Z. (2018). Effects of activation temperatures on the surface structures and supercapacitive performances of porous carbon fibers. *Surface and Coatings Technology*, *349*, 384–391. https://doi.org/https://doi.org/10.1016/j.surfcoat.2018.06.012

Zhao, W., Hao, C., Guo, Y., Shao, W., Tian, Y., & Zhao, P. (2023). Optimization of Adsorption Conditions Using Response Surface Methodology for Tetracycline Removal by MnFe2O4/Multi-Wall Carbon Nanotubes. *Water (Switzerland)*, *15*(13). https://doi.org/10.3390/w15132392

Zhao, W., Yang, L., Han, W., Gu, C., Xu, Z., Lv, X., & Zhang, H. (2024). Application and evaluation of a modified intraparticle diffusion model for mono-/multiadsorption of chlorobenzene pollutants on biochar. *Journal of Soils and Sediments*, *24*(11), 3626–3640. https://doi.org/10.1007/s11368-024-03910-x

Zheng, F., Zou, H., Xiang, Y., Zhi, D., Wang, X., & Zhou, Y. (2025). Efficient removal of tetracycline antibiotics in aquatic environment with ball-milled red mud modified biochars. *Journal of Environmental Sciences*. https://doi.org/https://doi.org/10.1016/j.jes.2025.07.047

Zhong, S.-F., Yang, B., Lei, H.-J., Xiong, Q., Zhang, Q.-Q., Liu, F., & Ying, G.-G. (2022). Transformation products of tetracyclines in three typical municipal wastewater treatment plants. *Science of The Total Environment*, *830*, 154647. https://doi.org/https://doi.org/10.1016/j.scitotenv.2022.154647

Zhou, L., Ying, G., Liu, S., Zhao, J., Yang, B., Chen, Z., & Lai, H. (2013). Science of the Total Environment Occurrence and fate of eleven classes of antibiotics in two typical wastewater treatment plants in South China. *Science of the Total Environment, The*, *452–453*, 365–376. https://doi.org/10.1016/j.scitotenv.2013.03.010

Zietzschmann, F., Stützer, C., & Jekel, M. (2016). Granular activated carbon adsorption of organic micro-pollutants in drinking water and treated wastewater - Aligning breakthrough curves and capacities. *Water Research*, *92*, 180–187. https://doi.org/10.1016/j.watres.2016.01.056

LIST OF APPENDIXES

Appendix A,

Tables and figures for Process optimization and equilibrium, kinetic, and isotherm studies analysis for adsorption removal of tetracycline from municipal wastewater treatment plants effluents using $ZnCl_2$ activation of biomass (cassava peels): Artificial Neural Network and Surface Response Methodology approach.

Table 1A, RSM-BBD, Adsorption experiments at Uv-vis spectrophotometer wavelength of 365nm.

Run	TC. Working conc. (mg/L)	pH	Time (min)	Dosage (g)	UV-vis spectrophotometer absorbance, initial and final		Initial and final TC. Conc. (mg/L)		Removal (%)
1	5	3	60	0.075	0.1654	0.0143	C_o= 4.3185	C_f = 0.3733	76.45
2	7.5	6	90	0.05	0.2082	0.0348	C_o = 5.436	C_f = 0.9086	83.28
3	5	9	30	0.05	0.1662	0.1174	C_o = 4.339	C_f =3.065	57.36
4	2.5	6	60	0.075	0.0912	0.0027	C_o = 2.3812	C_f =0.0704	97.09
5	5	3	90	0.05	0.1610	0.0192	C_o = 4.2036	C_f=0.5013	71.14
6	7.5	6	30	0.05	0.2100	0.0891	C_o =5.480	C_f = 2.326	57.55
7	5	6	90	0.075	0.1730	0.0080	C_o =4.516	C_f =0.208	95.39
8	5	6	60	0.05	0.1740	0.0172	C_o =4.543	C_f =0.4490	76.51
9	7.5	9	60	0.05	0.1959	0.0525	C_o =5.115	C_f =1.370	60.01
10	5	6	60	0.05	0.1711	0.0444	C_o = 4.467	C_f = 1.159	74.05
11	5	6	60	0.05	0.1698	0.0397	C_o =4.433	C_f = 1.036	76.61
12	5	6	60	0.05	0.1701	0.0514	C_o = 4.441	C_f = 1.342	72.78

13	2.5	3	60	0.05	0.0822	0.0214	$C_o = 2.129$	$C_f = 0.5587$	75.75
14	7.5	6	60	0.025	0.2185	0.0814	$C_o = 5.705$	$C_f = 2.125$	62.75
15	7.5	3	60	0.05	0.2086	0.0717	$C_o = 5.446$	$C_f = 1.872$	65.62
16	5	6	30	0.025	0.1696	0.0467	$C_o = 4.428$	$C_f = 1.219$	71.94
17	5	3	60	0.025	0.1769	0.0740	$C_o = 4.618$	$C_f = 1.932$	58.16
18	5	9	90	0.05	0.1712	0.0646	$C_o = 4.469$	$C_f = 1.671$	76.89
19	5	6	30	0.075	0.1698	0.0542	$C_o = 4.434$	$C_f = 1.446$	67.6
20	2.5	9	60	0.05	0.0831	0.00833	$C_o = 2.169$	$C_f = 0.217$	89.97
21	2.5	6	90	0.05	0.0911	0.00341	$C_o = 2.378$	$C_f = 0.0890$	96.25
22	5	9	60	0.075	0.1771	0.0380	$C_o = 4.624$	$C_f = 0.992$	74.14
23	5	9	60	0.025	0.1687	0.0560	$C_o = 4.404$	$C_f = 1.462$	66.8
24	2.5	6	60	0.025	0.0892	0.00966	$C_o = 2.328$	$C_f = 0.252$	89.16
25	2.5	6	30	0.05	0.0789	0.00899	$C_o = 2.060$	$C_f = 0.238$	88.04
26	7.5	6	60	0.075	0.2028	0.0741	$C_o = 5.295$	$C_f = 1.934$	76.98
27	5	6	90	0.025	0.1709	0.0498	$C_o = 4.462$	$C_f = 1.300$	70.86
28	5	6	60	0.05	0.1696	0.0458	$C_o = 4.428$	$C_f = 1.195$	73.3
29	5	3	30	0.05	0.1599	0.0629	$C_o = 4.175$	$C_f = 1.642$	60.66

Definition

C = concentration of tetracycline in solution after adsorption (mg/L).

C_o = Initial concentration of tetracycline in solution before adsorption (mg/L).

C/C_0 = This ratio indicates the fraction of tetracycline that remains in the solution after adsorption

Figure 1A UV-vis of spectrophotometry Calibration Absorbance for TC adsorption removal

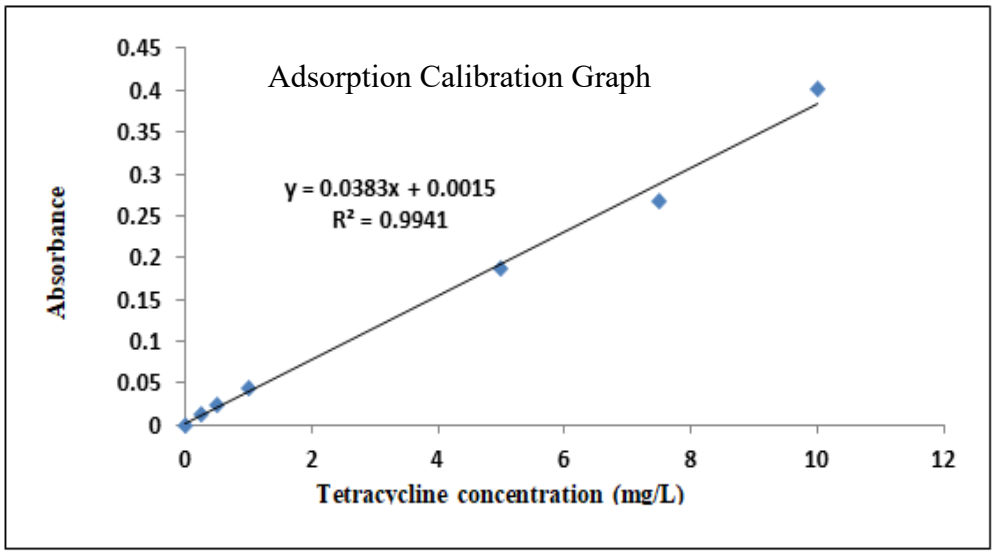

Adsorption kinetics models and Isothermal analysis

Figures 2A, **Pseudo-first-order** kinetic models' parameters.

(a)

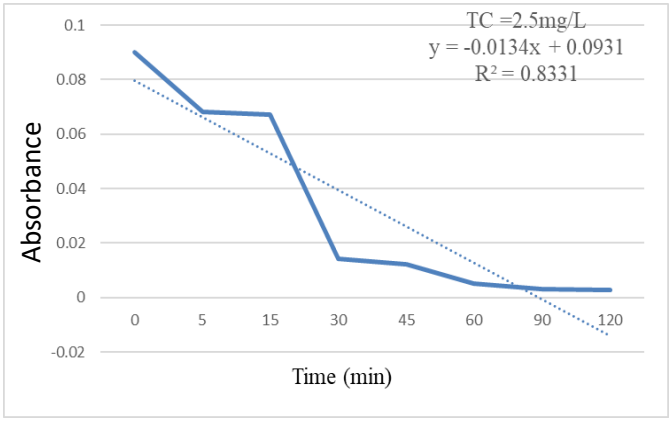

(b)

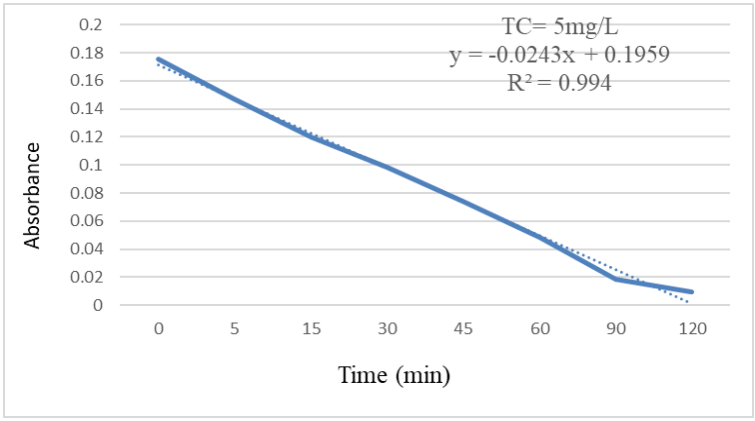

(c) (d)

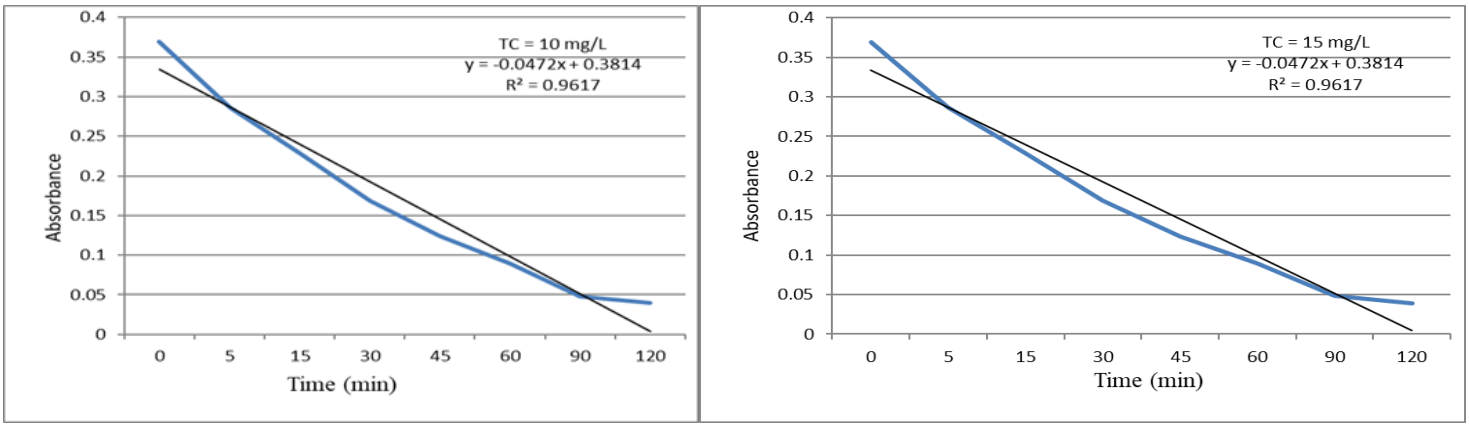

Figures 3A, **Pseudo-second-order** kinetic models' parameters.

(a) (b)

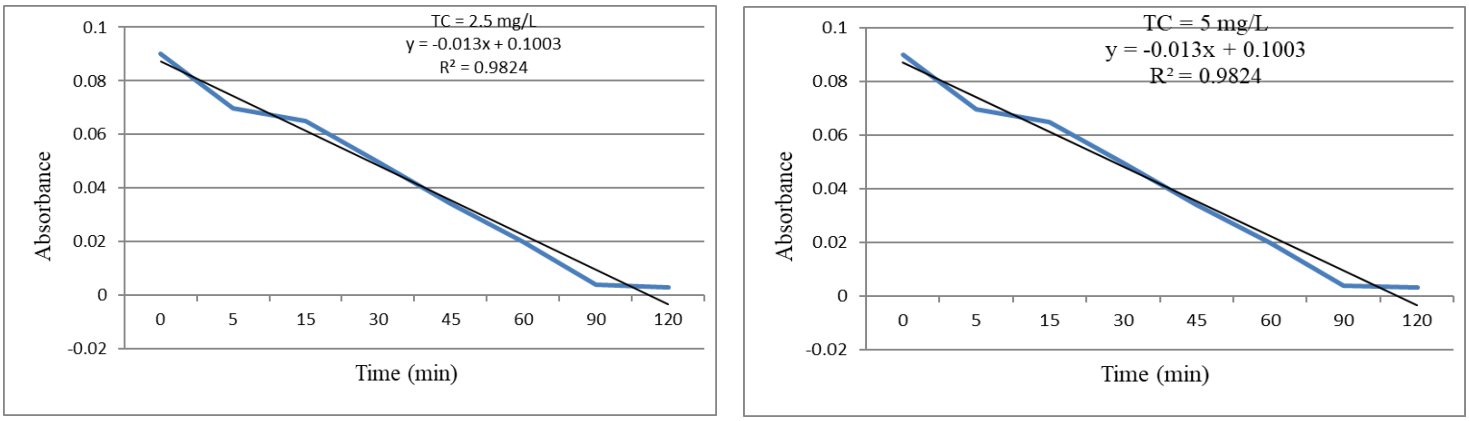

(C) (d)

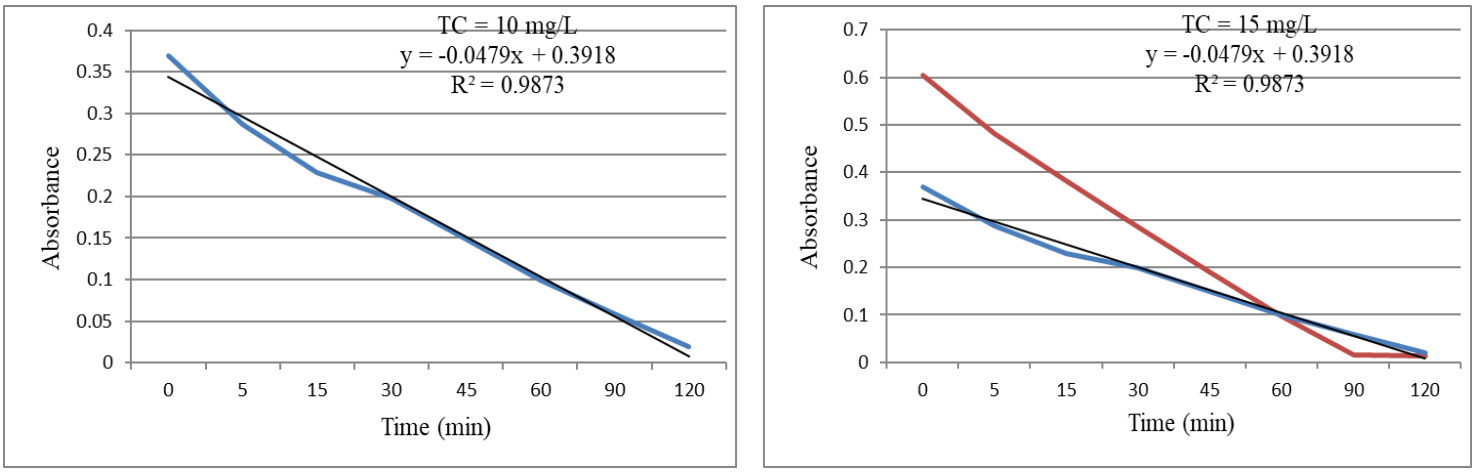

Figure 4A, Interparticle diffusion adsorption kinetics model at different concentration of contaminant (TC).

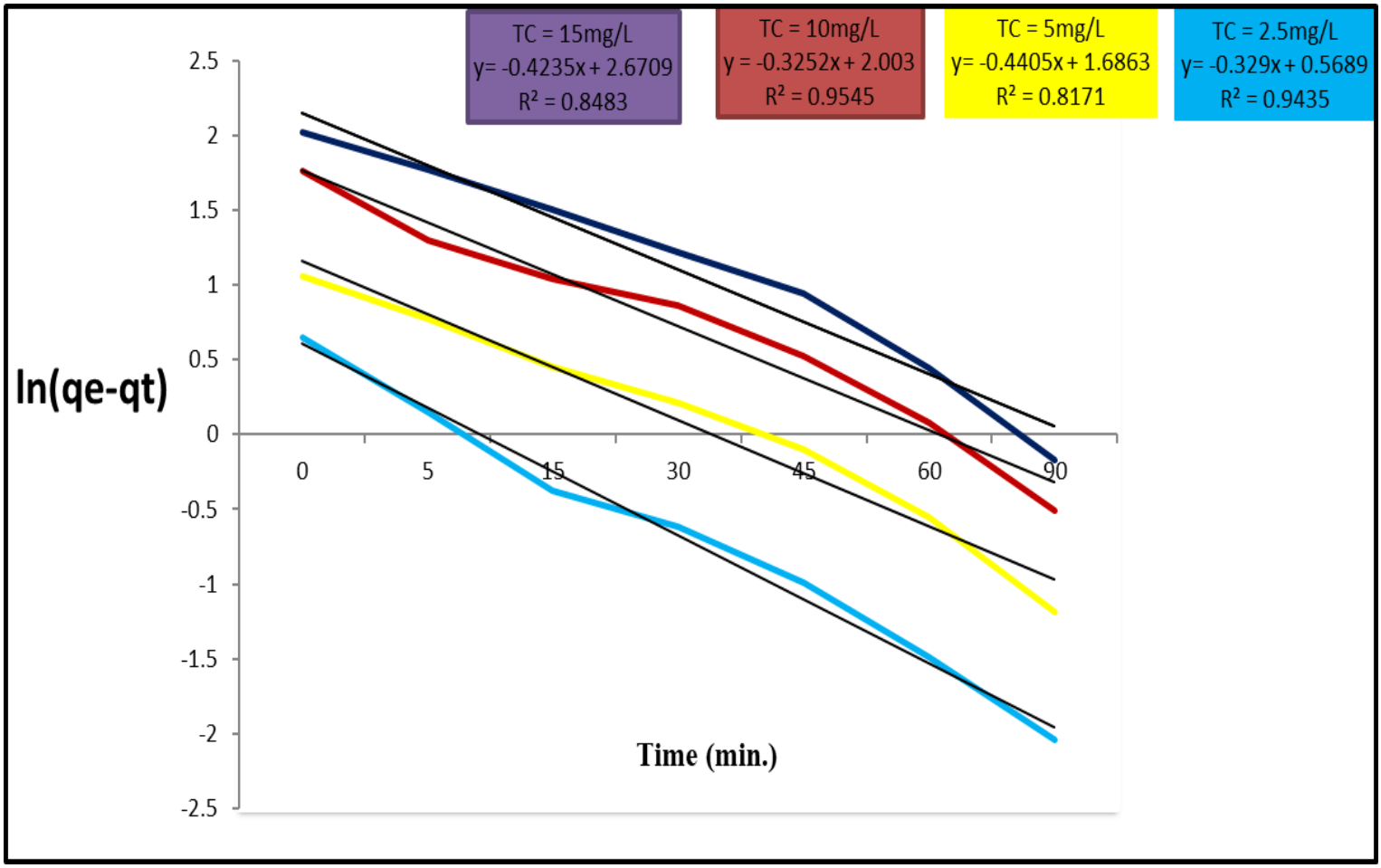

Appendix B,

Tables and figures for Process optimization and equilibrium, kinetic, and isotherm studies analysis for photocatalysis degradation of tetracycline from municipal wastewater treatment plants effluents using green synthesized ZnO-NPs: Artificial Neural Network and Surface Response Methodology approach.

Table 1B, RSM-BBD, Photocatalysis experiments at Uv-vis spectrophotometer wavelength of 365nm.

Run	TC.coc (mg/L)	pH	Time (min)	Catalyst dosage (g/L)	UV-vis spectrophotometer absorbance, initial and final		Initial and final TC. Conc. (mg/L)		Degradation efficiency (%)
1	10	5	120	1	0.3897	0.0344	Co=10.175	Cf =0.898	91.17
2	5	6	75	0.5	0.1176	0.0509	Co =3.070	Cf =1.305	53.38
3	10	6	75	1	0.3539	0.0925	Co =9.240	Cf =2.415	73.86
4	5	6	120	1	0.1184	0.0118	Co =3.010	Cf =0.308	92.19
5	5	6	75	1.5	0.1427	0.0206	Co =3.725	Cf=0.537	85.56
6	10	5	30	1	0.2396	0.0947	Co =6.255	Cf =2.473	60.47
7	15	6	75	1.5	0.3759	0.1850	Co =9.814	Cf =4.830	50.78
8	10	6	75	1	0.3353	0.0822	Co =8.751	Cf =2.160	75.27
9	10	6	30	1.5	0.2917	0.0574	Co =7.616	Cf =1.498	80.32
10	10	6	120	0.5	0.2284	0.0204	Co =5.963	Cf =0.532	91.06
11	10	5	75	1.5	0.2189	0.0353	Co =5.715	Cf =0.921	83.87
12	15	6	120	1	0.3763	0.1266	Co = 9.825	Cf =3.305	66.35
13	10	5	75	0.5	0.2333	0.0487	Co =6.091	Cf =1.271	79.13
14	10	6	75	1	0.2774	0.0386	Co =7.242	Cf =1.007	86.08
15	10	7	30	1	0.2651	0.0683	Co =6.938	Cf =1.783	74.94
16	10	6	75	1	0.2499	0.0574	Co =6.524	Cf =1.498	80.53
17	5	6	30	1	0.1270	0.0771	Co =3.315	Cf =2.013	39.27
18	5	5	75	1	0.1322	0.0608	Co =3.451	Cf =1.587	53.99
19	15	6	30	1	0.3501	0.2260	Co =9.140	Cf=5.900	35.44
20	5	7	75	1	0.1007	0.0149	Co =2.629	Cf =0.389	85.20

21	15	6	75	0.5	0.3575	0.1489	Co =9.334	Cf =3.887	58.34
22	10	6	75	1	0.2497	0.0495	Co =6.519	Cf =1.292	80.18
23	15	7	75	1	0.3365	0.2275	Co =8.785	Cf =5.939	32.39
24	15	5	75	1	0.3453	0.2361	Co =9.015	Cf =6.164	31.61
25	10	6	30	0.5	0.2536	0.0742	Co =6.621	Cf =1.937	70.73
26	10	7	75	0.5	0.2651	0.0661	Co =6.921	Cf =1.728	75.02
27	10	6	120	1.5	0.2412	0.0348	Co = 6.036	Cf =1.169	80.63
28	10	7	75	1.5	0.2621	0.08461	Co =6.843	Cf =2.209	67.71
29	10	7	120	1	0.2180	0.0648	Co =5.691	Cf =1.695	70.21

Figure 2B, UV-vis of spectrophotometry Calibration Absorbance for TC photocatalysis degradation.

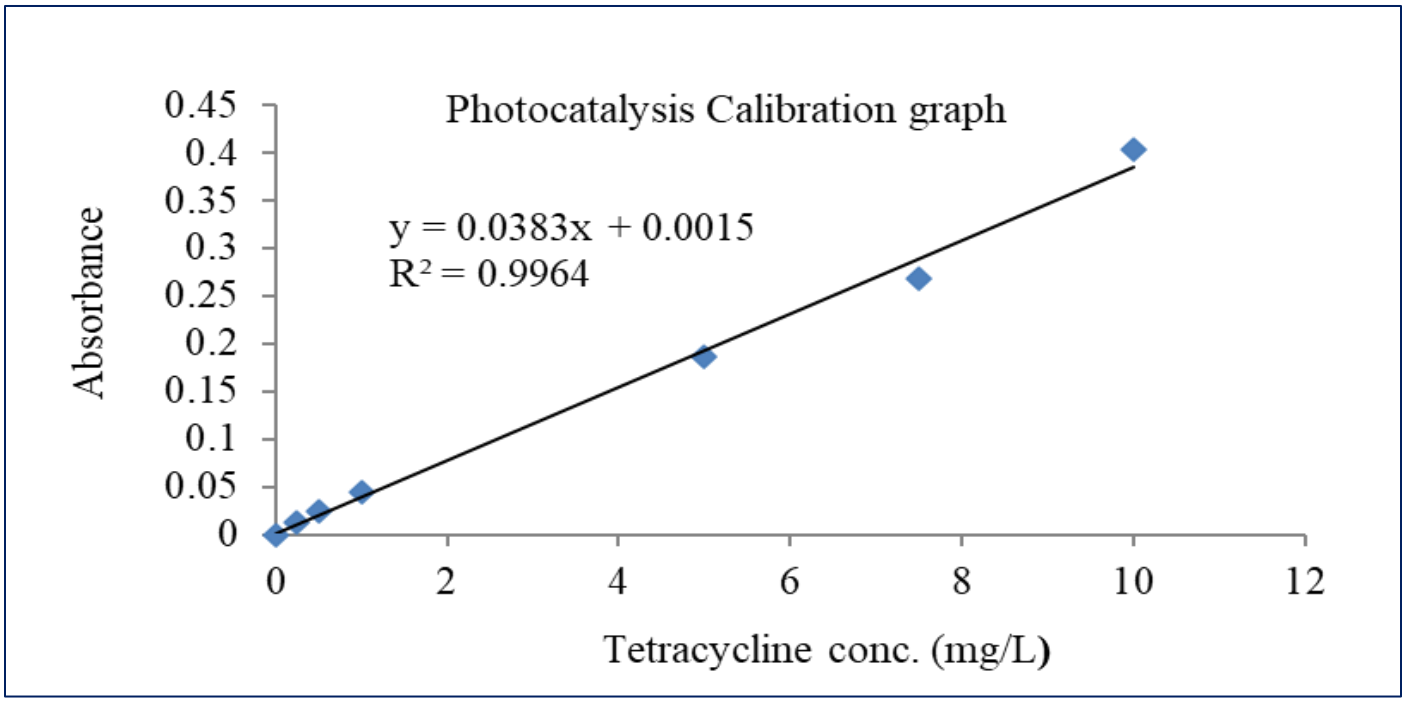

Figure 2B, Interparticle diffusion adsorption kinetics model at different concentration

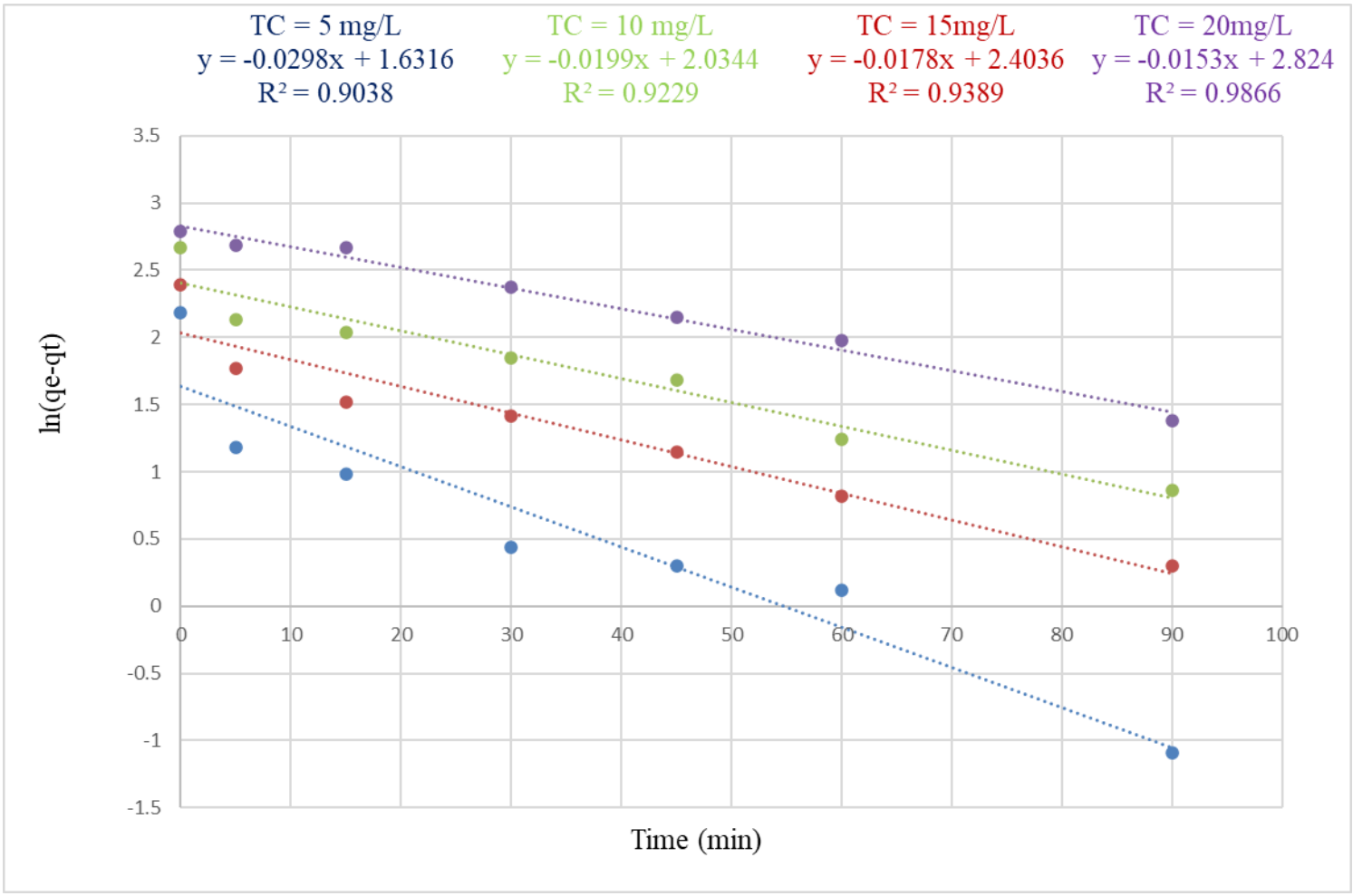

Appendix C,

Tables and figures for Simultaneous Adsorption and Photocatalysis Processes Based on the Synergetic effect of Composite Materials (Green-based AC/ZnO-NPs) for the removal of pharmaceutical pollutants of (Tetracycline) from Aqueous Solution

Table 1C, RSM-BBD, Simultaneously Adsorption-Photocatalysis experiments at Uv-vis spectrophotometer wavelength of 365nm.

Run	Parameters			Response		
	ZnO-NPs/AC Ratio	Initial (TC) Conc. (mg/L)	Composite Dosage (g/L)	Final TC Conc. (mg/L)	Abs. (%)	Removal Efficiency (%)
1	2:1	5	1	0.393	0.0850	92.12
2	4:1	5	1	0.954	0.0694	80.92
3	2:1	15	1	2.451	0.0870	83.65
4	4:1	15	1	3.095	0.1454	79.36
5	2:1	10	0.5	1.902	0.0320	80.98
6	4:1	10	0.5	2.224	0.0790	77.75
7	2:1	10	1.5	0.458	0.0162	95.41
8	4:1	10	1.5	1.813	0.0644	81.93
9	3:1	5	1.5	0.349	0.0489	93.02
10	3:1	15	0.5	4.008	0.0358	73.31
11	3:1	5	1.5	0.036	0.0012	99.41
12	3:1	15	1.5	1.958	0.0140	86.94
13	3:1	10	1	0.130	0.0036	98.70

Figure 1C, Simultaneously Adsorption-photocatalysis Calibration graph for TC degradation generated by UV-Vis NR CLB.

No	TC. Concentration (mg/L)	Absorbance.
1	0.5	0.0181
2	1	0.04936
3	5	0.1692
4	7.5	0.2704
5	10	0.3549